

---

---

---

---

JSCSEN 88(7–8)685–810(2023)

---

---

---

ISSN 1820-7421(Online)

---

---

---

---

---

---

# Journal of the Serbian Chemical Society

---

---

---

---

---

---

VOLUME 88

---

---

---

No 7–8

---

---

---

BELGRADE 2023

---

---

---

Available on line at



[www.shd.org.rs/JSCS/](http://www.shd.org.rs/JSCS/)

---

---

---

The full search of JSCS

is available through

DOAJ DIRECTORY OF

OPEN ACCESS

JOURNALS

[www.doaj.org](http://www.doaj.org)

The **Journal of the Serbian Chemical Society** (formerly Glasnik Hemijskog društva Beograd), one volume (12 issues) per year, publishes articles from the fields of chemistry. The **Journal** is financially supported by the **Ministry of Education, Science and Technological Development of the Republic of Serbia**.

Articles published in the **Journal** are indexed in Clarivate Analytics products: **Science Citation Index-Expanded™** – accessed via **Web of Science®** and **Journal Citation Reports®**.

**Impact Factor** announced on 28 June, 2023: **1.000; 5-year Impact Factor: 1.100.**

Articles appearing in the **Journal** are also abstracted by: **Scopus**, **Chemical Abstracts Plus (CAplus<sup>SM</sup>)**, **Directory of Open Access Journals**, **Referativni Zhurnal (VINITI)**, **RSC Analytical Abstracts**, **EuroPub**, **Pro Quest** and **Asian Digital Library**.

**Publisher:**

**Serbian Chemical Society**, Karnežijeva 4/III, P. O. Box 36, 1120 Belgrade 35, Serbia  
tel./fax: +381-11-3370-467, E-mails: **Society** – shd@shd.org.rs; **Journal** – jscs@shd.org.rs  
Home Pages: **Society** – <http://www.shd.org.rs/>; **Journal** – <http://www.shd.org.rs/JSCS/>  
Contents, Abstracts and full papers (from Vol 64, No. 1, 1999) are available in the electronic form at the Web Site of the **Journal** (<http://www.shd.org.rs/JSCS/>).

**Internet Service:**

**Nikola A. Pušin** (1930–1947), **Aleksandar M. Leko** (1948–1954),

**Panta S. Tutundžić** (1955–1961), **Miloš K. Mladenović** (1962–1964),

**Dorđe M. Dimitrijević** (1965–1969), **Aleksandar R. Despić** (1969–1975),

**Slobodan V. Ribnikar** (1975–1985), **Dragutin M. Dražić** (1986–2006).

**Editor-in-Chief:**

**BRANISLAV Ž. NIKOLIĆ**, Serbian Chemical Society (E-mail: [jscs-ed@shd.org.rs](mailto:jscs-ed@shd.org.rs))

**Deputy Editor:**

**DUŠAN SLADIĆ**, Faculty of Chemistry, University of Belgrade

**Sub editors:**

*Organic Chemistry*

**DEJAN OPSENICA**, Institute of Chemistry, Technology and Metallurgy, University of Belgrade

*Biochemistry and Biotechnology*

**JÁNOS CSANÁDI**, Faculty of Science, University of Novi Sad

**OLGICA NEDIĆ**, INEP – Institute for the Application of Nuclear Energy, University of Belgrade

*Inorganic Chemistry*

**MILOŠ ĐURAN**, Serbian Chemical Society

*Theoretical Chemistry*

**IVAN JURANIĆ**, Serbian Chemical Society

*Physical Chemistry*

**LJILJANA DAMJANOVIĆ-VASILIĆ**, Faculty of Physical Chemistry, University of Belgrade

*Electrochemistry*

**SNEŽANA GOJKOVIC**, Faculty of Technology and Metallurgy, University of Belgrade

*Analytical Chemistry*

**RADA BAOŠIĆ**, Faculty of Chemistry, University of Belgrade

*Polymers*

**BRANKO DUNJIĆ**, Faculty of Technology and Metallurgy, University of Belgrade

*Thermodynamics*

**MIRJANA KIJEVČANIN**, Faculty of Technology and Metallurgy, University of Belgrade

*Chemical Engineering*

**TATJANA KALUDEROVIĆ RADOIĆIĆ**, Faculty of Technology and Metallurgy, University of Belgrade

*Materials*

**RADA PETROVIĆ**, Faculty of Technology and Metallurgy, University of Belgrade

*Metallic Materials and Metallurgy*

**ANA KOSTOV**, Mining and Metallurgy Institute Bor, University of Belgrade

*Environmental and Geochemistry*

**VESNA ANTIĆ**, Faculty of Agriculture, University of Belgrade

*History of and Education in Chemistry*

**DRAGICA TRIVIĆ**, Faculty of Chemistry, University of Belgrade

**English Language Editors:**

**LYNNE KATSIKAS**, Serbian Chemical Society

**VLATKA VAJS**, Serbian Chemical Society

**Technical Editors:**

**JASMINA NIKOLIĆ**, Faculty of Technology and Metallurgy, University of Belgrade

**Journal Manager & Web Master:**

**VLADIMIR PANIĆ**, Institute of Chemistry, Technology and Metallurgy, University of Belgrade

**Office:**

**MARIO ZLATOVIĆ**, Faculty of Chemistry, University of Belgrade

**VERA ĆUŠIĆ**, Serbian Chemical Society

**Editorial Board**

**From abroad:** **R. Adžić**, Brookhaven National Laboratory (USA); **A. Casini**, University of Groningen (The Netherlands); **G. Cobb**, Baylor University (USA); **D. Douglas**, University of British Columbia (Canada); **G. Inzelt**, Etvos Lorand University (Hungary); **J. Kenny**, University of Perugia (Italy); **Ya. I. Korenman**, Voronezh Academy of Technology (Russian Federation); **M. D. Lechner**, University of Osnabrueck (Germany); **S. Macura**, Mayo Clinic (USA); **M. Spitteler**, INFU, Technical University Dortmund (Germany); **M. Stratakis**, University of Crete (Greece); **M. Swart**, University of Girona (Cataluna, Spain); **G. Vunjak-Novaković**, Columbia University (USA); **P. Worsfold**, University of Plymouth (UK); **J. Zagal**, Universidad de Santiago de Chile (Chile).

**From Serbia:** **B. Abramović**, **V. Antić**, **R. Baošić**, **V. Beškoski**, **J. Csanadi**, **Lj. Damjanović-Vasilić**, **A. Dekanski**, **V. Dondur**, **B. Dunjić**, **M. Duran**, **S. Gojković**, **I. Gutman**, **B. Jovančićević**, **I. Juranić**, **T. Kaluderović**, **Radiočić**, **L. Katsikas**, **M. Kijevčanin**, **A. Kostov**, **V. Leovac**, **S. Milonjić**, **V.B. Mišković-Stanković**, **O. Nedić**, **B. Nikolić**, **J. Nikolić**, **D. Osenica**, **V. Panić**, **M. Petkovska**, **R. Petrović**, **I. Popović**, **B. Radak**, **S. Ražić**, **D. Sladić**, **S. Sovilj**, **S. Šerbanović**, **B. Šolaja**, **Ž. Tešić**, **D. Trivić**, **V. Vajs**, **M. Zlatović**.

**Subscription:** The annual subscription rate is **150.00 €** including postage (surface mail) and handling. For Society members from abroad rate is **50.00 €**. For the proforma invoice with the instruction for bank payment contact the Society Office (E-mail: [shd@shd.org.rs](mailto:shd@shd.org.rs)) or see JSCS Web Site: <http://www.shd.org.rs/JSCS/>, option Subscription.

**Godišnja pretplata:** Za članove SHD: **2.500,00 RSD**, za penzionere i studente: **1000,00 RSD**, a za ostale: **3.500,00 RSD**: za organizacije i ustanove: **16.000,00 RSD**. Uplate se vrše na tekući račun Društva: **205-13815-62**, poziv na broj **320**, sa naznakom "pretplata za JSCS".

**Nota:** Radovi čiji su svi autori članovi SHD prioritetno se publikuju.  
Odlukom Odbora za hemiju Republičkog fonda za nauku Srbije, br. 66788/1 od 22.11.1990. godine, koja je kasnije potvrđena odlukom Savete Fonda, časopis je uvršten u kategoriju međunarodnih časopisa (**M-23**). Takođe, aktom Ministarstva za nauku i tehnologiju Republike Srbije, 413-00-247/2000-01 od 15.06.2000. godine, ovaj časopis je proglašen za publikaciju od posebnog interesa za nauku. **Impact Factor** časopisa objavljen 28. juna 2023. godine je **1,000**, a petogodišnji **Impact Factor 1,100**.



# Journal of the Serbian Chemical Society

JSCS-info@shd.org.rs • www.shd.org.rs/JSCS

*J. Serb. Chem. Soc.* Vol. 88, No. 7–8 (2023)

## CONTENTS\*

<i>K. D. Božić, M. M. Pavlović, G. M. Šekularac, S. V. Panić and M. R. Pantović Pavlović: Application aspects of joint anaphoresis/substrate anodization in production of biocompatible ceramic coatings (Survey).....</i>	<i>685</i>
<b>Organic Chemistry</b>	
<i>S. Farkas, G. Benedeković, S. M. Stanisljević, B. M. Srećo Zelenović, M. Popovin, V. Popovin and D. S. Jakimov: Synthesis and antiproliferative activity of (5R)-cleistenolide and analogues.....</i>	<i>705</i>
<i>A. Singhamahapatra, C. Pattnaik, B. Prasad Kar, G. C. Nayak, L. N. Sahoo and S. Sahoo: Click mediated synthesis of functionalized glycolipids with peptide-peptoid linkages.....</i>	<i>715</i>
<b>Biochemistry and Biotechnology</b>	
<i>J. Stevanović, D. Robajac, O. Nedić and Z. Dobrijević: Post-TRIzol protein extraction from peripheral blood mononuclear cells.....</i>	<i>729</i>
<b>Inorganic Chemistry</b>	
<i>C. Kaya, O. Bayindir, S. Saklar, O. Atakol and H. Çelikkan: Preventing hydrolysis of AlN powders with organophosphate coating in aqueous media.....</i>	<i>739</i>
<b>Electrochemistry</b>	
<i>S. K. Manu, N. V. Selvam and M. Ramachandran: Investigating inhibition characteristics of <i>Butea monosperma</i> leaf extracts to retard stainless steel biocorrosion in the presence of sulfate-reducing bacteria .....</i>	<i>749</i>
<b>Analytical Chemistry</b>	
<i>N. Turković, N. Andelković, D. Obradović, Z. Vujić and B. Ivković: Application of liquid chromatography in defining the interaction of newly synthesized chalcones and related compounds with human serum albumin.....</i>	<i>765</i>
<b>Environmental</b>	
<i>U. Marčeta, M. Vučinić Vasić, J. Ninkov, S. Ilić and B. Vujić: Health risk assessment of toxic elements in sedimentable dust from landfills .....</i>	<i>777</i>
<b>History of and Education in Chemistry</b>	
<i>S. A. Horvat, V. I. Popović, D. D. Rodić and T. N. Rončević: Analysis of the initial education of chemistry teachers and their attitudes towards teaching in the Republic of Serbia .....</i>	<i>793</i>

Published by the Serbian Chemical Society  
Karnegijeva 4/III, P.O. Box 36, 11120 Belgrade, Serbia  
Printed by the Faculty of Technology and Metallurgy  
Karnegijeva 4, P.O. Box 35-03, 11120 Belgrade, Serbia

\* For colored figures in this issue please see electronic version at the Journal Home Page:  
<http://www.shd.org.rs/JSCS/>



SURVEY

## Application aspects of joint anaphoresis/substrate anodization in production of biocompatible ceramic coatings

KATARINA Đ. BOŽIĆ<sup>1,2\*</sup>, MIROSLAV M. PAVLOVIĆ<sup>1,2\*#</sup>, GAVRILO M. ŠEKULARAC<sup>1</sup>, STEFAN V. PANIĆ<sup>1</sup> and MARIJANA R. PANTOVIĆ PAVLOVIĆ<sup>1,2#</sup>

<sup>1</sup>Institute of Chemistry, Technology and Metallurgy, National Institute of the Republic of Serbia, Department of Electrochemistry, University of Belgrade, Belgrade, Serbia and

<sup>2</sup>Center of Excellence in Environmental Chemistry and Engineering, Institute of Chemistry, Technology and Metallurgy, Belgrade, Serbia

(Received 18 January, revised 10 February, accepted 8 July 2023)

**Abstract:** Electrophoretic deposition (EPD) occurs as a cataphoretic deposition – the coating is deposited on the cathode, and anaphoretic deposition – the coating is deposited on the anode. The primary purpose of EPD is to obtain compact and uniform organic/inorganic coatings of the desired thickness and adhesion on metal surfaces by applying an electric field to the particles of coating precursor. EPD basic principles for coatings deposition concerning fundamental explanations and considerations of practical parameters of the process are presented. Cataphoretic deposition has become popular because it can apply organic coatings to complex structures that are otherwise very difficult to coat. These coatings were found to improve the characteristics of the substrate, such as biocompatibility, appearance and resistance to the corrosion processes. The key EPD parameters are composition, pH value and viscosity of deposition medium, as well as zeta potential of the particles, electric field strength, etc. A special survey is given to the process of anaphoretic deposition, which is relatively new, and its advantages over cataphoretic deposition are discussed. Through the process of joint anaphoresis/substrate anodization process, the surface of the substrate is simultaneously anodized and modified by incorporation of the foreign particles into the anodic layer. The coatings of mixed composition of better adhesion and corrosion resistance with respect to cataphoretically-deposited coatings are obtained as result.

**Keywords:** biomedical implants; titanium; anodization; cataphoresis; anaphoresis.

\* Corresponding author. E-mail: miroslav.pavlovic@ihtm.bg.ac.rs

# Serbian Chemical Society member.

<https://doi.org/10.2298/JSC230118034B>

## CONTENTS

1. INTRODUCTION
2. FACTORS AFFECTING EPD
  - 2.1. *Key parameters related to the suspension*
    - 2.1.1. Particle size
    - 2.1.2. Dielectric constant of the liquid
    - 2.1.3. Viscosity of solvent
    - 2.1.4. Conductivity of suspension
    - 2.1.5. Zeta potential
    - 2.1.6. pH of the suspension
  - 2.2. *Parameters related to the process*
    - 2.2.1. Deposition time
    - 2.2.2. Applied voltage
    - 2.2.3. Conductivity of substrate
    - 2.2.4. Concentration of a solid phase in the suspension
3. KINETICS OF EPD PROCESS
4. A NOVEL *IN SITU* METHOD OF ANODIZATION/ANAPHORETIC DEPOSITION OF CALCIUM PHOSPHATE COATINGS
5. CONCLUSION

## 1. INTRODUCTION

Various techniques are used to apply inorganic/organic composite coatings to metal substrates: the sol–gel process,<sup>1</sup> dip coating,<sup>2</sup> aerosol deposition/plasma spraying<sup>3,4</sup> and layer-by-layer deposition.<sup>5</sup> Electrophoretic deposition (EPD) has attracted attention as a simple and economical process which offers the possibility of applying uniform coatings on substrates of complex shapes at room temperature.<sup>6</sup> In EPD, the charged particles in suspension are attracted to and deposited on an oppositely charged electrode (substrate).<sup>7</sup>

EPD is a flexible technique suitable for the application of polymers, ceramics and composites. EPD involves two processes, electrophoresis and deposition. A positive or negative charge spontaneously generated on the surface of suspended particles, induces the particle movement towards the oppositely charged electrode as a pole of the applied electric field, in a process known as electrophoresis. Some materials already have a charge on their surface due to the presence of specific functional groups, or a species charge can be generated by adding to the suspension the ions of high adsorption ability. The second process is the coagulation of charged particles while they are depositing on the surface of the oppositely charged electrode. Consequently, a relatively compact and homogeneous coating is formed. The most straightforward apparatus for performing the EPD process consists of two parallel electrodes connected to a power source and immersed in a suspension of depositing particles.<sup>8</sup>

The EPD process can be cathodic (cataphoretic deposition) or anodic (anaphoretic deposition), depending on the electrode on which the deposition occurs,

according to the sign of the charge at particle surface. When the particles are positively charged, the deposition occurs on the cathode (negative electrode), and the process is called cathodic EPD. Anodic EPD is defined as the deposition of negatively charged particles on the anode (positive electrode).<sup>7</sup> Two types of electric fields can be applied for this process, alternating (AC) or direct (DC).<sup>8</sup>

## 2. FACTORS AFFECTING EPD

Two groups of parameters influence the EPD process: suspension-related parameters and process-related parameters. One of the most critical parameters for the deposition of uniform coatings is the formation of a stable suspension with well-dispersed charged particles. Particles are suspended in a medium by the interplay of three different forces: van der Waals attractive force, electrostatic repulsive force and a steric force of coagulate formation (not always present). For a suspension to be stable, electrostatic repulsive and/or steric forces must be dominant over van der Waals attraction. The charged particles move towards the appropriate electrode, where they are then electrostatically deposited upon charge neutralization.<sup>7</sup>

The main electrophoretic characteristic of a particle under the influence of an electric field is electrophoretic mobility.<sup>9</sup> Factors that affect the mobility of charged particles are mostly related to the particle characteristics in the specific suspending medium. Electrophoretic mobility ( $\mu$ ) is defined by Henry equation:<sup>10</sup>

$$\mu = \frac{2}{3} \frac{\varepsilon_0 \varepsilon_r \zeta}{\eta} f(\kappa r) \quad (1)$$

where  $\varepsilon_0$  is the electric permittivity of vacuum,  $\varepsilon_r$  is the relative electric permittivity of the suspending medium,  $\zeta$  is the zeta potential,  $\eta$  is the solvent viscosity,  $f(\kappa r)$  is the Henry coefficient, which depends on the relation between the thickness of the double layer ( $1/\kappa$ ) which is created between the electrode surface and charged particles, and the core radius ( $r$ ) of the particle.

According to Eq. (1), the electrophoretic mobility of a particle is directly proportional to the electric permittivity of the suspending medium, the potential gradient, *i.e.*, the zeta potential at the particle surface, and it is inversely proportional to the viscosity of the suspension.

### 2.1. Key parameters related to the suspension

#### 2.1.1. Particle size

The size of the particles deposited by the EPD method is an important parameter. The finely suspended particles are crucial for obtaining a uniform coating. Particle size and morphology directly affect the particle electrophoretic mobility, the coating thickness and the zeta potential.<sup>11</sup> It has been found that for many ceramic systems, a particle size of 1–20  $\mu\text{m}$  leads to good deposit properties.<sup>9</sup> The increase in the size of the particles leads to suspension inhomogeneity.

geneity and their precipitation due to the influence of gravity, causing an uneven coating thickness. In these cases, the mobility of the particles due to electrophoresis must be greater than the mobility of the particles under the influence of the gravitational field. Small particles have a large electrophoretic mobility. However, if there are larger particles in the suspension, it is necessary to apply a strong electric field or to increase the zeta potential to achieve good electrophoretic mobility.<sup>8</sup> The reduction in particle size also allows better control of cracks that may occur due to coating shrinkage during the drying phase.<sup>12</sup>

#### 2.1.2. Dielectric constant of the liquid

The dielectric constant of the suspending medium should have an optimum value. Liquids with a low dielectric constant value cause low mobility, and therefore no deposition can occur. At high values of the dielectric constant, the thickness of the electric double layer decreases due to the high concentration of polar solvent molecules within, which also reduces the electrophoretic mobility of the particles, especially for smaller particle size.<sup>13</sup>

#### 2.1.3. Viscosity of solvent

Solvent viscosity is an important parameter in the EPD process. According to Henry equation, the viscosity of a medium is inversely proportional to the electrophoretic mobility of the particles. A low-viscosity media are required for successful EPD process and high particle mobility.<sup>14</sup>

#### 2.1.4. Conductivity of suspension

The conductivity of the suspension should be in a specific range in order to be favourable for deposition and should be adjusted to maintain the mobility of the specific by tuning the excessive number of ions. Electrophoretic mobility and suspension conductivity are inversely proportional.<sup>15</sup> When the conductivity is very large, the particles move slowly (reduced electrophoretic mobility). On the other hand, when the conductivity is low, the suspension loses stability due to the deficit of a particle surface charge.<sup>16,17</sup>

#### 2.1.5. Zeta potential

One of the key parameters of the EPD process is the zeta potential or electrokinetic potential of charged particles in solution. Zeta potential is the difference in electrical potential that is established within the interphase between the most outer part of the electric double layer formed at the surface of the particle and a solid/liquid interface.<sup>18</sup> It is closely related to the surface properties of suspended particles and medium ionic composition. Direct measurement of the absolute charge on the particles in a liquid media related to an electric double layer established is not possible. Zeta potential can be calculated from experimental data using the Helmholtz–Smoluchowski equations. Zeta potential is of great practical importance for colloidal chemistry and the behaviour of solid particles

suspended/dispersed in liquids. For example, higher zeta potential indicates that particles are stable in dispersion, while lower values of zeta potential indicate lower stability of charged particles in a suspension. When zeta potential reaches a value of zero (isoelectric point) particles will agglomerate and coagulation will occur. It is possible to measure the adsorption of other molecules and modification of the particle surface by measuring the change of their zeta potential in different media. Additionally, in a few studies, the toxicological potential of nanoparticles was correlated with their zeta potential values. It is clear that zeta potential is of great practical importance for electrophoresis and colloidal chemistry.<sup>19</sup>

#### 2.1.6. pH of the suspension

One of the parameters on which zeta potential depends is pH due to high conductivities of hydrogen and hydroxide ions. If an alkali is added to a suspension containing particles with moderate negative zeta potential, the particles tend to acquire a more negative charge. If acid is added to this suspension, neutralization will occur, and consequently coagulation, or even precipitation, takes place. Similarly, adding more acid will generate a positive charge. Therefore, the zeta potential is positive at low pH values and negative at high pH values.<sup>20</sup> At higher concentrations, the acid or base will generate more charged particles in the double layer, which will increase the absolute zeta potential.

### 2.2. Parameters related to the process

#### 2.2.1. Deposition time

One of the most important parameters of the EPD process is the deposition time. At constant voltage, the deposition rate during the EPD process is constant at the beginning and then decreases. This phenomenon is explained by the formation of an insulating layer (coating) on the electrode, which reduces the strength of the electric field.<sup>21</sup> It is crucial to determine the optimal deposition time to obtain a homogeneous coating without cracks at the defined deposition rate.<sup>22</sup>

#### 2.2.2. Applied voltage

Although the amount of coating increases with increasing voltage, this increase deteriorates the coating uniformity. The application of high-strength electric field accelerates the deposition of particles, which does not allow them to pack uniformly within the coating. Additionally, the application of high voltages can increase the currents related to side electrochemical reactions such as hydrogen evolution reaction (cathodic), and oxygen evolution reaction (anodic), which will lead to pronounced release of H<sub>2</sub> and O<sub>2</sub> microbubbles and local change in pH which will cause cracking of the coating and its mechanical instability.

To avoid these issues, it is suggested to use moderate voltages.<sup>23</sup> It was also determined that the increase in applied voltage increases the surface roughness.

At low voltages, large particles cannot reach the substrate, and a uniform coating consisting of small particles is formed. By increasing the applied voltage, the particles move faster, which results in the formation of a less uniform coating consisting of large and small particles. In anaphoretic processes at passivating substrates, there is another issue of the increased rate of anodization of substrate at high voltages that will lead to simultaneous roughing of substrate and deposition of the rough coatings.<sup>24</sup>

#### 2.2.3. Conductivity of substrate

The conductivity of the substrate can affect the quality of the coating obtained by the EPD process. Low substrate conductivity results in non-uniform coating and slow deposition. Longer deposition times are required to coat poor-conductive substrates compared to conductive ones. This is explained by the decrease in the electric field similar to the presence of a separator introduced in modified EPD processes.<sup>25</sup>

#### 2.2.4. Concentration of a solid phase in the suspension

In general, the mass/thickness of the coating increase with increasing concentration. On the other hand, with an increase in thickness the cracks appear frequently, and the morphology of the coating is not uniform at a constant applied voltage.<sup>26</sup> In the case of multi-component systems, the partial rate of deposition depends on the volume fraction of particles in the suspension. When the volume fractions of solids is high, the particles are deposited at similar velocities. However, for small-volume fractions, the partial particle deposition rate depends on the electrophoretic mobility of each particle.<sup>9</sup>

### 3. KINETICS OF EPD PROCESS

Various attempts have been made to describe the kinetics of the EPD process. Hamaker<sup>27</sup> gave the first model of EPD kinetics for electrophoretic cells with planar geometry (Eq. (2)).<sup>28</sup> According to Hamaker, the deposited mass ( $m$ ) is proportional to the solid phase concentration of the suspension ( $C_s$ ), particle electrophoretic mobility ( $\mu$ ), the electrode surface area ( $S$ ), the strength of the applied electric field ( $E$ ) and deposition time ( $t$ ):

$$m = C_s \mu S E t \quad (2)$$

Avgustinik *et al.*<sup>29</sup> checked Hamaker's law of deposition on a cylindrical electrode with a coaxial counter electrode and came up with modified equation for  $m$  in which the electrophoretic mobility is represented in terms of the permittivity of the suspending medium ( $\epsilon = \epsilon_r \epsilon_0$ ), the zeta potential ( $\zeta$ ), and the viscosity of the solvent ( $\eta$ ):<sup>30</sup>

$$m = \frac{IV|\zeta|\epsilon C_s t}{3|\ln(a/b)|\eta} \quad (3)$$

where  $V$  is the voltage,  $l$  and  $a$  are the length and radius of the cylindrical electrode, respectively and  $b$  is the radius of the counter electrode ( $b > a$ ).

Hamaker's equation is applicable only for short deposition times because the linear variation of deposited mass with deposition time in Eq. (2) implies that all other parameters are constant during deposition. In order to consider other experimental conditions, Sarkar and Nicholson<sup>31</sup> proposed that for infinitesimal time intervals, the modified Hamaker equation holds:

$$\frac{\partial m}{\partial t} = f C_s \mu S E \quad (4)$$

where  $f \leq 1$  is the efficiency factor suggesting that not all particles brought to the electrode surface will precipitate, *i.e.*, if all the particles reaching the electrode surface are incorporated in the deposit:  $f = 1$ .<sup>17</sup> Based on this assumption, the authors modelled the variation of the deposited mass as a function of time for four different conditions, which are shown in Fig. 1.

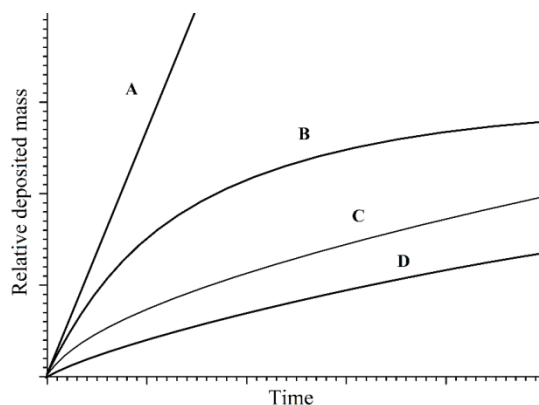


Fig. 1. Deposited mass as a fraction of  $C_s$  during EPD for four different deposition conditions: A) constant EPD current/constant concentration of suspension; B) constant EPD current,  $dC_s/dt < 0$ ; C) constant EPD voltage/constant concentration and D) constant EPD voltage,  $dC_s/dt < 0$ .<sup>31</sup>

A comparison of curves A and C leads to the conclusion that the rate of deposition for curve C (constant voltage) decreases initially, whereas it remains constant in curve A (when deposited under constant current regime), and the coating yield in curve A case is significantly higher. This deviation of curve C from curve A is a consequence of the formation of the insulating layer of the coating which weakens the imposed electric field. This insulating layer causes significant voltage drop per unit depth of the suspension, with the current decreasing during deposition at constant voltage (curve C).

Biesheuvel and Verweij<sup>30</sup> presented the following equation for deposit growth, based on the Kynch theory of sedimentation<sup>32</sup> which describes the bulk effect of the particle motion in the transport phenomena near the deposition electrode and it is based on the expression of the mass balance of the suspension–deposit boundary evolution:

$$\frac{\partial \delta}{\partial t} = -v \frac{\phi_s}{\phi_d - \phi_s} \quad (5)$$

where  $\delta$  is the coating thickness,  $v$  is the electrophoretic velocity of particles close to the electrode,  $\phi_s$  is the volume fraction of the solid phase in the suspension, and  $\phi_d$  is the volumetric parameter related to the deposit. For highly concentrated suspensions ( $\phi_s > 0.2$ ), a correction factor ( $X$ ):

$$X = \frac{\phi_d}{\phi_d - \phi_s} \quad (6)$$

can be included in the kinetic expression, and original Hamaker equation, Eq. (2), transforms into:

$$\frac{\partial m}{\partial t} = f C_s \mu S E \frac{\phi_d}{\phi_d - \phi_s} \quad (7)$$

The expression for the strength of the electric field as a function of suspension conductivity ( $\Lambda$ ) is:<sup>33</sup>

$$E = \frac{I}{\Lambda S} \quad (8)$$

where  $I$  is the particle migration current.

Finally:

$$\frac{\partial m}{\partial t} = f \mu C_s \frac{I}{\Lambda} \frac{\phi_d}{\phi_d - \phi_s} \quad (9)$$

To calculate the yield, Eq. (9) must be solved numerically. The accuracy of this equation was established using experimental data collected during the deposition.

Besides the direct current-EPD (DC-EPD) method where the deposition of charged particles occurs on the oppositely charged electrode in suspension under the influence of constant electric field there is the alternating current-EPD (AC-EPD) method in which the applied voltage is supplied from an AC field. In AC-EPD technique, the direction of electric field is reversed periodically which accounts for oscillation and migration of powder particles in the suspension between electrodes. It was shown that AC-EPD method leads to denser and less cracked coatings as compared to DC-EPD at similar thickness, having broader particle size distribution due to controlled particle migration according to the wave asymmetry and frequency. Fine tuning the asymmetry of AC wave as well as the frequency can further improve the coating characteristics.<sup>34,35</sup> Most models that explain the kinetics of the EPD process are based on the DLVO theory. This theory is named after the researchers Derjaguin, Landau, Verwey

and Overbeek.<sup>36,37</sup> According to this theory, the stability of suspended particles is determined by the interaction between attractive van der Waals forces and repulsive electrostatic forces between particles. At appropriate values of the ionic strength, the electrostatic stabilization of the colloid occurs. On the other hand, another important factor should be taken into account in the presence of hydrophilic polymers. In this case, the adsorption of macromolecules on the particles causes the repulsive forces between them and lead to steric stabilization.<sup>38</sup>

#### 4. A NOVEL *IN SITU* METHOD OF ANODIZATION/ANAPHORETIC DEPOSITION OF CALCIUM PHOSPHATE COATINGS

Cataphoretic deposition of hydroxyapatite (HAp) coatings on titanium is a well-known and widely used method.<sup>39</sup> However, the disadvantage of this type of deposition is the poor adhesion of the coating to the substrate. Cataphoretic coatings are usually sintered to overcome this issue.<sup>40</sup> Sintering of the coating increases the strength of the metal–ceramic bond. This involves generation of an oxide interlayer by the oxidation of Ti substrate, which permeates into the deposited coating. It should be noted that HAp is sensitive to high temperatures because it decomposes into different calcium phosphate structures. Hence the curing by sintering is not rational procedure to improve the coating adhesion.

Another issue in the production of HAp coatings on Ti substrate is the low compatibility of physicochemical properties between these two materials. This causes poor bonding at the HAp/Ti substrate interface, which will lead to the depletion of the coating from the substrate, and consequently to an acceleration of the corrosion and biodegradation, as well as deterioration of the mechanical properties. Many different substrate surface modification techniques, such as anodization, chemical substrate treatment, spraying, *etc.*, have been investigated to overcome poor coating adhesion.<sup>41</sup> Anodization of the substrate surface is one of the most commonly used methods due to its simplicity. In many studies, this method has been used to obtain microporous films of titanium oxide on the substrate surfaces for orthopedic applications.<sup>42</sup> In order to improve the adhesion of the HAp coating on the Ti substrate, Parcharoen *et al.*<sup>43</sup> first treated the Ti surface with alkali and then anodized it before applying the coating on the Ti by an EPD process. However, in the literature, it is difficult to find any data related to the simultaneous processes of modification of the surface of Ti substrate and EPD application of the HAp coating.

Pantović Pavlović *et al.*<sup>44–49</sup> have presented a new method of applying calcium phosphate and hybrid coatings based on calcium phosphate ceramics on Ti substrates. The method is based on the electrophoretic deposition of calcium phosphate coatings. What is unique about this method is the synergy and simultaneous enactment of several processes. The first process is the anodization of the substrate surface, during which a passive oxide layer is formed on the surface

( $\text{TiO}_2$ ), which changes the surface structure and increases the surface roughness. Another process that takes place in parallel is the deposition of a calcium phosphate coating onto substrate. Another novelty of this coating synthesis approach is the application of anaphoretic deposition, which means that the suspension contained negatively charged particles that were deposited on the working anode, *i.e.*, substrate (Fig. 2). Joint anaphoresis/substrate anodization process was performed by applying different voltages, namely 30, 60 and 90 V during the anodization process while keeping the applied electric charge on the anode constant. The polished sample surface appears smooth and homogenized. As the anodization voltage increases, the surface roughness increases for 30 and 60 V, respectively. Although the roughness appears higher for 90 V than for 60 V, some flattening of the surface occurs. This flattening is confirmed by linear and surface roughness analyses.<sup>44</sup>

The pH value of the suspension was 10, which is another difference in comparison to cataphoretic deposition where, in order to stabilize the suspension, the pH value is adjusted to very acidic pH values.

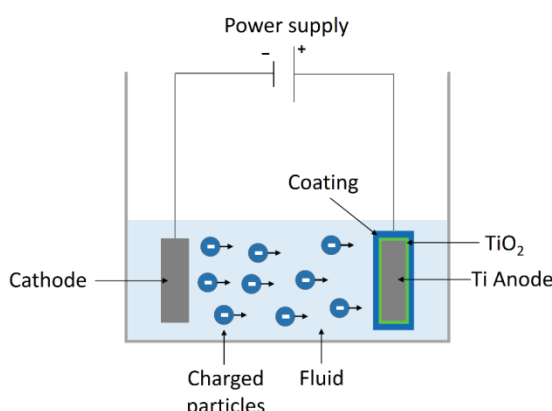


Fig. 2. Schematic representation of anaphoretic deposition.

For synthesized HAp/ $\text{TiO}_2$  composite coating on a Ti substrate, using this new *in situ* method of anodization/anaphoretic deposition of calcium phosphate coatings to strengthen the biocompatible composite coating, there is no need for a subsequent treatments to cure adhesion.

Fig. 3 displays SEM microphotographs of catHAp and anHAp/ $\text{TiO}_2$  coatings deposited via joint anaphoresis/substrate anodization process. As shown in Fig. 3a, the cataphoretically deposited HAp coating exhibits a large number of cracks. The granular structure of the catHAp coating can be observed in greater detail in Fig. 3b at higher magnification. These cracks are primarily caused by the mismatch in Young's modulus between the substrate and the coating. The titanium substrate is more elastic than the hydroxyapatite film, and as ceramic suspensions typically lose water content during drying, cracks in pure hydroxyapatite coatings

are inevitable. This water release occurs near the interface between the ceramic and the substrate, as well as within the bulk material, resulting in shrinkage of the ceramic coating surface and the formation of cracks even at low temperatures. It was found that catHAp coatings have very poor adhesion when deposited onto untreated Ti surfaces. Fig. 3c shows the SEM image of anHAp/TiO<sub>2</sub> composite coating on titanium deposited via joint anaphoresis/substrate anodization process, while Fig. 3d displays the detailed morphology of the composite coating, with needle-like and granular HAp shapes at higher magnification. The deposition of anHAp/TiO<sub>2</sub> is observed without any visible cracks, unlike catHAp. This is attributed to *in-situ* deposition of the anHAp/TiO<sub>2</sub> coating.

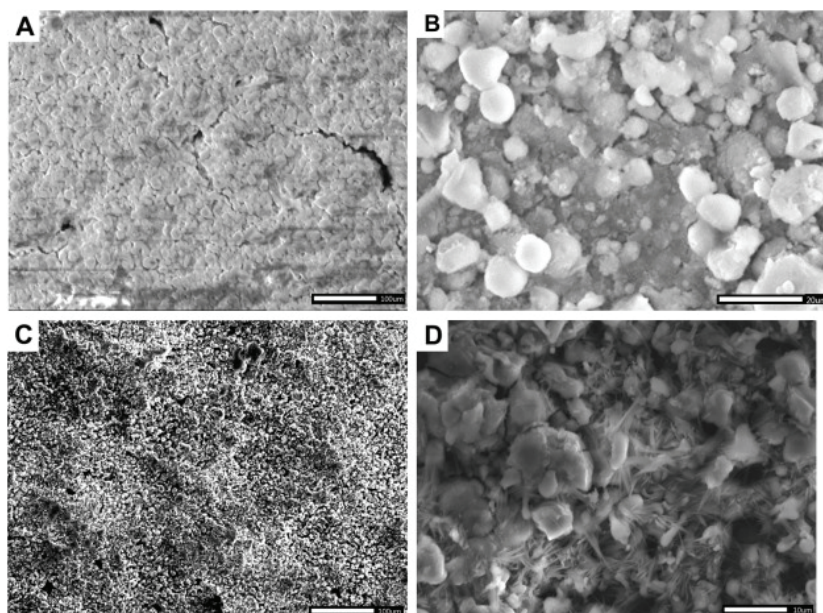


Fig. 3. SEM microphotographs of: a) catHAp coating, magnification  $\times 200$ , b) catHAp coating, magnification  $\times 1500$ , c) anHAp/TiO<sub>2</sub> coating, magnification  $\times 200$  and d) anHAp/TiO<sub>2</sub> coating, magnification  $\times 2000$ .<sup>45</sup> Reprinted with permission from Elsevier.

Fig. 4 presents an FE-SEM microphotograph showing the morphology of the anaphoretically obtained HAp/TiO<sub>2</sub> composite coating (anHAp/TiO<sub>2</sub>). On the surface of the coating, there are no visible cracks, unlike the cataphoretically obtained coating (catHAp). In Fig. 4, needle-like and granular forms of HAp can be observed, while catHAp has a granular structure.<sup>45</sup>

It can be concluded that rational preparation of the suspension and the correct choice of electrolyte, which results in the creation of a stable negatively charged micelle, leads to the formation of a compact and durable coating on the substrate. The resulting coating shows good properties for potential use in bone

implants. The results showed that the new *in situ* process gives much better results than the cataphoretic deposition of HAp in terms of adhesion.<sup>45</sup> Fig. 5 shows a photograph of anHAp/TiO<sub>2</sub> composite coating after adhesion testing according to ASTM D3359-02 standard.

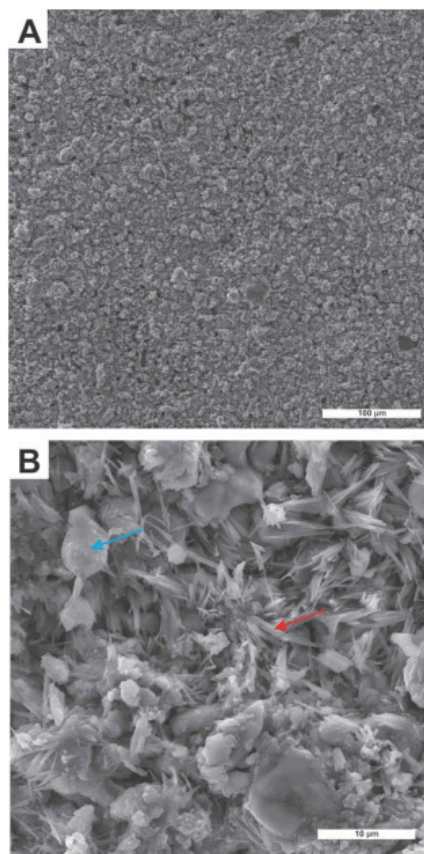


Fig. 4. FE-SEM microphotographs of composite anHAp/TiO<sub>2</sub> coating: a) magnification ×500 and b) magnification ×5000. Different HAp morphologies can be observed, blue arrow points granular and red one points needle-like HAp.<sup>45</sup> Reproduced with permission from Elsevier.

It was concluded that the adhesion of the anHAp/TiO<sub>2</sub> coating is level 4 compared to catHAp coatings which have adhesion level 1 or 2 even after the sintering process.<sup>44</sup> According to the ASTM D3359-02 standard, level 5 represents the best adhesion, while level 0 represents the worst adhesion.

Amorphous calcium orthophosphates (ACPs) are considered to be biomedically-relevant and bioactive calcium phosphates. ACPs possess adjustable chemical properties, but at the same time, they have glass-like physical properties with no long-range order in the atomic positions, whether orientational or translational, as described in reference<sup>47</sup>. Under certain conditions, ACPs can easily transform into thermodynamically stable hydroxyapatite. However, the stability

of ACPs and their transformation to crystalline HAp phases can be influenced by various additives and process parameters, as noted in reference.<sup>47</sup>



Fig. 5. Optical image of composite anHAp/TiO<sub>2</sub> coating after performing adhesion testing according to ASTM D 3359-02.<sup>44</sup>

The *in vitro* bioactivity of a substrate refers to its ability to form an apatite layer when in contact with biological or biological-like fluids. It was shown that the ACP/TiO<sub>2</sub> and ACP+ChOL/TiO<sub>2</sub> composites on Ti substrates can form a bone-like apatite layer on their surfaces when immersed in SBF solution. To assess the biocompatibility of these composite coatings, they were immersed in SBF solution and examined at different time intervals. The surface area physical appearance and particle size of the ACP/TiO<sub>2</sub> and ACP+ChOL/TiO<sub>2</sub> composite coatings on titanium substrates were characterized using SEM, along with the morphologies of the surfaces after immersion in SBF solution for various periods. Fig. 6a and b show the morphology of the ACP/TiO<sub>2</sub> and ACP+ChOL/TiO<sub>2</sub> composites surfaces before immersion in SBF solution, while Fig. 6c–f display the morphologies of the coatings immersed in SBF solution at different time periods.

The SEM images indicate that the composite coatings synthesized cover the substrate surface uniformly and consist of agglomerated nanosized particles with a size smaller than 100 nm. The ACP/TiO<sub>2</sub> and ACP+ChOL/TiO<sub>2</sub> coatings exhibit two different morphologies. The ACP/TiO<sub>2</sub> agglomerates appear larger, resulting in a coarser surface than the ACP+ChOL/TiO<sub>2</sub> coating. Additionally, small fractures are visible on the surface of the ACP+ChOL/TiO<sub>2</sub> composite coating, but it was found that the adhesion of these coatings is high, with a level of 5 according to ASTM D 3359-02: Standard Test Methods for Measuring Adhesion by Tape; cross-cut tape test (B), without any delamination or flaking. These findings suggest that pores are primarily formed during the one-step *in situ* anodization/anaphoretic electrodeposition process.<sup>47</sup>

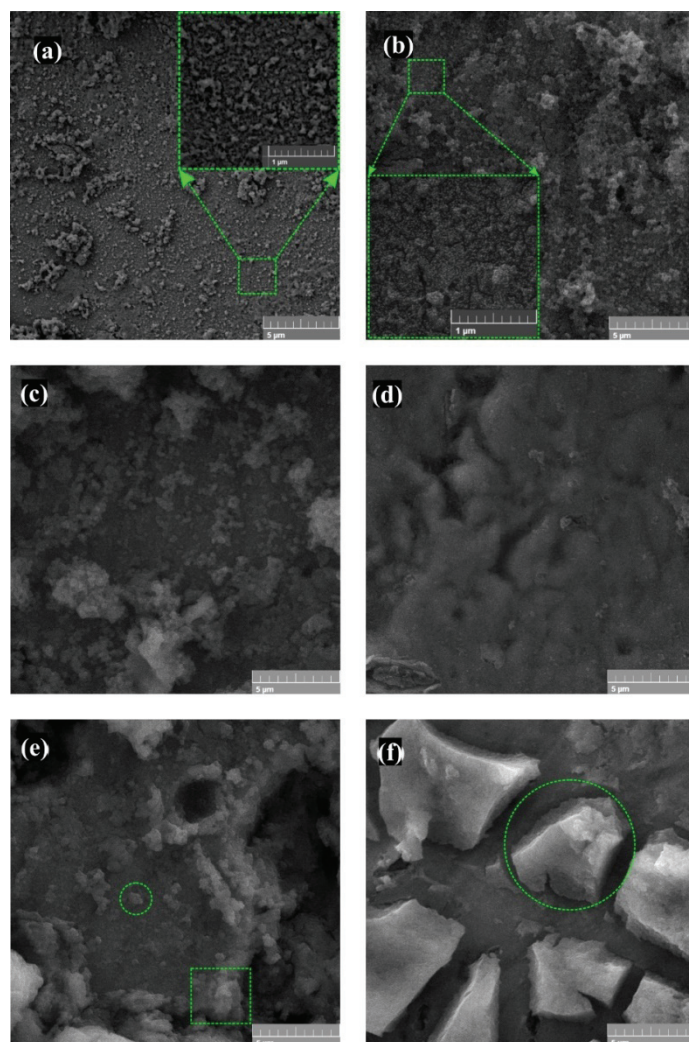


Fig. 6. FE-SEM micrographs presenting the morphology of: a) ACP/TiO<sub>2</sub> and b) ACP+ChOL/TiO<sub>2</sub> on Ti; ACP/TiO<sub>2</sub> coating on Ti immersed in SBF for: c) 72 and e) 240 h; ACP+ChOL/TiO<sub>2</sub> coating on Ti immersed in SBF for: d) 72 and f) 240 h.<sup>47</sup> Reprinted with permission from American Chemical Society.

The bioactivity of composite coatings of nano amorphous calcium phosphate/chitosan oligosaccharide lactate (ACP+ChOL)/titanium oxide (TiO<sub>2</sub>) and ACP/TiO<sub>2</sub> after immersion in simulated body fluid (SBF) for 72 and 240 h is shown in Fig. 6c–f. XRD diffraction patterns of both coatings show broad amorphous peaks that can be assigned to ACP, while the ACP+ChOL/TiO<sub>2</sub> coatings also show peaks assigned to chitosan. After immersion in SBF, both coatings showed XRD peaks assigned to hydroxyapatite (HAp), which is an evidence of the coat-

ings' bioactivity. The ACP+ChOL/TiO<sub>2</sub> coating shows greater bioactivity than the ACP/TiO<sub>2</sub> coating, as it is completely covered with HAp after 72 h of immersion, whereas the ACP/TiO<sub>2</sub> coating takes 72 h to begin forming a new HAp layer, and it grows preferentially in a vertical rather than planar direction. The FE-SEM images of the coatings after 240 h of immersion in SBF show that both coatings are bioactive, with the newly formed HAp layer covering the entire surface of the coating. The ACP/TiO<sub>2</sub> coating has an uneven distribution of HAp particles, while the ACP+ChOL/TiO<sub>2</sub> coating has a smooth and even distribution, and also has the formation of rock-like structures of HAp, which indicates greater bioactivity and osteoconductivity.<sup>47</sup>

A cross-sectional SEM image and its corresponding EDS spectra in the case of ACP+ChOL/TiO<sub>2</sub> coating is presented in Fig 7a. Based on the information provided in Fig. 7a, it can be observed that the ACP+ChOL/TiO<sub>2</sub> coating has a compact structure with two distinct morphologies. The first morphology, labeled  $\gamma$ , belongs to the TiO<sub>2</sub> layer which forms instantaneously when the voltage difference is applied. The thickness of this layer is  $170\pm15\ \mu\text{m}$ , and the EDS spectra (Fig. 7-a2) show the presence of only Ti and O from TiO<sub>2</sub>, along with some traces of Ca and P.

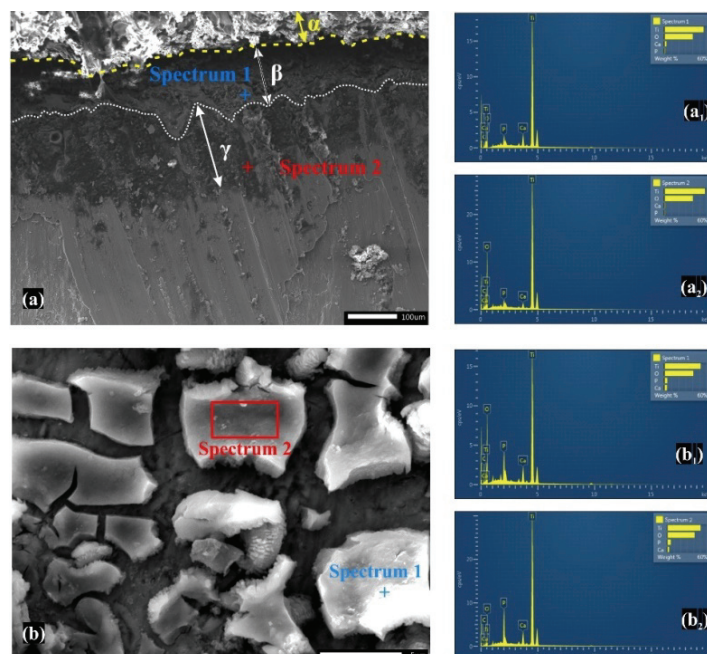


Fig. 7. Analysis of sample surfaces: a) SEM of cross-section of ACP+ChOL/TiO<sub>2</sub>, a<sub>1</sub>) EDS spectrum 1, a<sub>2</sub>) EDS spectrum 2, b) SEM of ACP+ChOL/TiO<sub>2</sub> sample after immersion in SBF for 240 h, b<sub>1</sub>) EDS spectrum 1 and b<sub>2</sub>) EDS spectrum 2.<sup>47</sup> Reprinted with permission from American Chemical Society.

The second morphology, labeled  $\beta$ , belongs to the ACP+ChOL/TiO<sub>2</sub> coating and is  $120\pm10$   $\mu\text{m}$  thick. Its deposition is a diffusion-limited process. The presence of ACP+ChOL in this layer can be inferred from the labeling, and it is confirmed by the EDS spectra. The top layer, labeled as  $\alpha$ , belongs to the epoxy resin used to protect the coating while it was cross-cut for the analysis.

The EDS measurements in Fig. 7-b1 and b2 show the presence of both Ca and P, indicating the formation of hydroxyapatite ( $\text{Ca}_{10}(\text{PO}_4)_6(\text{OH})_2$ ) on the surface of the ACP+ChOL/TiO<sub>2</sub> and ACP/TiO<sub>2</sub> samples after immersion in SBF for 240 h. The Ca/P ratio of the ACP+ChOL/TiO<sub>2</sub> sample was 1.71 for spectrum 1 and 1.62 for spectrum 2, while the Ca/P ratio of the ACP/TiO<sub>2</sub> sample was 1.63. Although the ideal Ca/P ratio for stoichiometric HAP is known to be 1.67, stable HAp phases have been found to exist over a range of Ca/P ratios between 1.3 and 1.8. The presence of C from ChOL can also be seen in both spectra in Fig. 7-b1 and b2. These quantitative EDS measurements are important for determining the elemental composition and Ca/P ratio of the synthesized films and confirming the formation of hydroxyapatite.

To summarize, the provided data describe the results of SEM and EDS analyses performed on ACP+ChOL/TiO<sub>2</sub> and ACP/TiO<sub>2</sub> coatings, both before and after immersion in SBF. The SEM images show a compact structure with two distinguishable morphologies – a TiO<sub>2</sub> layer formed instantaneously and an ACP+ChOL/TiO<sub>2</sub> coating formed *via* a diffusion-limited process.

Studies also showed that composite coatings of ACP/TiO<sub>2</sub> and ACP+ChOL/TiO<sub>2</sub> on titanium exhibit lower corrosion current density values in SBF solution compared to pure cp-Ti. The inclusion of ChOL in ACP solution improves the corrosion resistance by creating a stable, consistent coating on the titanium surface, resulting in a barrier layer that inhibits direct contact with the SBF solution. The ACP+ChOL/TiO<sub>2</sub> composite coating showed the lowest  $j_{\text{corr}}$  value ( $15.38\times10^{-9}$   $\text{A cm}^{-2}$ ), which was approximately three times lower compared to the pure cp-Ti sample. The study suggests that the improved corrosion stability of the composite coatings can be attributed to the formation of both inhomogeneous and homogeneous oxides, as well as ceramic and composite layers.<sup>47</sup>

Above the mentioned, coating was further developed. Multifunctional hybrid coating on a titanium substrate that can promote controlled inflammation and immunomodulation at the implant-tissue interface was developed. The coating was composed of nano amorphous calcium phosphate and chitosan oligosaccharide lactate, and was decorated with selenium. *In situ* anodization/anaphoretic deposition was performed in order to create the coating, and then it was investigated for its immunomodulatory and anti-inflammatory effects *in vivo*. The study has found that the ACP/ChOL/Se multifunctional hybrid composite coating on a titanium substrate has an immunomodulatory and anti-inflammatory effect,

compared to pure grade 2 titanium implants that are commonly used in medicine and dentistry.<sup>50</sup>

##### 5. CONCLUSION

A brief survey of the EPD process with a special attention on fundamental and applied aspects of the EPD process was described. The fundamental aspects were discussed with a focus on the basic principles of electrophoretic deposition and the kinetics of this process. The applied aspects of the EPD process were discussed with a focus on how practical process parameters influence the coating formation and its properties. The particular emphasis was given to the production of biocompatible HAp/Ti coatings produced by the EPD process on Ti substrate for biomedical applications. In the final section a novel process of anaphoretic deposition of HAp coatings on Ti was discussed. The advantage of novel HAp anaphoretic deposition coatings on Ti is the simultaneous oxidation of Ti substrates and the deposition of HAp coatings. As a result HAp coatings with better adhesion, biocompatibility and corrosion resistance are obtained when compared to cataphoretically produced HAp coating on Ti substrates. Novel anaphoretic deposition process of HAp coatings on Ti has excellent potential for further development through fundamental and applied aspects.

*Acknowledgement.* This work was supported by the Ministry of Education, Science and Technological Development of the Republic of Serbia (Grant No. 451-03-68/2022-14/200026).

##### ИЗВОД

##### АСПЕКТИ ПРИМЕНЕ ДВОЈНОГ ПРОЦЕСА АНАФОРЕЗЕ/АНОДИЗАЦИЈЕ СУПСТРАТА ЗА ФОРМИРАЊЕ БИОКОМПАТИБИЛНИХ КЕРАМИЧКИХ ПРЕВЛАКА

КАТАРИНА Ђ. БОЖИЋ<sup>1,2</sup>, МИРОСЛАВ М. ПАВЛОВИЋ<sup>1,2</sup>, ГАВРИЛО М. ШЕКУЛАРАЦ<sup>1</sup>, СТЕФАН В. ПАНИЋ<sup>1</sup>  
и МАРИЈАНА Р. ПАНТОВИЋ ПАВЛОВИЋ<sup>1,2</sup>

<sup>1</sup>Инситијуј за хемију, технологију и мешавине, Инситијуј ог националној значаја за Републику Србију, Центар за електрохемију, Универзитет у Београду, Београд и <sup>2</sup>Центар изузетних вредности за хемију и инжењерин животне средине, Институј за хемију, технологију и мешавине, Београд

Електрофоретско таложење (EPD) може се јавити као катафоретско таложење – превлака се таложи на катоди, и анафоретско таложење – превлака се таложи на аноди. Примарна сврха EPD је добијање компактних и уједначених органских/неорганских превлака жељене дебљине и адхезије на металне површине применом електричног поља на честице прекурсора превлаке. Приказани су основни принципи EPD за наношење превлака који се односе на основна објашњења и разматрања практичних параметара процеса. Катафоретско таложење постало је популарно јер може нанети органске превлаке на сложене структуре на које је иначе веома тешко нанети превлаку. Утврђено је да ове превлаке побољшавају карактеристике подлоге, као што су биокомпатибилност, изглед и отпорност на процесе корозије. Кључни EPD параметри су састав, pH вредност и вискозност медијума за таложење, као и зета потенцијал честица, јачина електричног поља, итд. Посебан осврт је усмерен на процес анафоретског таложења, који је релативно нов, и његовим предностима. Расправља се и о катафоретском таложењу. Про-

цесом здруженог процеса анафорезе/анодизације супстрата, површина подлоге се истовремено анодизује и модификује утрагивањем честица превлаке у анодни слој. Добијају се превлаке мешовитог састава, боље адхезије и отпорности на корозију у односу на катафоретски нанесене превлаке.

(Примљено 18. јануара, ревидирано 10. фебруара, прихваћено 8. јула 2023)

#### REFERENCES

1. G. Choi, A. H. Choi, L. A. Evans, S. Akyol, B. Ben-Nissan, *J. Am. Ceram. Soc.* **103** (2020) 5442 (<https://doi.org/10.1111/jace.17118>)
2. J. Peña, I. Izquierdo-Barba, M. A. García, M. Vallet-Regí, *J. Eur. Ceram. Soc.* **26** (2006) 3631 (<https://doi.org/10.1016/j.jeurceramsoc.2005.12.028>)
3. B. D. Hahn, D. S. Park, J. J. Choi, J. Ryu, W. H. Yoon, J. H. Choi, H. E. Kim, S. G. Kim, *Surf. Coatings Technol.* **205** (2011) 3112 (<https://doi.org/10.1016/j.surcoat.2010.11.029>)
4. I. Ullah, M. A. Siddiqui, H. Liu, S. K. Kolawole, J. Zhang, S. Zhang, L. Ren, K. Yang, *ACS Biomater. Sci. Eng.* **6** (2020) 1355 (<https://doi.org/10.1021/acsbiomaterials.9b01396>)
5. W. Yuan, J. Ji, J. Fu, J. Shen, *J. Biomed. Mater. Res., B* **85** (2008) 556 (<https://doi.org/10.1002/jbm.b.30979>)
6. N. Meyer, L. R. Rivera, T. Ellis, J. Qi, M. P. Ryan, A. R. Boccaccini, *Coatings* **8** (2018) 27 (<https://doi.org/10.3390/coatings8010027>)
7. L. Besra, M. Liu, *Prog. Mater. Sci.* **52** (2007) 1 (<https://doi.org/10.1016/j.pmatsci.2006.07.001>)
8. S. A. Batool, A. Wadood, S. W. Hussain, M. Yasir, M. A. Ur Rehman, *Surfaces* **4** (2021) 205 (<https://doi.org/10.3390/surfaces4030018>)
9. S. H. Lee, S. P. Woo, N. Kakati, D. J. Kim, Y. S. Yoon, *Energies* **11** (2018) 3122 (<https://doi.org/10.3390/en11113122>)
10. L. Kremser, D. Blaas, E. Kenndler, *Electrophoresis* **25** (2004) 2282 (<https://doi.org/10.1002/elps.200305868>)
11. A. Laska, M. Bartmański, *Inżynieria Mater.* **1** (2020) 20 (<https://doi.org/10.15199/28.2020.1.3>)
12. N. Sato, M. Kawachi, K. Noto, N. Yoshimoto, M. Yoshizawa, *Phys., C* **357–360** (2001) 1019 ([https://doi.org/10.1016/S0921-4534\(01\)00510-X](https://doi.org/10.1016/S0921-4534(01)00510-X))
13. S. Cabanas-Polo, A. R. Boccaccini, *J. Eur. Ceram. Soc.* **36** (2016) 265 (<https://doi.org/10.1016/j.jeurceramsoc.2015.05.030>)
14. A. A. Sadeghi, T. Ebadzadeh, B. Raissi, S. Ghashghaei, *Ceram. Int.* **39** (2013) 7433 (<https://doi.org/10.1016/j.ceramint.2013.02.087>)
15. B. Ouedraogo, *J. Sci. Res. Reports* **2** (2013) 190 (<https://doi.org/10.9734/jsrr/2013/2559>)
16. B. Ferrari, R. Moreno, *Mater. Lett.* **28** (1996) 353 ([https://doi.org/10.1016/0167-577X\(96\)00075-4](https://doi.org/10.1016/0167-577X(96)00075-4))
17. B. Ferrari, R. Moreno, *J. Eur. Ceram. Soc.* **30** (2010) 1069 (<https://doi.org/10.1016/j.jeurceramsoc.2009.08.022>)
18. I. Aznam, J. C. W. Mah, A. Muchtar, M. R. Somalu, M. J. Ghazali, *J. Zhejiang Univ. Sci. A* **19** (2018) 811 (<https://doi.org/10.1631/jzus.A1700604>)
19. M. Předota, M. L. Machesky, D. J. Wesolowski, *Langmuir* **32** (2016) 10189 (<https://doi.org/10.1021/acs.langmuir.6b02493>)
20. S. Kamble, S. Agrawal, S. Cherumukkil, V. Sharma, R. V. Jasra, P. Munshi, *ChemistrySelect* **7** (2022) e202103084 (<https://doi.org/10.1002/slct.202103084>)

21. A. A. Abdeltawab, M. A. Shoeib, S. G. Mohamed, *Surf. Coatings Technol.* **206** (2011) 43 (<https://doi.org/10.1016/j.surfcoat.2011.06.034>)
22. I. Zhitomirsky, *J. Eur. Ceram. Soc.* **18** (1998) 849 ([https://doi.org/10.1016/S0955-2219\(97\)00213-6](https://doi.org/10.1016/S0955-2219(97)00213-6))
23. R. N. Basu, C. A. Randall, M. J. Mayo, *J. Am. Ceram. Soc.* **84** (2001) 33 (<https://doi.org/10.1111/j.1151-2916.2001.tb00604.x>)
24. A. Rousta, D. Dorranian, *Trans. Inst. Met. Finish.* **99** (2021) 172 (<https://doi.org/10.1080/00202967.2021.1914382>)
25. P. Zhao, L. J. LeSargent, J. Farnese, J. Z. Wen, C. L. Ren, *Electrochim. Commun.* **108** (2019) 106558 (<https://doi.org/10.1016/j.elecom.2019.106558>)
26. A. M. A. Abudalazez, S. R. Kasim, A. B. Ariffin, Z. A. Ahmad, *Int. J. Eng. Res. Africa* **8** (2012) 47 (<https://doi.org/10.4028/www.scientific.net/JERA.8.47>)
27. H. C. Hamaker, *Trans. Faraday Soc.* **35** (1940) 279 (<https://doi.org/10.1039/TF9403500279>)
28. R. Moreno, B. Ferrari, in: *Electrophor. Depos. Nanomater.*, J.H. Dickerson, A.R. Boccaccini, Eds., Springer. New York, 2012, p. 73 ([https://doi.org/10.1007/978-1-4419-9730-2\\_2](https://doi.org/10.1007/978-1-4419-9730-2_2))
29. A. I. Avgustinik, V. S. Vigdergauz, G. I. Zhuravlev, *J. Appl. Chem. USSR (Engl. Transl.)* **35** (1962) 2090 ([https://jglobal.jst.go.jp/en/detail?JGLOBAL\\_ID=201602000824298251](https://jglobal.jst.go.jp/en/detail?JGLOBAL_ID=201602000824298251))
30. P. M. Biesheuvel, H. Verweij, *J. Am. Ceram. Soc.* **82** (1999) 1451 (<https://doi.org/10.1111/j.1151-2916.1999.tb01939.x>)
31. P. Sarkar, P. S. Nicholson, *J. Am. Ceram. Soc.* **79** (1996) 1987 (<https://doi.org/10.1111/j.1151-2916.1996.tb08929.x>)
32. G. J. Kynch, *Trans. Faraday Soc.* **48** (1952) 166 (<https://doi.org/10.1039/tf9524800166>)
33. G. Anné, K. Vanmeensel, J. Vleugels, O. Van Der Biest, *J. Am. Ceram. Soc.* **88** (2005) 2036 (<https://doi.org/10.1111/j.1551-2916.2005.00387.x>)
34. V. Ozhukil Kollath, Q. Chen, R. Closset, J. Luyten, K. Traina, S. Mullens, A. R. Boccaccini, R. Cloots, *J. Eur. Ceram. Soc.* **33** (2013) 2715 (<https://doi.org/10.1016/j.jeurceramsoc.2013.04.030>)
35. A. Braem, K. De Brucker, N. Delattin, M. S. Killian, M. B. J. Roeffaers, T. Yoshioka, S. Hayakawa, P. Schmuki, B. P. A. Cammue, S. Virtanen, K. Thevissen, B. Neirinck, *ACS Appl. Mater. Interfaces* **9** (2017) 8533 (<https://doi.org/10.1021/acsami.6b16433>)
36. E. J. W. Verwey, J. T. G. Overbeek, *Theory of the Stability of Lyophobic Colloids: The Interaction of Sol Particles Having an Electric Double Layer*, Elsevier, New York, 1948 ([http://www.damtp.cam.ac.uk/user/gold/pdfs/teaching/BPFD/Chap2\\_10\\_VerweyOverbeek.pdf](http://www.damtp.cam.ac.uk/user/gold/pdfs/teaching/BPFD/Chap2_10_VerweyOverbeek.pdf))
37. B. Derjaguin, L. Landau, *Prog. Surf. Sci.* **43** (1993) 30 ([https://doi.org/10.1016/0079-6816\(93\)90013-L](https://doi.org/10.1016/0079-6816(93)90013-L))
38. J. H. Adair, E. Suvaci, J. Sindel, in: *Encycl. Mater. Sci. Technol.*, K.H. Jürgen Buschow, R.W. Cahn, M.C. Flemings, B. Ilsehner, E.J. Kramer, S. Mahajan, P. Veyssiére, Eds., Elsevier, Amsterdam, 2001, p. 8996 (<https://doi.org/10.1111/j.2042-7158.1951.tb13130.x>)
39. S. Eraković, A. Janković, D. Veljović, E. Palcevskis, M. Mitić, T. Stevanović, D. Janačković, V. Miskovic-Stankovic, *J. Phys. Chem., B* **117** (2013) 1633 (<https://doi.org/10.1021/jp305252a>)
40. S. Erakovic, A. Jankovic, G. C. P. Tsui, C. Y. Tang, V. Miskovic-Stankovic, T. Stevanovic, *Int. J. Mol. Sci.* **15** (2014) 12294 (<https://doi.org/10.3390/ijms150712294>)

41. J. Li, P. Zhou, S. Attarilar, H. Shi, *Coatings* **11** (2021) 647  
(<https://doi.org/10.3390/coatings11060647>)
42. C. Yao, T. J. Webster, *J. Nanosci. Nanotechnol.* **6** (2006) 2682  
(<https://doi.org/10.1166/jnn.2006.447>)
43. Y. Parcharoen, P. Termsuksawad, S. Sirivisoot, *J. Nanomater.* **2016** (2016) 9143969  
(<https://doi.org/10.1155/2016/9143969>)
44. M. R. Pantović Pavlović, M. M. Pavlović, S. Eraković, T. Barudžija, J. S. Stevanović, N. Ignjatović, V. V. Panić, *J. Serb. Chem. Soc.* **84** (2019) 1305  
(<https://doi.org/10.2298/JSC190730105P>)
45. M. R. Pantović Pavlović, S. G. Eraković, M. M. Pavlović, J. S. Stevanović, V. V. Panić, N. L. Ignjatović, *Surf. Coatings Technol.* **358** (2019) 688  
(<https://doi.org/10.1016/j.surfcoat.2018.12.003>)
46. M. R. Pantović Pavlović, M. M. Pavlović, S. Eraković, J. S. Stevanović, V. V. Panić, N. Ignjatović, *Mater. Lett.* **261** (2020) 127121 (<https://doi.org/10.1016/j.matlet.2019.127121>)
47. M. R. Pantović Pavlović, B. P. Stanojević, M. M. Pavlović, M. D. Mihailović, J. S. Stevanović, V. V. Panić, N. L. Ignjatović, *ACS Biomater. Sci. Eng.* **7** (2021) 3088  
(<https://doi.org/10.1021/acsbiomaterials.1c00035>)
48. M. R. Pantović Pavlović, M. M. Pavlović, J. N. Kovačina, B. P. Stanojević, J. S. Stevanović, V. V. Panić, N. L. Ignjatović, *J. Ser. Chem. Soc.* **86** (2021) 555  
(<https://doi.org/10.2298/JSC210211024P>)
49. M. R. Pantović Pavlović, *PhD Thesis*, University of Belgrade, 2021 (in Serbian)  
(<https://147.91.1.130/handle/123456789/4424>)
50. M. R. Pantović Pavlović, N. L. Ignjatović, V. V. Panić, I. I. Mirkov, J. B. Kulaš, A. L. Malešević, M. M. Pavlović, *J. Funct. Biomater.* **14** (2023) 227  
(<https://doi.org/10.3390/jfb14040227>).



## Synthesis and antiproliferative activity of (*5R*)-cleistenolide and analogues

SÁNDOR FARKAS<sup>1</sup>, GORAN BENEDEKOVIĆ<sup>1</sup>, SLAĐANA M. STANISAVLJEVIĆ<sup>1</sup>,  
BOJANA M. SREĆO ZELENOVIĆ<sup>1</sup>, MIRJANA POPSAVIN<sup>1</sup>, VELIMIR POPSAVIN<sup>1,2\*</sup>  
and DIMITAR S. JAKIMOV<sup>3</sup>

<sup>1</sup>University of Novi Sad, Faculty of Sciences, Department of Chemistry, Biochemistry and Environmental Protection, Trg Dositeja Obradovića 3, 21000 Novi Sad, Serbia, <sup>2</sup>Serbian Academy of Sciences and Arts, Kneza Mihaila 35, 11000 Belgrade, Serbia and <sup>3</sup>University of Novi Sad, Faculty of Medicine, Oncology Institute of Vojvodina, Put dr Goldmana 4, 21204 Sremska Kamenica, Serbia

(Received 26 January, revised 25 March, accepted 9 April 2023)

*Abstract:* (*5R*)-Cleistenolide and a few related analogues have been synthesized starting from d-glucose. The key steps of the synthesis included a Z-selective Wittig olefination and an intramolecular Mitsunobu reaction with an inversion of configuration at the C-5 position. *In vitro* antiproliferative activity of synthesized compounds was tested on a panel of eight human tumour cells and against a single normal cell line (MRC-5). The majority of tested compounds showed strong antiproliferative effects on certain human tumour cells and all of them showed negligible toxicity to normal foetal lung fibroblasts (MRC-5). The most active compound obtained in this work is lactone **5**, which in MDA-MB 231 cell culture showed the same activity as doxorubicin ( $IC_{50}$  0.09  $\mu$ M). Strong antiproliferative activities of analogues **2**, **5** and **6** were recorded in the K562 cell line ( $IC_{50}$  0.21, 0.34 and 0.33  $\mu$ M, respectively), in which they showed very similar activities to doxorubicin ( $IC_{50}$  0.25  $\mu$ M). A performed SAR study revealed that a change in the stereochemistry at the C-5 position may increase the activity of resulting stereoisomers.

*Keywords:* antitumour agents; sugar  $\delta$ -lactones; (*5R*)-cleistenolide; Z-selective Wittig olefination; intramolecular Mitsunobu reaction; SAR analysis.

### INTRODUCTION

(–)-Cleistenolide (**1**, Fig. 1) is a naturally occurring  $\alpha,\beta$ -unsaturated  $\delta$ -lactone isolated from *Cleistochlamis kirkii* Oliver, a plant species that grows in southeast Africa.<sup>1</sup> The extract of this plant has been used in Tanzania and Mozambique in traditional medicine for the treatment of infected wounds, rheumat-

\*Corresponding author. E-mail: velimir.popasavin@dh.uns.ac.rs  
<https://doi.org/10.2298/JSC230126018F>

ism and tuberculosis.<sup>2</sup> Recently, Pereira *et al.*<sup>3</sup> isolated from the ethanolic extract of *C. kirkii* a new natural product (−)-cleistenolide, and eight other compounds of different structures: chamanetin, isochamanetin, dichamanetin, echunuline, *cis*-solamine, acetylmelodorinol, polycarpol and benzophenone. Noteworthy are recent findings that isolated fractions, dominated by pyranone (−)-cleistenolide, showed antibacterial activity against *Bacillus anthracis* and *Staphylococcus aureus* as well as antifungal activity against *Candida albicans*.<sup>1,2,4</sup> We have also confirmed that (−)-cleistenolide and some of its analogues demonstrated antimicrobial activity against a panel of nine microbial strains.<sup>5</sup> Finally, we were among the first to discover that (−)-cleistenolide and some new analogues of it may inhibit the growth of certain tumour cell lines.<sup>6–8</sup> After our first report dealing with this issue,<sup>6</sup> only one paper has been published on the cytotoxicity of natural product **1** towards a single malignant cell line.<sup>9</sup> Herein we describe a new total synthesis of the (5*R*)-cleistenolide (**2**), which is a C-5 epimer of natural product **1**. Our new synthesis of compound **2** is based on the chiral pool strategy, which involves the chirality transfer from D-glucose, which ensures obtaining the target in an optically pure form. The sequence contains only one step in which three benzyl-protecting groups are introduced, while their deprotection was carried out simultaneously with the introduction of acyl groups. Only one synthesis of **2** has been achieved so far;<sup>10</sup> however, no studies addressing its biological activity have been published yet. To elucidate the effects of stereochemistry at the C-5 position on the activity of lactones **1** and **2**, a study of their *in vitro* cytotoxicity on a panel of malignant cell lines was performed.

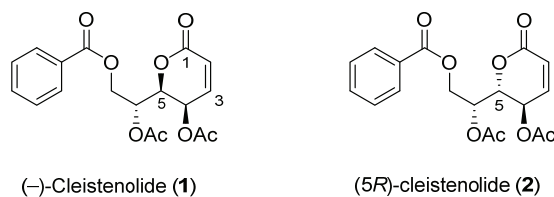


Fig. 1. Structures of (−)-cleistenolide (**1**) and (5*R*)-cleistenolide (**2**).

## EXPERIMENTAL

### General procedures

Melting points were determined on a hot stage microscope Nagema PHMK 05 apparatus, and were not corrected. Optical rotations were measured on a Rudolph Research Analytical automatic polarimeter, Autopol IV. IR spectra were recorded on a FTIR Nexus 670 (Thermo-Nicolet) spectrophotometer. <sup>1</sup>H- and <sup>13</sup>C-NMR spectra were recorded on a Bruker AC 250 E (at 250 and 62.5 MHz, respectively) or a Bruker Avance III spectrometer (at 400 and 100 MHz, respectively) using TMS as the internal standard. Chemical shifts were expressed in ppm ( $\delta$  values) and coupling constants ( $J$ ) in Hz. High-resolution mass spectra were taken on a Micromass LCT KA111 spectrometer or LTQ Orbitrap XL (Thermo Fisher Scientific Inc.) mass spectrometer. TLC was performed on DC Alufolien Kieselgel 60 F254 (E. Merck). Flash

column chromatography was performed using Kieselgel 60 (0.040–0.063, E. Merck). All organic extracts were dried with anhydrous Na<sub>2</sub>SO<sub>4</sub>. Organic solutions were concentrated in a rotary evaporator under reduced pressure at a bath temperature below 35 °C. The purity of the synthesized compounds was determined by HRMS or elemental microanalysis and was greater than 95 % (errors were less than 5 ppm).

#### Synthetic procedures

*Methyl (2Z)-4,6,7-tri-O-benzyl-2,3-dideoxy-D-arabino-hept-2-enoate (4).* To a cooled (0 °C) and stirred solution of compound **3** in anhydrous DMF (75 mL) was added NaH (1.66 g, 69.16 mmol) and after the vigorous evolution of H<sub>2</sub> had stopped, BnBr (4.8 mL, 40.3 mmol) was slowly added over 10 min. After 0.5 h, the cooling vessel was removed and the stirring was continued for an additional 2 h at room temperature. Anhydrous MeOH (12 mL) was slowly added to the reaction solution. And after the intense release of hydrogen had stopped, the mixture was evaporated. The resulting residue was dissolved in small volume of CH<sub>2</sub>Cl<sub>2</sub>/H<sub>2</sub>O, poured into H<sub>2</sub>O (250 mL) and extracted with CH<sub>2</sub>Cl<sub>2</sub> (3×40 mL). The organic phases were combined, washed with 10 % NaCl (3×150 mL), then dried and evaporated. The remaining crude compound **3a** was dissolved in 50 % aq. TFA (60 mL) and vigorously stirred at room temperature for 18 h. The reaction solution was evaporated by co-distillation with toluene to remove the acid and water, and the resulting residue was dried under high vacuum overnight. To a stirred solution of remaining crude lactol **3b** in anhydrous MeOH (500 mL) was added NaIO<sub>4</sub> (3.68 g, 17.29 mmol) and the stirring at room temperature was continued for 2 h, whereby crude intermediate **3c** was obtained. The reaction solution was then cooled to 0 °C and methyl 2-(triphenylphosphoranylidene)acetate (7.50 g, 22.46 mmol) was added. After 1 h, the cooling vessel was removed and the reaction was continued at room temperature for another 3 h. A new portion of reagent (4.05 g, 12.12 mmol) was added and stirring was continued for additional 20 h. The reaction solution was evaporated and the residue was dissolved in CH<sub>2</sub>Cl<sub>2</sub> and evaporated with silica gel. The residue was purified twice by flash chromatography (1:1 light petroleum/Et<sub>2</sub>O) to give pure **4** (4.10 g, 75 % from four steps) as a colourless syrup,  $[\alpha]_D = -19.1$  (*c* 1.0, CHCl<sub>3</sub>);  $R_f = 0.32$  (3:2 light petroleum/Et<sub>2</sub>O). Spectral data (IR, <sup>1</sup>H-NMR, <sup>13</sup>C-NMR and MS) were in good agreement with our previously reported values.<sup>6</sup>

*4,6,7-Tri-O-benzyl-2,3-dideoxy-D-arabino-hept-2-eno-1,5-lactone (5).* To a solution of compound **4** (2.05 g, 4.19 mmol) in CH<sub>2</sub>Cl<sub>2</sub> (85 mL) was added TsOH×H<sub>2</sub>O (0.021 g, 0.105 mmol). The mixture was stirred at room temperature for 96 h, then evaporated and the residue was purified by flash chromatography (1:1 light petroleum/Et<sub>2</sub>O). Pure product **5** (1.782 g, 96 %) was obtained as a colourless syrup. Crystallization from a mixture of light petroleum/Et<sub>2</sub>O gave analytical sample **5** as a white powder, mp 64 °C,  $[\alpha]_D = -194.6$  (*c* 0.5, CHCl<sub>3</sub>),  $R_f = 0.30$  (1:1 light petroleum/Et<sub>2</sub>O). Spectral data (IR, <sup>1</sup>H-NMR, <sup>13</sup>C-NMR and MS) were in good agreement with the values we reported previously.<sup>6</sup>

*4,6,7-Tri-O-benzyl-2,3-dideoxy-D-lyxo-hept-2-eno-1,5-lactone (6).* To a stirred mixture of lactone **5** (0.200 g, 0.45 mmol) and LiBr (0.391 g, 4.5 mmol) in CH<sub>3</sub>CN (5 mL) was added anhydrous Et<sub>3</sub>N (0.19 mL, 1.35 mmol). The mixture was stirred at room temperature for 24 h, then acidified with glacial AcOH (2.0 mL) while stirring at room temperature for additional 3 min. The reaction mixture was poured into H<sub>2</sub>O (80 mL) and extracted with EtOAc (3×20 mL). The organic solutions were combined, dried and evaporated, and the residue was dried under a vacuum for 4 h. To the stirred solution of the residue in anhydrous EtOAc (25 mL) was added Ph<sub>3</sub>P (0.295 g, 1.12 mmol) and 40 % DEAD (0.47 mL, 1.08 mmol) over 3 min. The reaction solution was stirred at room temperature for 20 h, then evaporated, and the residue was purified on two columns of flash silica (first with 1:1 light petroleum/Et<sub>2</sub>O, then with

99:1 CH<sub>2</sub>Cl<sub>2</sub>/Me<sub>2</sub>CO). Pure **6** (0.125 g, 62 %) was obtained as a glassy solid,  $[\alpha]_D = -86.4$  (*c* 0.5, CHCl<sub>3</sub>),  $R_f = 0.33$  (1:1 Et<sub>2</sub>O/light petroleum).

**(5R)-Cleistenolide (2).** To a stirred solution of compound **6** (0.100 g, 0.22 mmol), Bz<sub>2</sub>O (0.124 g, 0.55 mmol) and BzOH (0.134 g, 1.1 mmol) in anhydrous CH<sub>2</sub>Cl<sub>2</sub> (15 mL) was added anhydrous FeCl<sub>3</sub> (0.007 g, 0.04 mmol). After stirring at room temperature for 2 h, FeCl<sub>3</sub> (0.004 g, 0.02 mmol) and AcBr (0.16 mL, 2.2 mmol) were successively added and the reaction at room temperature continued for an additional 20 h. The reaction solution was diluted with CH<sub>2</sub>Cl<sub>2</sub> (10 mL), poured into 10 % NaHCO<sub>3</sub> (60 mL) and extracted with CH<sub>2</sub>Cl<sub>2</sub> (3×15 mL). The combined organic phases were washed with 10 % NaCl (30 mL), dried and evaporated. The residue was purified by flash chromatography (2:1 Et<sub>2</sub>O/light petroleum) to give pure product **2** (0.061 g, 76 %) as a colourless solid, which after recrystallization from a mixture of CH<sub>2</sub>Cl<sub>2</sub>/hexane, gave colourless needles, mp 152 °C (phase transition at 140–143 °C), lit.<sup>10</sup> mp 140 °C (the sample not recrystallized),  $[\alpha]_D = -30.0$  (*c* 0.5, CHCl<sub>3</sub>), lit.<sup>10</sup>  $[\alpha]_D = -22.0$  (*c* 1.0, CHCl<sub>3</sub>),  $R_f = 0.33$  (2:1 Et<sub>2</sub>O/light petroleum).

Analytical and spectral data of the compounds are given in the Supplementary material to this paper.

#### Antiproliferative activity

**Tested cells.** Eight human cancer cell lines were used to evaluate *in vitro* antiproliferative activity of tested compounds: myelogenous leukaemia, K562 (ATCC CCL-243), promyelocytic leukaemia, HL-60 (ATCC CCL-240), T cell leukaemia, Jurkat (ATCC CCL-1435), Burkitt's lymphoma, Raji (ATCC CCL-86), ER<sup>+</sup> breast adenocarcinoma, MCF-7 (ATCC HTB-22), ER<sup>-</sup> breast adenocarcinoma, MDA-MB 231 (ATCC HTB-26), cervix carcinoma, HeLa (ATCC CCL2), and epithelial lung carcinoma, A549 (ATCC HTB-38). The toxicity of each compound was also recorded in the culture of normal foetal lung fibroblasts, MRC-5 (ATCC CCL-185).

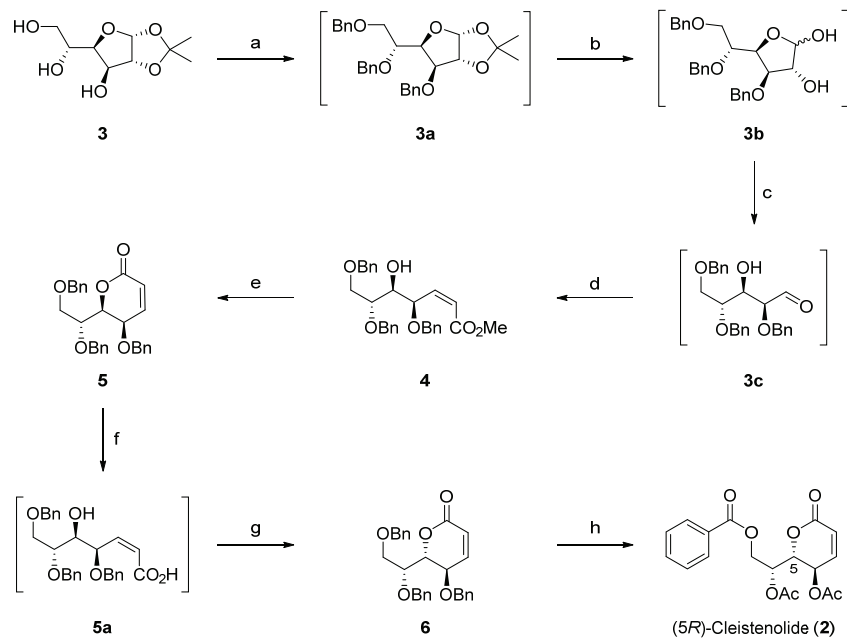
**MTT test.** After cells were exposed to the test compounds for 72 h, antiproliferative activities were assessed using the standard MTT assay.<sup>11</sup> Briefly, cells were harvested, counted using trypan blue and plated into 96-well microtiter plates (Costar) at the optimal seeding density of  $5 \times 10^3$  cells per well to assure a logarithmic growth rate throughout the assay period. Viable cells were placed in a volume of 90 µL per well, and preincubated in complete medium at 37 °C for 24 h to allow cell stabilization prior to the addition of test substances. The substances, at 10-fold the required final concentration, were added (10 µL well<sup>-1</sup>) to each well, except for the control ones, and the microplates were incubated for 72 h. The wells containing cells without tested substances were used as controls. MTT solution (10 µL) was added to each well 3 h before the end of incubation period. MTT was dissolved in medium at 5 mg mL<sup>-1</sup> and filtered to sterilize and remove the small amount of insoluble residue present in some batches of MTT. Acidified 2-propanol (100 µL of 0.04 M HCl in 2-propanol) was added to each well and mixed thoroughly to dissolve the dark blue crystals of formazan. After a few minutes at room temperature, the plates were read on a spectrophotometer plate reader (Multiscan MCC340, Labsystems) at 540 and 690 nm. The wells without cells containing complete medium and MTT acted as blanks.

## RESULTS AND DISCUSSION

#### Chemistry

The eight-step synthesis of (5*R*)-cleistenolide (**2**) was presented in Scheme 1. The synthesis commenced from a commercially available D-glucose derivative **3**. The first four steps of the synthesis, the preparation of enoate **4**, involve optimiz-

ation of the corresponding synthetic sequence that we recently published.<sup>6</sup> In contrast to the previous procedure, intermediates **3a**, **3b** and **3c** were not purified or characterized but were used in the following synthetic steps in their crude form. This provided the key intermediate **4** with an overall yield of 75 % (from four steps). Closure of the lactone ring was achieved as previously reported (TsOH, CH<sub>2</sub>Cl<sub>2</sub>, rt),<sup>6</sup> giving the desired  $\delta$ -lactone **5** in 96 % yield. For the configurational inversion at the C-5 position of **5**, a modified two-step procedure was applied, which involves the sequential hydrolysis of the lactone ring under the basic conditions (Et<sub>3</sub>N, LiBr, 98 % aq MeCN, rt), and intramolecular Mitsunobu reaction (Ph<sub>3</sub>P, DEAD, anhydrous EtOAc, rt).<sup>12</sup> The key intermediate **6** was thus obtained in a yield of 62 % (from **5**). The final step in the synthesis involved replacing the benzyl protecting groups with ester functions. It was achieved by successive treatment of **6** with Bz<sub>2</sub>O, BzOH and AcBr in the presence of catalytic amounts of FeCl<sub>3</sub>. These transformations gave (5*R*)-cleistenolide (**2**) in 76 % yield.



Scheme 1. a) BnBr, NaH, DMF, 0 °C, 0.5 h, rt, 2 h; b) 50 % aq. TFA, rt, 18 h; c) NaIO<sub>4</sub>, MeOH, rt, 2 h; d) Ph<sub>3</sub>P=CHCO<sub>2</sub>Me, MeOH, 0 °C, 1 h, rt, 3 h, 75 % from **3**; e) TsOH, CH<sub>2</sub>Cl<sub>2</sub>, rt, 96 h, 96 %; f) Et<sub>3</sub>N, LiBr, 98 % aq MeCN, rt, 24 h; g) Ph<sub>3</sub>P, DEAD, anhydrous EtOAc, rt, 20 h; 62 %; h) Bz<sub>2</sub>O, BzOH, FeCl<sub>3</sub>, AcBr, anhydrous CH<sub>2</sub>Cl<sub>2</sub>, rt, 22 h, 76 %.

This new synthesis of (5*R*)-cleistenolide (**2**) was achieved in eight synthetic steps and in a yield of 34 %. The first synthesis<sup>10</sup> of **2** was achieved in seven steps and in a total yield of 25 %.

*In vitro antiproliferative activities and SAR analysis*

The biological activities of synthesized compounds **1**, **2**, **5** and **6** were evaluated by an *in vitro* cytotoxicity test against a panel of eight human malignant cell lines, including human myelogenous leukaemia (K562), human promyelocytic leukaemia (HL-60), T cell leukaemia (Jurkat), Burkitt's lymphoma (Raji), ER<sup>+</sup> breast adenocarcinoma (MCF-7), ER<sup>-</sup> breast adenocarcinoma (MDA-MB 231), cervix carcinoma (HeLa) and lung adenocarcinoma epithelial cells (A549) and against single normal cell line, foetal lung fibroblasts (MRC-5). Cell growth inhibition was evaluated using the standard MTT colorimetric assay after exposure of cells to the test compounds for 72 h.<sup>11</sup> (−)-Cleistenolide (**1**), and the commercial antitumour agent doxorubicin (DOX) were used as positive controls. The results are shown in Table I. According to the resulting *IC*<sub>50</sub> values, all of cell lines tested were sensitive to the natural product **1**, as well as to the synthesized analogues **2**, **5** and **6**.

TABLE I. *In vitro* cytotoxicity (*IC*<sub>50</sub> / μM)<sup>a\*</sup> of (−)-cleistenolide (**1**), (5*R*)-cleistenolide (**2**), DOX and analogues (**5** and **6**)

Compound	Cell line								
	K562	HL-60	Jurkat	Raji	MCF-7	MDA-MB 231	HeLa	A549	MRC-5
<b>1<sup>a</sup></b>	7.65	1.21	14.22	36.94	26.07	2.25	7.32	16.34	>100
<b>2</b>	0.21	7.31	19.41	2.47	21.28	7.66	6.45	9.38	>100
<b>5</b>	0.34	12.55	9.24	29.66	1.39	0.09	3.58	1.85	64.39
<b>6</b>	0.33	8.27	17.03	1.05	20.06	7.04	5.90	17.21	>100
DOX	0.25	0.92	0.03	2.98	0.20	0.09	0.07	4.91	0.10

<sup>a</sup>Data taken from reference 6

All analogues (**2**, **5** and **6**) showed strong antiproliferative effects against K562 cells (*IC*<sub>50</sub> values in the range 0.21–0.33 μM). In contrast, lead **1** showed significantly lower activity against this cell line (*IC*<sub>50</sub> 7.65 μM). The most active compound in the K562 cell culture was target **2**, which showed more than 36 times stronger activity than lead **1**. At the same time, analogue **2** showed almost the same activity as doxorubicin against the mentioned malignant cell line. The most potent compounds against Raji cells are analogues **2** and **6**. Compound **2** was about fifteen times more active than lead **1** while showing similar activity to doxorubicin. Analogue **6** was the most active molecule against Raji cells. This compound showed even stronger potency than lead **1** (over 35 times), and about 3 times over doxorubicin. The most active compound in the MCF-7 cell culture is lactone **5**, which showed over 18 time greater potency than lead **1**. Also, lactone **5** is the most active compound obtained in this work, given that it showed an

\* *IC*<sub>50</sub> is the concentration of compound required to inhibit the cell growth by 50 % compared to an untreated control. Values are means of three independent experiments. Coefficients of variation were less than 10 %.

$IC_{50}$  0.09  $\mu\text{M}$  in the MDA-MB 231 cell culture. Compared to lead **1**, lactone **5** is 25 times more potent, and shows the same activity as the commercial drug doxorubicin against the mentioned malignant cell line. In HeLa and A549 cells, lactone **5** is consistently the most potent antiproliferative agent, being twice (HeLa) and 9 times (A549) more active than lead **1**. In the A549 cell culture, compound **5** showed, again, almost three times stronger antiproliferative activity than doxorubicin.

As can be further seen from Table I, all synthesized analogues (**2**, **5** and **6**), as well as lead compound **1**, were almost completely inactive toward normal MRC-5 cells. Compound **5** alone showed weak growth inhibition of this cell line ( $IC_{50}$  64.39  $\mu\text{M}$ ), with selectivity indices (SI)<sup>13</sup> as follows: 189.38 (K562 cells), 5.13 (HL-60), 6.97 (Jurkat), 2.17 (Raji), 46.32 (MCF-7), 715.44 (MDA-MB 231), 17.99 (HeLa) and 34.8 (A549). On the contrary, the commercial antitumour agent DOX exhibited a potent cytotoxicity against this cell line. This indicates the selectivity of synthesized compounds toward tumour cells, which is a desirable feature and represents a good basis for the further development of potent and selective antitumour agents.

In order to correlate the stereochemistry of synthesized compounds with their cytotoxic activities, we wanted to explore the effects of changing absolute stereochemistry at C-5 to antiproliferative activity of resulting analogues. The natural product **1**, and lactone **5** have been used as controls in this SAR analysis. The data in Table I reveal that target  $\delta$ -lactone **2**, which has (5*R*)-stereochemistry, represents a more potent cytotoxic agent compared to the natural product **1** of (5*S*)-stereochemistry, given that analogue **2** shows stronger activity against 5 of 8 tested malignant cells. Unfortunately, changing the absolute stereochemistry at the C-5 position (*5S*  $\rightarrow$  *5R*) in lactones of type **5** and **6** is not as effective, as an increase in activity was detected in only 3 out of 8 cancer cell lines tested (for more details see Supplementary material). However, these results still indicate that a change in stereochemistry at C-5 in cleistenolide-type lactones may increase the antiproliferative activity of the analogues.

#### CONCLUSION

In this work, a new total synthesis of (5*R*)-cleistenolide (**2**) was achieved in eight synthetic steps and in a total yield of 34 %. In terms of the economy of atoms and synthetic steps, this new synthesis of **2** utilizes 3 of 4 chiral centres of D-glucose. Although it was carried out in a sequence that is one step longer than the synthesis described in the literature,<sup>10</sup> our synthesis is more efficient, at least in terms of overall yield. The target compound **2** and the corresponding intermediates **5** and **6** were tested for their *in vitro* antiproliferative activity against a panel of eight human malignant cell lines as well as one normal cell line. All tested compounds had different antiproliferative effects on human malignant cell

lines but had no significant toxicity on normal foetal lung fibroblasts (MRC-5). The most active compound obtained in this work is lactone **5**, given that it showed an  $IC_{50}$  value of 0.09  $\mu\text{M}$  in the MDA-MB 231 cell culture. Compared to lead **1**, lactone **5** is 25 times more potent and shows the same activity as the commercial drug doxorubicin against the mentioned malignant cell line. The obtained results indicate that changing the stereochemistry at the C-5 position may improve antiproliferative activity toward some of evaluated cell lines. The obtained biological results further indicated that the change of stereochemistry at C-5 (from *5S* in natural product **1** to *5R* in analogue **2**) increases the cytotoxicity of the analogue toward majority of tested malignant cells.

#### SUPPLEMENTARY MATERIAL

Additional data and information are available electronically at the pages of journal website: <https://www.shd-pub.org.rs/index.php/JSCS/article/view/12250>, or from the corresponding author on request.

*Acknowledgements.* The authors gratefully acknowledge the financial support of the Ministry of Science, Technological Development and Innovation of the Republic of Serbia (Grant No. 451-03-47/2023-01/200125). This work has also received funding from the Serbian Academy of Sciences and Arts (Grant No. F-130).

#### ИЗВОД СИНТЕЗА И АНТИПРОЛИФЕРАТИВНА АКТИВНОСТ (5R)-КЛЕИСТЕНОЛИДА И АНАЛОГА

ШАНДОР ФАРКАШ<sup>1</sup>, ГОРАН БЕНДЕКОВИЋ, СЛАЂАНА М. СТАНИСАВЉЕВИЋ<sup>1</sup>, БОЈАНА М. СРЕЋО  
ЗЕЛЕНОВИЋ<sup>1</sup>, МИРЈАНА ПОПСАВИН<sup>1</sup>, ВЕЛИМИР ПОПСАВИН<sup>1,2</sup>, и ДИМИТАР С. ЈАКИМОВ<sup>3</sup>

<sup>1</sup>Универзитет у Новом Саду, Природно-математички факултет, Департман за хемију, биохемију и  
заштиту животне средине, Трг Доситеја Обрадовића 3, 21000 Нови Сад, <sup>2</sup>Српска академија наука и  
уметности, Кнеза Михаила 35, 11000 Београд и <sup>3</sup>Универзитет у Новом Саду, Медицински факултет,  
Институт за онкологију Војводине, Пут пр Голдмана 4, 21204 Сремска Каменица

(5*R*)-Клеистенолид и неколико сродних аналога су синтетизовани полазећи од d-глукозе. Кључни кораци синтезе укључивали су Z-селективну Витигову (Wittig) олефинацију и интрамолекулску Мицунобуову (Mitsunobu) реакцију уз инверзију конфигурације на C-5. *In vitro* антипролиферативна активност синтетизованих једињења је тестирана на панелу од осам хуманих туморских ћелија и према једној нормалној ћелијској линији (MRC-5). Већина тестиралих једињења показала је снажне антипролиферативне ефекте према одређеним хуманим туморским ћелијама, а сва су показала занемарљиву токсичност према нормалним ћелијама феталних фибробласта плућа (MRC-5). Најактивније једињење добијено у овом раду је лактон **5**, који је у ћелијској култури MDA-MB 231 показао исту активност као доксорубицин ( $IC_{50}$  0,09  $\mu\text{M}$ ). Јаке антипролиферативне активности аналога **2**, **5** и **6** су забележене у ћелијској култури K562 ( $IC_{50}$  0,21, 0,34 и 0,33  $\mu\text{M}$ , редом), показујући при томе веома сличне активности доксорубицину ( $IC_{50}$  0,25  $\mu\text{M}$ ). Прелиминарна CAP анализа указује да промена стереохемије на C-5 може повећати антипролиферативну активност резултујућих стереоизомера.

(Примљено 26. јануара, ревидирano 25. марта, прихваћено 9. априла 2023)

## REFERENCES

1. S. Samwel, S. J. M. Mdachi, M. H. H. Nkunya, B. N. Irungu, M. J. Moshi, B. Moulton, B. Luisi, *Nat. Prod. Commun.* **2** (2007) 737 (<https://doi.org/10.1177/1934578X0700200706>)
2. M. H. H. Nkunya, *Pure Appl. Chem.* **77** (2005) 1943 (<https://doi.org/10.1351/pac200577111943>)
3. F. Pereira, A. M. Madureira, S. Sancha, S. Mulhovo, X. Luo, A. Duarte, M. J. U. Ferreira, *J. Ethnopharm.* **178** (2016) 180 (<https://doi.org/10.1016/j.jep.2015.12.009>)
4. R. Verzár, G. Petri, *J. Ethnopharmacol.* **19** (1987) 67 ([https://doi.org/10.1016/0378-8741\(87\)90137-1](https://doi.org/10.1016/0378-8741(87)90137-1))
5. G. Benedeković, M. Popsavin, N. S. Radulović, Z. Stojanović-Radić, S. Farkas, J. Francuz, V. Popsavin, *Bioorg. Chem.* **106** (2021) 104491 (<https://doi.org/10.1016/j.bioorg.2020.104491>)
6. G. Benedeković, I. Kovačević, M. Popsavin, J. Francuz, V. Kojić, G. Bogdanović, V. Popsavin, *Bioorg. Med. Chem. Lett.* **26** (2016) 3318 (<https://doi.org/10.1016/j.bmcl.2016.05.044>)
7. G. Benedeković, M. Popsavin, I. Kovačević, V. Kojić, M. Rodić, V. Popsavin, *Eur. J. Med. Chem.* **202** (2020) 112597 (<https://doi.org/10.1016/j.ejmech.2020.112597>)
8. G. Benedeković, M. Popsavin, I. Kovačević, V. Kojić, J. Kesić, S. Farkas, V. Popsavin, *Tetrahedron* **96** (2021) 132385 (<https://doi.org/10.1016/j.tet.2021.132385>)
9. S. S. Nyandoro, G. Maeda, J. J. E. Munissi, A. Gruhonjic, P. A. Fitzpatrick, S. Lindblad, S. Duffy, J. Pelletier, F. Pan, R. Puttreddy, V. M. Avery, M. Erdélyi, *Molecules* **24** (2019) 2746 (<https://doi.org/10.3390/molecules24152746>)
10. P. S. Mahajan, R. G. Gonnade, S. B. Mhaske, *Eur. J. Org. Chem.* **2014** (2014) 8049 (<http://dx.doi.org/10.1002/ejoc.201403123>)
11. D. A. Scudiero, R. H. Shoemaker, K. D. Paull, A. Monks, S. Tierney, T. H. Nofziger, M. J. Currens, D. Seniff, M. R. Boyd, *Cancer Res.* **48** (1988) 4827 (<https://cancerres.aacrjournals.org/content/48/17/4827>)
12. A. Nakayama, H. Sato, S. Nagano, S. Karanjit, H. Imagawa, K. Namba, *Chem. Pharm. Bull.* **67** (2019) 953 (<http://dx.doi.org/10.1248/cpb.c18-00948>)
13. Selectivity Index (*SI*) is calculated as follows:  $SI = IC_{50}$  of normal cell line (MRC-5)/ $IC_{50}$  of cancer cell line. *SI* values greater than 2 are considered as a satisfactory selectivity (see ref. 14)
14. M. I. Ahmad, S. Dixit, R. Konwar, P. G. Vasdev, A. K. Yadav, S. Tripathi, M. M. Gupta, A. Sharma, A. Gupta, *Bioorg. Med. Chem. Lett.* **27** (2017) 5040 (<https://doi.org/10.1016/j.bmcl.2017.09.060>).



SUPPLEMENTARY MATERIAL TO  
**Synthesis and antiproliferative activity of (5*R*)-cleistenolide  
and analogues**

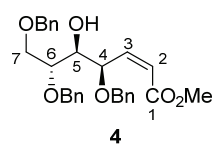
SÁNDOR FARKAS<sup>1</sup>, GORAN BENEDEKOVIĆ<sup>1</sup>, SLAĐANA M. STANISAVLJEVIĆ<sup>1</sup>,  
BOJANA M. SREĆO ZELENOVIĆ<sup>1</sup>, MIRJANA POPSAVIN<sup>1</sup>, VELIMIR POPSAVIN<sup>1,2\*</sup>  
and DIMITAR S. JAKIMOV<sup>3</sup>

<sup>1</sup>University of Novi Sad, Faculty of Sciences, Department of Chemistry, Biochemistry and Environmental Protection, Trg Dositeja Obradovića 3, 21000 Novi Sad, Serbia, <sup>2</sup>Serbian Academy of Sciences and Arts, Kneza Mihaila 35, 11000 Belgrade, Serbia and <sup>3</sup>University of Novi Sad, Faculty of Medicine, Oncology Institute of Vojvodina, Put dr Goldmana 4, 21204 Sremska Kamenica, Serbia

J. Serb. Chem. Soc. 88 (7–8) (2023) 705–713

SPECTROSCOPIC DATA OF MAIN COMPOUNDS

*Methyl (2Z)-4,6,7-tri-O-benzyl-2,3-dideoxy-D-arabino-hept-2-enoate (4)*



4

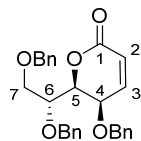
IR (film):  $\nu_{\text{max}}$  3479, 1723, 1658, 1604, 1586, 1028  $\text{cm}^{-1}$ .

$^1\text{H}$  NMR (400 MHz,  $\text{CDCl}_3$ ,  $\delta$ ): 7.24–7.39 (*m*, 15 H, 3  $\times$  Ph), 7.41 (*dd*, 1 H,  $J_{2,3} = 11.8$ ,  $J_{3,4} = 9.1$  Hz, H-3), 6.02 (*d*, 1 H,  $J_{2,3} = 11.8$  Hz, H-2), 5.42 (*bd*,  $J_{3,4} = 9.0$  Hz, H-4), 4.34–4.75 (*m*, 6 H, 3  $\times$   $\text{PhCH}_2$ ), 3.87 (*dd*, 1 H,  $J_{7a,7b} = 12.1$ ,  $J_{6,7b} = 4.9$  Hz, H-7b), 3.73 (*m*, 3 H, H-5, H-6 and H-7a), 3.69 (*s*, 3 H,  $\text{CO}_2\text{CH}_3$ ), 2.1–2.5 (*bs*, 1 H, OH).

$^{13}\text{C}$  NMR (100 MHz,  $\text{CDCl}_3$ ,  $\delta$ ): 166.15 ( $\text{CO}_2\text{CH}_3$ ), 147.32 (C-3), 138.53, 138.25, 137.95, 128.38, 128.35, 128.25, 128.14, 127.93, 127.82, 127.69, 127.60, 127.50 (3  $\times$  Ph), 122.38 (C-2), 77.85 (C-6), 74.49 (C-5), 73.54 (C-4), 73.52, 72.43, 71.27 (3  $\times$   $\text{PhCH}_2$ ), 70.74 (C-7), 51.44 ( $\text{CO}_2\text{CH}_3$ ).

(+)ESI-HRMS  $m/z$ : calculated for  $[\text{C}_{29}\text{H}_{32}\text{O}_6 + \text{K}^+]$  515.1830, observed 515.1822.

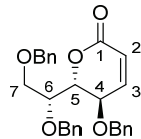
\*Corresponding author. E-mail: velimir.popavin@dh.uns.ac.rs

*4,6,7-Tri-O-benzyl-2,3-dideoxy-D-arabino-hept-2-eno-1,5-lactone (5)***5**IR (film):  $\nu_{\text{max}}$  1731, 1629, 1605, 1497, 1066, 1028  $\text{cm}^{-1}$ .

$^1\text{H}$  NMR (250 MHz,  $\text{CDCl}_3$ ,  $\delta$ ): 7.14–7.52 (*m*, 15 H, 3  $\times$  Ph), 6.99 (*dd*, 1 H,  $J_{2,3}$  = 9.8,  $J_{3,4}$  = 5.7 Hz, H-3), 6.20 (*d*, 1 H,  $J_{2,3}$  = 9.8 Hz, H-2), 4.46–4.86 (*m*, 7 H, H-5 and 3  $\times$   $\text{CH}_2\text{Ph}$ ), 4.28 (*dd*, 1 H,  $J_{4,5}$  = 2.5,  $J_{3,4}$  = 5.6 Hz, H-4), 4.18 (*ddd*, 1 H,  $J_{6,7\text{b}}$  = 2.0,  $J_{6,7\text{a}}$  = 4.0,  $J_{5,6}$  = 9.6 Hz, H-6), 3.96 (*dd*, 1 H,  $J_{7\text{a},7\text{b}}$  = 10.8,  $J_{6,7\text{b}}$  = 2.0 Hz, H-7b), 3.82 (*dd*, 1 H,  $J_{6,7\text{a}}$  = 3.9,  $J_{7\text{a},7\text{b}}$  = 10.8 Hz, H-7a).

$^{13}\text{C}$  NMR (62.5 MHz,  $\text{CDCl}_3$ ,  $\delta$ ): 162.68 (C-1), 143.13 (C-3), 138.25, 138.17, 137.69, 128.52, 128.42, 128.13, 128.05, 127.90, 127.75, 127.71, 127.66 (3  $\times$  Ph), 124.31 (C-2), 77.91 (C-5), 75.35 (C-6), 73.54, 72.36, 71.38 (3  $\times$   $\text{CH}_2\text{Ph}$ ), 67.92 (C-7), 65.46 (C-4).

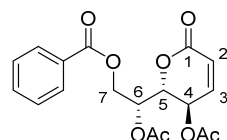
(+)ESI-HRMS *m/z*: calculated for  $[\text{C}_{28}\text{H}_{28}\text{O}_5 + \text{K}^+]$  483.1568, observed 483.1564.

*4,6,7-Tri-O-benzyl-2,3-dideoxy-D-lyxo-hept-2-eno-1,5-lactone (6)***6**IR (film):  $\nu_{\text{max}}$  3020, 1731, 1497, 1101, 1027  $\text{cm}^{-1}$ .

$^1\text{H}$  NMR (400 MHz,  $\text{CDCl}_3$ ,  $\delta$ ): 7.25–7.43 (*m*, 15 H, 3  $\times$  Ph), 6.85 (*dd*, 1 H,  $J_{2,3}$  = 10.0,  $J_{3,4}$  = 2.2 Hz, H-3), 5.99 (*dd*, 1 H,  $J_{2,3}$  = 10.0,  $J_{2,4}$  = 1.8 Hz, H-2), 4.34–4.84 (*m*, 8 H, 3  $\times$   $\text{CH}_2\text{Ph}$ , H-4 and H-5), 4.01 (*td*, 1 H,  $J_{6,7\text{a}}$  = 6.2,  $J_{6,7\text{b}}$  = 6.0,  $J_{5,6}$  = 1.9 Hz, H-6), 3.88 (*dd*, 1 H,  $J_{6,7\text{b}}$  = 5.8,  $J_{7\text{a},7\text{b}}$  = 9.8 Hz, H-7b), 3.84 (*dd*, 1 H,  $J_{6,7\text{a}}$  = 6.4,  $J_{7\text{a},7\text{b}}$  = 9.8 Hz, H-7a).

$^{13}\text{C}$  NMR (100 MHz,  $\text{CDCl}_3$ ,  $\delta$ ): 162.43 (C-1), 146.07 (C-3), 137.94, 137.78, 136.91, 128.51, 128.36, 128.31, 128.13, 127.94, 127.87, 127.78, 127.68, 127.63 (3  $\times$  Ph), 120.24 (C-2), 80.08 (C-5), 74.68 (C-6), 73.49, 72.64 and 71.6 (3  $\times$   $\text{CH}_2\text{Ph}$ ), 69.03 (C-7), 68.80 (C-4).

(+)ESI-HRMS *m/z*: calculated for  $[\text{C}_{28}\text{H}_{28}\text{O}_5 + \text{Na}^+]$  467.1834, observed 467.1827.

*(5R)-Cleistenolide (2)*(5*R*)-Cleistenolide (2)IR (film):  $\nu_{\text{max}}$  1744, 1604, 1176 cm<sup>-1</sup>.

<sup>1</sup>H NMR (400 MHz, CDCl<sub>3</sub>,  $\delta$ ): 7.40–8.05 (*m*, 5 H, Ph), 6.77 (*dd*, 1 H,  $J_{2,3}$  = 10.0,  $J_{3,4}$  = 2.7 Hz, H-3), 6.10 (*dd*, 1 H,  $J_{2,4}$  = 1.9,  $J_{2,3}$  = 10.0 Hz, H-2), 5.57 (*ddd*, 1 H,  $J_{2,4}$  = 1.9,  $J_{3,4}$  = 2.6,  $J_{4,5}$  = 8.5 Hz, H-4), 5.50 (*ddd*, 1 H,  $J_{5,6}$  = 2.2,  $J_{6,7b}$  = 5.3,  $J_{6,7a}$  = 7.3 Hz, H-6), 4.74 (*dd*, 1 H,  $J_{5,6}$  = 2.2,  $J_{4,5}$  = 8.5 Hz, H-5), 4.61 (*dd*, 1 H,  $J_{6,7b}$  = 5.3,  $J_{7a,7b}$  = 11.7 Hz, H-7b), 4.56 (*dd*, 1 H,  $J_{6,7a}$  = 7.3,  $J_{7a,7b}$  = 11.7 Hz, H-7a), 2.10 and 2.13 (2  $\times$  *s*, 3 H each, 2  $\times$  COCH<sub>3</sub>).

<sup>13</sup>C NMR (100 MHz, CDCl<sub>3</sub>,  $\delta$ ): 169.91 and 169.64 (2  $\times$  COCH<sub>3</sub>), 165.83 (COPh), 160.89 (C-1), 144.09 (C-3), 133.25, 129.91, 129.31, 128.45 (Ph), 121.82 (C-2), 77.80 (C-5), 67.80 (C-6), 63.20 (C-4), 62.40 (C-7), 20.60 (2  $\times$  COCH<sub>3</sub>).

(+)-ESI-LRMS *m/z*: 363 [M + H<sup>+</sup>].

Combustion analysis for C<sub>18</sub>H<sub>18</sub>O<sub>8</sub>: Calculated: C 59.67, H 5.01; found: C 59.49, H 4.89.

## SAR ANALYSIS

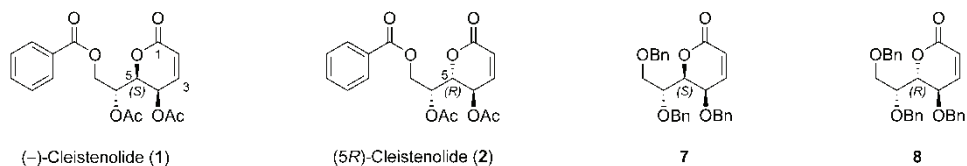


Fig. S-1. Structures of compounds used for SAR analysis

TABLE S-I. *In vitro* cytotoxicities used for SAR analysis.

Compounds	IC <sub>50</sub> ( $\mu$ M)							
	K562	HL-60	Jurkat	Raji	MCF-7	MDA-MB 231	HeLa	A549
<b>1</b>	7.65	1.21	14.22	36.94	26.07	2.25	7.32	16.34
<b>2</b>	0.21	7.31	19.41	2.47	21.28	7.66	6.45	9.38
<b>5</b>	0.34	12.55	9.24	29.66	1.39	0.09	3.58	1.85
<b>6</b>	0.33	8.27	17.03	1.05	20.06	7.04	5.90	17.21

The structure-activity relationships were accessed as follows: the IC<sub>50</sub> values of two compounds were compared, and the  $\Delta \log IC_{50}$  was calculated ( $\Delta \log IC_{50}$  is a difference between the log IC<sub>50</sub> values of an analogue and the corresponding control compound). Positive  $\Delta \log IC_{50}$  values show a decrease of

antiproliferative activity, whereas negative values indicate an increase in the activity upon the structural modification being considered. The results are presented in Fig. S2.

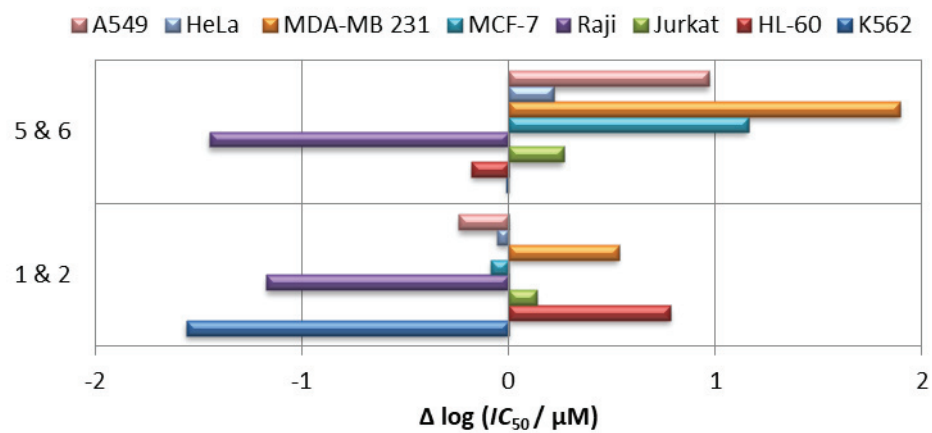
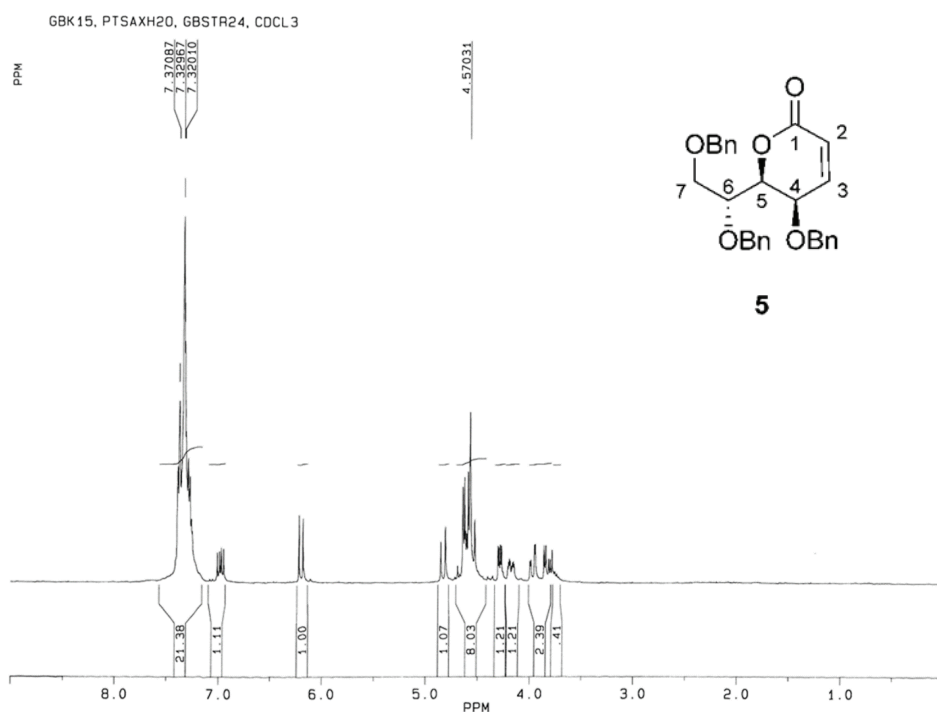


Fig. S-2. The effect of stereochemistry at the C-5 position on the cytotoxicity of stereoisomers.

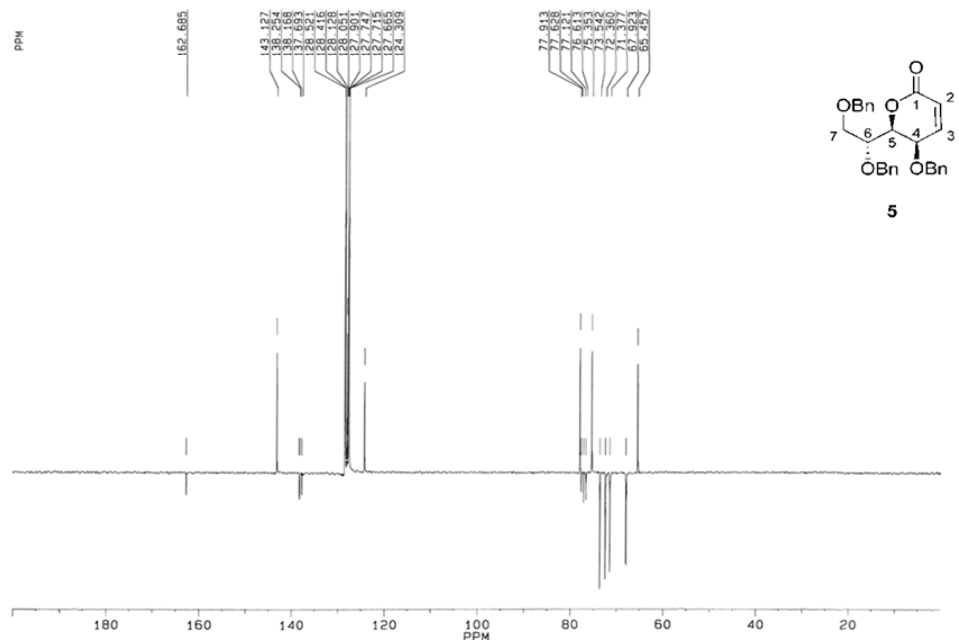
## NMR SPECTRA OF MAIN COMPOUNDS

250 MHz  $^1\text{H}$  NMR Spectrum of compound **5** ( $\text{CDCl}_3$ )



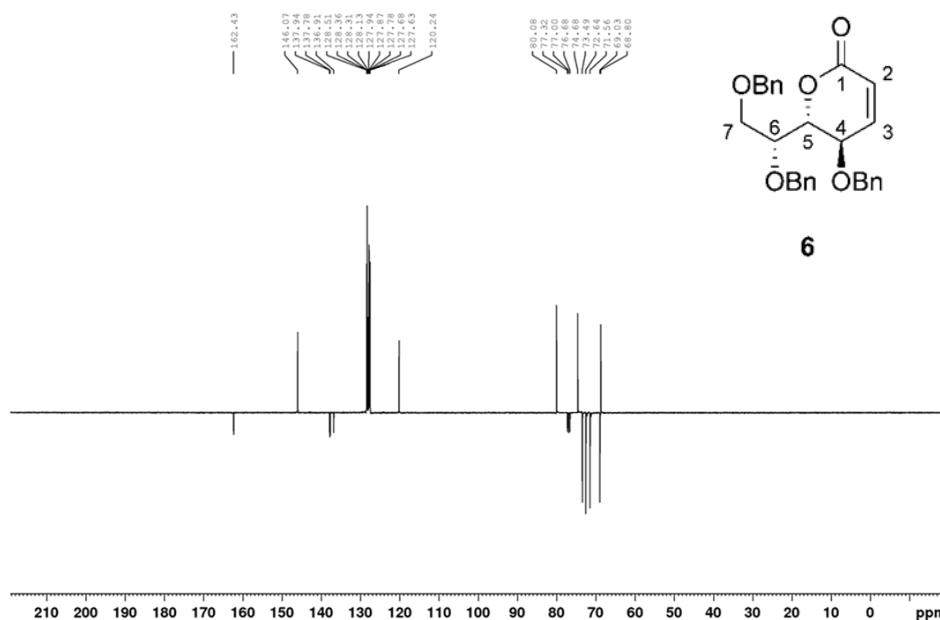
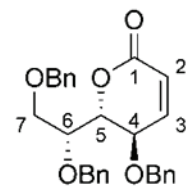
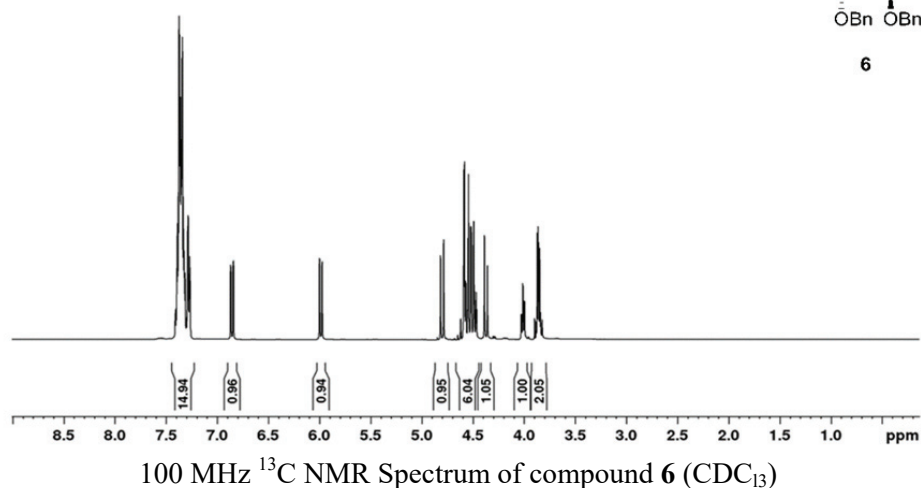
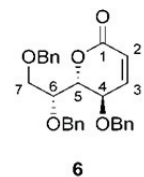
62.9 MHz  $^{13}\text{C}$  NMR Spectrum of compound **5** ( $\text{CDCl}_3$ )

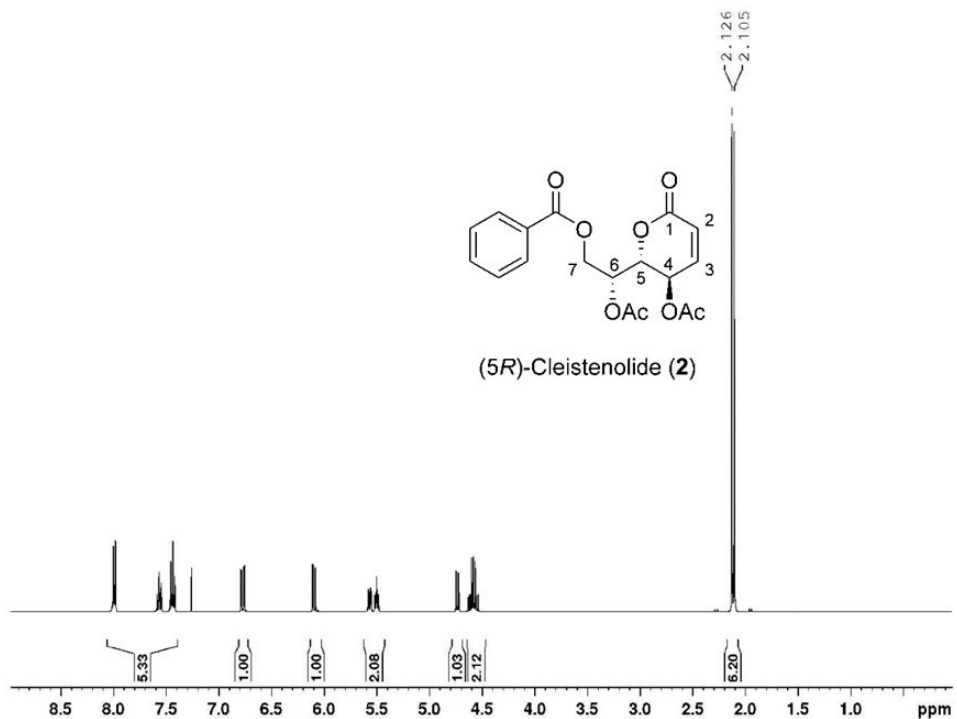
GBK15, CDCL3, PTSAXH20, GBSTR24

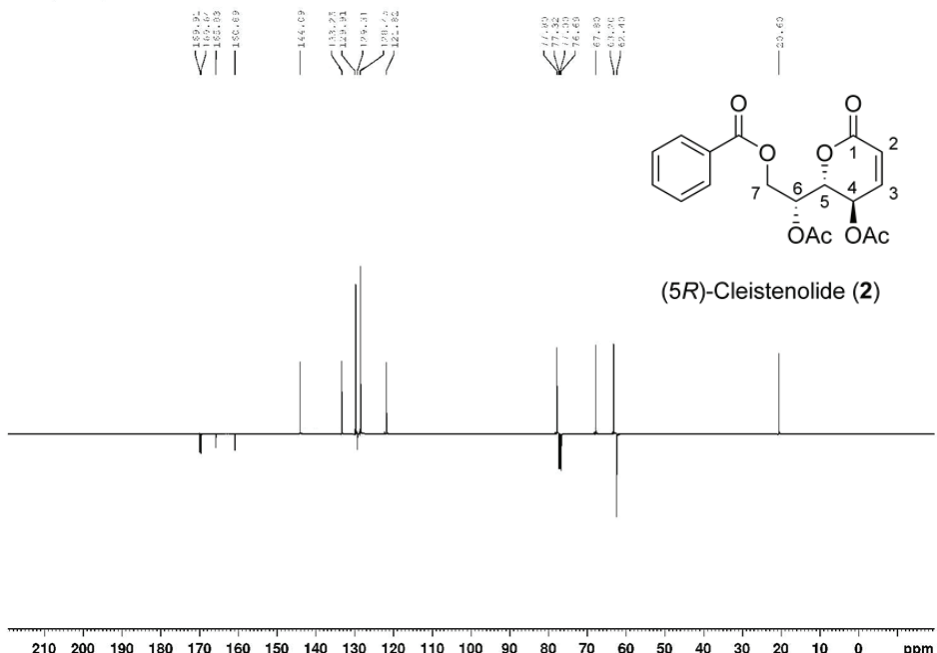
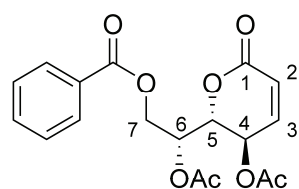


400 MHz  $^1\text{H}$  NMR Spectrum of compound **6** ( $\text{CDCl}_3$ )

GBK15L, CDCL3.10.3.17.



400 MHz  $^1\text{H}$  NMR Spectrum of compound **2** ( $\text{CDCl}_3$ )GBK3E,  $\text{CDCl}_3$ , 29.3.17.

100 MHz  $^{13}\text{C}$  NMR Spectrum of compound **2** ( $\text{CDCl}_3$ )GBK3E,  $\text{CDCl}_3$ , 29.3.17.COMPARISON OF NMR DATA OF FINAL PRODUCT **2** WITH PUBLISHED VALUES(5*R*)-Cleistenolide (**2**)TABLE S-II. Comparison of NMR data of final product **2** with published values ( $\text{CDCl}_3$ )

C/H	$\delta_{\text{H}}$ (J, Hz)		$\delta_{\text{C}}$	
	This work	Ref. 1	This work	Ref. 1
<b>1</b>	—	—	160.9	160.9
<b>2</b>	6.10 <i>dd</i> (1.9, 10.0)	6.12 <i>dd</i> (1.7, 10.0)	121.8	121.9
<b>3</b>	6.77 <i>dd</i> (10.0, 2.7)	6.79 <i>dd</i> (10.0, 2.8)	144.1	144.1
<b>4</b>	5.57 <i>ddd</i> (1.9, 2.6, 8.5)	5.59 <i>dt</i> (2.0, 2.0, 6.3)	63.2	63.3
<b>5</b>	4.74 <i>dd</i> (2.2, 8.5)	4.75 <i>dd</i> (2.0, 8.5)	77.8	78.0

TABLE S-II. Continued

C/H	$\delta_{\text{H}}$ (J, Hz)		$\delta_{\text{C}}$	
	This work	Ref. 1	This work	Ref. 1
6	5.50 <i>ddd</i> (2.2, 5.3, 7.3) 5.52 <i>ddd</i> (1.9, 5.3, 7.0)		67.8	67.9
7a	4.56 <i>dd</i> (7.3, 11.7)	4.58 <i>dd</i> (7.3, 11.5)	62.4	62.4
7b	4.61 <i>dd</i> (5.3, 11.7)	4.63 <i>dd</i> (5.3, 11.5)		
Me	2.10 and 2.13 (2 × <i>s</i> )	2.13 and 2.15 (2 × <i>s</i> )	20.6	20.7
MeCO	—	—	169.6 and 169.9	169.7 and 170.0
Ph	7.40–8.05 <i>m</i>	7.46–8.01 <i>m</i>	128.4, 129.3, 129.9, 133.2	128.5, 129.4, 129.7, 133.4
PhCO	—	—	166.0	165.9

## REFERENCES

- P. S. Mahajan, R. G. Gonnade, S. B. Mhaske, *Eur. J. Org. Chem.* **2014** (2014) 8049 (<https://dx.doi.org/10.1002/ejoc.201403123>).





## Click mediated synthesis of functionalized glycolipids with peptide-peptoid linkages\*

ANADI SINGHAMAHAPATRA<sup>1</sup>, CHINMAYEE PATTNAIK<sup>2</sup>, BISHNU PRASAD KAR<sup>3</sup>,  
GANESH CHANDRA NAYAK<sup>4</sup>, LAXMI NARAYAN SAHOO<sup>3\*</sup>  
and SATYANARAYAN SAHOO<sup>2\*\*</sup>

<sup>1</sup>Department of Chemistry, Saraswati Degree Vidyamandir, Neelakantha Nagar Berhampur, Odisha, India, 760002, <sup>2</sup>P. G. Department of Chemistry, Berhampur University, Odisha, India, 760007, <sup>3</sup>Department of Chemistry, Government Science College Chatrapur, Odisha, India, 761020 and <sup>4</sup>Department of Chemistry and Chemical Biology, Indian Institute of Technology (ISM) Dhanbad, Dhanbad, Jharkhand, India, 826004

(Received 1 February, revised 18 March, accepted 30 June 2023)

**Abstract:** The present work describes the synthesis of a new class of glycolipids with systematic variations in the linkage region, as well as in the aglycon part using Cu(I) catalyzed *click* reaction. The linkage region between sugar and the aglycon part was diversified using amide, amido-triazole and 5-benzoyl triazole moieties. The structural diversity of glycolipids was further amplified by incorporating several polar peptide foldamer groups such as triazole, amide, peptide, or *N*-aryl peptoid in the aglycon part. The newly designed glycolipids were derived from the amalgamation of different peptide bond mimics. This work reports the first use of *N*-aryl peptoid in the synthesis of glycolipids. The newly synthesized glycolipids were characterized using different spectroscopic and spectrometric analyses. The impact of the amide bond as well as the triazole ring in the linkage region on the morphology of the glycolipids was analysed by comparing their self-assemblies using SEM analysis. The geometries of the glycolipids were also optimized using density functional theory and the optimized structures were found to be minima in the potential energy surfaces.

**Keywords:** *click* reaction; [3+2] cycloaddition; triazole-amide; 5-benzoyl triazole; *N*-aryl peptoid; SEM study.

### INTRODUCTION

Glycolipids, an important class of biomolecules on the cell surface, have found a wide range of potential biological applications in addition to their applic-

\* Corresponding authors. E-mail: (\*)laxminarayanchem@gmail.com;  
(\*\*)sns.chem@buodisha.edu.in

• Dedicated to late Prof. Duraikkannu Loganathan.  
<https://doi.org/10.2298/JSC230201030S>

ations in detergents, agro-food chemicals, and cosmetics.<sup>1–6</sup> The glycan component of glycolipids has the affinity and the selectivity for different peptides and proteins, by virtue of which, glycolipids have the potential to be used as non-toxic and non-ionic surfactants for the extraction and the crystallization of integral membrane proteins. The bioactivity of glycolipids and their application as surfactants depends on the glycan part, the lipid chain, and the type of linkage between them, which emphasizes the need for the development of new methodologies for the synthesis of a series of glycolipids with diverse structures.<sup>7</sup> Among various methods reported for the synthesis of glycolipids, triazole ring containing glycolipids, synthesized by Cu(I) catalyzed *click* reaction of azide and alkyne<sup>8–11</sup> under aqueous conditions, has found the maximum acceptance in recent times, due to the easy synthetic method, higher yield and better proteolytic stability. Since the triazole ring is an isosteric replacement of the trans amide bond, it can act as a linker between the sugar and the aglycon part for the synthesis of *N*-linked glycoconjugates.<sup>12–19</sup> The C-5 proton of the triazole ring can be replaced by a suitable electrophile by the *click* reaction of azide and alkyne using Cu(I) catalyst under anhydrous conditions. Based on these assumptions, the authors have synthesized several glycoconjugates such as glycopeptoids,<sup>20</sup> halogenated glycolipids,<sup>21</sup> and aromatic glycoconjugates (Fig. 1).<sup>22</sup>

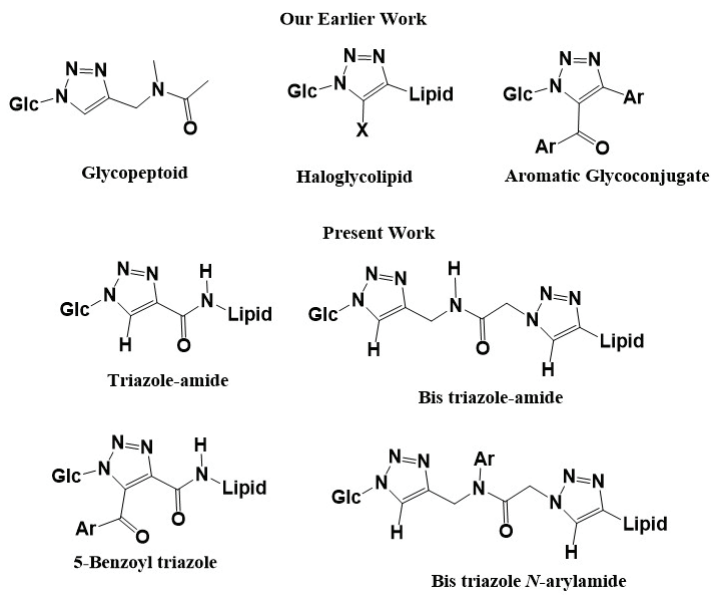


Fig. 1. Structural diversity in glycoconjugates using amide and its isosteres.

In addition to the rigid glycan part and the highly flexible aglycon part in glycolipid, the controlled flexibility of the linkage region by virtue of the re-

tricted rotation in the amide bond and its foldamers plays an important role in deciding its biological activity.<sup>23,24</sup> The present work has explored the use of Cu(I) catalysed *click* reaction for the synthesis of diversely functionalized triazole-linked glycolipids, where the linkage between the sugar and the lipid part has been modified using amide-linked triazole, 5-benzoyl triazole and bis-triazole rings connected by either amide or *N*-aryl amide bond.<sup>25</sup> Given the crucial role exemplified by amide bonds in controlling the structures and activities of proteins, the amide bonds and their isosteres like triazole rings are paramount constituents in drug molecules. A combination of the amide bond and triazole ring (*i.e.*, triazole–amide) in the linkage between sugar and lipid will introduce different conformations and modes of interaction with other molecules. This is the first report on the synthesis of an *N*-aryl peptoid-linked glycolipid by modifying the linkage region between the glycan and the aglycon part. The present work aims at the impact of the modification of the linkage region on the morphology of the glycolipids.

## EXPERIMENTAL

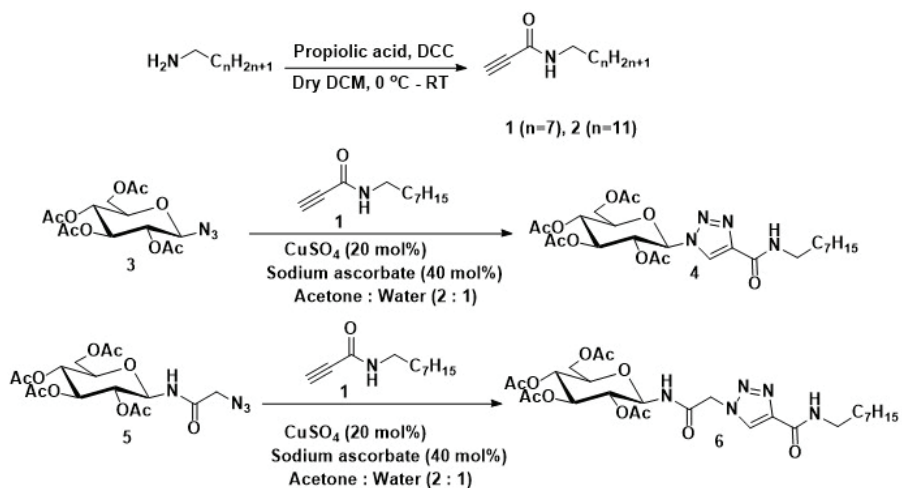
Experimental details and additional data are given in Supplementary material to this paper.

## RESULTS AND DISCUSSION

In order to demonstrate the impact of amide and its isosteres on the morphological properties by virtue of noncovalent interactions, triazole-linked glycoconjugates were synthesized using Cu(I) catalysed *click* reaction with the systematic variation in the alkyne or reaction condition. For the synthesis of triazole-amide linked glycolipid **4**, per-*O*-acetylated  $\beta$ -D-glucopyranosyl azide **3** was reacted with propiolamide **1** in presence of Cu(I) as the catalyst, generated *in situ* by the reaction of CuSO<sub>4</sub> and sodium ascorbate in an aqueous acetone medium. The propiolamides **1** and **2** were previously synthesized by a reaction of the corresponding amine with dicyclohexylcarbodiimide (DCC)-activated propionic acid (Scheme 1). The formation of compound **4** was confirmed by NMR spectroscopy and ESI-MS HRMS. In the <sup>1</sup>H-NMR spectrum of **4**, the triazole proton appeared as a singlet at 8.47 ppm whereas the –NH proton of the amide bond appeared as a triplet at 7.27 ppm. The anomeric proton appeared as a doublet at 5.98 ppm. The C-5 and C-4 carbon of the triazole ring appeared at 144.1 and 124.4 ppm, respectively, in the <sup>13</sup>C-NMR spectrum.

To introduce more structural diversity in the glycolipid, azidoacetamide-based triazole–amide linked glycolipid **6**, where the sugar moiety is linked to the triazole ring with an extra amide group spacer, was synthesized using a similar procedure as that of **4**. Per-*O*-acetylated  $\beta$ -D-glucopyranosyl azidoacetamide<sup>26</sup> **5** was reacted with *n*-octyl propiolamide **1** in presence of Cu(I) as the catalyst (Scheme 1). The C–H proton of the triazole ring in **6** appeared as a singlet at 8.31

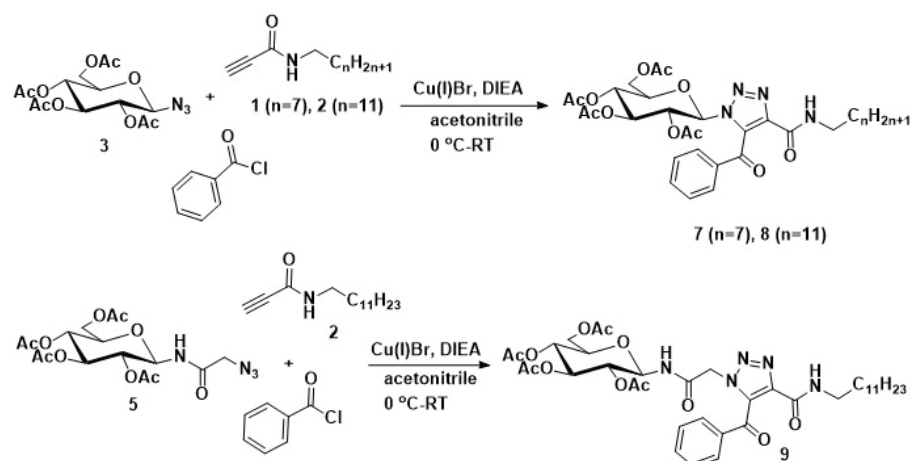
ppm in the  $^1\text{H}$ -NMR spectrum. The NH proton of the anomeric amide bond appeared as a doublet at 7.56 ppm and the NH proton of the triazole–amide appeared as a triplet at 7.29 ppm.



Scheme 1. Synthesis of triazole-amide-linked glycolipids.

A crucial role is played by the aromatic proton of the triazole ring in controlling its structure and activity. These protons can act as participants in noncovalent interactions (*e.g.*, C–H $\cdots$ O interactions) with other molecules. Replacement of the triazole proton with other functional groups, for instance, the benzoyl group will not only mutate the steric as well as the electronic atmosphere of the triazole ring but will also change its interaction with other molecules which is important for the activity of biomolecules like glycolipids. Keeping this in mind, glycolipids with 5-benzoyl triazole linkage were synthesized by the electrophilic addition of benzoyl chloride to the copper-triazolium intermediate, formed *in situ* by [3+2] cycloaddition reaction of azide functionalized sugar and alkyne functionalized long chain alkane under anhydrous condition. Azide **3** was reacted with propiolamide **1** and benzoyl chloride in presence of Cu(I)Br and diisopropylethylamine in dry acetonitrile (Scheme 2) which gave 5-benzoyl triazole-linked glycolipid **7** upon purification. In the  $^1\text{H}$ -NMR spectrum of **7**, the absence of the triazole proton and the appearance of carbonyl carbon of the 5-benzoyl triazole group at 186.2 ppm in the  $^{13}\text{C}$ -NMR spectrum confirmed the formation of the 5-benzoyl triazole ring. The formation of **7** was further confirmed by the ESI-MS HRMS spectrum. Glycolipid **8** with a longer lipid chain was synthesized by reacting protected glycosyl azide **3** with propiolamide **2** under similar reaction conditions as that of **7**.

For the introduction of another amide bond between the sugar and 5-benzoyl triazole ring, azidoacetamide **5** was reacted with propiolamide **2** and benzoyl chloride using Cu(I)Br and DIEA in dry acetonitrile (Scheme 2). The NH proton of the triazole–amide group appeared as a triplet at 7.20 ppm whereas the NH proton of the anomeric amide group appeared as a doublet at 7.06 ppm in the <sup>1</sup>H-NMR spectrum. In the <sup>13</sup>C-NMR spectrum of **9**, the carbonyl carbon of the 5-benzoyl triazole group appeared at 186.8 ppm.

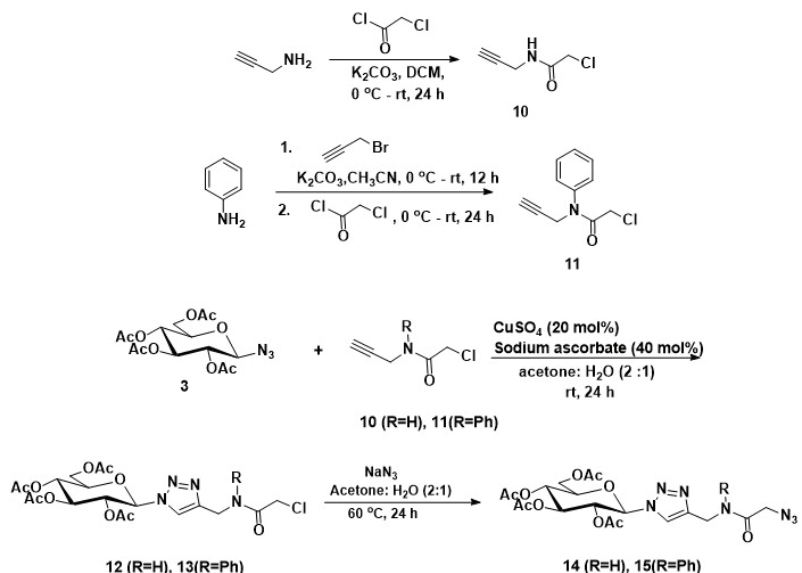


Scheme 2. Synthesis of 5-benzoyl triazole-linked glycolipids.

The reactivity of the triazole ring will be changed by the substitution of its proton by the benzoyl group, whereas on the other side, the presence of an additional triazole ring in the existing molecule may support its binding with other molecules or acquaint supplementary traits to its structure and activity. For the synthesis of bis-triazole linked glycolipid, azide functionalized triazole linked glycoconjugates **14** and **15** were synthesized for further reaction with alkyne functionalized long chain alkanes. Propargyl amine was reacted with chloroacetyl chloride in the presence of potassium carbonate to give the corresponding chloroacetamide **10** which upon reaction with per-*O*-acetylated *β*-D-glucopyranosyl azide **3** in presence of Cu(I) furnished triazole-linked chloroacetamide **12**. Further reaction of **12** with sodium azide in a mixture of acetone and water (2:1) at 60 °C resulted in the formation of the corresponding azidoacetamide **14** (Scheme 3).

To use the structural and conformational features of *N*-aryl peptoids as a linkage in glycolipids known in the literature of peptidomimetics, bis-triazole-linked glycolipid was synthesized with an *N*-aryl peptoid backbone. Azidoacetamide functionalized *N*-aryl peptoid glycoconjugate **15** was synthesized for further *click* reaction with alkyne functionalized lipid. The synthesis started with the monoalkylation of aniline using propargyl bromide (1.1 equiv.) in the presence of

potassium carbonate, followed by a reaction with chloroacetyl chloride, to give *N*-propargylated *N*-chloroacetamide of aniline **11** (Scheme 3). The reaction of **11** with per-*O*-acetylated  $\beta$ -D-glucopyranosyl azide **3** using copper sulphate and sodium ascorbate in an aqueous acetone medium gave triazole-linked *N*-aryl glycopeptoid chloroacetamide **13**. The chloroacetamide **13** was reacted with sodium azide in a mixture of acetone and water (2:1) at 60 °C to give the corresponding azidoacetamide **15** (Scheme 3). Unlike *N*-alkyl peptoids which exist as a mixture of *cis* and *trans* isomers, *N*-aryl peptoids prefer to exist as *trans* isomers. In the  $^1\text{H-NMR}$  spectra of **14** and **15**, the triazole protons appeared as singlets at 7.84 and 7.97 ppm, respectively.

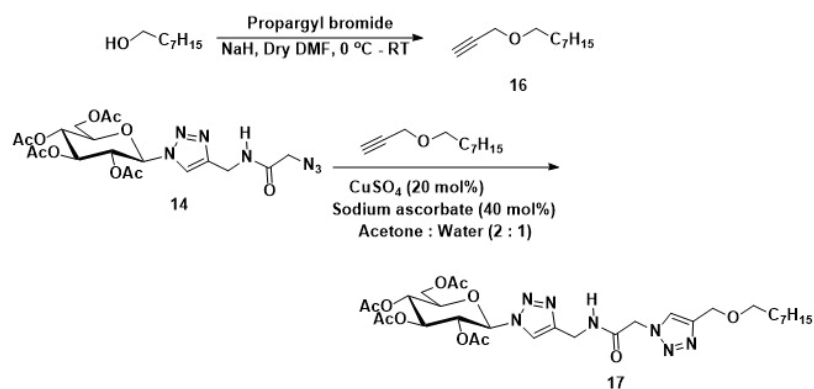


Scheme 3. Synthesis of azide functionalized triazole linked glycoconjugates.

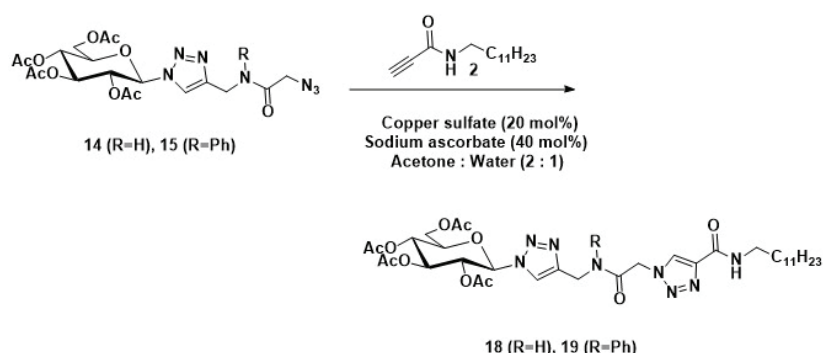
The triazole-linked azidoacetamide functionalized glycoconjugate **14** was reacted with *n*-octyl propargyl ether **16** using Cu(I) catalyzed *click* reaction to give bis-triazole linked glycolipid **17** after purification by column chromatography (Scheme 4). In the  $^1\text{H-NMR}$  spectrum of **17**, two triazole protons appeared as singlets at 8.32 and 7.86 ppm, whereas the NH proton of amide appeared as a singlet at 7.33 ppm.

The reaction of **14** with propiolamide **2** by Cu(I) catalyzed *click* reaction gave bis-triazole-linked glycolipid **18** (Scheme 5). There are two types of triazole rings and two amide bonds in **18**, one of them is a triazole-amide. In the  $^1\text{H-NMR}$  spectrum of **18**, two triazole protons appeared as singlets at 8.29 and 7.85 ppm whereas the two NH protons of two amide bonds appeared as multiplets in the range of 7.26–7.18 ppm.

A bis-triazole-linked glycolipid with an *N*-aryl peptoid backbone was designed by replacing the NH proton of the amide bond connecting two triazole rings with a phenyl group. The synthesis was done by Cu(I) catalysed *click* reaction of triazole-linked *N*-aryl glycopeptoid azidoacetamide **15** with propiolamide **2** to give bis-triazole linked glycolipid **19** after purification (Scheme 5). The two triazole protons of **19** appeared as singlets at 8.20 and 7.91 ppm, and the NH proton of the triazole-amide appeared as a triplet at 7.11 ppm in the <sup>1</sup>H-NMR spectrum.



Scheme 4. Synthesis of bis-triazole linked glycolipid **17**.



Scheme 5. Synthesis of bis-triazole-linked glycolipids.

The synthesized glycolipids contain aromatic triazole ring and other  $\pi$ -electron systems (*e.g.*, 5-benzoyl triazole and *N*-aryl amide) in the linkage region of sugar and lipid part, which can participate in noncovalent interactions with other bio-molecules and conjugated  $\pi$ -electron systems, thereby facilitating the study of these interactions by the spectroscopic methods like UV–Vis spectroscopy. To understand the diversity in the conjugated  $\pi$ -electron system, the UV–Vis spectra of the glycolipids were recorded. The UV–Vis spectra of triazole amide-linked

glycolipids **4** and **6** showed absorption maxima ( $\lambda_{\max}$ ) at 210 and 223 nm, respectively (Fig. 2A and B). For the corresponding 5-benzoyl triazole-linked glycolipids **7** and **9**, there were additional peaks at  $\lambda_{\max}$  256 and 261 nm, respectively (Fig. 2A and B). With the change in lipid chain length or changes in linkage region, there was no significant change in the absorption spectrum as shown in the case of **7**, **8** and **9** (Fig. 2C). Bis-triazole-linked glycolipids **17–19** showed absorption maxima ( $\lambda_{\max}$ ) at 215, 213 and 211 nm, respectively, in the UV–Vis spectra (Fig. 2D).

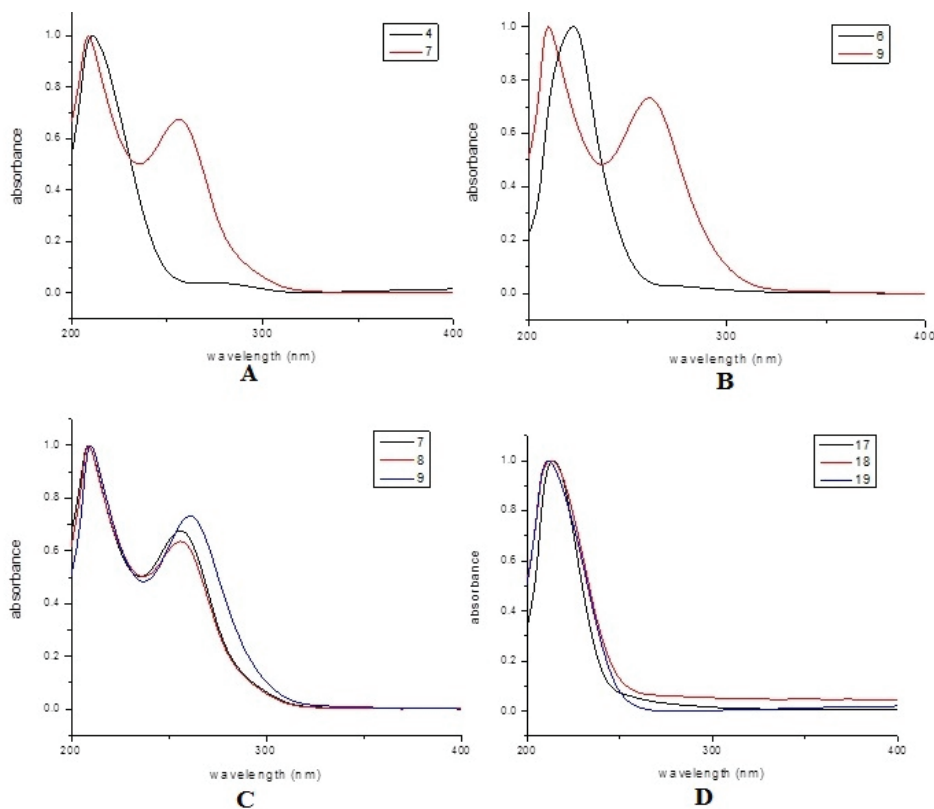


Fig. 2. UV–Vis spectra in methanol at  $10^{-5}$  M concentration; A) glycolipids **4** and **7**; B) glycolipids **6** and **9**; C) glycolipids **7–9**; D) glycolipids **17–19**.

The ability of the functional groups present in the linkage region connecting the sugar and the lipid part to participate in non-covalent interaction plays an important role in controlling the physical properties of synthetic glycolipids. With a systematic variation in the sugar–lipid linkage region, twelve different glycolipids were selected from this work and our earlier work for the SEM study (Fig. 3). The synthesized glycolipids have different functional groups such as amide,

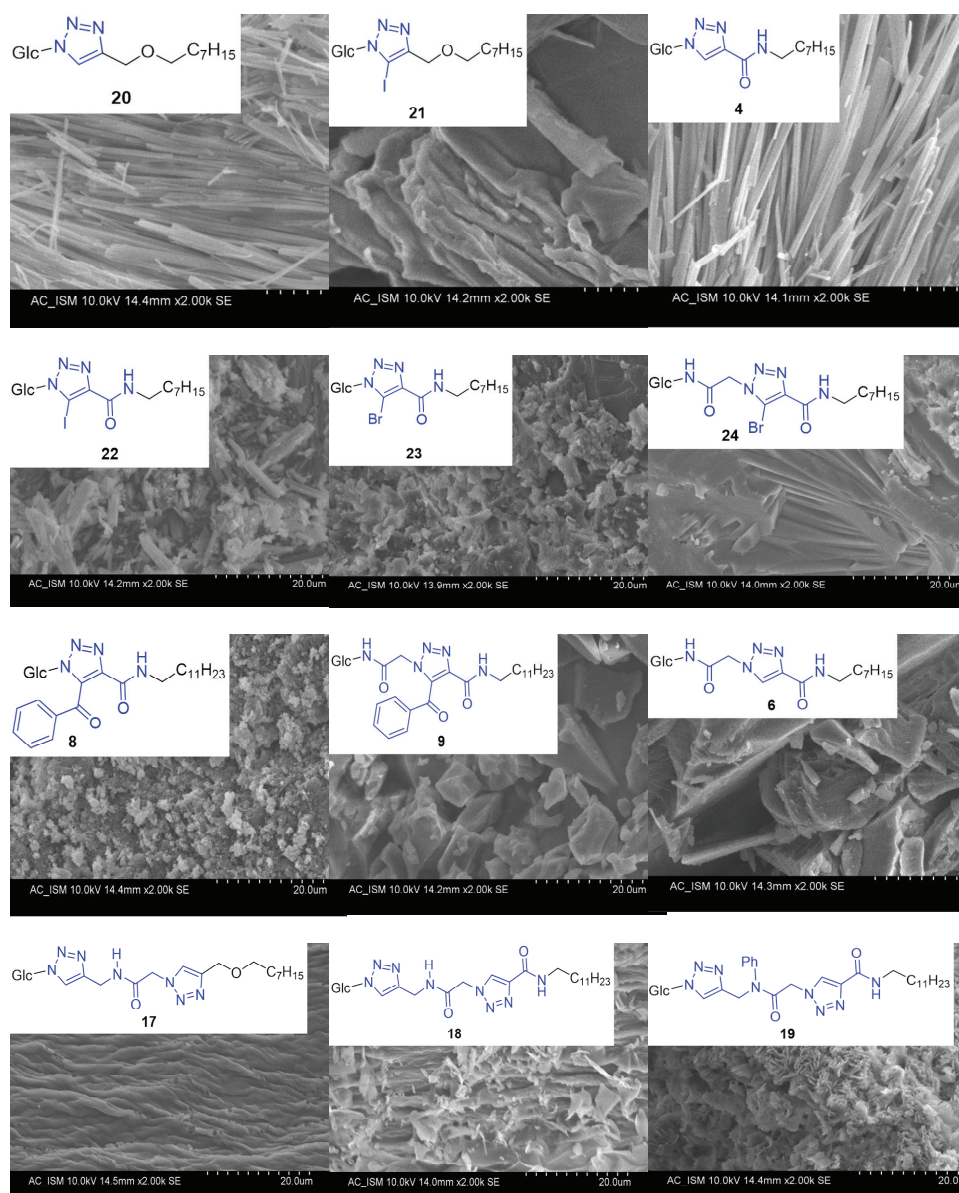


Fig. 3. SEM Images of the synthesized glycolipids.

triazole, amido triazole, halotriazole and bis-triazole in the sugar–lipid linkage region. To understand the influence of these functionalized triazole rings on the morphology of synthesized glycolipids, the self-assembled structures of the protected glycolipids were studied using a scanning electron microscope. Fig. 3 (A–L) displays the SEM images of the self-assembled structures of glycolipids in

a mixture of ethyl acetate and hexane. It was observed that a C-5 protonated triazole containing glycolipid exhibited fiber-like structures, probably due to an extended noncovalent interaction (*e.g.*, C–H···O interaction) as observed in **4** and **20**, whereas substitution of the C-5 proton by a halogen atom such as Br or I diminished such noncovalent interactions. This can be clearly visible from the SEM images of **21–24** where no regular arrangements were observed. In the case of an amido-triazole the effect of non-covalent interaction can be observed from the fibre-like arrangements in the SEM image of **4**, but replacing the triazole proton with a benzoyl group at the C-5 position of the triazole reduced the ability to form fibre-like arrangements as shown in the case of **8** and **9**.

The irregular arrangements of the glycolipids in the SEM images of **17–19** can be attributed to the replacement of an amide bond by either a triazole or *N*-aryl peptoid or ether linkage which reduced the noncovalent interactions. The above study clearly explained the impact of non-covalent interactions on the morphology of glycolipids.

To understand the stability of the glycolipids, the geometries of these molecules were optimized using B3LYP density functional theory. The optimized structures thus obtained were used for frequency calculations. In each case, positive frequencies were obtained, which implies that the optimized structures are minima in the potential energy surfaces and hence are stable. The optimized structures of **8** and **9** are given in Fig. 4.

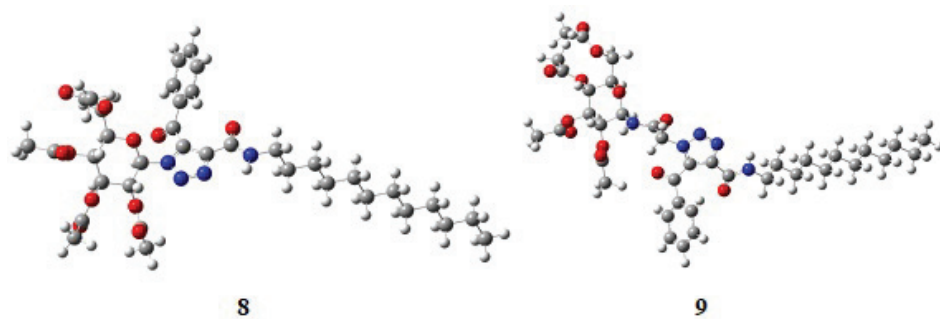


Fig. 4. DFT optimized geometries of synthesized glycolipids **8** and **9**.

#### CONCLUSION

Diversely functionalized triazole-linked glycolipids were synthesized with systematic variation in the linkage region between glycan and aglycon unit. These Cu(I) catalyzed [3+2] cycloaddition reactions not only gave higher yields under mild reaction conditions, but also have the advantage of functionalizing the triazole rings with modification in reaction condition (5-benzoyl triazole) or sequence of reactions (bis-triazole). The structure of the linkage region between sugar and lipid was systematically varied with different amide bonds and its iso-

sters like triazole-amide, 5-benzoyl triazole, bis-triazole with peptide or *N*-aryl peptoid backbone. The stability of the synthesized glycolipids was also determined based on DFT calculations. The scanning electron microscopy (SEM) study of self-assembled structures of the synthesized glycolipids showed the importance of the amide bond as well as the triazole ring in deciding the morphology of the glycolipids. Since these functional groups are important constituents in peptides or peptidomimics, synthetic glycolipids can be modified accordingly for the interactions with natural peptides, enzymes or other medically important biomolecules. This methodology can be extended to other monosaccharides and disaccharides, with variations in the length of the lipid chain, for the synthesis of a library of compounds. The application of synthesized glycolipids as nonionic surfactants as well as potential drug candidates is in progress.

#### SUPPLEMENTARY MATERIAL

Additional data and information are available electronically at the pages of journal website: <https://www.shd-pub.org.rs/index.php/JSCS/article/view/12254>, or from the corresponding author on request.

*Acknowledgements.* The authors thank Indian Institute of Technology Madras, Indian Institute of Technology (ISM), Dhanbad and Berhampur University for the instrumentation facility. The authors are thankful to OSHEC, Government of Odisha for the seed grant under OURIIP (1034/69/OSHEC) and SERB, New Delhi, for the TARE fellowship (Grant no. TAR/2018/000764).

ИЗВОД

#### СИНТЕЗА ГЛИКОЛИПИДА СА ПЕПТИД–ПЕПТОИД СПОЈЕМ ПРИМЕНОМ „CLICK“ РЕАКЦИЈЕ

ANADI SINGHAMAHAPATRA<sup>1</sup>, CHINMAYEE PATTNAIK<sup>2</sup>, BISHNU PRASAD KAR<sup>3</sup>, GANESH CHANDRA NAYAK<sup>4</sup>,  
LAXMI NARAYAN SAHOO<sup>3</sup> и SATYANARAYAN SAHOO<sup>2</sup>

<sup>1</sup>Department of Chemistry, Saraswati Degree Vidyamandir, Neelakantha Nagar Berhampur, Odisha, India, 760002, <sup>2</sup>P. G. Department of Chemistry, Berhampur University, Odisha, India, 760007, <sup>3</sup>Department of Chemistry, Government Science College Chatrapur, Odisha, India, 761020 and <sup>4</sup>Department of Chemistry and Chemical Biology, Indian Institute of Technology (ISM) Dhanbad, Dhanbad, Jharkhand, India, 826004

У овом раду је описана синтеза нове класе гликолипида са системским променама споја између два дела структуре, као и агликонског дела молекула, применом „click“ Cu(I)-катализоване реакције. Модификације споја између шећера и агликонског дела подразумевају амидне, амидо-триазолоске и 5-бензоил триазолске структурне мотиве. Структурне разлике гликолипида су додатно истакнуте укључивањем неколико поларних завојних пептидних група са као што су триазоли, амиди, пептиди или *N*-арил пептоиди у агликонском делу. Нови гликолипиди су креирани комбиновањем различитих пептомиметичких спојева. У раду је први пут приказана примена *N*-арил пептоида у синтези гликолипида. Нова синтетисана једињења су окарактерисана применом спектроскопских и спектрометријских анализа. Утицај амидне везе као и триазолског прстена на морфологију гликолипида је упоређен са њиховом способношћу самоорганизовања, коришћењем SEM анализе. Геометрија гликолипида је оптимизована теоријом

функционалне густине и оптимизоване структуре се налазе у минимуму потенцијалне енергије површине.

(Примљено 1. фебуара, ревидирано 18. марта, прихваћено 30. јуна 2023)

#### REFERENCES

- R. C. R. Jala, S. Vudhgiri, C. G. Kumar, *Carbohydr. Res.* **516** (2022) 108556 (<https://doi.org/10.1016/j.carres.2022.108556>)
- Y. Queneau, S. Chambert, C. Basset, R. Cheaib, *Carbohydr. Res.* **343** (2008) 1999 (<https://doi.org/10.1016/j.carres.2008.02.008>)
- L. Chaveriat, I. Gosselin, C. Machut, P. Martin, *Eur. J. Med. Chem.* **62** (2013) 177 (<https://doi.org/10.1016/j.ejmech.2012.12.032>)
- D. Wu, M. Fujio, C.-H. Wong, *Bioorg. Med. Chem.* **16** (2008) 1073 (<https://doi.org/10.1016/j.bmc.2007.10.026>)
- T. Lee, M. Cho, S.-Y. Ko, H.-J. Youn, D. J. Baek, W.-J. Cho, C.-Y. Kang, S. Kim, *J. Med. Chem.* **50** (2007) 585 (<https://doi.org/10.1021/jm061243q>)
- R. A. Falconer, I. Toth, *Bioorg. Med. Chem.* **15** (2007) 7012 (<https://doi.org/10.1016/j.bmc.2007.07.048>)
- L. Sahoo, A. Singhamahapatra, S. Sahoo, *J. Serb. Chem. Soc.* **83** (2018) 539 (<https://doi.org/10.2298/JSC170905030S>)
- H. C. Kolb, M. G. Finn, K. B. Sharpless, *Angew. Chem. Int. Ed.* **40** (2001) 2004 ([https://doi.org/10.1002/1521-773\(20010601\)40:11<2004::AIDANIE2004>3.0.CO;2-5](https://doi.org/10.1002/1521-773(20010601)40:11<2004::AIDANIE2004>3.0.CO;2-5))
- J. E. Moses, A. D. Moorhouse, *Chem. Soc. Rev.* **36** (2007) 1249 (<https://doi.org/10.1039/B613014N>)
- V. K. Tiwari, B. B. Mishra, K. B. Mishra, N. Mishra, A. S. Singh, X. Chen, *Chem. Rev.* **116** (2016) 3086 (<https://doi.org/10.1021/acs.chemrev.5b00408>)
- A. K. Agrahari, P. Bose, M. K. Jaiswal, S. Rajkhowa, A. S. Singh, S. Hotha, N. Mishra, V. K. Tiwari, *Chem. Rev.* **121** (2021) 7638 (<https://doi.org/10.1021/acs.chemrev.0c00920>)
- K. J. V. Paul, D. Loganathan, *Tetrahedron Lett.* **49** (2008) 6356 (<https://doi.org/10.1016/j.tetlet.2008.08.073>)
- H.-L. Zhang, X.-P. He, L. Sheng, Y. Yao, W. Zhang, X.-X. Shi, J. Li, G.-R. Chen, *Mol. Divers.* **15** (2011) 889 (<https://doi.org/10.1007/s11030-011-9318-1>)
- V. Neto, R. Granet, P. Krausz, *Tetrahedron* **66** (2010) 4633 (<https://doi.org/10.1016/j.tet.2010.03.115>)
- A. Baron, Y. Blériot, M. Sollogoub, B. Vauzeilles, *Org. Biomol. Chem.* **6** (2008) 1898 (<https://doi.org/10.1039/B805528A>)
- F. A. Sani, T. Heidelberg, R. Hashim, Farhanullah, *Colloids Surfaces., B* **97** (2012) 196 (<https://doi.org/10.1016/j.colsurfb.2012.03.030>)
- S.-X. Song, H.-L. Zhang, C.-G. Kim, L. Sheng, X.-P. He, Y.-T. Long, J. Li, G.-R. Chen, *Tetrahedron* **66** (2010) 9974 (<https://doi.org/10.1016/j.tet.2010.10.033>)
- M. J. Clemente, J. Fitremann, M. Mauzac, J. L. Serrano, L. Oriol, *Langmuir* **27** (2011) 15236 (<https://doi.org/10.1021/la203447e>)
- K. Pérez-Labrada, I. Brouard, I. Méndez, C. S. Pérez, J. A. Gavin, D. G. Rivera, *Eur. J. Org. Chem.* (2014) 3671 (<https://doi.org/10.1002/ejoc.201402117>)
- A. Singhamahapatra, L. Sahoo, D. Loganathan, *J. Org. Chem.* **78** (2013) 10329 (<https://doi.org/10.1021/jo401720s>)
- L. Sahoo, A. Singhamahapatra, D. Loganathan, *Org. Biomol. Chem.* **12** (2014) 2615 (<https://doi.org/10.1039/C3OB42308E>)

22. L. Sahoo, S. Kundu, A. Singhamahapatra, N. K. Jena, G. C. Nayak, S. Sahoo, *Carbohydr. Res.* **469** (2018) 23 (<https://doi.org/10.1016/j.carres.2018.08.015>)
23. S. M. Miller, R. J. Simon, S. Ng, R. N. Zuckermann, J. M. Kerr, W. H. Moos, *Drug Dev. Res.* **35** (1995) 20 (<https://doi.org/10.1002/ddr.430350105>)
24. J. T. Nguyen, C. W. Turck, F. E. Cohen, R. N. Zuckermann, W. A. Lim, *Science* **282** (1998) 2088 (<https://doi.org/10.1126/science.282.5396.2088>)
25. N. H. Shah, G. L. Butterfoss, K. Nguyen, B. Yoo, R. Bonneau, D. L. Rabenstein, K. Kirshenbaum, *J. Am. Chem. Soc.* **130** (2008) 16622 (<https://doi.org/10.1021/ja804580n>)
26. K. J. V. Paul, L. Sahoo, V. Sorna, D. Loganathan, *Trends Carbohydr. Res.* **2** (2010) 21 ([https://www.trendscarbo.com/getf\\_shoppingcart.php?id=726840555](https://www.trendscarbo.com/getf_shoppingcart.php?id=726840555)).



SUPPLEMENTARY MATERIAL TO  
**Click mediated synthesis of functionalized glycolipids with  
peptide-peptoid linkages**

ANADI SINGHAMAHAPATRA<sup>1</sup>, CHINMAYEE PATTNAIK<sup>2</sup>, BISHNU PRASAD KAR<sup>3</sup>,  
GANESH CHANDRA NAYAK<sup>4</sup>, LAXMI NARAYAN SAHOO<sup>3\*</sup>  
and SATYANARAYAN SAHOO<sup>2\*\*</sup>

<sup>1</sup>Department of Chemistry, Saraswati Degree Vidyamandir, Neelakantha Nagar Berhampur, Odisha, India, 760002, <sup>2</sup>P. G. Department of Chemistry, Berhampur University, Odisha, India, 760007, <sup>3</sup>Department of Chemistry, Government Science College Chatrapur, Odisha, India, 761020 and <sup>4</sup>Department of Chemistry and Chemical Biology, Indian Institute of Technology (ISM) Dhanbad, Dhanbad, Jharkhand, India, 826004

J. Serb. Chem. Soc. 88 (7–8) (2023) 715–727

EXPERIMENTAL

*A. General Information:* The solvents used during the reaction were distilled before use, and dry solvents were prepared using standard methods. All reagents purchased from commercial sources were used without any purification. Column chromatography was performed over 100–200 mesh silica with ethyl acetate and hexane as the eluent. <sup>1</sup>H and <sup>13</sup>C NMR spectra were recorded on a Bruker 400 MHz NMR spectrometer. All mass spectra were recorded in a Q-TOF electrospray ionization spectrometer. UV-Visible spectra were recorded on a Systronics PC-based double-beam UV-visible spectrophotometer (model-2202). Scanning Electron Microscopic studies were carried out using a Hitachi S3400 N microscope. All the Density Functional Theory (DFT) based computations were performed using the Gaussian 09W package. The geometries of Compounds **21** and **22**, which include iodine atoms in their structures, were optimized at B3LYP/def2svp level, and for all other compounds given in Figure 3, the geometry optimization was performed at B3LYP/6-31G(d) level. No symmetry was imposed in the molecules during optimization. The optimized structures obtained in the above processes were subjected to frequency calculations to find out whether these are maxima or minima in the potential energy surfaces.

*B 1. General method for Cu(I) catalysed synthesis of 1,4-triazole linked glycolipids **4** & **6**:* To a stirred mixture of azide (**3** or **5**, 1 mmol)<sup>26</sup> and alkyne (**1**, 1.1 mmol) in acetone (5 mL), solutions of copper sulphate (20 mol% in 1 mL water) and sodium ascorbate (40 mol% in 1.5 mL water) were added. The reaction continued until the starting material (**3** or **5**) was completely consumed at room temperature, as indicated by TLC. The crude product obtained after the aqueous workup was purified by column chromatography to obtain an analytically pure sample.

\*Corresponding authors. E-mail: (\*)laxminarayanchem@gmail.com;  
(\*\*)sns.chem@buodisha.edu.in

**Compound 4:** Yield 95% (520 mg), m.p. 175-179 °C,  $[\alpha]_D$ -28.6° (c = 1.0, CHCl<sub>3</sub>, 25 °C), <sup>1</sup>H NMR (400 MHz, CDCl<sub>3</sub>): δ 8.47 (s, 1H, triazole -CH), 7.27 (t, 1H, J = 9.6 Hz, NH), 5.98 (d, 1H, J = 8.4 Hz, H-1), 5.53-5.44 (m, 2H, H-2 & H-3), 5.31 (t, 1H, J = 9.6 Hz, H-4), 4.32-4.28 (dd, 1H, H-6a), 4.18-4.15 (dd, 1H, H-6b), 4.09-4.06 (m, 1H, H-5) 3.48-3.42 (m, 2H, NH-CH<sub>2</sub>-), 2.08, 2.06, 2.03, 1.87 (4s, 12H, 4 x -COCH<sub>3</sub>), 1.64-1.60 (m, 2H, -NHCH<sub>2</sub>CH<sub>2</sub>CH<sub>2</sub>), 1.38-1.27 (bs, 10H, 5 x CH<sub>2</sub>), 0.87 (t, 3H, -CH<sub>3</sub>) ppm; <sup>13</sup>C NMR (100 MHz, CDCl<sub>3</sub>): δ 170.6, 170.0, 169.4, 168.7, 159.4, 144.1, 124.4, 85.8, 75.1, 72.6, 70.5, 67.5, 61.4, 39.3, 31.8, 29.6, 29.3, 29.2, 27.0, 22.7, 20.7, 20.6 (x 2), 20.2, 14.1 ppm; ESI-MS HRMS: calculated 555.2666 for [M+H]<sup>+</sup>, found 555.2667 for C<sub>25</sub>H<sub>39</sub>N<sub>4</sub>O<sub>10</sub>.

**Compound 6:** Yield 90% (550 mg), m.p. 155-157 °C,  $[\alpha]_D$ +11.2° (c = 1.3, CHCl<sub>3</sub>, 25 °C), <sup>1</sup>H NMR (400 MHz, CDCl<sub>3</sub>): δ 8.31 (s, 1H, triazole -CH), 7.56 (d, 1H, J = 8.8 Hz, NH), 7.29 (t, 1H, NH), 5.33-5.27 (m, 2H, H-1 & H-2), 5.21-5.11 (ABq, 2H, NHCOCH<sub>2</sub>), 5.05 (t, 1H, J = 9.6 Hz, H-4), 4.94 (t, 1H, J = 9.6 Hz, H-3), 4.30-4.25 (dd, 1H, H-6a), 4.10-4.07 (dd, 1H, H-6b), 3.87-3.86 (m, 1H, H-5) 3.47-3.42 (m, 2H, NH-CH<sub>2</sub>-), 2.06, 2.03, 2.00 (3s, 12H, 4 x -COCH<sub>3</sub>), 1.64-1.59 (m, 2H, -NHCH<sub>2</sub>CH<sub>2</sub>CH<sub>2</sub>), 1.37-1.27 (bs, 10H, 5 x CH<sub>2</sub>), 0.87 (t, 3H, -CH<sub>3</sub>) ppm; <sup>13</sup>C NMR (100 MHz, CDCl<sub>3</sub>): δ 170.7, 170.6, 169.8, 169.5, 165.4, 159.7, 143.7, 127.1, 78.2, 73.8, 72.7, 70.4, 68.1, 61.7, 52.6, 39.3, 31.7, 29.5, 29.2, 29.1, 26.9, 22.6, 20.6, 20.5, 14.0 ppm; ESI-MS HRMS: calculated 612.2881 for [M+H]<sup>+</sup>, found 612.2903 for C<sub>27</sub>H<sub>42</sub>N<sub>5</sub>O<sub>11</sub>.

## 2. General method for synthesis of 5-benzoyl 1,4-triazole linked glycolipids 7, 8, & 9:

Per-*O*-acetylated glucopyranosyl azide/ azidoacetamide (**3** or **5**, 1 mmol) was taken along with *n*-alkyl propiolamide (**1** or **2**, 1.1 mmol) and Cu(I)Br (1.1 mmol) in a two necked RB flask under nitrogen. Dry acetonitrile (5 mL) was added to it, followed by DIEA (0.45 mL, 2.5 mmol). The reaction mixture was stirred at 0 °C for 10 minutes and benzoyl chloride (0.13 mL, 1.1 mmol) was added dropwise. The reaction was continued at room temperature until the per-*O*-acetylated glucopyranosyl azide/azidoacetamide was completely consumed, as indicated by TLC. The crude product, after aqueous workup, was purified by column chromatography and characterized based on NMR and ESI-MS spectroscopic data.

**Compound 7:** Yield 75% (490 mg), m.p. 58-61 °C,  $[\alpha]_D$ -39.8° (c = 0.7, CHCl<sub>3</sub>, 25 °C), <sup>1</sup>H NMR (400 MHz, CDCl<sub>3</sub>): δ 7.78 (d, 2H, J = 7.6 Hz), 7.61 (t, 1H, J = 7.6 Hz), 7.45 (t, 2H, J = 7.6 Hz), 7.07 (t, 2H, J = 6.0 Hz, NH), 5.89-5.80 (m, 2H, H-1 & H-2), 5.34 (t, 1H, J = 9.2 Hz, H-3), 5.11 (t, 1H, J = 9.6 Hz, H-4), 3.92-3.88 (dd, 1H, H-6a), 3.80-3.76 (m, 2H, H-6b & H-5), 3.33-3.28 (q, 2H, NH-CH<sub>2</sub>-), 2.03, 2.00, 1.96, 1.81 (4s, 12H, 4 x -COCH<sub>3</sub>), 1.53-1.50 (m, 2H, -NHCH<sub>2</sub>CH<sub>2</sub>), 1.29-1.25 (bs, 10H, 5 x CH<sub>2</sub>), 0.86 (t, 3H, -CH<sub>3</sub>) ppm; <sup>13</sup>C NMR (100 MHz, CDCl<sub>3</sub>): δ 186.2 (Triazole-C=O), 170.3, 170.2, 169.2, 168.7 (4 x -COCH<sub>3</sub>), 158.3 (NH-CO), 142.2, 136.5, 135.8, 134.7, 129.6, 128.7, 85.3 (C-1), 75.0, 72.8, 70.1, 67.3, 61.3, 39.4, 31.8, 29.8, 29.6, 29.3, 29.2, 27.0, 22.7, 20.6 (x 2), 20.5, 20.4, 14.2 ppm; ESI-MS HRMS: calculated 659.2928 for [M+H]<sup>+</sup>, found 659.2924 for C<sub>32</sub>H<sub>43</sub>N<sub>4</sub>O<sub>11</sub>.

**Compound 8:** Yield 70% (500 mg), syrup,  $[\alpha]_D$ -53.0° (c = 0.2, CHCl<sub>3</sub>, 25 °C), <sup>1</sup>H NMR (400 MHz, CDCl<sub>3</sub>): δ 7.78 (d, J = 7.6 Hz, 2H), 7.61 (t, J = 7.6 Hz, 1H), 7.45 (t, J = 7.6 Hz, 2H), 7.07 (t, 1H, NH), 5.89-5.80 (m, 2H, H-1 & H-2), 5.34 (t, 1H, J = 9.2 Hz, H-3), 5.11 (t, 1H, J = 9.6 Hz, H-4), 3.91-3.88 (dd, 1H, H-6a), 3.79-3.76 (m, 2H, H-6b & H-5), 3.33-3.28 (q, 2H, NH-CH<sub>2</sub>-), 2.03, 2.00, 1.96, 1.81 (4s, 12H, 4 x -COCH<sub>3</sub>), 1.53 (m, 2H, -NHCH<sub>2</sub>CH<sub>2</sub>), 1.25 (bs, 18H, 9 x CH<sub>2</sub>), 0.87 (t, 3H, -CH<sub>3</sub>) ppm; <sup>13</sup>C NMR (100 MHz, CDCl<sub>3</sub>): δ 186.1 (Triazole-C=O), 170.2, 170.1, 169.0, 168.6 (4 x -COCH<sub>3</sub>), 158.2, 142.1, 136.4, 135.7, 134.5, 129.4, 128.6, 85.2, 74.9, 72.7, 70.0, 67.2, 61.2, 39.2, 31.8, 29.6, 29.5, 29.4, 29.2, 26.8,

22.6, 20.5, 20.4, 20.3, 14.2 ppm; ESI-MS HRMS: calculated 715.3554 for  $[M+H]^+$ , found 715.3528 for  $C_{36}H_{51}N_4O_{11}$ .

**Compound 9:** Yield 70% (540 mg), syrup,  $[\alpha]_D -14.2^\circ$  ( $c = 0.3$ ,  $CHCl_3$ , 25 °C),  $^1H$  NMR (400 MHz,  $CDCl_3$ ):  $\delta$  7.83 (d,  $J = 7.6$  Hz, 2H), 7.62 (t,  $J = 7.2$  Hz, 1H), 7.46 (t, 2H,  $J = 7.6$  Hz.), 7.20 (t, 1H,  $J = 6.0$  Hz, NH), 7.06 (d, 1H,  $J = 9.2$  Hz, C-NH-), 5.26-5.19 (m, 3H, H-2 & -NHCOCH<sub>2</sub>-), 5.13 (t, 1H,  $J = 9.2$  Hz, H-1), 5.02 (t, 1H,  $J = 9.2$  Hz, H-4), 4.86 (t, 1H,  $J = 9.6$  Hz, H-3), 4.26-4.22 (dd, 1H, H-6a), 4.03-4.00 (dd, 1H, H-6b), 3.76-3.73 (m, 1H, H-5) 3.32-3.27 (q, 2H, NH-CH<sub>2</sub>), 2.05, 2.01, 1.99 (x 2) (4s, 12H, 4 x -COCH<sub>3</sub>), 1.53-1.50 (m, 2H, -NHCH<sub>2</sub>CH<sub>2</sub>), 1.24 (bs, 18H, 9 x CH<sub>3</sub>), 0.87 (t, 3H, -CH<sub>3</sub>) ppm;  $^{13}C$  NMR (100 MHz,  $CDCl_3$ ):  $\delta$  186.8 (Triazole-C=O), 171.4, 170.7, 169.9, 169.6 (4 x -COCH<sub>3</sub>), 165.1, 158.6 (2 x NH-CO), 142.5, 136.5, 135.3, 134.7, 129.8, 128.9, 128.6, 78.3 (C-1), 73.7, 72.5, 70.5, 68.1, 61.7, 51.7, 39.4, 32.0, 29.7, 29.6 (x 2), 29.4, 29.3, 26.9, 22.7, 20.8, 20.6, 14.2 ppm; ESI-MS HRMS: calculated 772.3769 for  $[M+H]^+$ , found 772.3758 for  $C_{38}H_{54}N_5O_{12}$ .

**3. Synthesis of 11:** To a mixture of aniline (0.3 mL, 3.2 mmol) and potassium carbonate (900 mg, 6.5 mmol) in dry acetonitrile (10 mL), propargyl bromide (0.3 mL, 3.5 mmol) was added at 0 °C. After stirring the reaction mixture for 12 h at room temperature, chloroacetyl chloride (5 mmol) was added to the reaction mixture at 0 °C. The reaction mixture was allowed to cool to room temperature over a period of 30 minutes and stirred for 24 h at room temperature. After completion of the reaction, as indicated by TLC, the reaction mixture was filtered and the filtrate was concentrated to dryness. The crude reaction mixture was purified by column chromatography to give the title compound in 50% overall yield.

**Compound 11:** Yield 50% (330 mg),  $^1H$ -NMR ( $CDCl_3$ , 400 MHz):  $\delta$  7.48-7.46 (m, 3H), 7.35-7.33 (m, 2H), 4.50 (d, 2H,  $J = 2.4$  Hz, N-CH<sub>2</sub>-), 3.84 (s, 2H, CO-CH<sub>2</sub>-Cl), 2.24 (t, 1H,  $J = 2$  Hz, alkyne CH) ppm;  $^{13}C$ -NMR ( $CDCl_3$ , 100 MHz):  $\delta$  165.9, 140.2, 130.1, 129.3, 128.2, 120.2, 78.2, 72.9, 41.7, 39.2 ppm. ESI-MS HRMS: Calculated for  $C_{11}H_{11}NOCl$  ( $[M+H]^+$ ): 208.0529; found 208.0527.

#### 4. Synthesis of triazole-linked chloroacetamide functionalized glycoconjugates 12 & 13:

Synthesis was done following the same procedure as that of compounds 4 and 6.

**Compound 12:** Yield 90% (450 mg), m.p. 80-81 °C,  $[\alpha]_D -10.0^\circ$  ( $c = 0.4$ ,  $CHCl_3$ , 25 °C),  $^1H$ -NMR ( $CDCl_3$ , 400 MHz):  $\delta$  7.80 (s, 1H, triazole CH), 7.16 (s, 1H, NH), 5.87-5.85 (m, 1H, H-1), 5.45-5.38 (m, 2H, H-2 & H-3), 5.26-5.21 (m, 1H, H-4), 4.62-4.55 (m, 2H, CH<sub>2</sub>NH), 4.33-4.28 (m, 1H, H-6a), 4.17-4.14 (m, 1H, H-6b), 4.07 (s, 2H, CH<sub>2</sub>Cl), 4.02-3.98 (m, 1H, H-5), 2.09, 2.06, 2.03, 1.87 (4s, 12H, 4 x -COCH<sub>3</sub>) ppm;  $^{13}C$ -NMR ( $CDCl_3$ , 100 MHz):  $\delta$  170.6, 170.0, 169.4, 168.9, 166.2, 144.7, 121.0, 85.9, 75.3, 72.7, 70.5, 67.8, 61.6, 42.6, 35.3, 20.8, 20.6 (x 2), 20.2 ppm; ESI-MS HRMS: Calculated for  $C_{19}H_{26}N_4O_{10}Cl$  ( $[M+H]^+$ ): 505.1337; found 505.1330.

**Compound 13:** Yield: 92% (530 mg), m.p. 89-90 °C,  $[\alpha]_D -8.3^\circ$  ( $c = 0.4$ ,  $CHCl_3$ , 25 °C),  $^1H$ -NMR ( $CDCl_3$ , 400 MHz):  $\delta$  7.96 (s, 1H, triazole CH), 7.42-7.37 (m, 3H), 7.18-7.16 (m, 2H), 5.83 (d, 1H,  $J = 8.8$  Hz, H-1), 5.43-5.39 (m, 2H, H-2 & H-3), 5.25 (t, 1H,  $J = 9.6$  Hz, H-4), 5.09-4.79 (ABq, 2H, NCH<sub>2</sub>), 4.35-4.30 (m, 1H, H-6a), 4.18-4.15 (m, 1H, H-6b), 4.02-3.98 (m, 1H, H-5), 3.87 (s, 2H, CH<sub>2</sub>Cl), 2.11, 2.07, 2.03, 1.87 (4s, 12H, 4 x -COCH<sub>3</sub>) ppm;  $^{13}C$ -NMR ( $CDCl_3$ , 100 MHz):  $\delta$  170.7, 170.0, 169.4, 168.8, 166.4, 144.3, 141.0, 130.1, 129.1, 128.0, 122.3, 86.0, 75.3, 72.5, 70.7, 67.7, 61.5, 45.7, 42.0, 20.8, 20.6, 20.2 ppm; ESI-MS HRMS: Calculated for  $C_{25}H_{30}N_4O_{10}Cl$  ( $[M+H]^+$ ): 581.1650; found 581.1673.

#### 5. Synthesis of triazole-linked azide functionalized glycoconjugates 14 & 15:

Triazole-linked chloroacetamide functionalized glycoconjugate (12 or 13, 0.5 mmol) was dissolved in acetone (14 mL) and an aqueous solution (7 mL) of sodium azide (160 mg, 2.5

mmol) was added to it. The reaction mixture was stirred at 60 °C for 24 h. After completion of the reaction, acetone was removed by applying vacuum. Ethyl acetate (50 mL) was added to the reaction mixture and the organic layer after aqueous workup gave the desired compound (**14** or **15**).

**Compound 14:** Yield 92% (240 mg), m.p. 89-90 °C,  $[\alpha]_D$  -3.5° (c = 0.3, CHCl<sub>3</sub>, 25 °C), <sup>1</sup>H-NMR (CDCl<sub>3</sub>, 400 MHz): δ 7.84 (s, 1H, triazole C-H), 7.09 (s, 1H, NH), 5.89-5.87 (m, 1H, H-1), 5.46-5.40 (m, 2H, H-2 & H-3), 5.28-5.23 (m, 1H, H-4), 4.62-4.53 (m, 2H, NHCH<sub>2</sub>), 4.33-4.28 (m, 1H, H-6a), 4.17-4.14 (m, 1H, H-6b), 4.05-3.99 (m, 3H, H-5 & CH<sub>2</sub>N<sub>3</sub>), 2.09, 2.07, 2.03, 1.87 (4s, 12H, 4 x -COCH<sub>3</sub>) ppm; <sup>13</sup>C-NMR (CDCl<sub>3</sub>, 100 MHz): δ 170.6, 170.0, 169.4, 169.0, 167.0, 144.8, 121.1, 85.8, 75.2, 72.6, 70.5, 67.7, 61.5, 52.6, 34.8, 20.8, 20.6 (x 2), 20.2 ppm; ESI-MS HRMS: Calculated for C<sub>19</sub>H<sub>25</sub>N<sub>7</sub>O<sub>10</sub>Na ([M+Na]<sup>+</sup>): 534.1561; found 534.1556.

**Compound 15:** Yield 94% (275 mg), m.p. 81-84 °C,  $[\alpha]_D$  -22.7° (c = 0.3, CHCl<sub>3</sub>, 25 °C), <sup>1</sup>H-NMR (CDCl<sub>3</sub>, 400 MHz): δ 7.97 (s, 1H, triazole C-H), 7.41-7.37 (m, 3H), 7.14-7.12 (m, 2H), 5.84 (d, 1H, J = 8.8 Hz, H-1), 5.46-5.37 (m, 2H, H-2 & H-3), 5.26 (t, 1H, J = 9.6 Hz, H-4), 5.09-4.80 (ABq, 2H, NHCH<sub>2</sub>-), 4.35-4.30 (m, 1H, H-6a), 4.18-4.15 (m, 1H, H-6b), 4.03-3.99 (m, 1H, H-5), 3.64-3.61 (m, 2H, CH<sub>2</sub>N<sub>3</sub>), 2.11, 2.07, 2.03, 1.87 (4s, 12H, 4 x -COCH<sub>3</sub>) ppm; <sup>13</sup>C-NMR (CDCl<sub>3</sub>, 100 MHz): δ 170.7, 170.0, 169.4, 168.9, 167.6, 144.3, 140.5, 130.2, 129.1, 128.0, 122.3, 85.9, 75.2, 72.5, 70.7, 67.7, 61.5, 50.9, 45.3, 20.8, 20.6, 20.2 ppm; ESI-MS HRMS: Calculated for C<sub>25</sub>H<sub>30</sub>N<sub>7</sub>O<sub>10</sub> ([M+H]<sup>+</sup>): 588.2054; found 588.2048.

#### 6. Synthesis of bis-triazole-linked glycolipids **17**, **18**, & **19**:

Synthesis was done following the same procedure as that of compounds **4** and **6**.

**Compound 17:** Yield 94% (240 mg),  $[\alpha]_D$  +23.5° (c = 0.2, CHCl<sub>3</sub>, 25 °C), <sup>1</sup>H-NMR (CDCl<sub>3</sub>, 400 MHz): δ 8.32 (s, 1H, triazole C-H), 7.86 (s, 1H, triazole C-H), 7.33 (s, 1H, NH), 5.87-5.85 (m, 1H, H-1), 5.43-5.41 (m, 2H, H-2 & H-3), 5.27-5.23 (m, 1H, H-4), 5.16-5.08 (m, 2H, COCH<sub>2</sub>-N), 4.56-4.54 (m, 2H, -O-CH<sub>2</sub>-triazole), 4.35-4.28 (m, 3H, H-6a & O-CH<sub>2</sub>-CH<sub>2</sub>-), 4.18-4.14 (m, 1H, H-6b), 4.04-4.02 (m, 1H, H-5), 2.07, 2.02, 1.84 (3s, 12H, 4 x -COCH<sub>3</sub>), 1.77-1.72 (m, 2H, O-CH<sub>2</sub>-CH<sub>2</sub>-), 1.40-1.26 (bs, 10H, 5 x CH<sub>2</sub>), 0.88 (t, 3H, -CH<sub>3</sub>) ppm; <sup>13</sup>C-NMR (CDCl<sub>3</sub>, 100 MHz): δ 170.6, 170.0, 169.4, 169.0, 164.7, 160.7, 144.6, 140.7, 129.3, 121.5, 85.9, 75.3, 72.6, 70.6, 67.8, 65.6, 61.6, 52.7, 35.2, 31.9, 29.3, 29.2, 28.7, 26.0, 22.7, 20.8, 20.7, 20.6, 20.2, 14.1 ppm; ESI-MS HRMS: Calculated for C<sub>30</sub>H<sub>45</sub>N<sub>7</sub>O<sub>11</sub>K ([M+K]<sup>+</sup>): 718.2814; found 718.2816.

**Compound 18:** Yield 92% (275 mg),  $[\alpha]_D$  +22.8° (c = 0.3, CHCl<sub>3</sub>, 25 °C), <sup>1</sup>H-NMR (CDCl<sub>3</sub>, 400 MHz): δ 8.29 (s, 1H, triazole C-H), 7.85 (s, 1H, triazole C-H), 7.26-7.18 (m, 2H, 2x NH), 5.87-85 (d, 1H, H-1), 5.43-5.41 (m, 2H, H-2 & H-3), 5.29-5.25 (m, 1H, H-4), 5.14 (s, 2H, N-CH<sub>2</sub>-CO), 4.53-4.52 (m, 2H, NH-CH<sub>2</sub>-triazole), 4.32-4.28 (m, 1H, H-6a), 4.19-4.15 (m, 1H, H-6b), 4.04-4.02 (m, 1H, H-5), 3.45-3.40 (m, 2H, CO-NH-CH<sub>2</sub>), 2.07, 2.06, 2.02, 1.85 (4s, 12H, 4 x -COCH<sub>3</sub>), 1.62-1.59 (m, 2H, NH-CH<sub>2</sub>-CH<sub>2</sub>), 1.25 (bs, 18H, 9 x CH<sub>2</sub>), 0.87 (t, 3H, -CH<sub>3</sub>) ppm; <sup>13</sup>C-NMR (CDCl<sub>3</sub>, 100 MHz): δ 170.6, 170.0, 169.4, 169.1, 164.9, 159.8, 144.6, 144.0, 127.2, 121.5, 85.9, 75.3, 72.6, 70.6, 67.8, 61.6, 52.9, 39.4, 35.1, 32.0, 29.8, 29.7, 29.6, 29.4, 27.1, 22.8, 20.8, 20.6, 20.2, 14.2 ppm; ESI-MS HRMS: Calculated for C<sub>34</sub>H<sub>52</sub>N<sub>8</sub>O<sub>11</sub>Na ([M+Na]<sup>+</sup>): 771.3653; found 771.3659.

**Compound 19:** Yield 92% (275 mg),  $[\alpha]_D$  -26.5° (c = 0.3, CHCl<sub>3</sub>, 25 °C), <sup>1</sup>H-NMR (CDCl<sub>3</sub>, 400 MHz): δ 8.20 (s, 1H, triazole C-H), 7.91 (s, 1H, triazole C-H), 7.48-7.43 (m, 3H), 7.26-7.23 (m, 2H), 7.11 (t, 1H, NH), 5.82 (d, 1H, J = 8.8 Hz, H-1), 5.43-5.36 (m, 2H, H-2 & H-3), 5.26 (t, 1H, J = 9.6 Hz, H-4), 5.14-4.75 (m, 4H, CO-CH<sub>2</sub>-triazole & N-CH<sub>2</sub>-triazole), 4.33-4.29 (m, 1H, H-6a), 4.19-4.16 (m, 1H, H-6b), 4.01-3.97 (m, 1H, H-5), 3.45-3.40 (m, 2H,

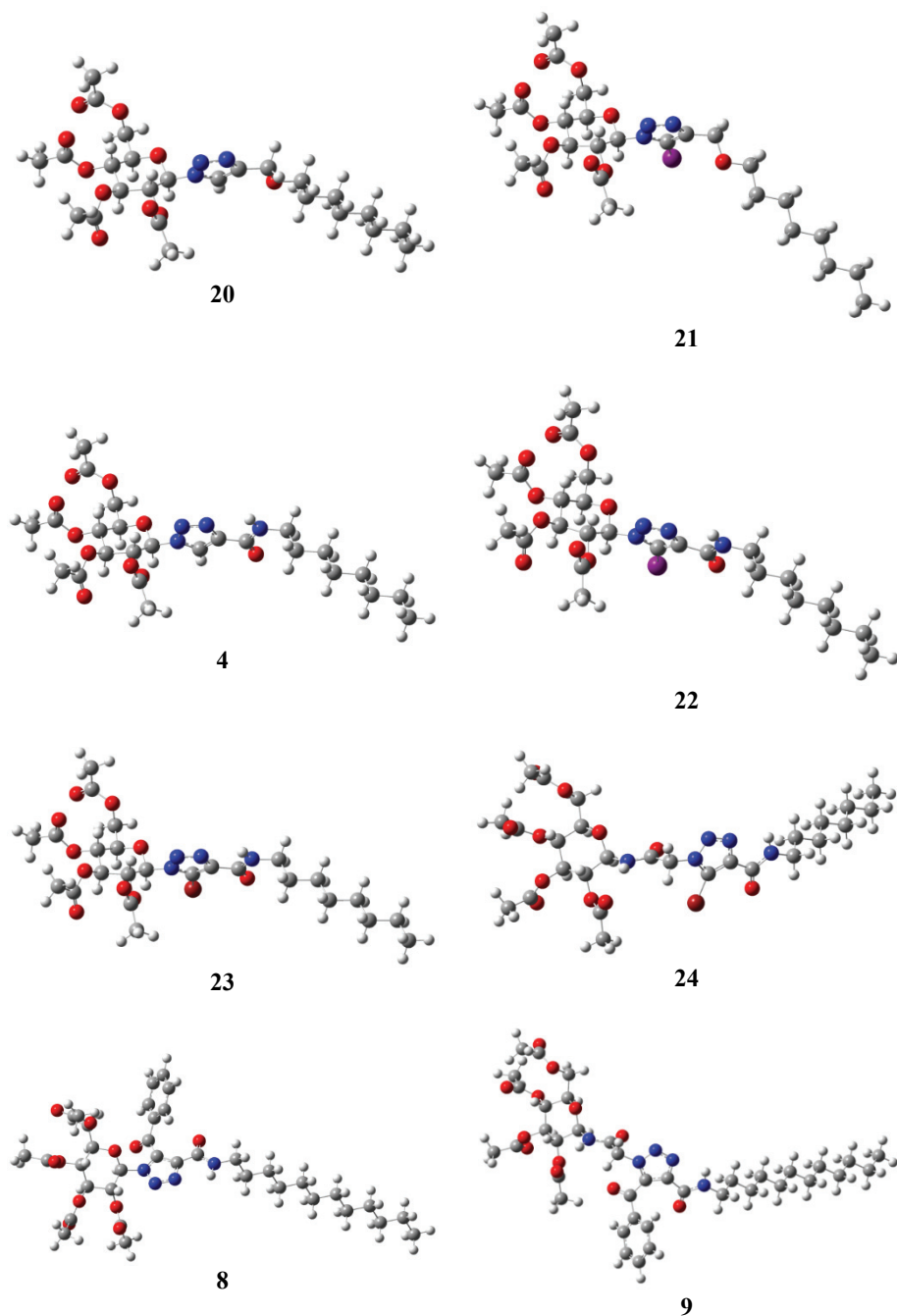
NH-CH<sub>2</sub>), 2.10, 2.06, 2.04, 1.88 (4s, 12H, 4 x -COCH<sub>3</sub>), 1.62-1.58 (m, 2H, CO-NH-CH<sub>2</sub>-CH<sub>2</sub>), 1.37-1.26 (bs, 18H, 9 x CH<sub>2</sub>), 0.87 (t, 3H, -CH<sub>3</sub>) ppm; <sup>13</sup>C-NMR (CDCl<sub>3</sub>, 100 MHz): δ 170.6, 170.0, 169.3, 168.9, 164.6, 160.0, 144.0, 143.7, 140.2, 130.5, 129.5, 128.3, 127.3, 122.5, 86.0, 75.4, 72.5, 70.9, 67.9, 61.5, 51.7, 45.6, 39.3, 32.0, 29.7, 29.6, 29.4, 27.0, 22.8, 20.8, 20.6, 20.3, 14.2 ppm; ESI-MS HRMS: Calculated for C<sub>40</sub>H<sub>56</sub>N<sub>8</sub>O<sub>11</sub>K ([M+K]<sup>+</sup>): 863.3705; found 863.3708.

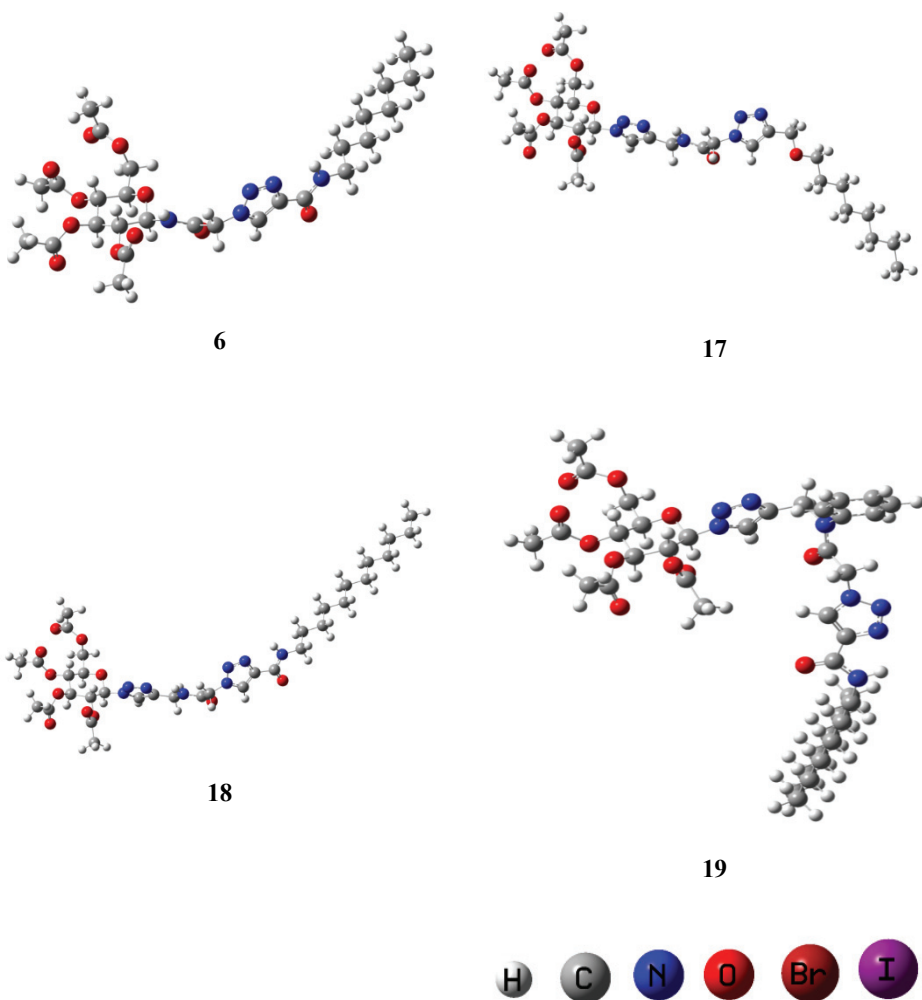
C. Optimized structures of the synthesized glycolipids<sup>1</sup>

To understand the stability of the glycolipids, the geometries of these molecules were optimized using B3LYP density functional theory method. The optimized structures thus obtained were used for frequency calculations. In each case, positive frequencies were obtained, which implies that the optimized structures have the minimum potential energy surfaces and hence are stable. The optimized energies, zero point energies, and the energies obtained after zero point energy correction are given in Table S-I. Table S-I also includes the corresponding computed dipole moments of the optimized structures.

TABLE S-I. The computed optimized energies and dipole moments of different glycolipids

Glycolipids	Energy (Hartree)	Zero Point Energy (ZPE) (Hartree)	ZPE corrected Energy (Hartree)	Dipole moment (Debye)
Compound <b>20</b>	-1892.6572228	0.6452809	-1892.011942	4.6002
Compound <b>21</b>	-2188.4529957	0.6300699	-2187.822926	4.2163
Compound <b>4</b>	-1946.8434404	0.640086	-1946.203354	1.7310
Compound <b>22</b>	-2242.6021772	0.6249956	-2241.977182	1.4714
Compound <b>23</b>	-4517.9400722	0.6300275	-4517.310045	1.2438
Compound <b>24</b>	-4725.9556611	0.685842	-4725.269819	4.7129
Compound <b>8</b>	-2448.4788797	0.8450222	-2447.633858	1.9814
Compound <b>9</b>	-2656.4962833	0.9017656	-2655.594518	4.2192
Compound <b>6</b>	-2154.8592204	0.6963938	-2154.162827	5.9574
Compound <b>17</b>	-2381.0080409	0.7691367	-2380.238904	7.9441
Compound <b>18</b>	-2592.4501362	0.8781671	-2591.571969	8.1417
Compound <b>19</b>	-2823.4965783	0.9592672	-2822.537311	2.1175





## REFERENCES

1. *GAUSSIAN 09, REVISION D.01*, GAUSSIAN, INC., WALLINGFORD, CT, 2013.

## TABLE OF FIGURES

- Figure S1**  $^1\text{H}$  NMR (400 MHz,  $\text{CDCl}_3$ ) spectrum of **4**
- Figure S2**  $^{13}\text{C}$  NMR (100 MHz,  $\text{CDCl}_3$ ) spectrum of **4**
- Figure S3**  $^1\text{H}$  NMR (400 MHz,  $\text{CDCl}_3$ ) spectrum of **6**
- Figure S4**  $^{13}\text{C}$  NMR (100 MHz,  $\text{CDCl}_3$ ) spectrum of **6**
- Figure S5**  $^1\text{H}$  NMR (400 MHz,  $\text{CDCl}_3$ ) spectrum of **7**
- Figure S6**  $^{13}\text{C}$  NMR (100 MHz,  $\text{CDCl}_3$ ) spectrum of **7**
- Figure S7**  $^1\text{H}$  NMR (400 MHz,  $\text{CDCl}_3$ ) spectrum of **8**
- Figure S8**  $^{13}\text{C}$  NMR (100 MHz,  $\text{CDCl}_3$ ) spectrum of **8**
- Figure S9**  $^1\text{H}$  NMR (400 MHz,  $\text{CDCl}_3$ ) spectrum of **9**
- Figure S10**  $^{13}\text{C}$  NMR (100 MHz,  $\text{CDCl}_3$ ) spectrum of **9**
- Figure S11**  $^1\text{H}$  NMR (400 MHz,  $\text{CDCl}_3$ ) of compound **11**
- Figure S12**  $^{13}\text{C}$  NMR (100 MHz,  $\text{CDCl}_3$ ) of compound **11**
- Figure S13**  $^1\text{H}$  NMR (400 MHz,  $\text{CDCl}_3$ ) of compound **12**
- Figure S14**  $^{13}\text{C}$  NMR (100 MHz,  $\text{CDCl}_3$ ) of compound **12**
- Figure S15**  $^1\text{H}$  NMR (400 MHz,  $\text{CDCl}_3$ ) of compound **13**
- Figure S16**  $^{13}\text{C}$  NMR (100 MHz,  $\text{CDCl}_3$ ) of compound **13**
- Figure S17**  $^1\text{H}$  NMR (400 MHz,  $\text{CDCl}_3$ ) of compound **14**
- Figure S18**  $^{13}\text{C}$  NMR (100 MHz,  $\text{CDCl}_3$ ) of compound **14**
- Figure S19**  $^1\text{H}$  NMR (400 MHz,  $\text{CDCl}_3$ ) of compound **15**
- Figure S20**  $^{13}\text{C}$  NMR (100 MHz,  $\text{CDCl}_3$ ) of compound **15**
- Figure S21**  $^1\text{H}$  NMR (400 MHz,  $\text{CDCl}_3$ ) of compound **17**
- Figure S22**  $^{13}\text{C}$  NMR (100 MHz,  $\text{CDCl}_3$ ) of compound **17**
- Figure S23**  $^1\text{H}$  NMR (400 MHz,  $\text{CDCl}_3$ ) of compound **18**
- Figure S24**  $^{13}\text{C}$  NMR (100 MHz,  $\text{CDCl}_3$ ) of compound **18**
- Figure S25**  $^1\text{H}$  NMR (400 MHz,  $\text{CDCl}_3$ ) of compound **19**
- Figure S26**  $^{13}\text{C}$  NMR (100 MHz,  $\text{CDCl}_3$ ) of compound **19**

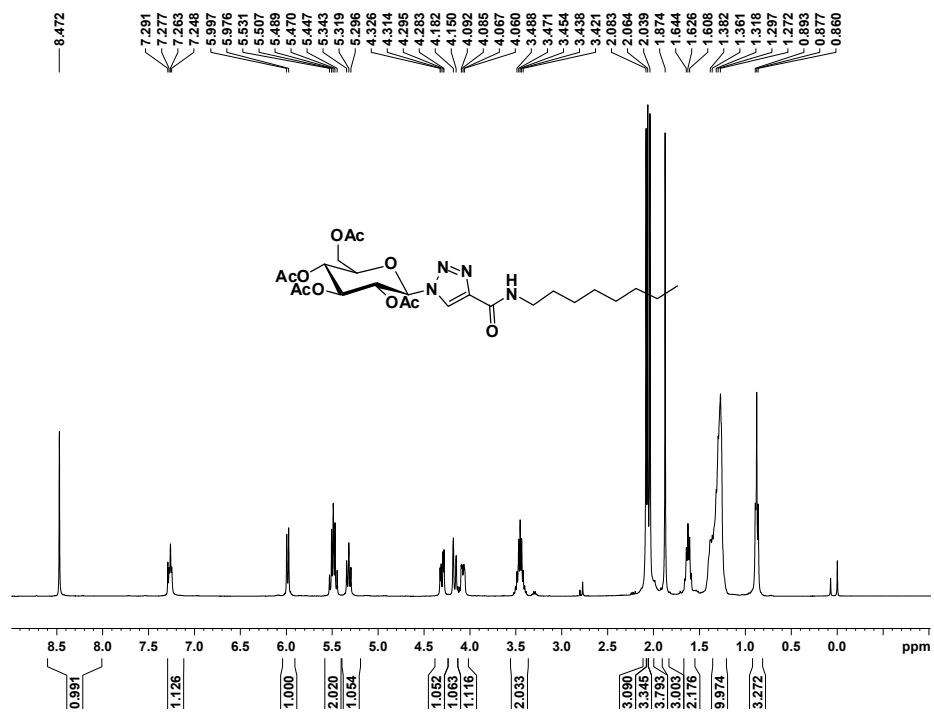


Figure S1  $^1\text{H}$  NMR (400 MHz,  $\text{CDCl}_3$ ) spectrum of 4

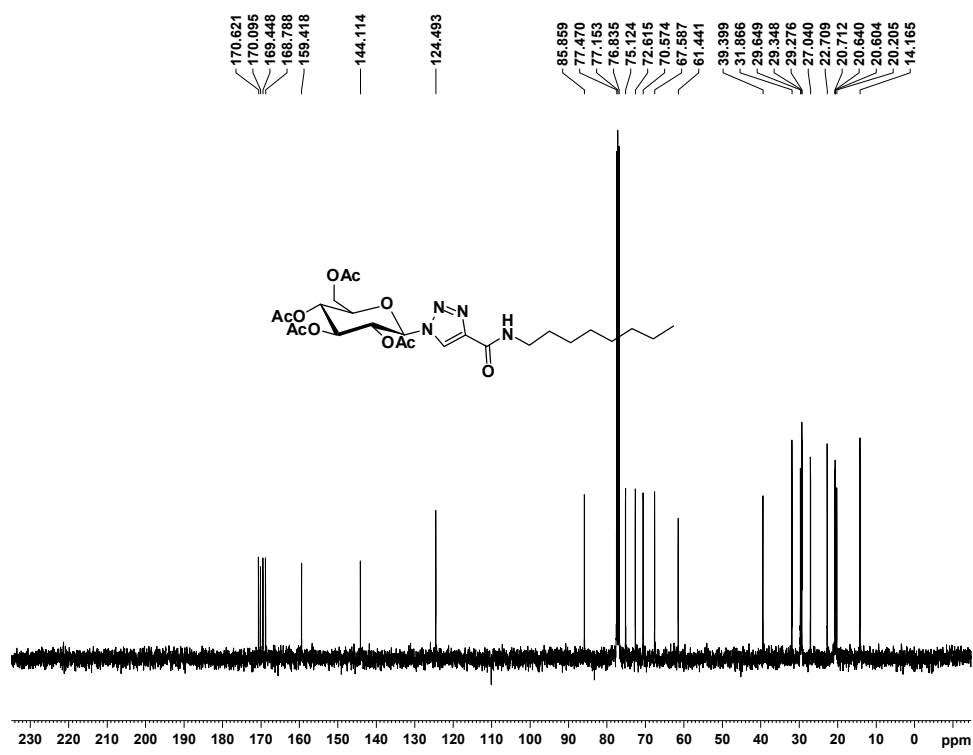


Figure S2  $^{13}\text{C}$  NMR (100 MHz,  $\text{CDCl}_3$ ) spectrum of 4

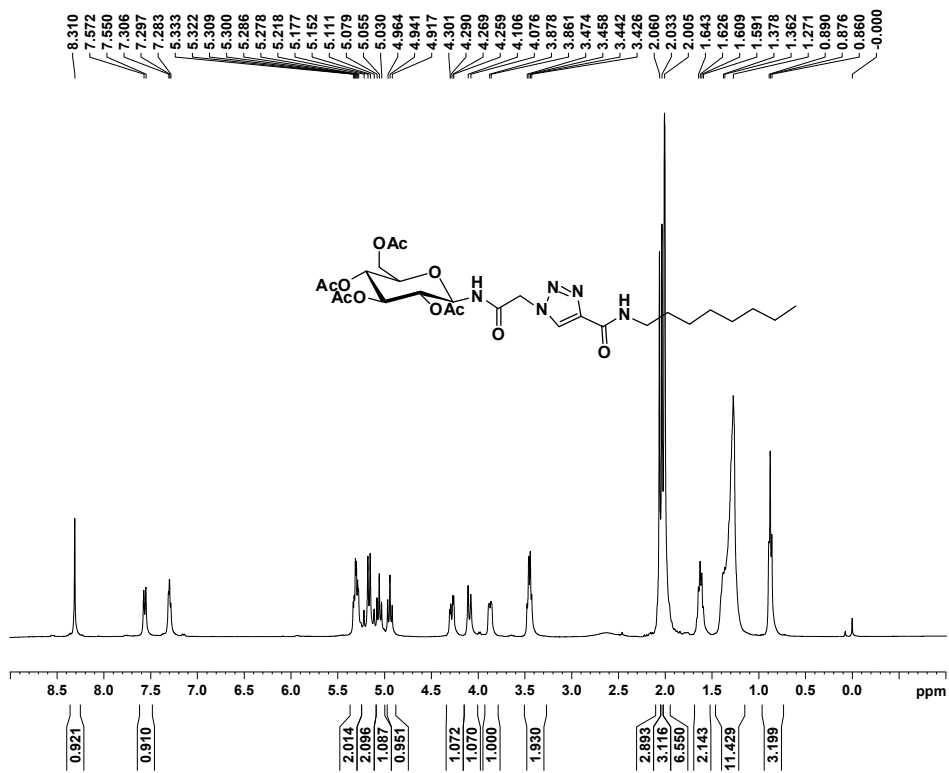
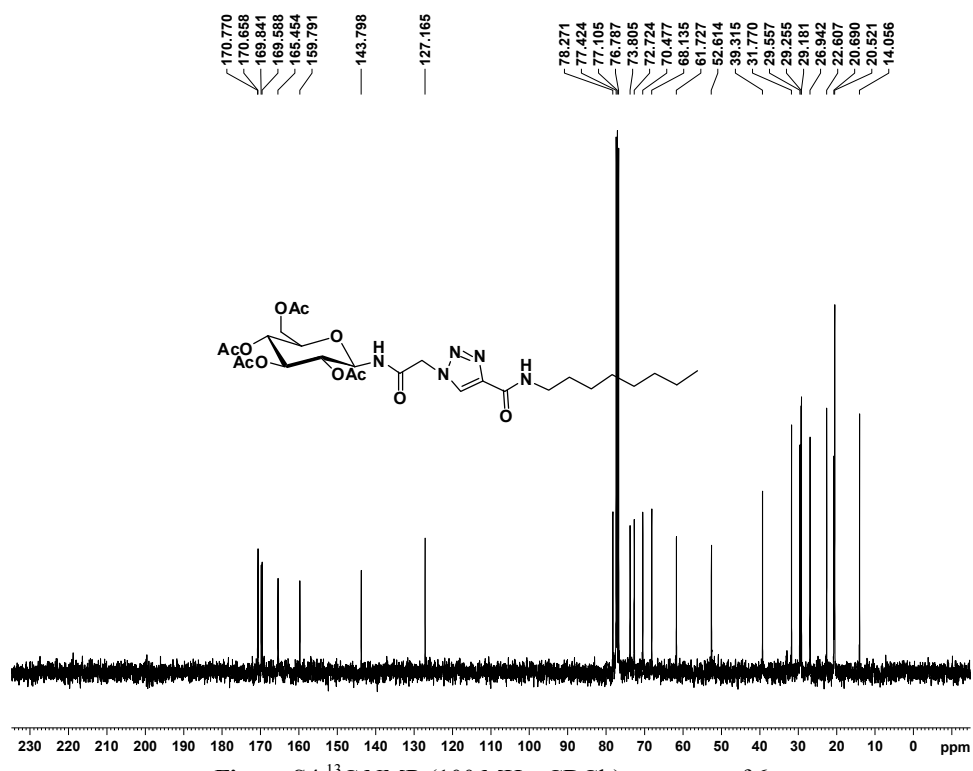
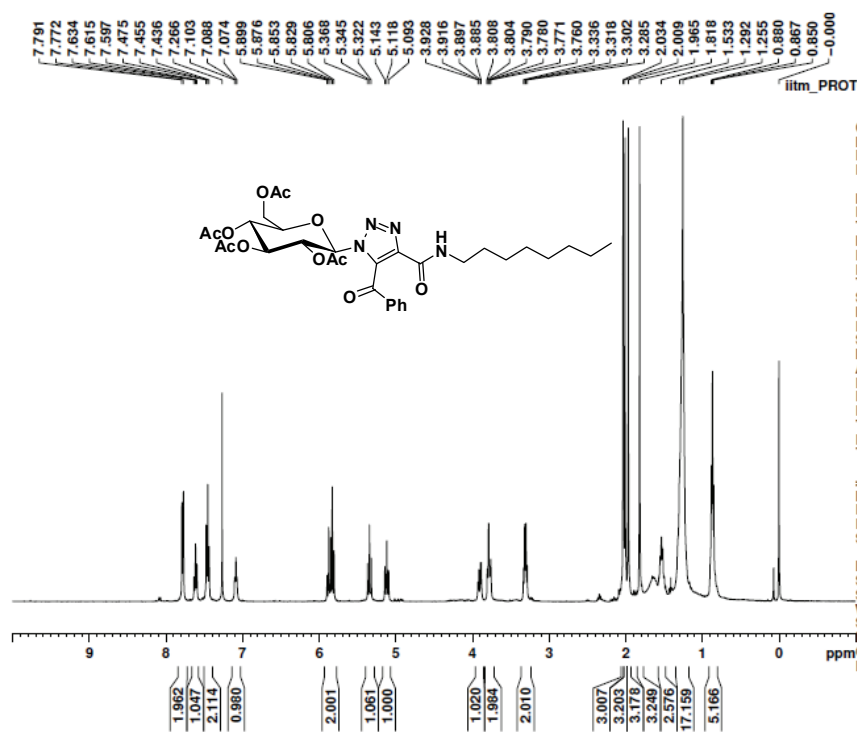


Figure S3 <sup>1</sup>H NMR (400 MHz, CDCl<sub>3</sub>) spectrum of 6



**Figure S4**  $^{13}\text{C}$  NMR (100 MHz,  $\text{CDCl}_3$ ) spectrum of **6**



**Figure S5** <sup>1</sup>H NMR (400 MHz, CDCl<sub>3</sub>) spectrum of **7**

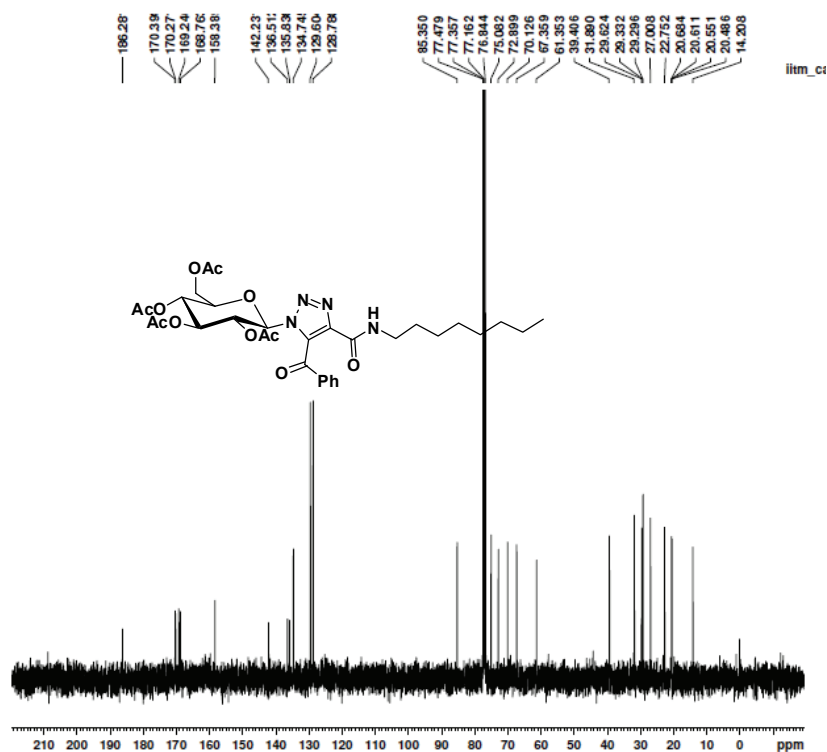


**Figure S6**  $^{13}\text{C}$  NMR (100 MHz,  $\text{CDCl}_3$ ) spectrum of 7

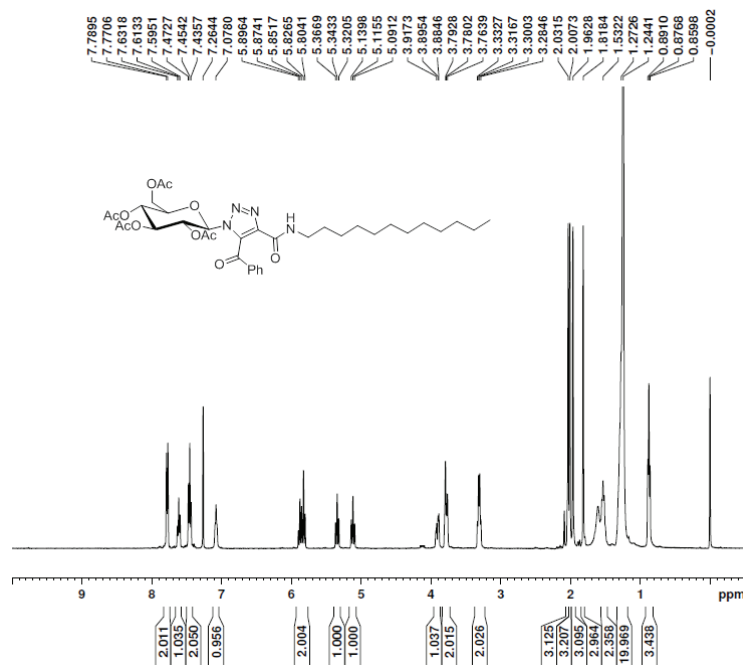


**Figure S7** <sup>1</sup>H NMR (400 MHz, CDCl<sub>3</sub>) spectrum of **8**

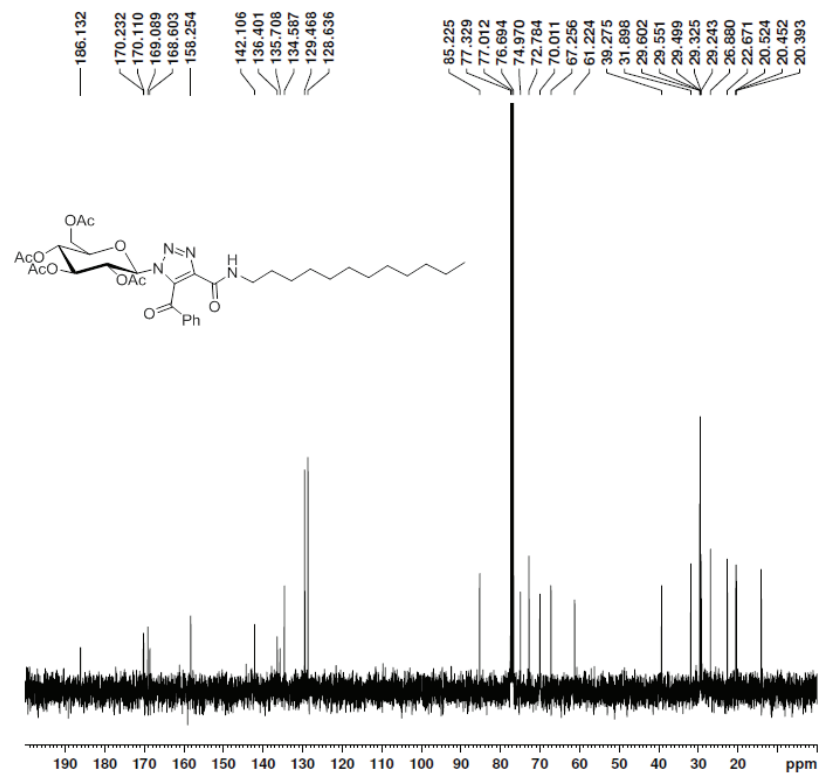


**Figure S8**  $^{13}\text{C}$  NMR (100 MHz,  $\text{CDCl}_3$ ) spectrum of **8**

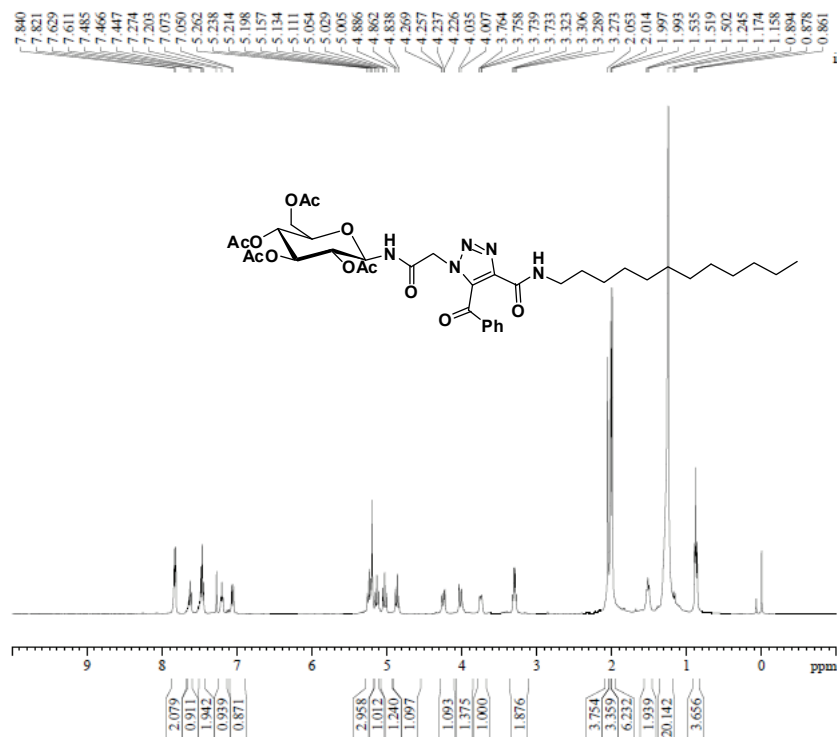


**Figure S9** <sup>1</sup>H NMR (400 MHz, CDCl<sub>3</sub>) spectrum of **9**

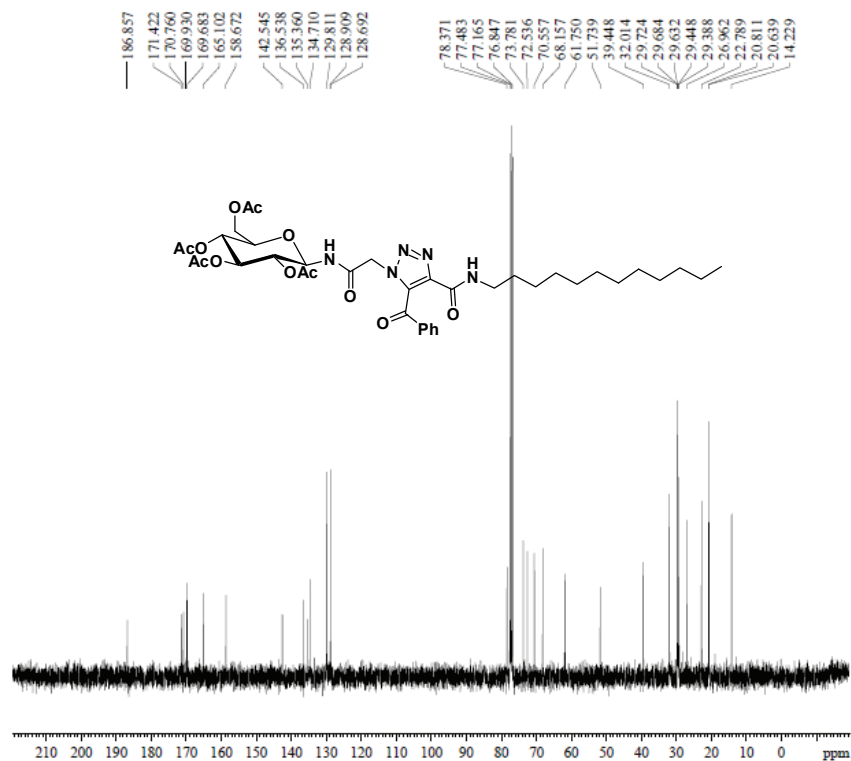


**Figure S10**  $^{13}\text{C}$  NMR (100 MHz,  $\text{CDCl}_3$ ) spectrum of **9**

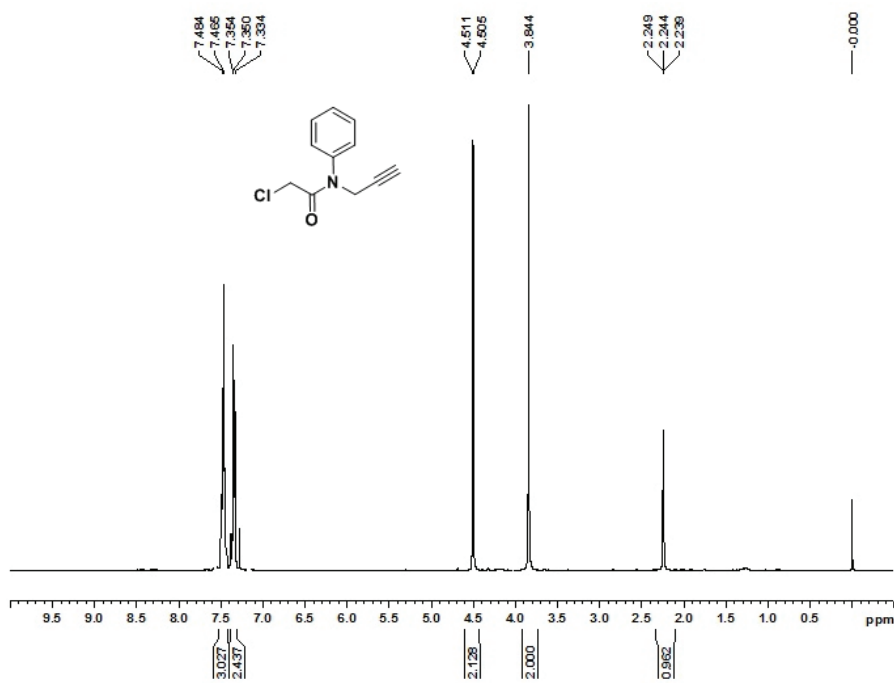


**Figure S11**  $^1\text{H}$  NMR (400 MHz,  $\text{CDCl}_3$ ) of compound 11

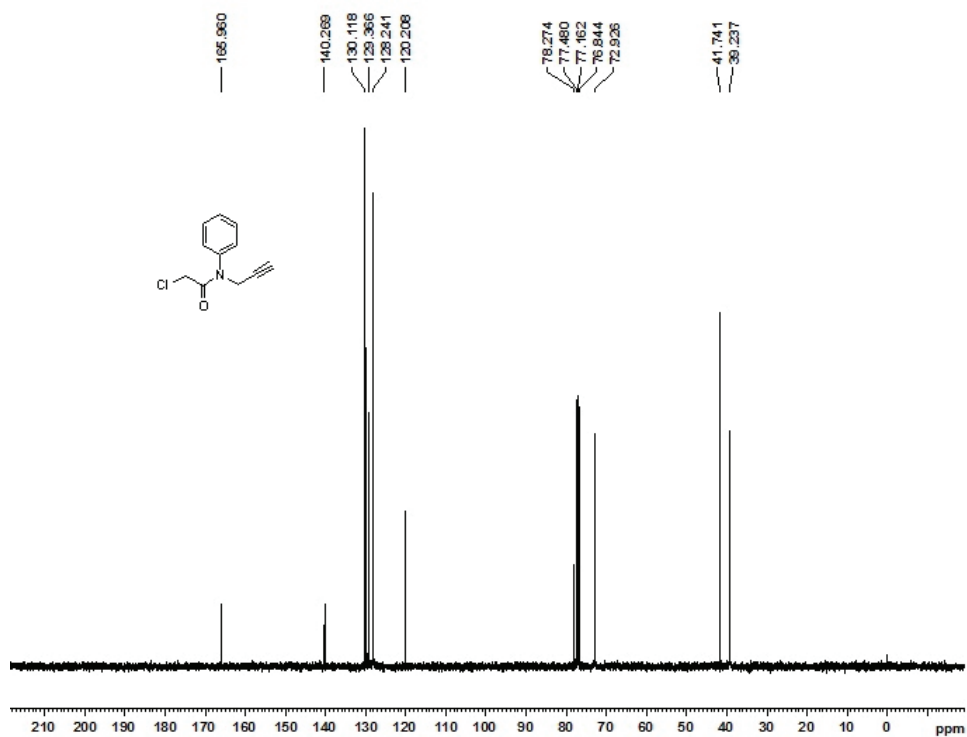


**Figure S12**  $^{13}\text{C}$  NMR (100 MHz,  $\text{CDCl}_3$ ) of compound 11

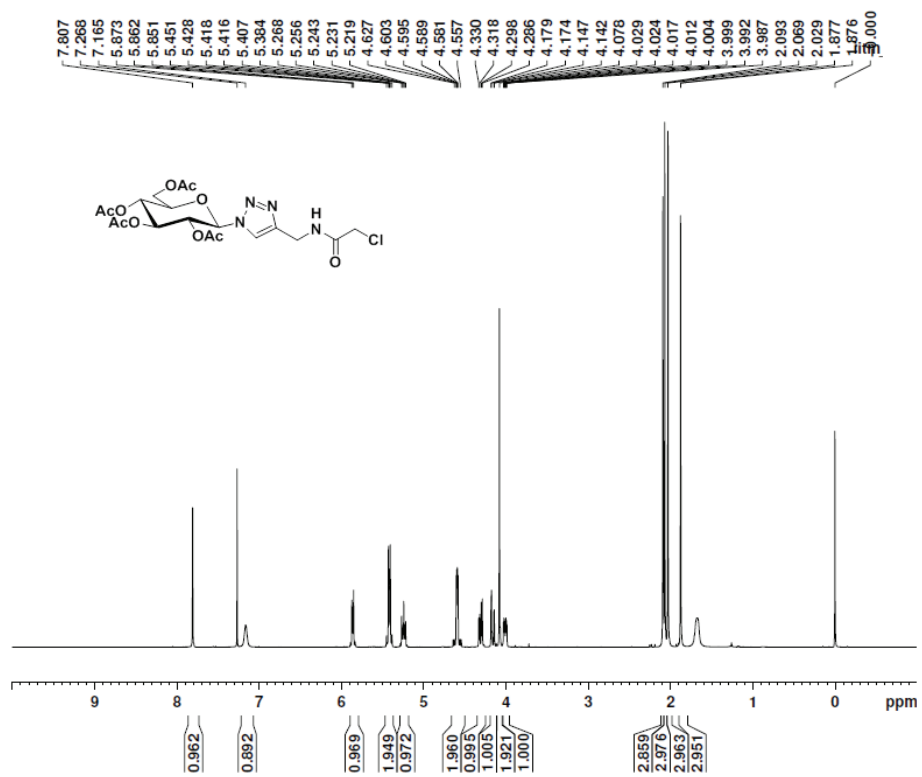
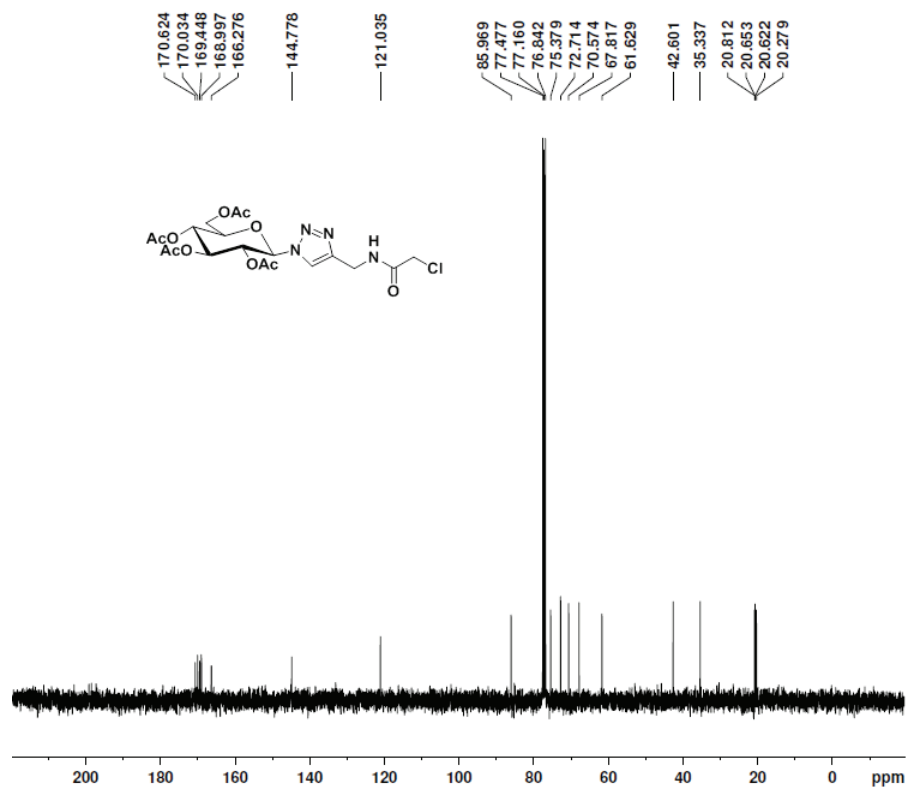
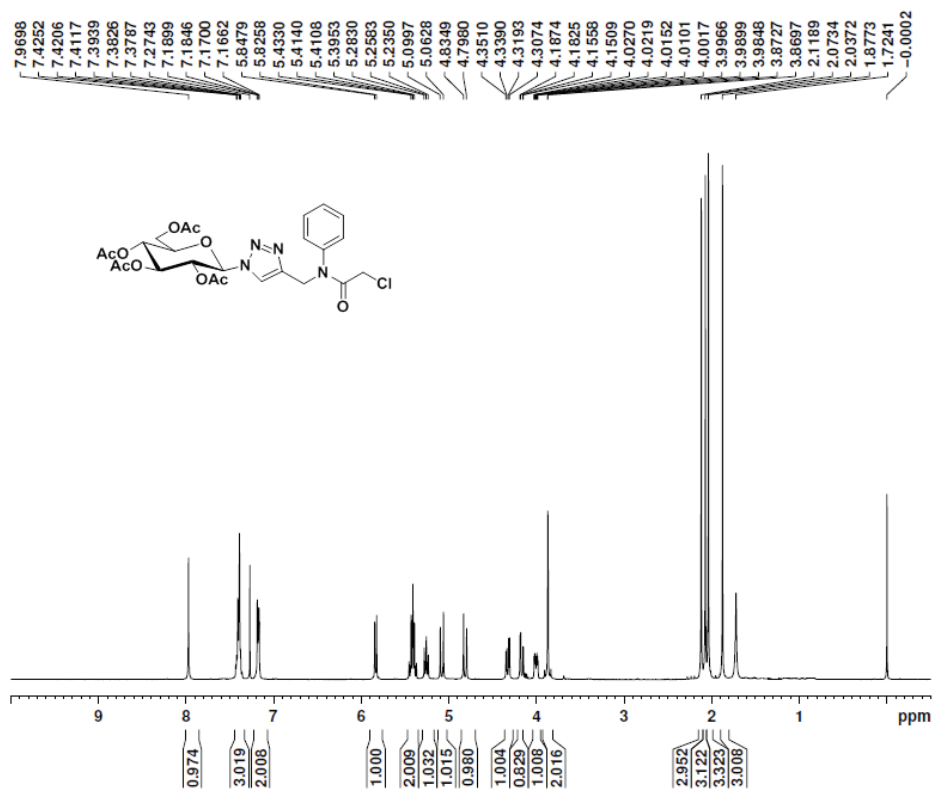


Figure S13 <sup>1</sup>H NMR (400 MHz, CDCl<sub>3</sub>) of compound 12



**Figure S14**  $^{13}\text{C}$  NMR (100 MHz,  $\text{CDCl}_3$ ) of compound 12



**Figure S15** <sup>1</sup>H NMR (400 MHz, CDCl<sub>3</sub>) of compound 13

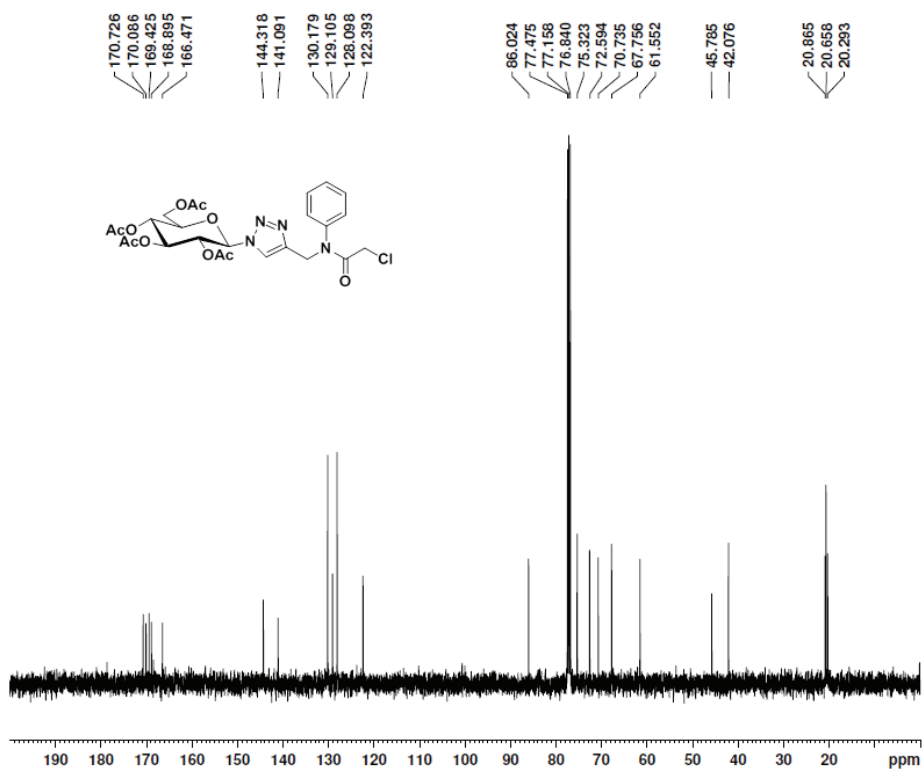


**Figure S16**  $^{13}\text{C}$  NMR (100 MHz,  $\text{CDCl}_3$ ) of compound 13

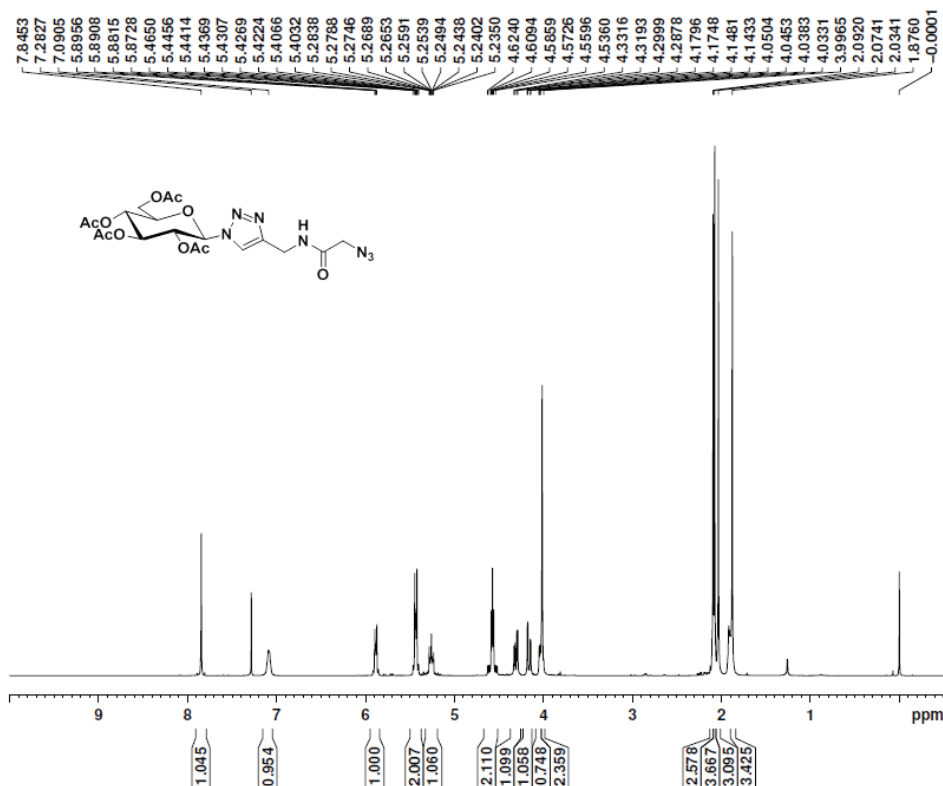


**Figure S17** <sup>1</sup>H NMR (400 MHz, CDCl<sub>3</sub>) of compound 14

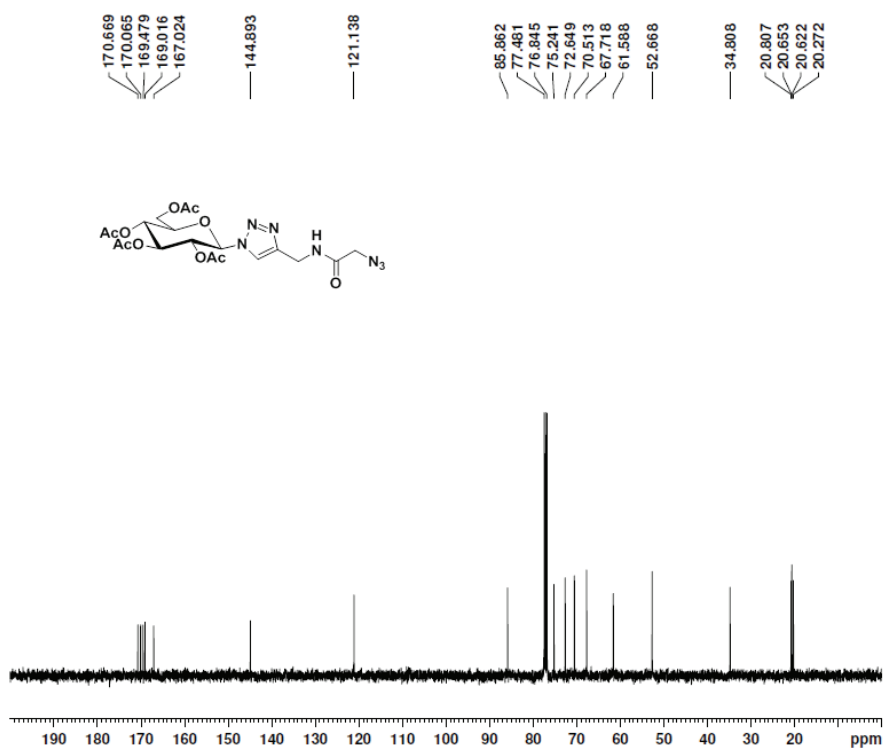


**Figure S18**  $^{13}\text{C}$  NMR (100 MHz,  $\text{CDCl}_3$ ) of compound 14

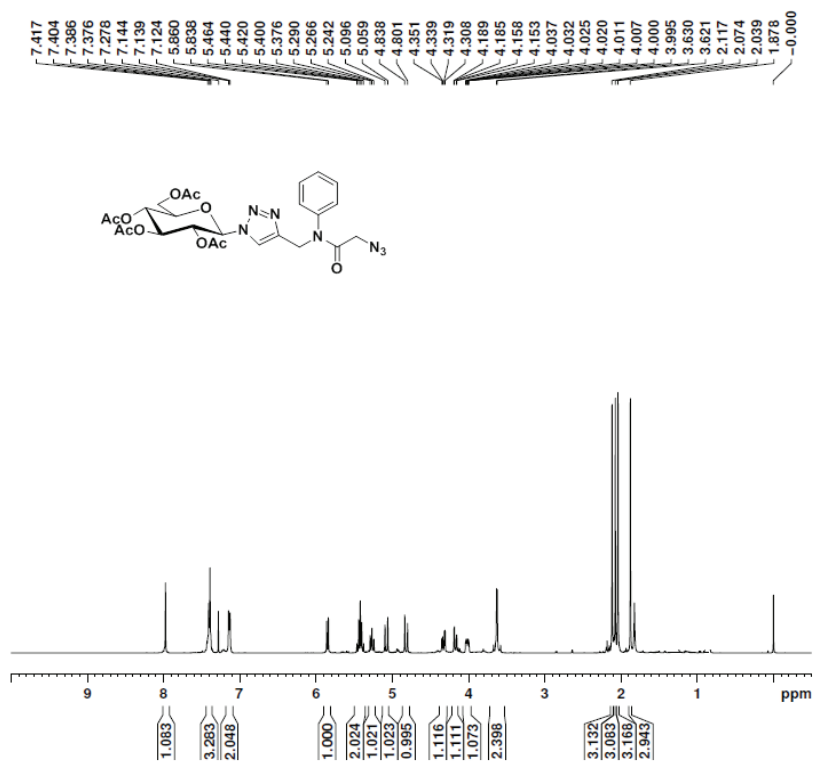
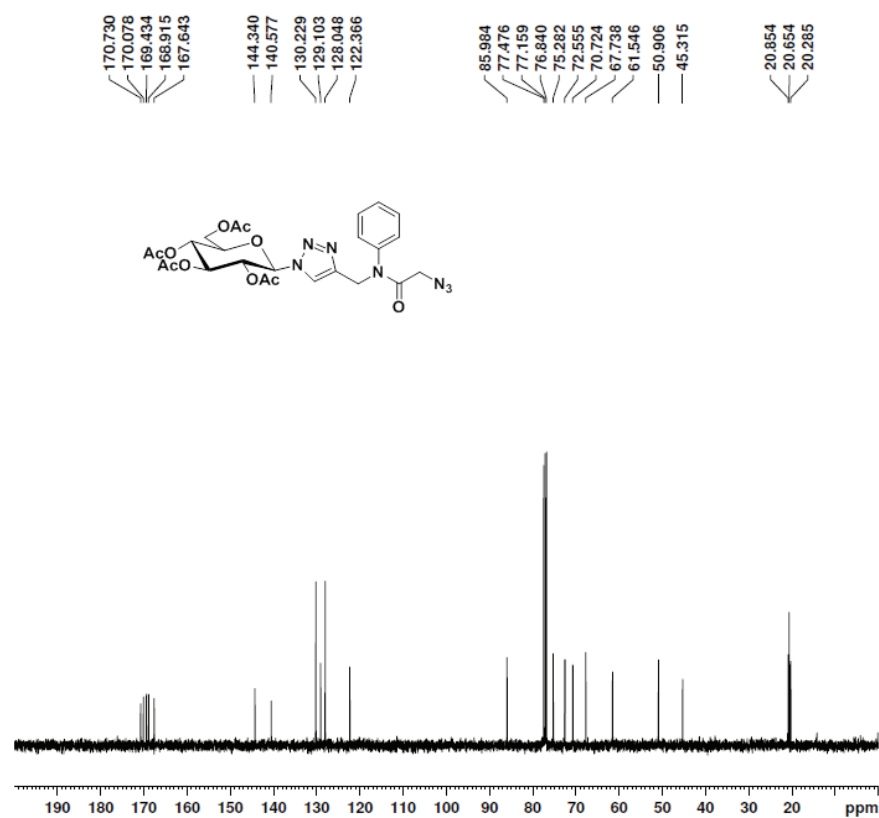
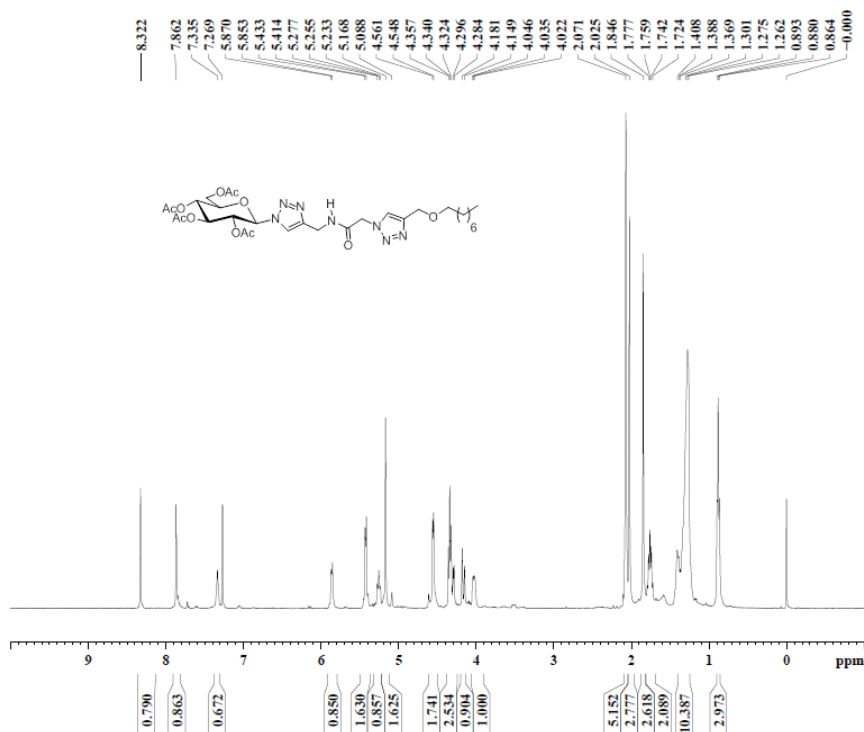


Figure S19 <sup>1</sup>H NMR (400 MHz, CDCl<sub>3</sub>) of compound 15



**Figure S20**  $^{13}\text{C}$  NMR (100 MHz,  $\text{CDCl}_3$ ) of compound 15



**Figure S21** <sup>1</sup>H NMR (400 MHz, CDCl<sub>3</sub>) of compound 17

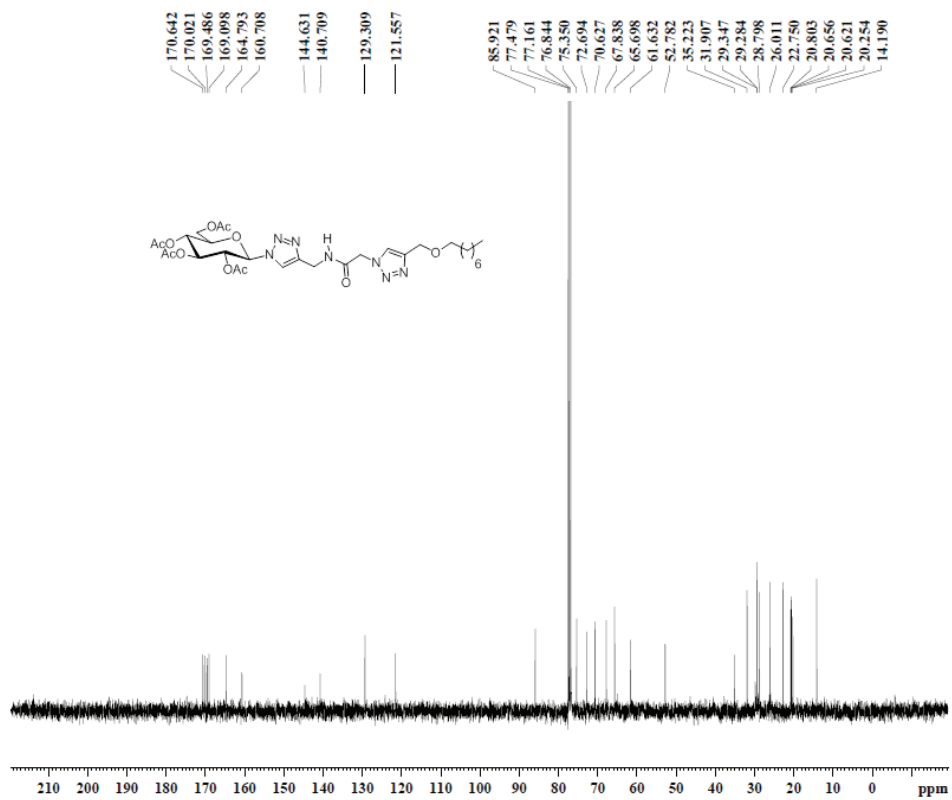


**Figure S22**  $^{13}\text{C}$  NMR (100 MHz,  $\text{CDCl}_3$ ) of compound **17**

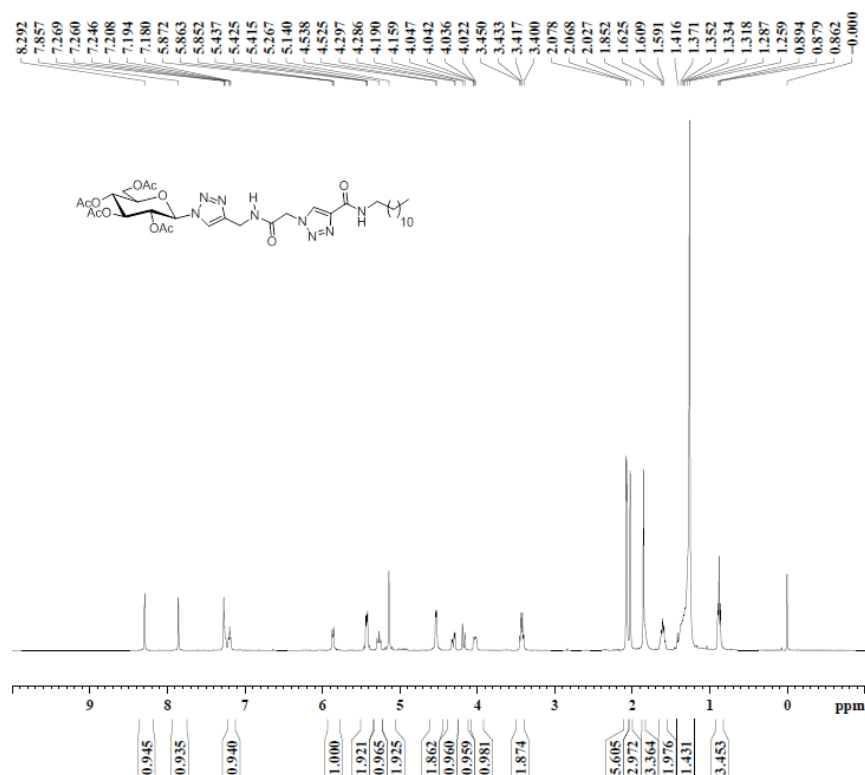
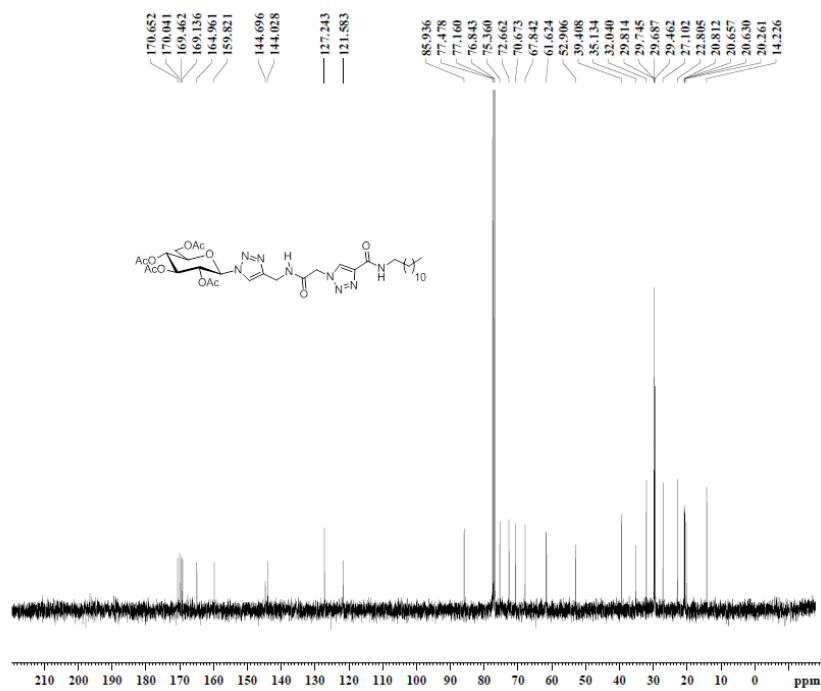


Figure S23  $^1\text{H}$  NMR (400 MHz,  $\text{CDCl}_3$ ) of compound 18



**Figure S24**  $^{13}\text{C}$  NMR (100 MHz,  $\text{CDCl}_3$ ) of compound 18

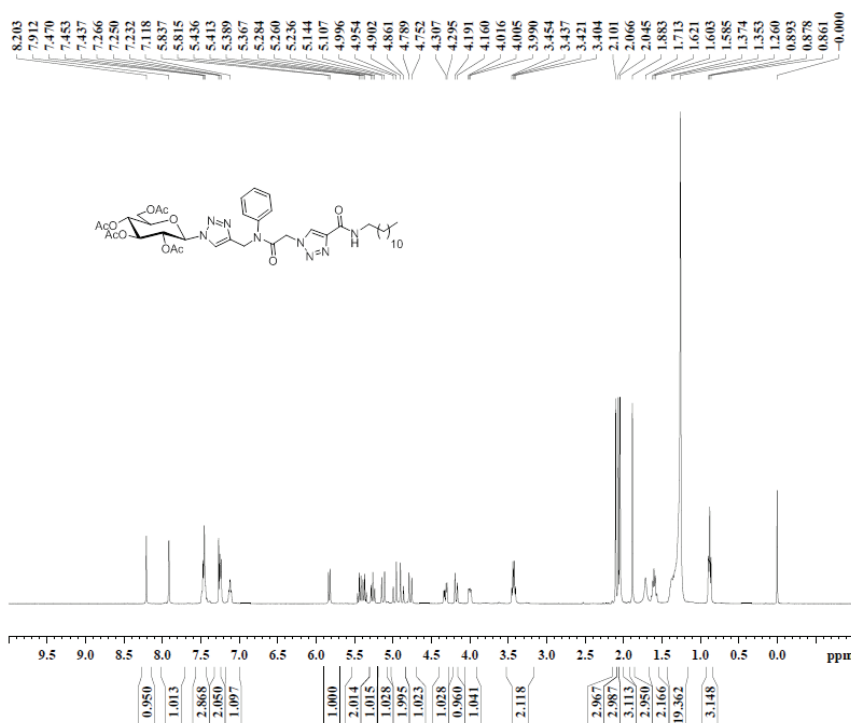
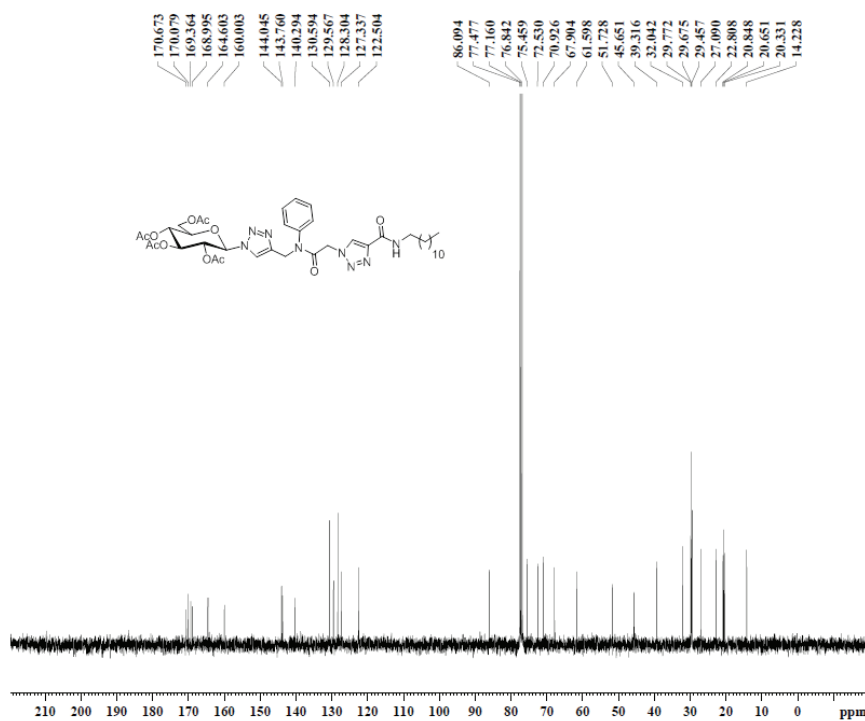


Figure S25  $^1\text{H}$  NMR (400 MHz,  $\text{CDCl}_3$ ) of compound 19



**Figure S26**  $^{13}\text{C}$  NMR (100 MHz,  $\text{CDCl}_3$ ) of compound **19**.





## Post-TRIzol protein extraction from peripheral blood mononuclear cells

JOVANA STEVANOVIĆ, DRAGANA ROBAJAC<sup>#</sup>, OLGICA NEDIĆ<sup>#</sup>  
and ZORANA DOBRIJEVIĆ\*

Institute for the Application of Nuclear Energy, University of Belgrade, Banatska 31b,  
11080 Belgrade, Serbia

(Received 30 March, revised 27 April, accepted 8 July 2023)

**Abstract:** After sample processing for RNA and DNA analysis, the leftover protein pellets are usually discarded due to the limited efficiency of pellet reconstitution/solubilisation. As the pelleted proteins are tightly packed, they are most often solubilised using chaotropic agents (e.g., guanidine hydrochloride or urea), detergents (e.g., SDS), salts (NaCl) or basic buffer (Tris). The aim of this study was to define and optimise the procedure for the efficient extraction of proteins from human peripheral blood mononuclear cells (PBMCs), obtained by a single blood draw and lysed in TRIzol reagent, by varying experimental conditions in terms of protein precipitation solvent (iso-propanol or acetone), washing (with or without guanidine hydrochloride) and solubilisation solution (containing SDS, NaCl, urea and/or Tris). We evaluated the efficacy of the final, optimised protocol to solubilise both small cytoplasmic and larger transmembrane proteins, and the compatibility with methods employed for the subsequent analysis of protein posttranslational modifications, such as glycosylation. The optimised protocol for the extraction and isolation of post-TRIzol leftover proteins from PBMCs can be defined as follows: protein precipitation from the organic phase with ice-cold acetone, pellet washing with absolute ethanol and solubilisation in 1 % SDS, employing 20 min heating at 50 °C and vortexing.

**Keywords:** protein solubilisation; TRIzol extraction; PBMC.

### INTRODUCTION

Extraction of RNA, DNA and proteins from the same sample enables the exploration of cellular mechanisms at different levels of gene expression. A comprehensive evaluation of RNA-based and protein-based changes related to physiological and pathological stimuli is crucial for understanding the molecular basis

\* Corresponding author. E-mail: zorana.dobrijevic@inep.co.rs

<sup>#</sup> Serbian Chemical Society member.

<https://doi.org/10.2298/JSC230330037S>

of cellular processes, due to the dynamics and the complexity of gene regulation. Simultaneous extraction of different types of biomolecules becomes extremely important when experimental samples are hard to obtain and/or process, or when the number of harvested cells or tissue size per sampling is relatively small.<sup>1</sup>

Since leucocyte counts and alterations in their signalling pathways and gene expression pattern reflect the immunological status, peripheral blood mononuclear cells (PBMCs) and cultured lymphocytes are frequently used as biological material in immunological studies, cancer and diabetes research, as well as in pathogen-host interaction examinations.<sup>2</sup> In many of these experimental settings, the comprehensive assessment of changes in different biomolecules and their correlations is biologically relevant and crucial for the interpretation of results. Therefore, a method for rapid, efficient and reproducible simultaneous extraction of RNA and proteins from PBMCs or their cellular fractions is much needed, as the sample size and the number of individual sample acquisitions is limited.

The widely applied method for this simultaneous extraction of all mentioned biomolecules includes the usage of phenol, guanidine isothiocyanate and isoamyl alcohol mixture, commercially branded as TRIzol. Procedures which employ TRIzol are mostly optimised for RNA extraction, while the leftover organic phase, separated after the addition of chloroform, can be used for the isolation of DNA and proteins from the same sample, which is more cost-effective than the purchase of specialised commercially available kits for the simultaneous extraction of different biomolecules.<sup>1</sup> Most post-TRIzol protein-leftover processing methods include the employment of guanidine hydrochloride, urea and SDS, in specific concentrations, in order to solubilise a protein precipitate.<sup>3,4</sup> Solubilisation efficiency depends on the composition of the solubilisation buffer and temperature regime, as well as on the pellet size and the initial protein composition of the sample.<sup>4,5</sup> Therefore, the optimal protocol for the protein extraction from TRIzol lysates is expected to vary between different tissue/cell types.

The aim of the present study was to define and optimise the procedure for the efficient protein extraction from human PBMCs, obtained by a single blood draw and lysed in TRIzol reagent, by varying experimental conditions in a several-step process. In an effort to maximise the protein yield, limit the utilisation of strong chaotropic agents, avoid dialysis and shorten the total duration of the extraction procedure, we tested alternative organic solvents for protein precipitation, different pellet washing procedures, as well as several alternative solubilisation solutions/buffers, in terms of NaCl, SDS, urea and Tris concentration. We evaluated the efficacy of the optimised protocol for the solubilisation of small soluble cytoplasmic and larger transmembrane proteins, as well as the compatibility with the subsequent analysis of protein posttranslational modifications, such as glycosylation.

## EXPERIMENTAL

*PBMC isolation and lysis*

Peripheral blood samples were collected from healthy adult volunteers ( $n = 16$ ) in EDTA-containing tubes after an overnight fasting. Samples were pooled and centrifuged at 400g (deceleration brakes off) at 4 °C for 10 min in a centrifuge with the swing-bucket rotor (centrifuge 5804R, Eppendorf, Hamburg, Germany). The buffy coat was collected, diluted with phosphate-buffered saline (PBS, 10 mM, pH 7.4) in a 1:2 volume ratio, and layered onto lymphocyte separation medium (1.077 g/mL, Capricorn Scientific, Ebsdorfergrund, Germany). The manufacturer's protocol was modified for the isolation of PBMCs, by including centrifugation during the separation step at 700g (slow acceleration, deceleration brakes off, swing-bucket rotor) at 18–21 °C for 30 min (centrifuge 5804R, Eppendorf, Hamburg, Germany). PBMC layer was collected, washed twice with PBS and once with erythrocyte lysis buffer (155 mM NH<sub>4</sub>Cl, 10 mM KHCO<sub>3</sub>, 0.1 mM EDTA), and centrifuged at 100g at room temperature for 10 min. PBMC pellet was dissolved in TRIzol reagent (TRIsure, Bioline, London, UK), assuring complete solubilisation and homogenization, and aliquots stored at –80 °C for further processing, which is a standard requirement of sample storage for RNA extraction, necessary for preserving the integrity of RNA molecules. The amount of TRIzol reagent used for the lysis of PBMCs extracted from the initial 3 mL (*ca.* 2.5×10<sup>6</sup> cells) of whole peripheral blood was 400 µL.

*Protein extraction and solubilisation*

As shown in Fig. 1, thawed PBMC lysates in TRIzol reagent were subjected to phase separation according to the manufacturer's instruction,<sup>6</sup> by adding chloroform (0.2 mL per 1 mL of TRIzol reagent) and centrifugation at 12000g at 4 °C for 15 min. The aqueous phase was removed and absolute ethanol added (0.3 mL per 1 mL of TRIzol reagent) to the remaining interphase and phenol–chloroform organic phase in order to precipitate DNA. Samples were mixed by gentle inversion and DNA pelleted by centrifugation at 2000g, at 4 °C for 5 min. The remaining supernatants (phenol–ethanol solutions) were pooled together and separated into equal aliquots in 1.5 mL microtubes for further protein precipitation, washing and solubilisation following different protocols.

Either ice-cold isopropanol or ice-cold acetone (1.5 mL per 1 mL of TRIzol reagent used for PBMC homogenization) was added to phenol–ethanol supernatant to precipitate proteins and incubated at –20 °C for 30 min. The centrifugation step at 12000g, at 4 °C for 10 min was performed to pellet proteins. Pellets were washed twice following two alternative protocols: using 0.3 M guanidine hydrochloride (Gu-HCl) in 95% ethanol or absolute ethanol (2 mL per 1 mL of TRIzol reagent), at 4 °C for 20 min and centrifugation at 7500g at 4 °C for 5 min. For pellets washed with Gu-HCl, a third washing step was performed with absolute ethanol under the same conditions. Protein pellets were air-dried and resuspended in 100 µL of the tested solubilisation solutions/buffers:

Solut. 1 – 1% SDS in ddH<sub>2</sub>O;

Solut. 2 – 100 mM Tris pH 8.0, 5 mM EDTA, 1 % SDS;

Solut. 3 – 100 mM Tris pH 8.0, 5 mM EDTA, 140 mM NaCl, 1 % SDS;

Solut. 4 – 100 mM Tris pH 8.0, 5 mM EDTA, 6 M urea, 5 % SDS.

Each mixture was vortexed and incubated in a thermoshaker at 50 °C and 300 rpm to enable protein solubilisation, for varying incubation times (10–40 min) and with intermittent vortexing, and finally left at 90 °C for 10 min. After cooling down for 2–3 min, centrifuging at 10000g for 10 min was conducted to remove any remaining insoluble aggregates.

### PBMCs in Trizol

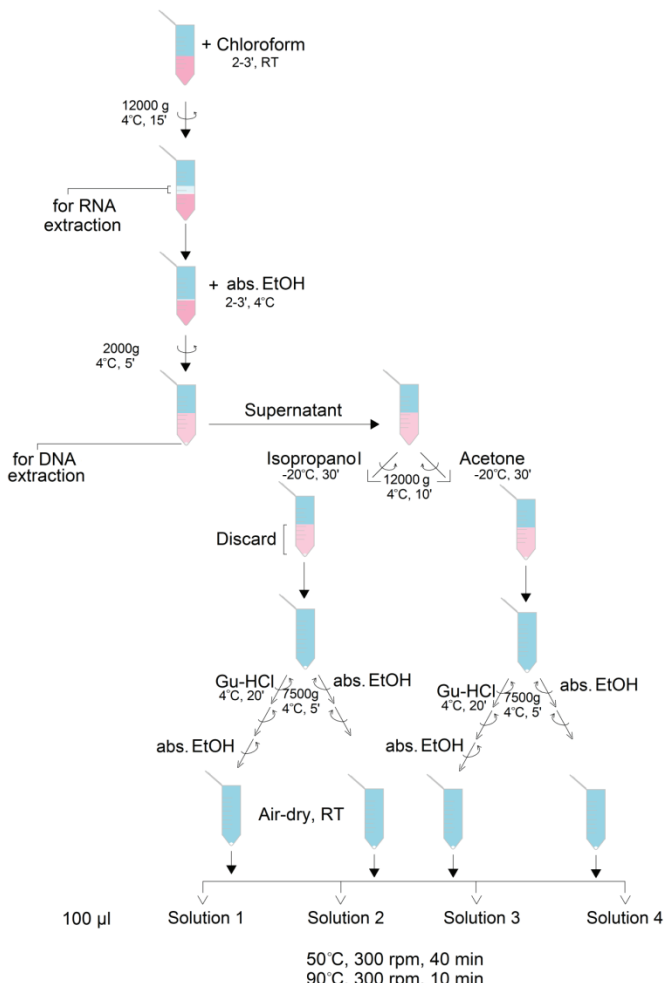


Fig. 1. Schematic presentation of the experimental setup.

In a separate experimental setup, we tested the effect of selected organic solvents used for protein precipitation on the time-dependency of the pellet solubilisation. Protein pellets were solubilised in solution 1, vortexed and incubated at 50 °C and 300 rpm for 40 min, and then heated at 90 °C for 10 min with continuous shaking. Every 10 min, samples were cooled down for 2–3 min to the room temperature, 2 µL aliquots were taken to measure the absorbance at A280 (Epoch microplate spectrophotometer, BioTek Instruments – Agilent, Santa Clara, CA, USA), and 10 µL aliquots were saved for electrophoresis.

#### Electrophoretic separation

Sample aliquots were mixed in 1:1 volume ratio with 2× concentrated Laemmli buffer containing 2-mercaptoethanol as a reducing agent (100 mM Tris-HCl, pH 6.8, 4 % SDS, 20 %

glycerol, 10 % 2-mercaptoethanol, 0.1 % bromophenol blue) and heated at 95 °C for 5 min. Samples were centrifuged prior to SDS-polyacrylamide gel electrophoresis (SDS-PAGE) to remove possible aggregates. SDS-PAGE was used for the electrophoretic separation of proteins on 10 or 8 % gels under reducing conditions. Ten percent gels were used to examine potential presence of aggregates, whereas 8 % gels were employed for separation of higher molecular weight proteins, further enabling their immunodetection. Samples (concentration 2 mg/mL) were applied at different volumes (10, 15 or 30 µL). The molecular weight of proteins was estimated using Pink Plus prestained protein ladder with a 14–175 kDa range (Cleaver Scientific, Rugby, UK). Following electrophoretic separation, proteins were either stained on gel or transferred to a nitrocellulose membrane. In-gel protein staining was performed using the standard procedure with Coomassie brilliant blue R250 (CBB) solution.<sup>7</sup> Selected lectins and specific antibodies were employed for detection of (glyco)proteins.

#### Lectin- and immuno-blotting

Following protein transfer onto nitrocellulose membrane (wet transfer: constant voltage, 100 V for 1 h, with cooling unit, as recommended by the producer), protein-free sites were blocked with 5 % BSA in Tris-buffered saline (10 mM Tris, 0.15 M NaCl, pH 7.4) containing 0.1 % Tween-20 (TBST) overnight (for lectin blotting) or for 45 min (for immunoblotting). Membranes were washed in TBST before immunodetection. For lectin blotting, membranes were incubated in a solution of biotinylated *Sambucus nigra* lectin (SNA) or *Aleuria aurantia* lectin (AAL) in TBST (0.2 µg/mL) at room temperature for 1 h, washed with TBST 4×5 min, further incubated with fluorescein-conjugated streptavidin (0.025 µg/mL) at room temperature for 1 h and washed again with TBST 4×5 min. The fluorescent signal was recorded using the ChemiDoc MP imaging system (Bio-Rad Laboratories Inc., Hercules, CA, USA). SNA, AAL and fluorescein-conjugated streptavidin were purchased from Vector Laboratories (Burlingame, CA, USA). For immunodetection, membranes were incubated in a solution of primary antibodies in TBST, at 4 °C overnight, washed with TBST 6×5 min and further incubated with biotinylated secondary antibodies (0.15 µg/mL) at room temperature for 30 min. Another washing step was applied (6×5 min), and the membranes incubated with fluorescein-conjugated streptavidin as previously described. The following primary antibodies were employed: mouse monoclonal anti-CD45 antibody (1 µg/mL; Bio-Rad, Hercules, CA, USA), rabbit anti-β-actin antiserum (1:500 volume ratio; Sigma Aldrich) and goat polyclonal anti-GAPDH antibody (0.625 µg/mL; Sigma Aldrich). Biotinylated secondary antibodies were: horse-anti-mouse, horse-anti-goat, and goat-anti-rabbit IgG (Vector Laboratories, Burlingame, CA, USA).

#### RESULTS AND DISCUSSION

The aim of our study was to define and optimise the procedure for the efficient protein extraction from human PBMC. Following the manufacturer's procedure for TRIzol application, proteins from PBMCs precipitated with isopropanol and washed with Gu-HCl and ethanol were completely dissolved in all examined solutions under the defined conditions. Our selection of the solubilisation solutions was based on the previous attempts to define procedures for the efficient extraction of proteins from TRIzol lysates of other biological samples. As the pelleted proteins are tightly packed, they are usually solubilised using some chaotropic agents (e.g., guanidine hydrochloride or urea), detergent (e.g., SDS) or salts (NaCl, Tris). It is recommended to avoid chemicals that are harm-

ful and toxic, as well as those that can interact with proteins resulting in misleading data and conclusions. Profile of protein bands as well as their intensities were similar in all tested conditions, as shown in Fig. 2A. This result differs from those reported by others,<sup>8–13</sup> who have found the increased efficiency of the solutions containing (thio)urea compared to alternative solubilisation solutions for proteins isolated by TRIzol method from tissues and cultured cell other than PBMCs. Urea is a non-toxic, strong protein denaturant that facilitates protein solubilisation in combination with disulphide bond disruption.<sup>14</sup> Still, the side effect of urea employment is carbamylation, a process in which urea dissociates to ammonia and cyanate with concomitant formation of isocyanic acid. The acid further interacts with the N-termini of proteins and amino groups of lysine and arginine. Approximately 20 % of N-termini and 2 % of lysine residues are modified with as much as 2 M urea.<sup>15</sup> Carbamylation interferes with downstream processes, *e.g.*, enzymatic digestion and peptide separation, identification and quantification, as well as protein labelling. Therefore, we excluded urea from further experiments.

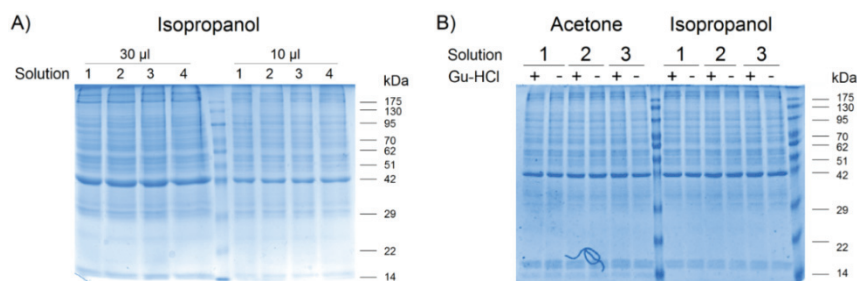


Fig. 2. SDS-PAGE electrophoresis on 10 % gel under reducing conditions. A) Proteins precipitated with isopropanol, washed with the addition of guanidine hydrochloride (Gu-HCl) and solubilised in one of the four tested solutions; B) proteins precipitated with isopropanol or acetone, washed with or without the addition of Gu-HCl. Solutions used for solubilisation are labelled as follows: 1 (1 % SDS), 2 (100 mM Tris, pH 8.0, 5 mM EDTA, 1 % SDS), 3 (100 mM Tris, pH 8.0, 5 mM EDTA, 1 % SDS, 140 mM NaCl) and 4 (100 mM Tris, pH 8.0, 5 mM EDTA, 5 % SDS, 6 M urea). Molecular weight markers are given on the right.

None of the variables examined, in respect to the type of the organic solvent and the composition of the washing or solubilisation solution, demonstrated deviations from other experimental combinations regarding the yield of the extracted proteins or the distribution of proteins after SDS-PAGE (Fig. 2B). Acetone was equally suitable for protein precipitation as the recommended isopropanol. The exclusion of Gu-HCl from the pellet washing step did not affect the protein yield and the solubilisation efficiency. Our finding is in accordance with the results of Kopec *et al.*<sup>4</sup> who analysed the efficacy of protein extraction from brain tissue by varying concentrations of NaCl, Tris, SDS and EDTA in the lysis buffer. Both

results confirmed that guanidine hydrochloride is not a crucial component in the washing step, thus, the usage of this highly toxic chaotropic agent can be omitted. According to our results, any of the tested solubilisation solutions could be used for protein solubilisation giving similar protein yields (Fig. 2B). Therefore, we selected the simplest solution (1 % SDS in ddH<sub>2</sub>O) for the protein solubilisation step. SDS, a strong anionic detergent, is widely employed protein denaturing agent and is often incorporated in lysis/solubilisation buffers. Furthermore, SDS is more compatible with some sophisticated techniques (such as HPLC and FPLC) and, hence, more suitable than urea. SDS will not crystallize under often-used conditions (1 % or 34 mM), unlike urea whose concentrations are much higher (6–8 M) and crystallization is inevitable.<sup>16</sup>

It was noticed that proteins in acetone-precipitated pellet were less tightly packed and aggregates tended to dissolve faster than those precipitated with isopropanol. Since all washing and solubilisation procedures resulted in the same outcome, to examine the efficiency of the solubilisation with time, the absorbance of dissolved proteins was measured in 10-min intervals during 40 min, employing heating at 50 °C, plus the additional 10 min heating at 90 °C (termed a 50-min time point). The simplest method employing absolute ethanol for pellet washing and 1 % SDS for solubilisation was used to dissolve acetone- or isopropanol-precipitated proteins. Acetone pellet was dissolved more efficiently at 50 °C, while heating at 90 °C had no additional effect (Fig. 3).

All tested procedures resulted in comparable specific protein bands corresponding to small soluble proteins GAPDH (37 kDa) and β-actin (42 kDa), as well as high molecular mass transmembrane protein CD45 (~180–~220 kDa), as shown in Fig. 4A.

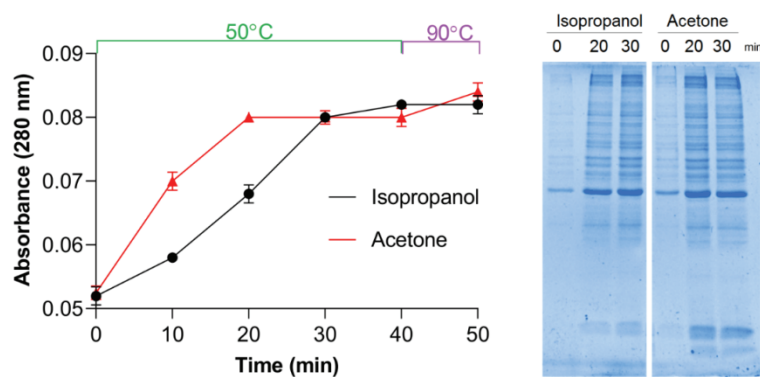


Fig. 3. Solubilisation curve of the protein pellet precipitated with isopropanol or acetone and CBB staining of the solubilised proteins precipitated with isopropanol or acetone (washed with absolute ethanol, dissolved in 1 % SDS) after electrophoretic separation (SDS-PAGE under reducing conditions) on 10 % gels. Sample aliquots were collected before incubation at 50 °C and every 10 min during 40 min incubation, and additional 10 min incubation at 90 °C.

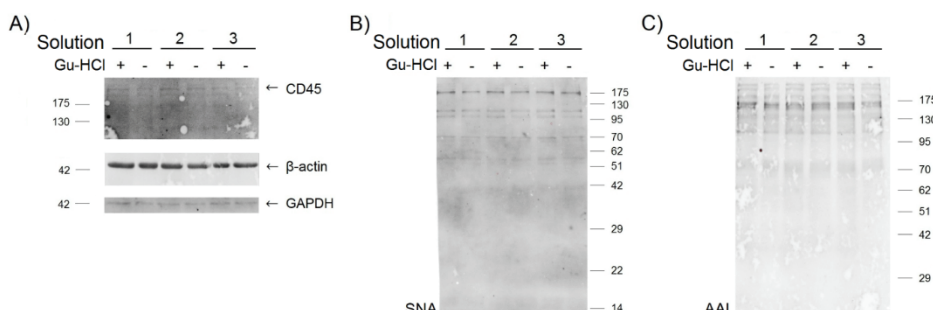


Fig. 4. Proteins precipitated with acetone, washed with ethanol and dissolved in 1 % SDS resolved by reducing SDS-PAGE on 10 % gel (for GAPDH,  $\beta$ -actin and SNA-reactive glycoproteins) or 8 % gel (for CD45 and AAL-reactive glycoproteins). Immunoblot with anti-CD45, anti- $\beta$ -actin or anti-GAPDH antibodies (A) and lectin blots with SNA (B) or AAL lectin (C).

In order to detect whether posttranslational modifications of proteins remained preserved during the isolation procedure, the presence of sialylated (recognised by SNA lectin) and fucosylated (recognized by AAL lectin) glycoforms in solubilisates obtained after acetone precipitation was examined and confirmed by lectin blotting. As can be seen from Fig. 4B and C, neither sialylation nor fucosylation pattern of the extracted proteins was affected by the presence/absence of Gu-HCl in the pellet washing step or by the choice of the tested solubilisation solutions. The distribution of the bands in the lectin blot and their intensities were similar regardless of the protein extraction procedure, both in the region of small and high molecular weight glycoproteins.

#### CONCLUSION

By varying solutions and conditions for protein precipitation, pellet washing and protein solubilisation, the optimised protocol for the extraction and isolation of post-TRIzol leftover proteins from PBMCs can be defined as follows: protein precipitation from the organic phase with ice-cold acetone, pellet washing with absolute ethanol and solubilisation in 1 % SDS employing 20 min heating at 50 °C and vortexing. The addition of urea, NaCl and Tris, as well as an increase in the concentration of SDS did not improve the solubilisation of PBMC protein pellet. Furthermore, the exclusion of Gu-HCl from the pellet washing solution did not affect the quality/quantity of the extracted proteins. Acetone was shown to be equally suitable for the protein precipitation as recommended isopropanol. Even more, acetone pellet was more easily solubilised during shorter periods of incubation (up to 20 min). The proposed protocol is specifically tailored for PBMCs, as a frequently analysed type of biological sample for biomedical and biochemical research. It may be considered as a simple, cost-effective and efficient protocol to extract PBMC proteins from post-TRIzol leftover material.

*Acknowledgements.* This work was supported by the Ministry of Science, Technological Development and Innovations (No 451-03-47/2023-01/200019).

#### ИЗВОД

#### ЈЕДНОСТАВНА МЕТОДА ИЗОЛОВАЊА ПРОТЕИНА БЕЗ УПОТРЕБЕ ГУАНИДИН-ХИДРОХЛОРИДА ИЗ ОСТАТАКА ЕКСТРАКЦИЈЕ РЕАГЕНСОМ TRIZOL ИЗ ПЕРИФЕРНИХ МОНОНУКЛЕАРНИХ ЋЕЛИЈА

ЈОВАНА СТЕВАНОВИЋ, ДРАГАНА РОБАЈАЦ, ОЛГИЦА НЕДИЋ И ЗОРАНА ДОБРИЈЕВИЋ

*Институут за промену нуклеарне енергије, Банатска 31б, 11080 Београд*

Након екстракције RNA и DNA, преостали протеински остатак најчешће бива одстрањен услед његовог отежаног растворавања. Исталожени протеини су густо паковани, због чега је најчешће потребно користити неки хаотропни агенс (нпр. гуанидин-хидрохлорид или уреа), детергент (нпр. SDS), со (NaCl) или базни пуфер (Tris). Циљ студије био је да се дефинише и оптимизује поступак ефикасне екстракције протеина из хуманих мононуклеарних ћелија периферне крви (PBMC), добијених из једног узимања крви и лизираних у реагенсу TRIzol. Варирани су експериментални услови у смислу избора растворача за таложење протеина (изопропанол или ацетон), испирања гуанидин-хидрохлоридом или без испирања и растворова за солубилизацију (садржај SDS, NaCl, уреа и/или Tris). Процењена је ефикасност оптимизованог протокола за солубилизацију малих солубилних протеина цитоплазме и већих трансмембраних протеина, као и компатибилност методе са даљом анализом пост-транслационих модификација протеина (нпр. гликозиловања). Протокол оптимизован за екстракцију и изоловање протеина из остатака TRIzol лизата PBMC, дефинисан је као: преципитација протеина из органске фазе ледено-хладним ацетоном, испирање талога апсолутним етанолом и солубилизација протеина у 1 % SDS грејањем на 50 °C уз мешање, у трајању од 20 min.

(Примљено 30. марта, ревидирано 27. априла, прихваћено 8. јула 2023)

#### REFERENCES

1. W. Mathieson, G. A Thomas, *Anal. Biochem.* **433** (2013) 10  
(<https://dx.doi.org/10.1016/j.ab.2012.10.006>)
2. P. Sen, E. Kemppainen, M. Orešić, *Front. Mol. Biosci.* **4** (2018)  
(<https://dx.doi.org/10.3389/fmolb.2017.00096>)
3. H. Riol, B. Jeune, A. Moskovic, L. Bathum, E. Wang, *Anal. Biochem.* **275** (1999) 192  
(<https://dx.doi.org/10.1006/abio.1999.4328>)
4. A. M. Kopec, P. D. Rivera, M. J. Lacagnina, R. Hanamsagar, S. D. Bilbo, *J. Neurosci. Methods* **280** (2017) 64 (<https://dx.doi.org/10.1016/j.jneumeth.2017.02.002>)
5. R. B. Braakman, K. Bezstarostí, A. M. Sieuwerts, V. de Weerd, A. M. van Galen, C. Stingl, T. M. Luider, M. A. Timmermans, M. Smid, J. W. Martens, J. A. Foekens, J. A. Demmers, A. Umar, *J. Proteome Res.* **14** (2015) 1627  
(<https://dx.doi.org/10.1021/acs.jproteome.5b00046>)
6. TRIsure™ Product Specifications,  
[https://www.bioline.com/mwdownloads/download/link/id/953/trisure\\_product\\_manual.pdf](https://www.bioline.com/mwdownloads/download/link/id/953/trisure_product_manual.pdf)  
(accessed 25 July, 2023)
7. C. Arndt, S. Koristka, A. Feldmann, R. Bergmann, M. Bachmann, *Methods Mol. Biol.* **1853** (2018) 27 (<https://dx.doi.org/10.1007/978-1-4939-8745-04>)

8. A. B. Hummon, S. R. Lim, M. J. Difilippantonio, T. Ried, *Biotechniques* **42** (2007) 467 (<https://dx.doi.org/10.2144/000112401>)
9. A. E. Simões, D. M. Pereira, J. D. Amaral, A. F. Nunes, S. E. Gomes, P. M. Rodrigues, A. C. Lo, R. D'Hooge, C. J. Steer, S. N. Thibodeau, P. M. Borralho, C. M. P. Rodrigues, *BMC Genomics* **14** (2013) 181 (<https://dx.doi.org/10.1186/1471-2164-14-181>)
10. A. P. Joy, D. C. Ayre, I. C. Chute, A. P. Beauregard, G. Wajnberg, A. Ghosh, S. M. Lewis, R. J. Ouellette, D. A. Barnett, *J. Extracell. Vesicles* **7** (2018) 1438727 (<https://dx.doi.org/10.1080/20013078.2018.1438727>)
11. Y. Wen, I. J. Vechetti, T. R. Valentino, J. J. McCarthy, *Biotechniques* **69** (2020) 264 (<https://dx.doi.org/10.2144/btn-2020-0083>)
12. C. Young, P. Truman, *Anal Biochem.* **421** (2012) 330 (<https://doi.org/10.1016/j.ab.2011.10.045>)
13. C. Pop, S. Ameling, D. Vishnu, F. Loghin, U. Völker, E. Hammer, *JIOMICS* **5** (2015) 58 (<https://dx.doi.org/10.5584/jionomics.v5i1.185>)
14. L. Hua, R. Zhou, D. Thirumalai, B.J. Berne, *Proc. Natl. Acad. Sci. USA* **105** (2008) 16928 (<https://doi.org/10.1073/pnas.0808427105>)
15. L. Kollipara, R.P. Zahedi, *Proteomics* **13** (2013) 941 (<https://dx.doi.org/10.1002/pmic.201200452>)
16. B. Schlager, A. Straessle, E. Hafen, *BMC Biotechnol.* **12** (2012) (<https://dx.doi.org/10.1186/1472-6750-12-95>).



## Preventing hydrolysis of AlN powders with organophosphate coating in aqueous media

CEREN KAYA<sup>1</sup>, OĞUZ BAYINDIR<sup>1,2</sup>, SARUHAN SAKLAR<sup>3</sup>, ORHAN ATAKOL<sup>4</sup>  
and HÜSEYİN ÇELİKKAN<sup>1\*</sup>

<sup>1</sup>Department of Chemistry, Science Faculty, Gazi University, 06560, Ankara, Türkiye,

<sup>2</sup>Sabancı University Nanotechnology Research and Application Center, 34956, İstanbul, Türkiye,

<sup>3</sup>General Directorate of Mineral Research and Exploration, 06800, Ankara, Türkiye  
and <sup>4</sup>Department of Chemistry, Science Faculty, Ankara University, 06500, Ankara, Türkiye

(Received 21 March, revised 26 April, accepted 28 June 2023)

**Abstract:** The coating of aluminum nitride powder has a great importance industrially and environmentally. AlN can be rapidly hydrolyzed to aluminum hydroxide and ammonia in the atmosphere or water media. To prevent the hydrolysis of AlN, the inorganic or organic based coatings are used frequently. For the first time, this study describes the phosphate esters as organophosphate coating used for the inhibition of hydrolysis reaction of AlN in its water suspension. Phenyl phosphate showed the best inhibition against AlN hydrolysis with an easy application technique and at low concentration of 0.005 M. AlN coating efficiency was proved by spectroscopic and imaging methods. It was concluded that the coating acquired the protective properties of phenyl phosphate through its water repellence.

**Keywords:** aluminum nitride; organophosphate; coating; hydrolysis protection.

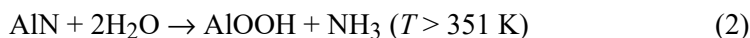
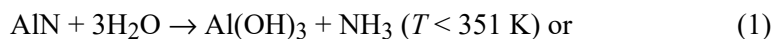
### INTRODUCTION

Aluminum nitride is an industrially important ceramic with its low dielectric coefficient, high electrical resistance and thermal conductivity, and low thermal expansion coefficient.<sup>1</sup> AlN is frequently used ceramic in the production of ceramics and electronic devices as an additive,<sup>2,3</sup> semiconductor,<sup>4</sup> supercapacitors<sup>5</sup> and surface coating.<sup>3</sup> AlN must be utilized under controlled conditions because of its sensitivity to oxidation and hydrolysis in atmosphere.<sup>6</sup> In water, it highly decomposes to aluminum hydroxide and ammonia depending on the temperature and pH.<sup>7</sup>

In AlN production, 700 °C is a critical temperature, and aluminum powder can be reacted by the nitrogen in atmosphere to form AlN.<sup>8</sup> For that, there is a

\*Corresponding author. E-mail: celikkan@gazi.edu.tr  
<https://doi.org/10.2298/JSC230321029K>

high amount of AlN in the dross of aluminum recycling facilities, especially the secondary dross could contain approximately 14 % of AlN in the total quantity.<sup>9</sup> The high reactivity of AlN causes the storage and disposal problems for AlN products and the dross of Al recovery plants. In addition, protecting AlN particles against hydrolysis is critical in preventing ammonia related environmental effects.<sup>10</sup> Hydrolysis of AlN occurs by both mechanisms in several steps in which NH<sub>3</sub> and Al(OH)<sub>3</sub> are produced, and the hydrolysis mechanism are related to temperature as shown below.<sup>11</sup> On the other hand, crystalline Al(OH)<sub>3</sub> (bayerite) to become more stable phase can form from amorphous AlOOH (boehmite) at room temperature:<sup>11</sup>



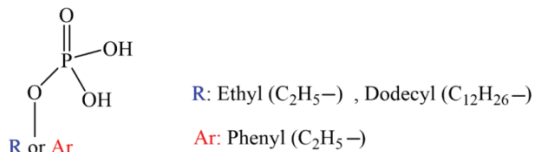
For these reasons, the coating of AlN surface to avoid its decomposition is essential for manufacturing and waste management<sup>12</sup> also the surface modification is a necessity for the deagglomeration and mixing problems of the ceramics production with AlN.<sup>12</sup> Inorganic and organic modifiers can be utilized for coating AlN surface against oxidation and hydrolysis in atmosphere. While phosphoric acid,<sup>13,14</sup> silicate<sup>15</sup> and their derivatives could be used to get water immiscible surface on AlN in the inorganic treatment, the organic molecules with their long chain carboxylic acids, or hydroxyl/amine groups could be utilized to obtain a water repelling surface on AlN such as sebacic acid,<sup>16</sup> citric acid,<sup>17</sup> oleic acid,<sup>18</sup> silicic acid,<sup>19</sup> dodecylamine,<sup>20</sup> cetyl alcohol<sup>20</sup> and stearic acid.<sup>20</sup>

In this study, we investigated to prevent AlN hydrolysis by forming a protective layer on the surface of AlN using organophosphate (OP) molecules such as ethyl phosphate (EP), phenyl phosphate (PP) and dodecyl phosphate (DP) esters. The resistance of treated powders of AlN to hydrolysis was characterized by X-ray diffraction (XRD), fourier transform infrared (FTIR), contact angle, scanning electron microscopy (SEM) techniques and pH measurements. It was observed that the hydrolysis resistance was directly related to the water repellency of the OP used in treatment process of AlN.

## EXPERIMENTAL

### *Materials*

AlN powder was purchased by Alfa Aesar (with the particle size under 4  $\mu\text{m}$ ). EP, PP and DP (presented in Scheme 1) were obtained from TCI. Ethanol in high purity was purchased from Sigma. The solutions of OP esters were prepared with the appropriate amount of AlN and 30 % ethanol in deionized water. 0.1 M HCl and NaOH were used to adjust the pH of the solutions. All the experiments were performed at room temperature.



Scheme 1. Chemical structure of OPs.

*Apparatus*

Mettler Toledo SevenCompact was used for pH measurements in the AlN suspensions. The wettability of the treated AlN samples was performed by SEO Phoenix 300 contact meter with a static water contact angle technique. A Panalytical Empyrean with a CuK $\alpha$  source at a 0.154 nm wavelength (Tokyo, Japan) was used to record XRD spectra. FTIR spectra were obtained using Shimadzu IR-Affinity 1 (Kyoto, Japan). SEM micrographs were obtained with a Jeol 6390 LV SEM operated at 10 kV after gold coating by a sputter coater.

*Methods*

pH responses of AlN suspensions in the existence of various OP esters were performed at 2 % AlN and 0.025 M of OP ester. The XRD spectra, contact angel measurements, FTIR spectra and SEM micrographs were obtained from the samples filtered and dried at 60 °C in vacuum oven after treating with OP esters and water in the appropriate solutions.

## RESULTS AND DISCUSSION

The pH change in a particular hydrolysis condition has an importance since the hydrolysis product, NH<sub>3</sub>, of AlN increases the pH of the solution. Because of the effect of OP ester on the hydrolysis of AlN in water, the pH test is useful for monitoring the hydrolysis of AlN vs. time. In Fig. 1, the results of pH vs. time for the suspensions of various OP ester and AlN were presented. Initial pH of the OP ester solution was adjusted in the range of pH 6–7 to monitor pH accurately before the addition of AlN into the media. The pH monitoring reached maximum value at pH 10, for the suspension of water and AlN, in 1500 min. This result confirmed the NH<sub>3</sub> production after hydrolysis reaction of AlN in water. On the other hand, the addition of OP esters into the media inhibited the hydrolysis reaction completely with a non-significant difference at pH, Fig. 1, with a result similar to the literature.<sup>17,18,20</sup> Since the principle of the chemical coverage of AlN surface against hydrolysis reaction was modifying the surface with organic molecules to increase the hydrophobicity of its surface,<sup>21</sup> it could be said that all three modifiers were suitable to succeed in covering the AlN surface regardless the type of organic group attached to phosphate in OP esters such as EP, PP and DP. On the other hand, Egashira *et al.* proved that the oxide sensitive group binding to AlN as well as the organic group in a modifier molecule is important in preventing hydrolysis by showing lower efficiency of dodecylamine to cethyl alcohol, while dodecyl group has a longer carbon skeleton than cethyl group.<sup>20</sup> After the results shown in Fig. 1, the water contact angle method was needed as a technique to measure surface hydrophobicity of OP ester treated AlN. For this

purpose, the surface treated AlN powders obtained in the same conditions from Fig. 1 were filtered and dried at 60 °C in vacuum oven, while the water-treated AlN was obtained by the same way for comparison.

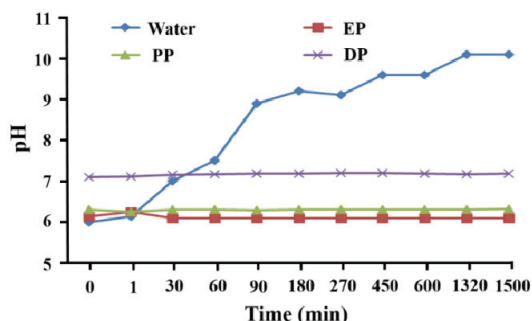


Fig. 1. pH responses vs. time for AlN suspensions in water and water/OP esters.

The contact angel measurements in Fig. 2 showed that maximum water repelling was obtained from the samples treated with DP (75.7°) and PP (69.8°), while EP (25.9°) treated sample showed a limited repelling. In addition, the water treated AlN sample in Fig. 2 interestingly gave a higher value, than EP treated sample, namely 42.9°. As expected, non-treated AlN sample in Fig. 2 showed no water repelling because of its reactivity.

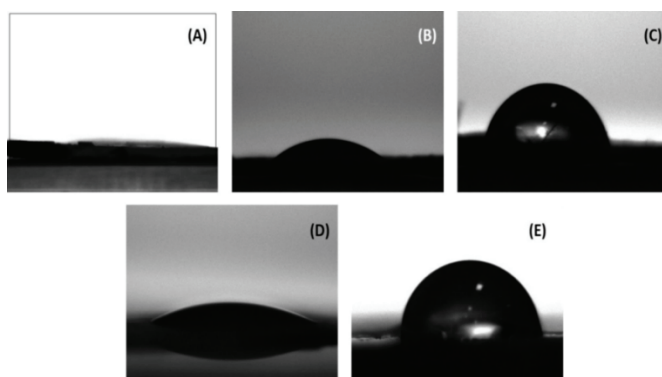


Fig. 2. The water contact angle measurements of non-treated AlN (A), water (B), PP (C), EP (D) and DP treated (E) AlN powders.

FTIR spectra of non-treated and treated AlN samples are presented in Fig. 3. The broad band around 700 cm<sup>-1</sup> was attributed to the absorption of Al–N vibration.<sup>12</sup> The water treated sample of AlN showed two bands at 696 and 1032 cm<sup>-1</sup> from the adsorption of Al–O vibrations, at the range of 3443–3650 cm<sup>-1</sup> of O–H vibrations arisen from water vapor adsorbed on the powder sample. In PP and EP treated AlN samples, there was not a significant adsorption band without the

broad band of Al–N vibrations because of low alkyl chain and aromatic group attached to the surface of AlN particle. DP treated AlN showed distinctly aliphatic adsorption bands for C–C and C–H symmetric/ asymmetric vibrations in its long carbon skeleton at 1070, 1144, 1220, 1470, 2847, 2915 and 2961 cm<sup>-1</sup>.

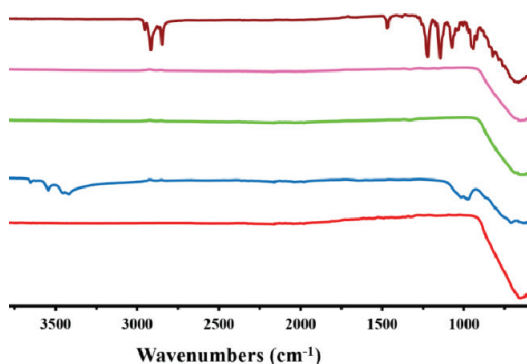


Fig. 3. FTIR spectra of non-treated (A), water treated (B), PP treated (C), EP treated (D) and DP treated (E) AlN samples.

XRD spectra of the samples of treated and non-treated AlN powders are presented in Fig. 4. In Fig. 4, the characteristic peaks of AlN powder at  $2\theta$  33.3, 36.1, 37.9, 49.9, 59.4 and 66.1° corresponding to (100), (002), (101), (102), (110) and (103), respectively (JCPDS card number: 00-001-0287). After water treatment of AlN powders, the appearance of the diffraction peaks at  $2\theta$  18.8, 20.4, 27.9, 40.7 and 53.2° corresponding to (001), (100), (101), (111) and (112), respectively, was resulting from the formation of  $\text{Al}_2\text{O}_3 \cdot 2\text{H}_2\text{O}$  due to the hydrolysis reaction of AlN in water. From Fig. 4, while it was understood that DP and PP protected AlN well against the hydrolysis reaction, it was concluded that EP did not provide a complete protection against hydrolysis since both the diffraction peaks for AlN and  $\text{Al}_2\text{O}_3 \cdot 2\text{H}_2\text{O}$  were observed in the diffraction spectrum of EP treated AlN sample.<sup>22</sup> However, it was concluded that PP provided complete protection for AlN against hydrolysis while DP protected only partially, since very weak  $\text{Al}_2\text{O}_3 \cdot 2\text{H}_2\text{O}$  peaks were observed in AlN sample treated with DP, while  $\text{Al}_2\text{O}_3 \cdot 2\text{H}_2\text{O}$  peaks were not observed in AlN sample treated with PP. This result showed that the PP treatment provide the best protection for AlN against the hydrolysis reaction in water.

Particle morphologies of AlN powders after treatment with OP esters were critical for the microstructural evolution. The SEM micrographs of AlN samples treated by water and OP esters are presented in Fig. 5. The formation of aluminum oxide was confirmed from the polymorphs of Al–O formation between the adjacent particles for the sample of water treated AlN powder. While there was no significant change in particle morphology for DP and PP treated AlN, a

similar degradation was observed in the EP treated AlN sample similar to the water treated AlN sample due to Al-O formation on the sample surface.<sup>6</sup>

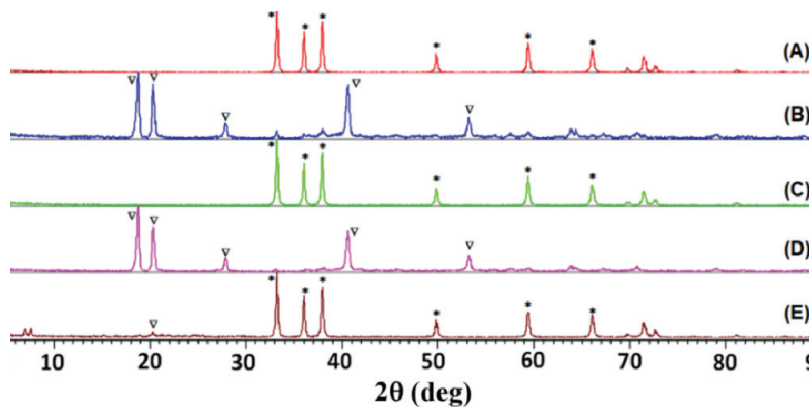


Fig. 4. XRD spectra of non-treated (A), water treated (B), PP treated (C), EP treated (D) and DP treated (E) of AlN samples.

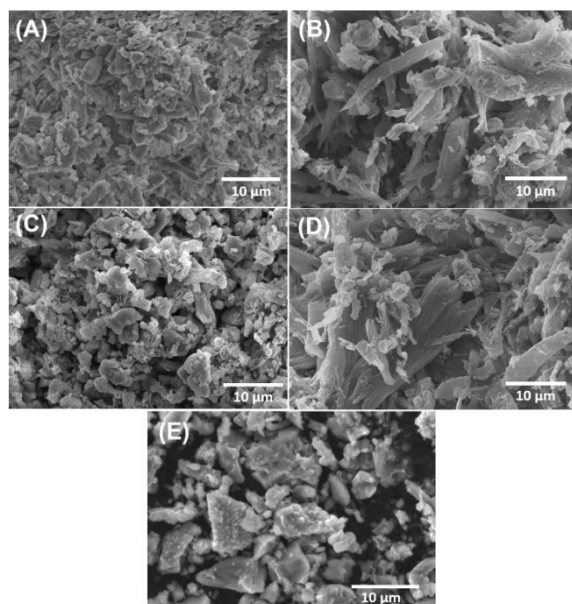


Fig. 5. SEM micrographs of water (A), PP (B), EP (C) and DP treated (D) of AlN samples, and (E) untreated AlN.

After it was concluded that the best protection was obtained as a result of treatment of AlN with PP, in order to examine the effect of PP concentration on AlN protection against the hydrolysis reaction, the pH changes of AlN water suspensions containing PP in different concentrations were monitored and plotted

Fig. 6. From the pH change of 0.0001 M PP treatment of AlN in water in Fig. 6, it was concluded that the AlN samples treated with PP at 0.001 M and higher concentrations protected the AlN powders against the hydrolysis reaction. This result showed that PP could inhibit the hydrolysis reaction of AlN at lower concentrations better than water-repellent and hydrolysis protective materials used for similar purposes in the literature.

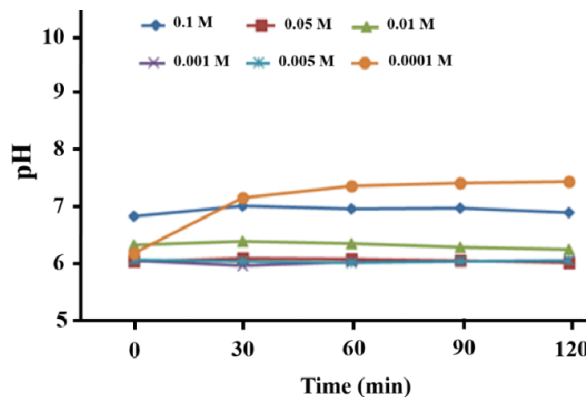


Fig. 6. pH responses vs. time for AlN suspensions in water with various PP concentrations.

#### CONCLUSION

The capability of water repelling and hydrolysis inhibition with the coating of AlN surface are very important in order to avoid the environmental poisoning and the degradation of AlN. The inorganic treatment with mostly phosphate compounds and organic treatment with mostly oxygen functional compounds have been utilized for this purpose. In this paper, alkyl and aryl functional phosphate esters were used for inhibition of hydrolysis reaction first time, and PP as aryl functional coating of AlN powder showed the best performance in very dilute concentration for avoiding hydrolysis and degradation of AlN, so it seems that this type of materials are very useful and promising for coating AlN against hydrolysis reaction with an easy application.

*Acknowledgements.* This research was supported by Gazi University Scientific Research Funding (Project No: 05/2017-04), in addition, Oğuz Bayındır thanks the TUBITAK 2218 National Postdoctoral Research Scholarship Programme (P. No. 1929B011800196) for the scholarship support.

## ИЗВОД

## СПРЕЧАВАЊЕ ХИДРОЛИЗЕ ПРАХА AlN ПОМОЋУ ОРГАНОФОСФАТНИХ ПРЕВЛАКА У ВОДЕНОЈ СРЕДИНИ

CEREN KAYA<sup>1</sup>, OĞUZ BAYINDIR<sup>1,2</sup>, SARUHAN SAKLAR<sup>3</sup>, ORHAN ATAKOL<sup>4</sup> и HÜSEYİN ÇELİKKAN<sup>1</sup>

<sup>1</sup>Department of Chemistry, Science Faculty, Gazi University, 06560, Ankara, Türkiye, <sup>2</sup>Sabancı University Nanotechnology Research and Application Center, 34956, İstanbul, Türkiye, <sup>3</sup>General Directorate of Mineral Research and Exploration, 06800, Ankara, Türkiye и <sup>4</sup>Department of Chemistry, Science Faculty, Ankara University, 06500, Ankara, Türkiye

Облагање прахом алуминијум-нитрида има велики индустријски и еколошки значај. У атмосфери или воденој средини AlN брзо подлеже реакцији хидролизе при чему настају алуминијум-хидроксид и амонијак. Да би се спречила хидролиза AlN, често се користе неоргански или органски премази. Први пут у овом раду описана је примена фосфатних естара као органофосфатних премаза за инхибицију реакције хидролизе AlN у воденој средини. Најбољи резултати инхибиције хидролизе AlN добијени су у случају фенил-фосфата који се користи једноставном техником наношења и при ниској концентрацији од 0,005 М. Ефикасност превлаке AlN је потврђена спектроскопским и *imaging* методама. Закључено је да фенил-фосфат инхибира реакцију хидролизе захваљујући његовој слабој апсорпцији воде.

(Примљено 21. марта, ревидирано 26. априла, прихваћено 28. јуна 2023)

## REFERENCES

1. L. M. Sheppard, *Am. Ceram. Soc. Bull.* **69** (1990) 1801
2. G. Hu, C. Q. Chen, K. T. Ramesh, J. W. McCauley, *Acta Materialia* **60** (2012) 3480 (<https://doi.org/10.1016/j.actamat.2012.03.011>)
3. J. L. Qi, L. P. Wang, Y. Zhang, X. Guo, W. Yu, Q. Wang, K. Zhang, P. Ren, M. Wen, *Surf. Coat. Technol.* **405** (2021) 126724 (<https://doi.org/10.1016/j.surfcoat.2020.126724>)
4. Q. Wang, Y. Lu, S. Mishin, Y. Oshmyansky, D. A. Horsley, *J. Microelectromechanical Syst.* **26** (2017) 1132 (<https://doi.org/10.1109/JMEMS.2017.2712101>)
5. S. Hao, L. Zhang, X. Wang, G. Zhao, P. Hou, X. Xu, *Energy Fuels* **35** (2021) 12628 (<https://doi.org/10.1021/acs.energyfuels.1c01420>)
6. J. Li, M. Nakamura, T. Shirai, K. Matsumaru, C. Ishizaki, K. Ishizaki, *J. Am. Ceram. Soc.* **89** (2006) 937 (<https://doi.org/10.1111/j.1551-2916.2005.00767.x>)
7. A. Kocjan, A. Dakskobler, K. Krnel, T. Kosmač, *J. Eur. Ceram. Soc.* **31** (2011) 815 (<https://doi.org/10.1016/j.jeurceramsoc.2010.12.009>)
8. G. Long, L. M. Foster, *J. Am. Ceram. Soc.* **42** (1959) 53 (<https://doi.org/10.1111/j.1151-2916.1959.tb14066.x>)
9. H. Feng, G. Zhang, Q.. Yang, L. Xun, S. Zhen, D. Liu, *Processes* **8** (2020) 1269 (<https://doi.org/10.3390/pr8101269>)
10. M. Mahinroosta, A. Allahverdi, *J. Environ. Manage.* **223** (2018) 452 (<https://doi.org/10.1016/j.jenvman.2018.06.068>)
11. S. Fukumoto, T. Hookabe, H. Tsubakino, *J. Materials Sci.* **35** (2000), 2743 (<https://doi.org/10.1023/A:1004718329003>)
12. M. Oliveira, S. Olhero, J. Rocha, J. M. F. Ferreira, *J. Colloid Interface Sci.* **261** (2003), 456 ([https://doi.org/10.1016/S0021-9797\(03\)00065-1](https://doi.org/10.1016/S0021-9797(03)00065-1))
13. R. Senthil Kumar, K. Rajeswari, B. Praveen, U. N. S. Hareesh, R. Johnson, *J. Am. Ceram. Soc.* **93** (2010) 429 (<https://doi.org/10.1111/j.1551-2916.2009.03418.x>)

14. Q. Wang, S. M. Olhero, J. M. F. Ferreira, W. Cui, K. Chen, Z. Xie, R. Rimani, *J. Am. Ceram. Soc.* **96** (2013) 1383 (<https://doi.org/10.1111/jace.12288>)
15. Y. H. Koh, J. J. Choi, H. E. Kim, *J. Am. Ceram. Soc.* **83** (2000) 306 (<https://doi.org/10.1111/j.1151-2916.2000.tb01190.x>)
16. Y. Shimizu, J. Hatano, T. Hyodo, M. Egashira *J. Am. Ceram. Soc.* **83** (2000) 2793 (<https://doi.org/10.1111/j.1151-2916.2000.tb01633.x>)
17. S. Wildhack, G. Rixecker, F. Aldinger, *J. Am. Ceram. Soc.* **83** (2000) 2391 (<https://doi.org/10.1111/j.1151-2916.2005.00467.x>)
18. H. B. Shan, Y. Zhu, Z. T. Zhang, *Br. Ceram. Trans.* **98** (1999) 146 (<https://doi.org/10.1179/096797899680363>)
19. G. Yu, J. Xie, S. Wang, Y. Wang, T. Wang, L. Fan, L. Zhang, F. Lei, Y. Shi, L. Yu, *Ceram. Int.* **47** (2021) 29253 (<https://doi.org/10.1016/j.ceramint.2021.07.089>)
20. M. Egashira, Y. Shimizu, S. Takatsuki, *J. Mater. Sci. Lett.* **10** (1991) 994 (<https://doi.org/10.1007/BF00721824>)
21. A. Kocjan, A. Dakskobler, T. Kosmac, *Int. J. Appl. Ceram. Technol.* **8** (2011) 853 (<https://doi.org/10.1111/j.1744-7402.2010.02516.x>)
22. R. S. Kumar, U. S. Hareesh, P. Ramavath, R. Johnson, *Ceram. Int.* **37** (2011) 2583 (<https://doi.org/10.1016/j.ceramint.2011.04.131>).





## Investigating inhibition characteristics of *Butea monosperma* leaf extracts to retard stainless steel biocorrosion in the presence of sulfate-reducing bacteria

SHIV KUMAR MANU, NOYEL VICTORIA SELVAM  
and MANIVANNAN RAMACHANDRAN\*

Department of Chemical Engineering, National Institute of Technology Raipur,  
Chhattisgarh – 492010, India

(Received 30 December 2022, revised 10 January, accepted 12 May 2023)

**Abstract:** The influence of sulfate-reducing bacteria *Desulfovibrio desulfuricans* on stainless steel SS 202 corrosion in neutral media was studied in detail using weight loss and electrochemical routes. The bacterial activity resulted in material loss with an average rate of 0.015 mm/year. The scanning electron microscopy (SEM) analysis showed a significant increase in the sessile bacterial population with the immersion period. Use of 500 ppm palash (*Butea monosperma*) leaf extract (PLE) reduced the average corrosion rate to 0.002 mm/year. SEM analysis showed a very thin external film formation in the presence of the inhibitor. The X-ray photoelectron spectroscopy studies confirmed the presence of corrosion products such as Fe<sub>2</sub>O<sub>3</sub> and FeS. The gas chromatography–mass spectrometry studies showed the dominant percentage of various terpenoids along with vitamin E as the main components of the PLE. Electrochemical analysis showed the existence of a diffusion barrier. The resistance offered by the diffusion barrier is high in the inhibited sample when compared to uninhibited samples.

**Keywords:** biocorrosion; *Butea monosperma*; electrochemical study; X-ray photoelectron spectroscopy.

### INTRODUCTION

The presence of bacteria in the environment surrounding a metal structure leads to its destruction by the corrosive products generated of their metabolic activity. This negative effect is frequently referred as biocorrosion or microbially influenced corrosion (MIC). Biocorrosion is caused by a wide variety of micro-organisms ranging from bacteria, algae and fungi.<sup>1</sup> MIC is prevalent in many process utilities and often leads to equipment breakdown, resulting in severe fin-

\* Corresponding author. E-mail: rmani.che@nitrr.ac.in  
<https://doi.org/10.2298/JSC221230026M>

ancial losses.<sup>1</sup> Corrosion caused by aggressive chemicals is widespread in all process plants and it can be identified, understood, and controlled with less difficulty. It is difficult to understand and control the MIC because of the interdependent activities of many microbes that change with local environmental factors involved in the MIC.<sup>2</sup>

Though the incidence percentage of MIC is not as high as chemical corrosion, 20 % of the total corrosion cost in any process unit is due to MIC.<sup>1</sup> It is well known that the effects of sulfate-reducing bacteria (SRB) are severe when compared to other bacterial species. The products of SRB metabolism are conducive and enhance the corrosion processes. The products of their metabolism produce corrosive polysulfides and sulfur that react with the metal ions leading to the production of respective metal sulfides which in turn are conducive and promote the formation of localized concentration cells to enhance corrosion and pitting.<sup>2</sup>

Stainless steel grade SS202 is widely used in many industrial applications, especially in the food industry. The characteristic feature of stainless steel is its corrosion-resistant properties. However, under aggressive environments, stainless steel is prone to corrosion. Inhibitors are playing an effective role in shielding metal substrates against corrosion. Despite their high efficiency, synthetic corrosion inhibitors cannot be employed regularly for corrosion prevention due to their severe environmental impacts. As a result, scientists have concentrated their efforts on developing green corrosion inhibitors. Plants, fruits, and their peels are excellent sources of phytochemical compounds that are less expensive and environmentally safer than the synthetic type of inhibitor.

Plant-based compounds contain certain natural compounds (phenolics compounds, lectins, essential oils, alkaloids, polypeptides, terpenoids and polyacetylenes) with powerful anti-biofilm properties.<sup>3</sup> These phytochemical compounds work on bacteria by substrate deprivation, rupture of microbe membrane, preventing bacterial attachment on surfaces, affecting the metabolism of exopolymeric substance formation, and inducing mutations.<sup>4,5</sup> The efficacy of Palash (*Butea monosperma*) leaf extract as green corrosion inhibitor on mild steel corrosion in 1 M HCl was studied and reported 96 % of corrosion inhibition efficiency.<sup>6</sup> The palash leaf extract has antibacterial activity against microbes including *Escherichia coli*, *Pseudomonas aeruginosa* and *Staphylococcus aureus* due to the presence of active substances like sterols, triterpenes, glycosides, flavonoids and proteins.<sup>7</sup> However, information on antibacterial activity against *Desulfovibrio desulfuricans* is not available in the literature. Hence, this is the first work reporting the antibacterial activity of palash leaf extract on *D. desulfuricans*. Tao *et al.* studied the role of total flavonoids of *Potentilla kleiniana* (TFP) against the stainless steel biocorrosion caused by *P. aeruginosa* bacterium by disrupting *P. aeruginosa*'s cell membrane.<sup>8</sup> Lekbach *et al.* studied the efficiency of catechin

hydrate as biocorrosion inhibitor caused by *P. aeruginosa* in 304L stainless steel and obtained a maximum inhibition efficiency of 99 %.<sup>9</sup>

The present work reports detailed studies on *D. desulfuricans*-induced corrosion in SS 202 and control of the same using 500 ppm (palash leaves) extract.

#### EXPERIMENTAL

In this investigation, *Desulfovibrio desulfuricans* sp. strains (NCIM, Pune, India) were employed. The modified Baar's medium consists of K<sub>2</sub>HPO<sub>4</sub>-0.5 g, NH<sub>4</sub>Cl-1.0 g, CaSO<sub>4</sub>-2.0 g, MgSO<sub>4</sub>·7H<sub>2</sub>O-2.0 g, sodium lactate-7.0 g, Fe(NH<sub>4</sub>)<sub>2</sub>(SO<sub>4</sub>)<sub>2</sub>-0.5 g in 1000 ml distilled water. The pH of the medium used for the studies was 7. Stainless steel coupons (SS 202) were cut to a size of 1 cm×1 cm×0.05 cm, and polished well. One side of the polished samples was sealed with Teflon tape. For the electrochemical studies, a copper contact was attached to the sealed surface and this was used as the working electrode. The composition of stainless-steel coupons used in this study was as follows (wt. %): 0.18 C, 0.53 Si, 9.48 Mn, 0.075 P, 0.012 S, 13.71 Cr, 0.01 Mo, 1.32 Ni, 0.01 Al, 0.84 Cu and balance Fe. The *Butea monosperma* (Palash) leaves were dried in sunlight to remove moisture and powdered with the help of a grinder. The obtained powder was soaked in ethanol for a period of 24 h and then filtered using a Whatman filter paper No. 1. Ethanol was removed by vacuum evaporation to yield palash leaf extract (PLE).

Weight loss experiments were carried out as two sets, one employing modified Baar's medium containing SRB culture (UB) and the other with modified Baar's medium, SRB and 500 ppm PLE (IB). The abiotic experiments were performed by immersing the coupons in modified Baar's medium (U)/modified Baar's medium and 500 ppm PLE (I). The numbers at the end of U/UB and I/IB represents the immersion period in weeks. The metal coupons prepared for the studies were weighed and immersed in individual test tubes filled with the UB/IB medium and incubated at 37 °C. Total duration of the study was four weeks. To study the progress of corrosion, every week four samples were withdrawn and the weight of the samples after cleaning and drying was measured. The nutrient medium into which the respective samples were immersed was also analyzed for the dissolved sulfide concentration using the standard protocol.<sup>10</sup> A comparison of the sample weight before and after immersion gives the weight loss of the sample, the average of which is used to estimate the corrosion rate CR using the method explained in the literature.<sup>1</sup> Similarly, for the electrochemical analysis techniques, the samples kept immersed were withdrawn from the media periodically for conducting potentiodynamic polarization (DP) and electrochemical impedance spectroscopy studies (EIS). Prior to each analysis, the samples were kept at open circuit potential (OCP) for 10 min. The scan rate used for DP was 5 mV/s. For EIS runs, the scan was done from 0.01 to 10<sup>3</sup> Hz with an AC amplitude of 10 mV. The electrochemical techniques were performed at 37 °C on an electrochemical analyser (PARSTAT). An Ag/AgCl reference electrode and a platinum counter electrode were used for the studies. A scanning electron microscopy (SEM, Carl Zeiss UHR model) combined with an energy-dispersive X-ray system was used to study morphology and elemental composition of the samples. To study the various functional groups, present in the external film adhered to the surface of the sample Fourier transform infrared (FTIR) spectroscopy (Bruker, Alpha model) and X-ray photoelectron spectroscopy (XPS) were used. The composition of the PLE was found using a gas chromatography and mass spectrometry (GC-MS) unit (Agilent 5977).

## RESULTS AND DISCUSSION

*Weight loss study*

The corrosion calculation by weight loss method was performed for stainless steel 202 coupons for a period of 28 days in both UB and IB media and the results are shown in Fig. 1a. In the UB sample, the CR of tested coupons was greater than in the IB medium. In the UB sample, the CR increases for the first two weeks and then remains stable till the fourth week. This could be due to the diffusion limitation caused by the deposition of corrosion products on the metal surface.

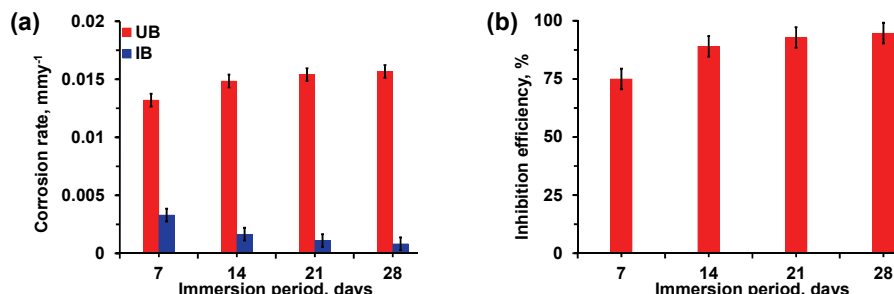


Fig. 1. a) Corrosion rate of stainless steel immersed in UB and IB medium and b) inhibition efficiency as a function of immersion period.

The CR of the IB sample presents a continuously decreasing trend indicating the formation of a stable, continuous external film that protects the surface. Fig. 1b shows the effect of the immersion period on the inhibition efficiency using 500 ppm of PLE. An average inhibition efficiency of 88 % was obtained.

Fig. S-1a and b of the Supplementary material to this paper show the corrosion rate of SS 202 in modified Baar's medium with (I) and without (U) Palash leaf extract in the absence of bacteria and inhibition efficiency as a function of immersion time, respectively. From Fig. 1a and S-1, it is clear that the corrosion rate in the abiotic case is significantly less when compared with the biotic case for both uninhibited and inhibited samples. The corrosion inhibition efficiency decreases with an increase in the immersion period, as seen in Fig. S-1b.

It is noteworthy to follow the sulfide concentration of the UB and IB samples during these periods which is presented in Fig. S-2 of the Supplementary material. During incubation the test tubes, containing UB and IB medium with SS samples immersed in them, turned black indicating the formation of iron sulfide set up by reaction between iron and  $\text{HS}^-$  caused by the SRB activity. The formation of  $\text{H}_2\text{S}$  is confirmed by the rotten egg odor upon opening the test tubes. From Fig. S-2, after the supplementation of the PLE, a decrease in dissolved sulfide content is clearly seen. This shows that the extract affects the metabolic activity of the bacteria resulting in reduced concentration of dissolved

sulfide. The literature suggests the neem leaf extract intervened in the metabolic activity of the *Desulfovibrio sp.* and inhibited the biocorrosion of API 5L X80 linepipe steel.<sup>11</sup> However, the palash leaf extract was reported for the inhibition of chemical corrosion of mild steel in HCl medium<sup>6</sup> and not for biocorrosion except by our previous publication for galvanized steel.<sup>12</sup> The sulfide content in the UB sample increased from 48 ppm in the first week to 69 ppm in the fourth week. On the other hand, the IB sample showed a continuously decreasing trend in the sulfide values which ultimately goes to zero in the fourth week. There will be some variation in the bacterial count due to the death phase of the bacteria. The dissolved sulfide can also react with the metal and form metal sulfides. This is corroborated by the increase in the sulfide content of the UB sample. A similar trend in the sulfide concentration has been reported in the literature.<sup>13</sup> Harrison and Thode studied the kinetic mechanism involved in the reduction of sulfate to sulfide by *D. desulfuricans* in Starkey's medium and optimized the temperature, metabolite concentrations and growth conditions.<sup>14</sup> The literature is available with respect to the kinetic study of anaerobic reduction of sulfate to sulfide caused by the mixed consortium.<sup>15</sup>

#### *Electrochemical impedance spectroscopy*

The electrical characteristics of the biofilm and corrosion products layer can be analyzed using EIS. Fig. S-3 a and b of the Supplementary material show the impedance modulus measured at different frequencies in UB and IB samples at varied immersion times. Fig. S-3c and d show the phase angle variations with frequency for the same. From S-3a and c, it can be noticed that the addition of the inhibitor extract increases the impedance modulus approximately by ten times. The impedance modulus at low frequency for the UB sample decreases significantly during the third week and increases to a greater extent in the fourth week. This is due to the development of a thicker corrosion products film during the fourth week which prevents the movement of the electrolyte. In the case of IB samples, the maximum impedance modulus at low frequency is observed for the third week. This decreases again in the fourth week which is due to the change in the thickness and composition of the external film formed on the metal. The formation of a thicker corrosion products layer during third week in IB sample matches well with the SEM findings. Overall, the impedance modulus of the IB samples is approximately ten-times higher at low frequencies for all the immersion durations indicating higher resistance to material degradation. The Bode phase angle plot shows the presence of two-time constants in both cases. In the case of UB samples, the phase angle at the lowest frequency decreases for the second and third weeks indicating an increase in corrosion. For the fourth week, the low-frequency peak is broader and shows a shift towards low frequency

which indicates good adsorption of the external film on the metal surface which offers protection against corrosion.<sup>16</sup>

In the case of IB samples, the phase angle peak at low frequency increases slightly for the second week. For the third week, the phase angle peak at the lower frequency region is much broader when compared to other weeks. The impedance modulus plot for the same period shows a maximum value at the lowest frequency which indicates that the film formed during the third week is continuous with good corrosion protection. Similarly, for the fourth week, the phase angle peak shows a shift towards lower frequency accompanied by an increase in peak value indicating good corrosion protection with immersion time.<sup>16</sup>

Fig. 2a and b illustrate the Nyquist plot for the SS sample in UB and IB media at different times. The high-frequency zone presents a semi-circular pattern and the low-frequency region shows the presence of diffusion limitation. The high-frequency semi-circular pattern shows the features of a depressed semicircle which is caused by surface roughness. Hence the system is modeled with a constant phase element (CPE) instead of an ideal capacitor. The impedance of any CPE element "i" ( $Z_i$ ) is given as:

$$Z_{i\text{CPE}} = Y_i^{-1} (j\omega)^{-n} \quad (1)$$

In the above equation,  $Y_i$  is the admittance in  $\text{S s}^n \text{ cm}^{-2}$ ,  $\omega$  is the angular frequency in  $\text{rad s}^{-1}$ ,  $j$  is  $-1$  and  $n$  is the roughness parameter the value of which becomes 1 for an ideal capacitor.

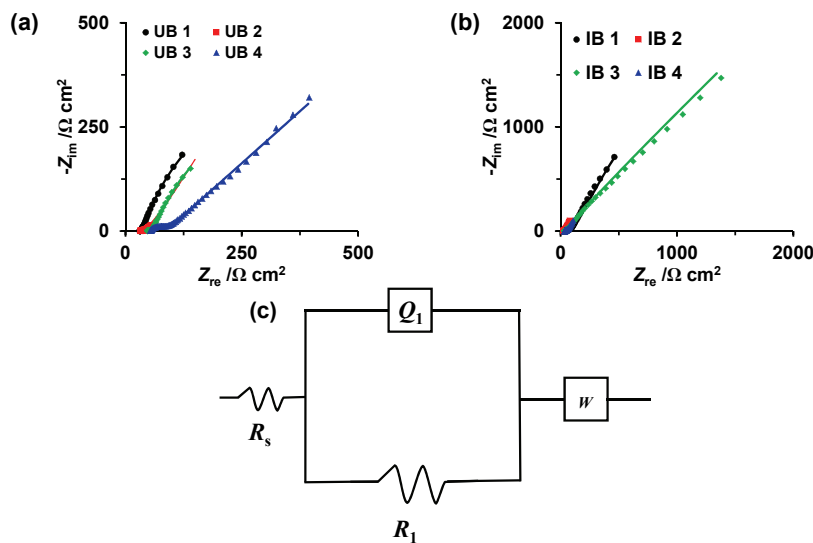


Fig. 2. Nyquist plot for stainless steel in: a) UB and b) IB medium. The experimental data is represented using a continuous line and dots depict equivalent electrical circuit (EEC) fit. c) EEC used for fitting the EIS data.

The equivalent circuit used to model the system is represented in Fig. 2c. The CPE is represented by  $Q_1$  and the diffusion element is represented using Warburg impedance ( $W$ ). The impedance ( $Z_W$ ) of the Warburg diffusion element is given as:<sup>17</sup>

$$Z_W = Y_0^{-1} (2\omega)^{-0.5} (1-j) \quad (2)$$

where  $Y_0$  is the admittance in  $S s^n cm^{-2}$ ,  $\omega$  is the angular frequency in  $rad s^{-1}$ .

Table I shows the best-fit parameters obtained for the EEC. The continuously decreasing trend of  $R_1$ , with immersion time in the case of the UB sample, and the continuously increasing trend of the same with immersion time for the IB sample match well with the results obtained from the weight loss studies. The capacitance ( $C_1$ ) of the CPE element can be found from the admittance  $Y_1$ , resistance  $R_1$  associated with the CPE unit, and the corresponding roughness parameter  $n_1$  calculated using:<sup>18</sup>

$$C_1 = (Y_1 (R_1^{1-n_1}))^{1/n_1} \quad (3)$$

The capacitance values are inversely proportional to the film thickness.<sup>2</sup> The calculated capacitance values in Table I show that the thickness of the film in the UB sample increases with immersion time while the inhibited sample presents a stable capacitance value which shows that the external film thickness is not altered significantly with immersion time.

TABLE I. EEC fitted value for the stainless steel in biotic and inhibited cases

Parameter	Biotic (UB)				Inhibitor (IB)			
	UB 1	UB 2	UB 3	UB 4	IB 1	IB 2	IB 3	IB 4
$R_s / \Omega cm^2$	31.26	37.34	49.67	53.8	53.19	29.03	33.81	38.59
$Y_1 \times 10^4 / S s^n cm^{-2}$	765	2290	1576	3	138	75	100	125
$n_1$	0.9187	1	1	0.6441	1	0.9007	0.9504	1
$R_1 / \Omega cm^2$	654.3	543.8	320.1	33.52	2061	2402	2581.5	2761
$W \cdot Y_0 / S s^{0.5} cm^{-2}$	0.0803	0.0272	0.0464	0.0082	0.0047	0.0102	0.0080	0.0059
$C_1 / \mu F cm^{-2}$	0.24	0.23	0.16	0.004	0.01	0.03	0.02	0.01

The inverse of Warburg admittance gives the resistance offered by the diffusion barrier. It is clearly seen that the diffusion resistance offered by the barrier is high with the PLE inhibitor.

#### Potentiodynamic polarization study (Tafel)

Tafel plot for the SS sample in UB and IB media after immersion for defined durations (up to four weeks) is shown in Fig. S-4 of the Supplementary material. The Tafel parameters obtained by Tafel region extrapolation are listed in Table II. It can be seen that the  $E_{corr}$  shows a positive shift with the immersion period in both UB and IB samples. This shows the formation of passive layer which pre-

vents the diffusion of the corrosive medium. When inhibitor molecules are added to the aggressive medium, the cathodic reaction is slowed, resulting in a negative shift in the open circuit potential observed for the first week which could be attributed to the decreased hydrogen generation at the cathode due to the adsorption of the inhibitor molecules.<sup>19,20</sup> Potentiodynamic polarization plots show a significant change with the addition of an inhibitor and hence alter the mechanism of hydrogen generation and anodic dissolution reactions.<sup>1,21,22</sup> From the second week positive shift in the potential with inhibitor addition can be observed. Moreover, it is clearly observed that both the cathodic and the anodic current densities are drastically decreased with the inhibitor addition. This gives information that both the cathodic hydrogen generation and anodic dissolution reactions are affected with the inhibitor addition. Thus, the inhibitor acts as a mixed inhibitor. Previously, the sulfide analysis results indicated that the inhibitor affected the metabolic activities of the SRB. Thus, the inhibitor works as a corrosion inhibitor and also as an antibacterial agent. Moreover, the  $j_{corr}$  values are lowered with the addition of the inhibitor and with immersion time it shows a continuously decreasing trend which shows the improved corrosion resistance properties of the inhibitor layer with time. In the absence of the inhibitor continuously increasing trend in the same can be observed. On the other hand, a continuously decreasing tendency is observed for  $j_{corr}$  with the inhibitor extract. As the stainless steel 202 grade contains manganese instead of nickel, the  $j_{corr}$  values are higher. Vignesh *et al.* reported  $j_{corr}$  value of 246.1  $\mu\text{A cm}^{-2}$  for SS202 in NaCl medium.<sup>23</sup>

TABLE II. Tafel fit parameters for stainless steel in biotic (a) and inhibited (b) to study various parameter to study biocorrosion

Sample		$E_{corr}$ V vs. Ag/AgCl	$j_{corr}$ $\mu\text{A cm}^{-2}$	$b_a$ mV dec <sup>-1</sup>	$-b_c$ mV dec <sup>-1</sup>	CR mm y <sup>-1</sup>	IE %
Biotic (UB)	UB1	-0.58	78	88.19	48.69	0.83	—
	UB2	-0.51	92.6	164.55	87.21	0.98	—
	UB3	-0.41	137	220	157.38	1.45	—
	UB4	-0.33	197.6	208.32	119.07	2.10	—
Inhibitor (IB)	IB1	-0.82	14.2	176	92.57	0.15	81.8
	IB2	-0.35	9.3	157	96.27	0.10	90.1
	IB3	-0.28	4.5	79.62	55.5	0.05	96.7
	IB4	-0.09	3.7	142.36	102.58	0.04	98.1

#### FTIR analysis

Fig. 3a–c shows the FTIR spectra for the samples immersed in the UB and IB media along with the spectrum of the Palash leaf extract. The FTIR spectrum of samples in the UB medium show strong peaks between 650–660  $\text{cm}^{-1}$  which correspond to the presence of the acetal group, one of the major components of

the bacterial biofilm.<sup>24</sup> The peak at 1500–1520 cm<sup>-1</sup> corresponds to the amide II functional groups (NH bending and CN stretching) in the biofilm.<sup>25</sup> The peak at 2353 cm<sup>-1</sup> corresponds to N–H or C=O stretching vibrations.<sup>26</sup> The peak at 3737 cm<sup>-1</sup> corresponds to the hydroxyl groups of the biofilms.<sup>27</sup> The samples immersed in IB samples show the presence of amide II functional groups (1530 cm<sup>-1</sup>) and esters (1680–1700 cm<sup>-1</sup>). Apart from that peak at 2353 cm<sup>-1</sup> corresponding to N–H or C=O group can also be observed. The sample also shows the presence of O–H group (3740 cm<sup>-1</sup>).

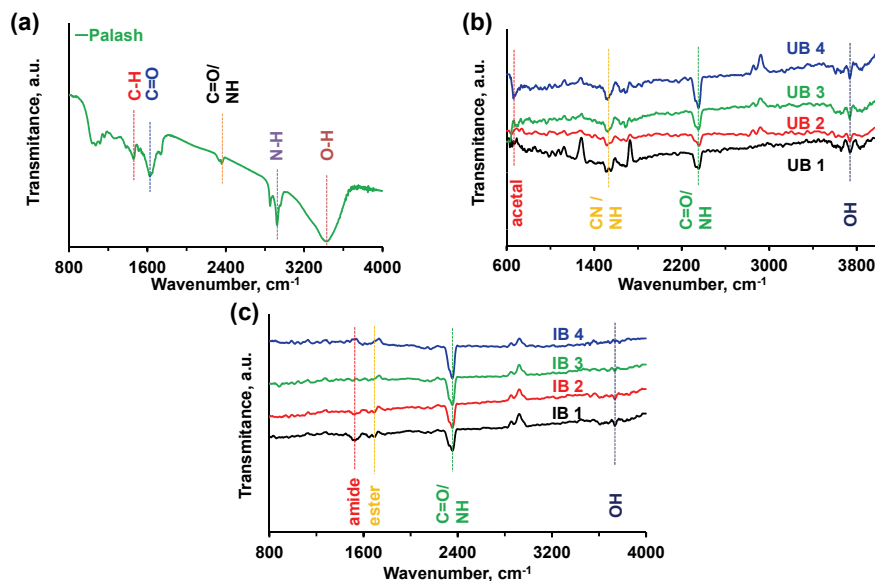


Fig. 3. FTIR analysis of ethanolic extract of: a) Palash leaf extract, b) biotic case and c) inhibited case in the medium.

#### Scanning electron microscopy

The SEM images of the UB and IB samples with the external film formed on them after one and three weeks of immersion period are shown in Fig. 4. The UB sample at the end of first week shows many sessile cells with two distinct layers - One compact inner layer and an outer layer that shows spherical structures scattered all over the sample surface. The third-week UB sample shows the presence of numerous sessile bacteria and a compact external biofilm layer. The compactness of the external layer in the case of UB sample increases with the immersion period which adds strength to the weight loss results where the corrosion rate stays stable after two weeks of immersion. The IB sample shows the presence of a very thin external layer in the first week. In the third week's sample, tiny scattered granular structures can be observed which could be due to the adsorbed cor-

rosion products and inhibitor molecules. Table S-I of the Supplementary material shows the elemental composition of the UB and IB samples at different immersion period. The IB samples show higher carbon content when compared to UB samples which could be due to the adsorbed inhibitor molecules. The sulfide and iron concentrations are high in the UB samples due to the formation and deposition of iron sulfide.

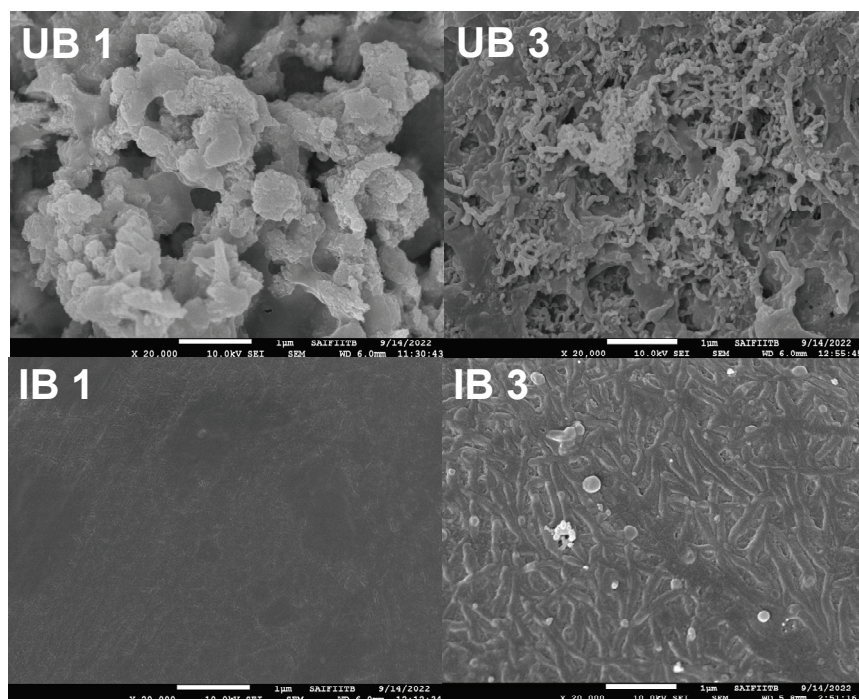


Fig. 4. SEM images of the layer formed on the stainless-steel coupons immersed in UB and IB medium for 1- and 3-week immersion periods.

#### *GC–MS analysis*

The findings of the GC–MS analysis of PLE are given in Table S-II of the Supplementary material. The analysis shows that about 78.9 % of the extract is composed of terpenoids which are known for their antioxidant and antibacterial properties. Similarly, compounds such as vitamin E and W-18 are also helpful in controlling bacterial growth and corrosion.

#### *X-ray photoelectron spectroscopy*

Fig. 5a–e show the deconvoluted XPS spectra for the elements: iron, nitrogen, carbon, oxygen and sulfur, respectively. The Fe2p deconvolution peak at 706.6 eV confirms the presence of  $\text{FeS}_2$ .<sup>28</sup> The peaks at 710.8 and 716.6 eV arise

due to the presence of  $\text{Fe}^{3+}$ . The presence of metallic Fe is denoted by the peak at 719.2 eV.<sup>20</sup> The N1s deconvolution gives two peaks one at 399.4 eV and the second at 400.7 eV. These belong to the amine groups of the biological system.<sup>29</sup> The deconvoluted C1s spectra for the third week UB sample with an external film formed on it shows peaks at 284.1, 285.6 and 287.6 eV corresponding to C=C, C-C, O-C-O and C=O functional groups, respectively.<sup>30</sup> These peaks are contributions from the organic compounds present in the biofilm. The O1s spectra for the UB sample show two significant peaks at 531.3 and 530.9 eV corresponding to carbonyl compounds of biofilm and the iron oxides formed due to corrosion reactions.<sup>31</sup> The S2p deconvolution shows a peak at 163.5, 166.6 and 168.6 eV corresponding to the presence of iron sulfide ( $\text{Fe}_{0.89}\text{S}$ ),  $\text{SO}_3$  and  $\text{SO}_4^{2-}$ , respectively.<sup>32-34</sup>

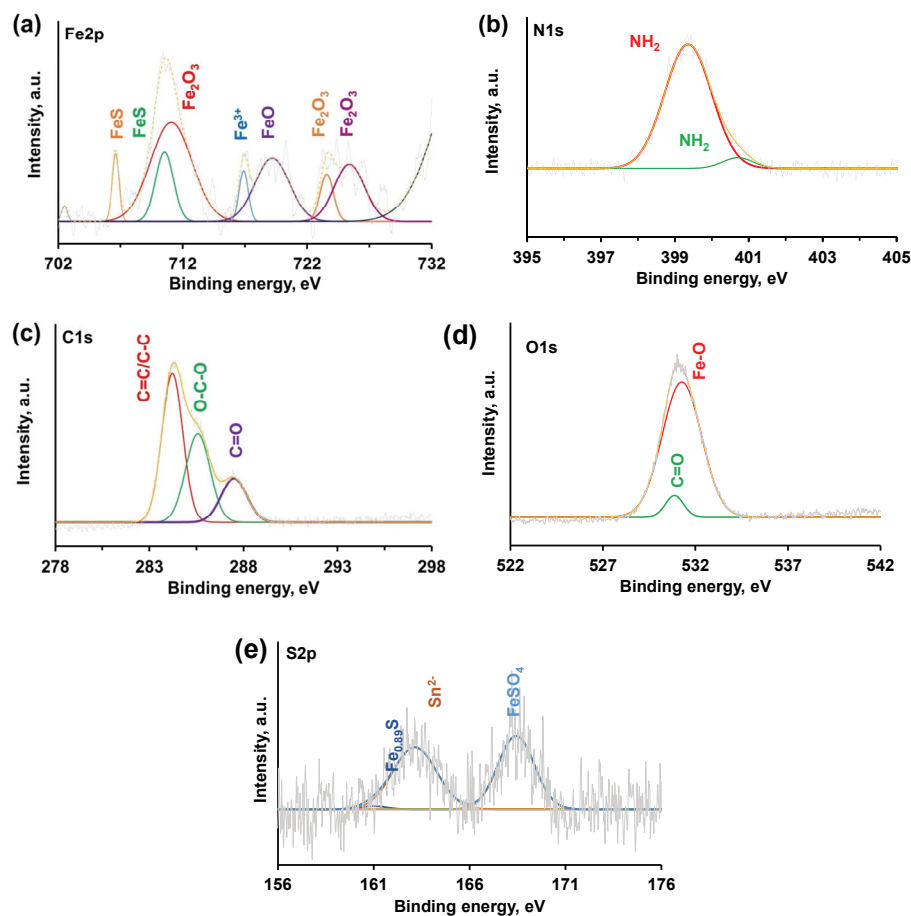


Fig. 5. Deconvoluted XPS spectra of SS 202 in UB medium: a) Fe2p, b) N1s, c) C1s, d) O1s and e) S2p.

Fig. 6a–e shows the deconvoluted XPS spectra of various elements in IB sample. The C1s spectra show the presence of C=C (284.3 eV) which could be a contribution from inhibitor component W-18.<sup>30,35</sup> The peak at 285.7 eV corresponds to C–O group. The O1s deconvolution gives peak at 530.6 eV which represents iron oxides and the peak at 531.5 eV affirms the presence of organic C–O bond.<sup>36</sup> The N1s deconvolution shows primary peak at 398.3 eV that is characteristic of pyridinic group which could have come from the W-18 compound of the inhibitor extract.<sup>37</sup> The peaks at 399.9 and 402.4 eV signify amide and N–O groups, respectively.<sup>38,39</sup> The peak at 407.9 eV corresponds to NO<sub>3</sub><sup>-</sup>.<sup>40</sup> The peaks at 709.4 and 723 eV, and the satellite peak at 715.3 eV show the presence of Fe<sup>2+</sup>.<sup>41</sup> The peak at 160.8 eV in the deconvoluted s2p spectra shows the existence of S<sup>2-</sup> and the peaks at 162.4 and 169 eV, respectively, show the presence of S<sub>2</sub><sup>2-</sup> and SO<sub>4</sub><sup>2-</sup>.<sup>42</sup> The sulfide group could have originated from the sulfonamide products of inhibitor molecules or from FeS. The products of corrosion from the XPS studies based on literature include iron sulfides and oxides.

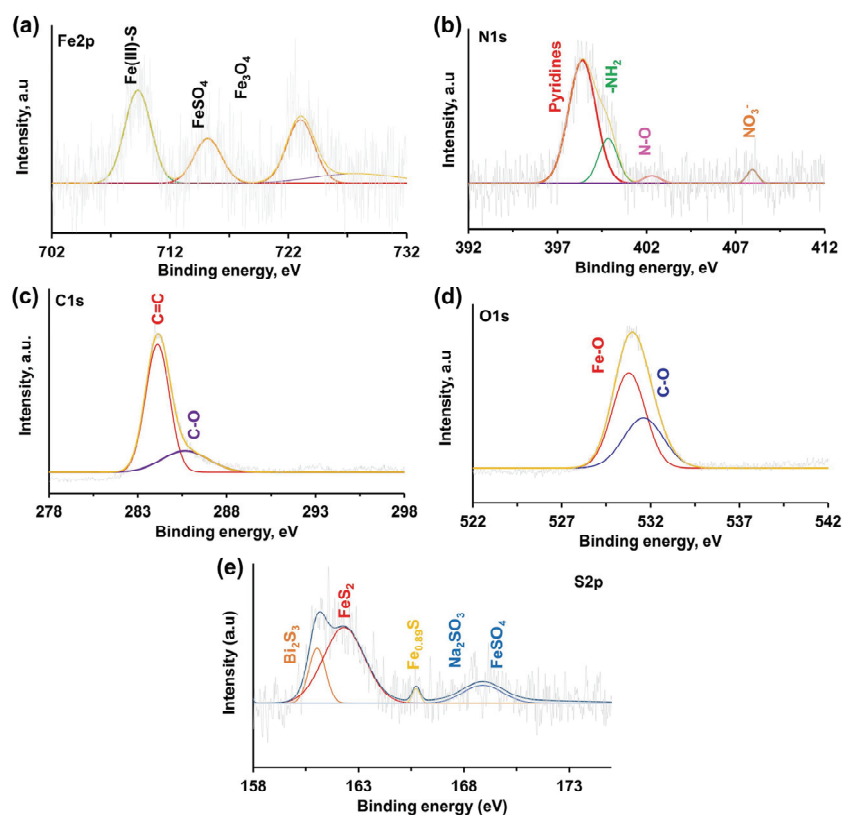
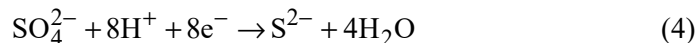


Fig. 6. Deconvoluted XPS spectra of SS 202 in IB medium: a) Fe2p, b) N1s, c) C1s, d) O1s and e) S2p.

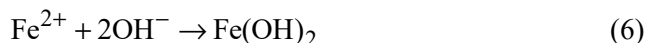
Table S-I shows the elemental composition of the samples analyzed by EDAX. The increased amount of carbon in the inhibited sample is due to the adsorbed inhibitor molecules. The sulfide and iron content are very low in the IB sample.

#### *Mechanism*

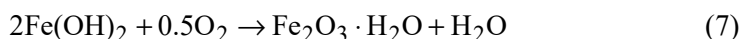
Analysis of the external film formed on the UB and IB samples have shown that the samples mainly consisted of iron sulfides and oxides. The dissolution of iron in SS 202 causes formation of  $\text{Fe}^{2+}$ . The SRB utilize the hydrogen ions generated by the water dissociation, sulfate in the environment and the electrons from iron dissolution for the reduction reaction to produce  $\text{FeS}$ .<sup>43,44</sup> The following reactions can be written:



Apart from the formation of  $\text{FeS}$ , the hydroxyl radicals formed from water dissociation react with  $\text{Fe}^{2+}$  to yield  $\text{Fe(OH)}_2$ :



In the alkaline environment the  $\text{Fe(OH)}_2$  reacts to give rust ( $\text{Fe}_2\text{O}_3 \cdot \text{H}_2\text{O}$ ):<sup>43,45</sup>



The sulfides produced by SRB are more reactive, soluble and exist in more reduced form. In the present study pH measurement after four weeks shows a pH close to 9. At these alkaline conditions, the sulfides produced easily react to produce polysulfides and sulfur.<sup>46,47</sup> With the inhibitor extract the number of sessile bacteria is reduced as observed from the SEM images and the metabolic activity of the bacteria is also decreased which is reflected in the decreased dissolved sulfide concentration, corrosion products and corrosion rate.

#### CONCLUSIONS

The effect of palash leaf extract in the control of SRB caused corrosion in SS 202 was studied in detail. Over an immersion period of four weeks, 500 ppm of PLE was able to control the corrosion by 88 %. The SEM analysis showed the formation of different kinds of external layer on the sample in the presence and absence of PLE. In the case of uninhibited samples, the biofilm thickness and the number of sessile bacteria increased with immersion period. In the inhibited sample a very thin external film was observed. The XPS analysis showed significant products of corrosion as  $\text{FeS}$  and  $\text{Fe}_2\text{O}_3$ . The inhibitor consisted of 78 % terpenoids which are known for their antioxidant and antibacterial effects. The

PLE was found to work well in the control of SS 202 corrosion caused by SRB activity in the neutral medium.

#### SUPPLEMENTARY MATERIAL

Additional data and information are available electronically at the pages of journal website: <https://www.shd-pub.org.rs/index.php/JSCS/article/view/12207>, or from the corresponding author on request.

#### ИЗВОД

#### ИСПИТИВАЊЕ ИНХИБИТОРСКИХ КАРАКТЕРИСТИКА ЕКСТРАКТА ЛИШЋА *Butea monosperma* НА УСПОРАВАЊЕ БИОКОРОЗИЈЕ НЕРЂАЈУЋЕГ ЧЕЛИКА У ПРИСУСТВУ СУЛФАТ-РЕДУКУЈУЋИХ БАКТЕРИЈА

SHIV KUMAR MANU, NOYEL VICTORIA SELVAM и MANIVANNAN RAMACHANDRAN

*Department of Chemical Engineering, National Institute of Technology Raipur, Chhattisgarh – 492010, India*

Утицај сулфат-редукујућих бактерија *Desulfovibrio desulfuricans* на корозију нерђајућег челика SS 202 у неутралној средини је детаљно испитиван коришћењем методе губитка масе и електрохемијских метода. Активност бактерија доводи до губитка материјала просечном брзином од 0,015 mm/год. Анализа скенирајућом електронском микроскопијом (СЕМ) је показала значајан пораст популације сесилних бактерија током периода урењања. Примена екстракта лишћа биљке шумски пламен (*Butea monosperma*) концентрације 500 ppm је смањила просечну брзину корозије на 0,002 mm/год. СЕМ анализом је показано да се у присуству инхибитора формира веома танак спољашњи филм. Фотоелектронска спектроскопија X-зрацима је потврдила присуство корозионих продуката као што су Fe<sub>2</sub>O<sub>3</sub> и FeS. Испитивањима гасном хроматографијом–масеном спектрометријом је утврђено да су главне компоненте екстракта листа шумског пламена различити терпеноиди и витамин E. Електрохемијска анализа је показала присуство дифузионе баријере током корозије. Отпорност која потиче од дифузионе баријере се значајно повећава у присуству инхибитора.

(Примљено 30. децембра 2022, ревидирано 10. јануара, прихваћено 12. маја 2023)

#### REFERENCES

1. A. Sharma, M. Ramachandran, N. V. Selvam, *Corr. Rev.* **40** (2021) 87 (<https://doi.org/10.1515/corrrev-2021-0019>)
2. B. S. Swaroop, S. N. Victoria, R. Manivannan, *J. Taiwan Inst. Chem. Eng.* **64** (2016) 269 (<https://doi.org/10.1016/j.jtice.2016.04.007>)
3. Y. Y. Yong, G. A. Dykes, W. S. Choo, *Crit. Rev. Microbiol.* **45** (2019) 201 (<http://doi.org/10.1080/1040841X.2019.1573802>)
4. M. M. Cowan, *Clin. Microbiol. Rev.* **12** (1999) 564 (<https://doi.org/10.1128/CMR.12.4.564>)
5. L. Lu, W. Hu, Z. Tian, D. Yuan, G. Yi, Y. Zhou, *Chin. Med.* **14** (2019) 11 (<http://doi.org/10.1186/s13020-019-0232-2>)
6. A. Singh, M. A. Quraishi, E. E. Ebenso, *Int. J. Electrochem. Sci.* **7** (2012) 12545 (<http://www.electrochemsci.org/papers/vol7/71212545.pdf>)
7. M. C. Sahu, R.N. Padhy, *Asian Pac. J. Trop. Dis.* **3** (2013) 217 ([https://doi.org/10.1016/S2222-1808\(13\)60044-4](https://doi.org/10.1016/S2222-1808(13)60044-4))
8. J. Tao, S. Yan, H. Wang, L. Zhao, H. Zhu, Z. Wen, *LWT* **154** (2022) 112631, (<https://doi.org/10.1016/j.lwt.2021.112631>)

9. Y. Lekbach, Y. Dong, Z. Li, D. Xu, S. El Abed, Y. Yi, L. Li, S. I. Koraichi, T. Sun, F. Wang, *Corros. Sci.* **157** (2019) 98 (<https://doi.org/10.1016/j.corsci.2019.05.021>)
10. *ASTMG31-12a, Standard Guide for Laboratory Immersion Corrosion Testing of Metals*, 2012 (<http://www.astm.org/Standards/G31>)
11. S. M. Bhola, F. M. Alabbas, R. Bhola, J. R. Spear, B. Mishra, D. L. Olson, A. E. Kakpovbia, *Eng. Fail. Anal.* **36** (2014) 92 (<https://doi.org/10.1016/j.engfailanal.2013.09.015>)
12. S. K. Manu, S. N. Victoria, R. Manivannan, *J. Indian Chem. Soc.* **99** (2022) 100652 (<https://doi.org/10.1016/j.jics.2022.100652>)
13. S. Kebbouche-Gana, M.L. Gana, *Ann. Microbiol.* **62** (2012) 203 (<https://doi.org/10.1007/s13213-011-0247-0>)
14. A.G. Harrison, H.G. Thode, *Trans. Faraday Soc.* **54** (1958) 84 (<https://doi.org/10.1039/TF9585400084>)
15. S. Moosa, M. Nemat, S. T. L. Harrison, *Chem. Eng. Sci.* **57** (2002) 2773 ([https://doi.org/10.1016/S0009-2509\(02\)00152-5](https://doi.org/10.1016/S0009-2509(02)00152-5))
16. S. Meng, Z. Liu, X. Zhao, B. Fan, H. Liu, M. Guo, H. Hao, *RSC Adv.* **11** (2021) 31693 (<https://doi.org/10.1039/d1ra04976c>)
17. C. N. Cao, J. Q. Zhang, *An Introduction to Electrochemical Impedance Spectroscopy*, Science Press, Beijing, 2002
18. H. Ma, X. Cheng, G. Li, S. Chen, Z. Quan, S. Zhao, L. Niu, *Corros. Sci.* **42** (2000) 1669 ([https://doi.org/10.1016/S0010-938X\(00\)00003-2](https://doi.org/10.1016/S0010-938X(00)00003-2))
19. R. S. Abdel Hameed, *Int. J. Electrochem. Sci.* **17** (2022) 221017 (<https://doi.org/10.20964/2022.10.31>)
20. Y. Guo, T. Meng, D. Wang, H. Tan, R. He, *Eng. Fail. Anal.* **78** (2017) 87 (<https://doi.org/10.1016/j.engfailanal.2017.03.003>)
21. H. Liu, G. Meng, W. Li, T. Gu, H. Liu, *Front. Microbiol.* **10** (2019) 1298 (<https://doi.org/10.3389/fmicb.2019.01298>)
22. G. Vignesh, C. S. Narayanan, P. Chinnaiyan, K. Shanmugapriya, *Mater. Res. Express* **6** (2019) 126540 (<https://doi.org/10.1088/2053-1591/ab5606>)
23. A. Kumar, P.C. Srivastava, *Mater. Sci.-Pol.* **37** (2019) 116 (<https://doi.org/10.2478/msp-2019-0001>)
24. C. Mayer, R. Moritz, C. Kirschner, W. Borchard, R. Maibaum, J. Wingender, H. C. Flemming, *Int. J. Biol. Macromol.* **26** (1999) 3 ([https://doi.org/10.1016/S0141-8130\(99\)00057-4](https://doi.org/10.1016/S0141-8130(99)00057-4))
25. A. Z. M. Rus, in *Biopolymers and biotech admixtures for eco-efficient construction materials*, F. Pacheco-Torgal, V. Ivanov, N. Karak, H. Jonkers, Eds., Woodhead Publishing, Sawston, 2016, p. 427 (<https://doi.org/10.1016/C2014-0-02075-8>)
26. S. Vijayakumar, B. Vaseeharan, B. Malaikozhundan, N. Gopi, P. Ekambaram, R. Pachaiappan, P. Velusamy, K. Murugan, G. Benelli, R. S. Kumar, M. Suriyanarayananamoorthy, *Microbial Pathogenesis* **102** (2017) 173 (<https://doi.org/10.1016/j.micpath.2016.11.029>)
27. M. M. Haque, M. K. Mosharaf, M. A. Haque, M. Z. H. Tanvir, M. K. Alam, *Front. Microbiol.* **12** (2021) 615113 (<https://doi.org/10.3389/fmicb.2021.615113>)
28. H. Qi, Y. Wang, J. Feng, R. Peng, Q. Shi, X. Xie, *Int. J. Environ. Res. Public Health* **19** (2022) 15416 (<https://doi.org/10.3390/ijerph192215416>)
29. P. Li, M. Yu, X. Ke, X. Gong, Z. Li, X. Xing, *ACS Appl. Bio Mater.* **5** (2022) 3290 (<https://doi.org/10.1021/acsabm.2c00292>)

30. H.-W. Tien, Y.-L. Huang, S.-Y. Yang, J.-Y. Wang, C.-C. M. Ma, *Carbon* **49** (2011) 1550 (<https://doi.org/10.1016/j.carbon.2010.12.022>)
31. N. Sarmadi, M. Gharabaghi, M. T. Saray, M. Darestani, D. Garman, P. Koshy, S. S. Mofarah, C. C. Sorrell, *Inorg. Chem.* **60** (2021) 175 (<https://dx.doi.org/10.1021/acs.inorgchem.0c02762>)
32. Y. Yuan, L. Wang, L. Gao, *Front. Chem.* **8** (2020) 818 (<https://doi.org/10.3389/fchem.2020.00818>)
33. M. Watanabe, H. Ando, T. Handa, T. Ichino, N. Kuwaki, *Zairyo-to-Kankyo* **56** (2007) 10 (<https://doi.org/10.3323/jcorr.56.10>)
34. *NIST X-ray Photoelectron Spectroscopy Database*, 2012 (<http://dx.doi.org/10.18434/T4T88K>)
35. E. E. Knaus, B. K. Warren, T. A. Ondrus (University of Alberta, Bayer Corp) US Patent Publication 4,468,403 (1984)
36. Y. Wu, Y. Lin, J. Xu, *Photochem. Photobiol. Sci.* **18** (2019) 1081 (<https://doi.org/10.1039/C8PP00493E>)
37. D. Kim, Y. Kwon, J.-H. Lee, S.-J. Kim, Y.-I. Park, *Membranes* **12** (2022) 93 (<https://doi.org/10.3390/membranes12010093>)
38. R. J. J. Jansen, H. van Bekkum, *Carbon* **33** (1995) 1021 ([https://doi.org/10.1016/0008-6223\(95\)00030-H](https://doi.org/10.1016/0008-6223(95)00030-H))
39. X. Yan, T. Xu, G. Chen, S. Yang, H. Liu, Q. Xue, *J. Phys., D* **37** (2004) 907 (<https://doi.org/10.1088/0022-3727/37/6/015>)
40. Y. R. Park, M. J. Ko, Y.-H. Song, C. J. Lee, *J. Appl. Phys.* **114** (2013) 153516 (<https://doi.org/10.1063/1.4826206>)
41. G. Dong, M. Fang, J. Zhang, R. Wei, L. Shu, X. Liang, S. Yip, F. Wang, L. Guan, Z. Zheng, J. C. Ho, *J. Mater. Chem., A* **5** (2017) 11009 (<https://doi.org/10.1039/C7TA01134B>)
42. Z. Otgonbayar, W. C. Oh, *J. Inorg. Organomet. Polym.* **32** (2022) 2910 (<https://doi.org/10.1007/s10904-022-02319-8>)
43. V. C. Nettikaden, D. Ifezue, F. H. Tobins, *J. Fail. Anal. Preven.* **14** (2014) 43 (<https://doi.org/10.1007/s11668-013-9757-3>)
44. F. Guan, X. Zhai, J. Duan, M. Zhang, B. Hou, *PLoS One* **11** (2016) e0162315. (<https://dx.doi.org/10.1371/journal.pone.0162315>)
45. Z. Ahmad, *Principles of Corrosion Engineering and Corrosion Control*, Butterworth-Heinemann, Oxford, 2006 (<https://doi.org/10.1016/B978-0-7506-5924-6.X5000-4>)
46. S. L. Johnston, G. Voordouw, *Environ. Sci. Technol.* **46** (2012) 9183 (<https://doi.org/10.1021/es3019594>)
47. R. Cord-Ruwisch, W. Kleinitz, F. Widdel, *J. Pet. Technol.* **39** (1987) 97 (<https://doi.org/10.2118/13554-PA>).

SUPPLEMENTARY MATERIAL TO  
**Investigating inhibition characteristics of *Butea monosperma* leaf extracts to retard stainless steel biocorrosion in the presence of sulfate-reducing bacteria**

SHIV KUMAR MANU, NOYEL VICTORIA SELVAM  
and MANIVANNAN RAMACHANDRAN\*

Department of Chemical Engineering, National Institute of Technology Raipur,  
Chhattisgarh – 492010, India

J. Serb. Chem. Soc. 88 (7–8) (2023) 749–764

Fig. S-1a and b show the corrosion rate of SS 202 in modified Baar's medium containing with (I) and without (U) palash leaf extract in the absence of bacteria and inhibition efficiency as a function of immersion time respectively. From Fig. 1a and S-1, it is clear that the corrosion rate in the abiotic case is significantly less when compared with the biotic case for both uninhibited and inhibited samples. The corrosion inhibition efficiency decreases with an increase in the immersion period, as seen in Fig. S-1b.

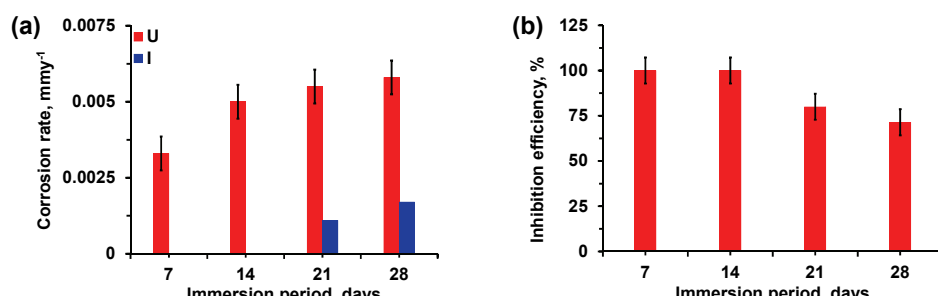


Fig. S-1. (a) Corrosion rate of stainless steel immersed in U and I medium in the absence of bacteria and (b) inhibition efficiency as a function of immersion period.

From Fig. S-2, after the supplementation of the PLE, a decrease in dissolved sulfide content is clearly seen. This shows that the extract affects the metabolic activity of the bacteria resulting in reduced dissolved sulfide concentration. The sulfide content in the UB sample increased from 48 ppm in the first week to 69 ppm in the fourth week. On the other hand, the IB sample showed a continuously

\* Corresponding author. E-mail: rmani.che@nitrr.ac.in

decreasing trend in the sulfide values which ultimately goes to zero in the fourth week.

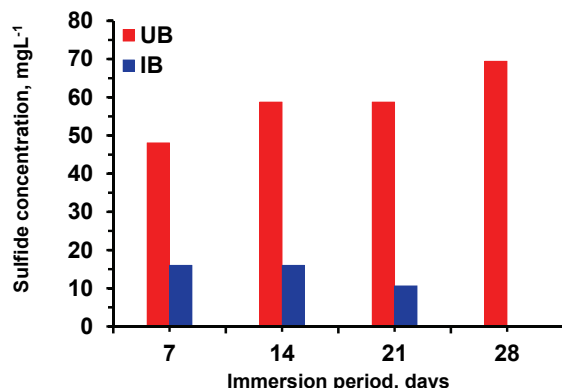


Fig. S-2. Effect of immersion time on dissolved sulfide concentrations for SS 202 in UB and IB medium.

Fig. S-3a and b show the impedance modulus measured at different frequencies in UB and IB samples at varied immersion times. Fig. S-3c and d show the phase angle variations with frequency for the same. From Fig. S-3a and c, it can be noticed that the addition of the inhibitor extract increases the impedance modulus approximately by ten times. The impedance modulus at low frequency for the UB sample decreases significantly during the third week and increases to a greater extent in the fourth week. This is due to the development of a thicker corrosion products film during the fourth week which prevents the movement of the electrolyte. In the case of IB samples, the maximum impedance modulus at low frequency is observed for the third week. This decreases again in the fourth week which is due to the change in the thickness and composition of the external film formed on the metal. The formation of a thicker corrosion products layer during third week in IB sample matches well with the SEM findings. Overall, the impedance modulus of the IB samples is approximately ten-times higher at low frequencies for all the immersion durations indicating higher resistance to material degradation. The Bode phase angle plot shows the presence of two-time constants in both cases. In the case of UB samples, the phase angle at the lowest frequency decreases for the second and third weeks indicating an increase in corrosion. For the fourth week, the low-frequency peak is broader and shows a shift towards low frequency which indicates good adsorption of the external film on the metal surface which offers protection against corrosion.<sup>1</sup>

In the case of IB samples, the phase angle peak at low frequency increases slightly for the second week. For the third week, the phase angle peak at the

lower frequency region is much broader when compared to other weeks. The impedance modulus plot for the same period shows a maximum value at the lowest frequency which indicates that the film formed during the third week is continuous with good corrosion protection. Similarly, for the fourth week, the phase angle peak shows a shift towards lower frequency accompanied by an increase in peak value indicating good corrosion protection with immersion time.<sup>1</sup>

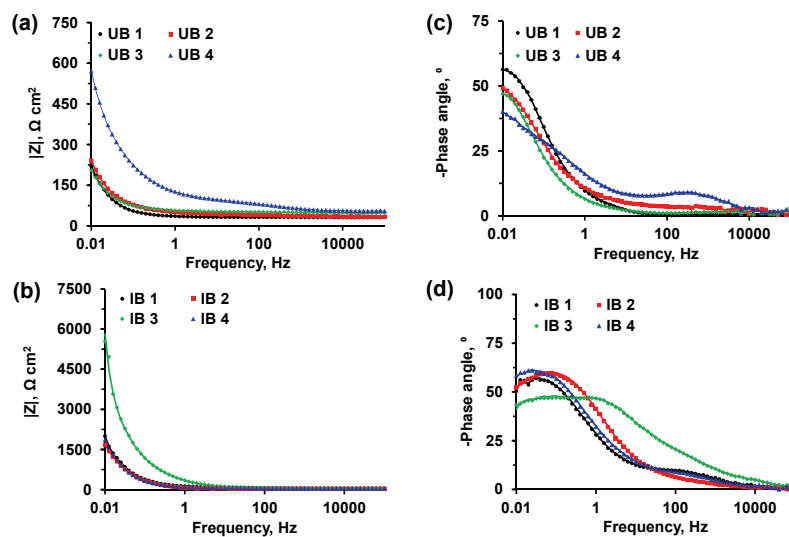


Fig. S-3. Bode impedance modulus for SS 202 in (a) UB and (b) IB medium at different immersion periods. Bode phase angle plot for SS 202 in (c) UB and (d) IB medium at different immersion periods.

Tafel plot for the SS sample in UB and IB media after immersion for defined durations is shown in Fig. S-4. The Tafel parameters obtained after Tafel region extrapolation are listed in Table II. It can be seen that the  $E_{\text{corr}}$  shows a positive shift with the immersion period in both UB and IB samples. This shows the formation of passive layer which prevents the diffusion of the corrosive medium. With the inhibitor addition, a significant negative shift in  $E_{\text{corr}}$  is observed for the first week which could be attributed to the decreased hydrogen generation at the cathode due to the adsorption of the inhibitor molecules.<sup>2</sup> From the second week positive shift in the potential with inhibitor addition can be observed. Moreover, it is clearly observed that both the cathodic and the anodic current densities are drastically decreased with the inhibitor addition. This gives information that both the cathodic hydrogen generation and anodic dissolution reactions are affected with the inhibitor addition. Thus, the inhibitor acts as a mixed inhibitor.

Previously, the sulfide analysis results indicated that the inhibitor affected the metabolic activities of the SRB. Thus, the inhibitor works as a corrosion inhibitor and also as an antibacterial agent. Moreover, the  $j_{corr}$  values are lowered with the addition of the inhibitor for all weeks and with immersion time it shows a continuously decreasing trend which shows the improved corrosion resistance properties of the inhibitor layer with time. In the absence of the inhibitor continuously increasing trend in the same can be observed. On the other hand, a continuously decreasing tendency is observed for  $j_{corr}$  with the inhibitor extract.

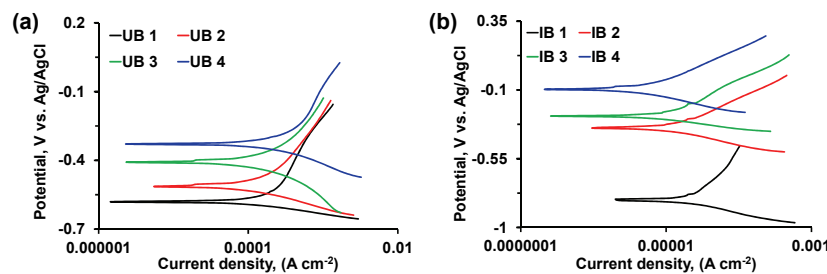


Fig. S-4. Polarization plots for SS 202 coupons immersed in (a) UB (b) IB media at four immersion periods.

Table S-I shows the elemental composition of the UB and IB samples at different immersion period. The IB samples show higher carbon content when compared to UB samples which could be due to the adsorbed inhibitor molecules. The sulfide and iron concentrations are high in the UB samples due to the formation and deposition of iron sulfide.

TABLE S-I. Elemental analyses of the layer formed on the stainless-steel coupons immersed in UB and IB medium for 1- and 3-week immersion periods. All values are in at. %

Element	UB 1	UB 3	IB 1	IB 3
C	30.40	33.49	70.18	70.74
O	48.07	37.85	20.60	20.22
Na	0.60	1.56	0.02	0
Mg	1.57	1.86	0	0.03
Si	0.06	0.83	0.44	0.63
P	5.19	6.12	8.13	7.77
S	3.14	3.33	0.18	0.10
Ca	7.00	3.80	0.21	0.33
Cr	0.04	1.13	0.06	0
Mn	1.81	0.49	0.02	0.03
Fe	1.80	9.02	0.16	0.05
Ni	0.06	0.05	0	0.12
Cu	0.27	0.46	0	0

The findings of the GC-MS analysis of PLE are given in Table S-II. The analysis shows that about 78.9 % of the extract is composed of terpenoids which

are known for their antioxidant and antibacterial properties. Similarly, compounds such as vitamin-E and W-18 are also helpful in controlling bacterial growth and corrosion.

TABLE S-II. List of few compounds present in significant quantities in palash leaf extract identified from GC-MS analysis

Compound name	Time (min)	Area (%)	Group
3-O-Methyl-d-glucose	20.49	3.22	D-aldohexose
Hexadecanoic acid, 2-hydroxy-1-(hydroxymethyl)ethyl ester	37.97	3.33	Ester
Di(pentamethylphenyl)ketone	44.08	6.20	Ketones
W-18	44.70	3.79	Opioid
Vitamin E	46.80	4.53	Methylated phenol
Lup-20(29)-en-3-one	49.85	40.95	Triterpenoid
Betulin	50.14	19.79	Pentacyclic triterpenoid
$\gamma$ -Sitostenone	50.99	18.20	Tetracyclic terpene

#### REFERENCES

1. S. Meng, Z. Liu, X. Zhao, B. Fan, H. Liu, M. Guo, H. Hao, *RSC Adv.* **11** (2021) 31693 (<https://doi.org/10.1039/d1ra04976c>)
2. A. Kumar, P.C. Srivastava, *Mater. Sci.-Pol.* **37** (2019) 116 (<https://doi.org/10.2478/msp-2019-0001>).



## Application of liquid chromatography in defining the interaction of newly synthesized chalcones and related compounds with human serum albumin

NEMANJA TURKOVIĆ<sup>1,2\*</sup>, NASTASIJA ANĐELKOVIĆ<sup>3</sup>, DARIJA OBRADOVIĆ<sup>4</sup>,  
ZORICA VUJIĆ<sup>3</sup> and BRANKA IVKOVIĆ<sup>3</sup>

<sup>1</sup>*Institute for Medicines and Medical Devices of Montenegro (CInMED), Blvd. Ivana Crnojevića 64a, Podgorica, Montenegro, <sup>2</sup>University of Montenegro, Faculty of Medicine, Krusevac bb, Podgorica, Montenegro, <sup>3</sup>Faculty of Pharmacy, Department of Pharmaceutical Chemistry, University of Belgrade, Vojvode Stepe 450, Belgrade, Serbia and <sup>4</sup>Innovation Centar, Institute of Physics Belgrade, Pregrevica 118, 11080 Zemun, Belgrade, Serbia*

(Received 12 December 2022, revised 21 January, accepted 6 July 2023)

**Abstract:** Defining the interaction of newly synthesized compounds with plasma proteins is an important step in the drug development process. Chromatographic techniques can be successfully used in predicting the biopharmaceutical and pharmacokinetic properties of newly synthesized compounds. The aim of this study is to investigate and isolate the most important molecular properties that affect the interaction of 20 newly synthesized chalcones and commercial compounds (lopinavir, ritonavir, darunavir and ivermectin) with human serum albumin (HSA). The retention behaviour of the selected compounds was tested on a CHIRALPAK®HSA column. A mixture of phosphate buffer (pH 7.0) and isopropanol (80:20 volume ratio) was used as the mobile phase, and the support vector method was used to form the quantitative structure retention relationship (QSRR) model. Based on the obtained values of retention parameters, it was observed that halogenated derivatives show the strongest, and methylated chalcone derivatives the weakest interaction with HSA. By correlating the retention and physicochemical properties of the tested compounds, it was shown that the structural (SDSCH) and electronic properties (MAXQ, EEM\_F1) groups have the greatest influence on the retention behaviour and the interaction of the tested compounds with HSA. The obtained QSRR model can be applied in the prediction of the retention characteristics of new, structurally related chalcone derivatives on HSA stationary phase.

**Keywords:** high performance affinity chromatography; support vector method; quantitative structure retention relationship; chalcone; human serum albumin.

\*Corresponding author. E-mail: nemanja.turkovic@cinmed.me  
<https://doi.org/10.2298/JSC221212033T>

## INTRODUCTION

Chromatographic techniques can be successfully applied in predicting and defining basic biopharmaceutical and pharmacokinetic properties in the first stages of discovery and development of new medicinal substances. Chromatographic techniques can be used along with *in silico* predictions and other *in vitro* studies. High performance affinity chromatography (HPAC) is often used in order to more precisely define the interaction of drugs with plasma proteins. HPAC enables precise and less time-consuming analysis of the sample. For these purposes, a phase modified with human serum albumin (HSA) is used as a stationary phase. The mobile phase simulates the physiological composition of blood plasma and enables satisfactory retention behaviour of the tested compounds.<sup>1–3</sup>

Serum albumins are the main soluble proteins of the blood. They make up 55 % of total plasma proteins and have numerous physiological functions: maintenance of osmotic pressure in the blood, transport of various endogenous molecules, various xenobiotics (medicines), *etc.* It is known that the interaction of drugs with HSA significantly affects the volume of distribution and the rate of their elimination. The volume of distribution, free concentration and metabolism of medicinal substances can be significantly changed depending on the value of the binding constant for HSA, which is important from the aspect of drug safety and efficacy. Therefore, the characterization of the drug-HSA interaction in the first stages of the development of new drugs affects the further optimization of the structural and physicochemical characteristics of the newly synthesized compounds. HSA is a protein consisting of three structurally similar domains I–III. Each domain of this protein consists of two subdomains (A and B) stabilized by 17 disulfide bridges.<sup>1,4</sup>

Chalcones are occurring in natural plant products, but they are today mostly obtained by semi- or total synthesis using the aldol condensation reaction (Claisen-Schmidt). Chemically, chalcones are 1,3-diphenylprop-2-en-1-ones, in which two aromatic rings are connected by  $\alpha,\beta$ -unsaturated carbonyl system. In nature, chalcones are precursors in the biosynthesis of flavones, flavanones and chromanones and play an important role in protecting plants from ultraviolet radiation, pathogens and insects. Chalcones have been shown to have a wide range of biological activities such as: antitubercular, antityrosine kinase, anti-proliferative, anti-HIV-1-protease, antimicrobial and antioxidant activities.<sup>5</sup>

Previous studies have shown that chalcones, thanks to the presence of  $\alpha,\beta$ -unsaturated carbonyl chain in the molecule, react with amino groups of enzymes and other proteins (Michael's addition). In this reaction, the enone functional group is as an electron acceptor. Michael's addition is facilitated by the presence of electron acceptor groups in the B ring of the chalcone, while the presence of electron donor groups at the same position hinders this reaction. This could be one of the assumed mechanisms of interaction with plasma proteins.<sup>6,7</sup>

A literature review showed that more detailed studies of the interaction of chalcone with plasma proteins at the molecular level have not been done so far.

In this regard, the aim of this study was to examine the retention behaviour of selected newly synthesized chalcones and related compounds, which show anti-HIV-1-protease activity, on a stationary phase modified with HSA and to use the quantitative structure (chromatographic) retention relationships (QSRR) method to extract the most important structural features that affect the binding of the tested compounds to HSA.<sup>8</sup>

## EXPERIMENTAL

### *Chemicals and reagents*

The tested chalcones were synthesized at the Faculty of Pharmacy, Department of Pharmaceutical Chemistry, Belgrade, Serbia, while the commercial compounds are lopinavir, ritonavir, darunavir and ivermectin produced by Sigma Aldrich.<sup>8</sup> The chemical structures of the tested compounds are shown in Figs. 1 and 2.

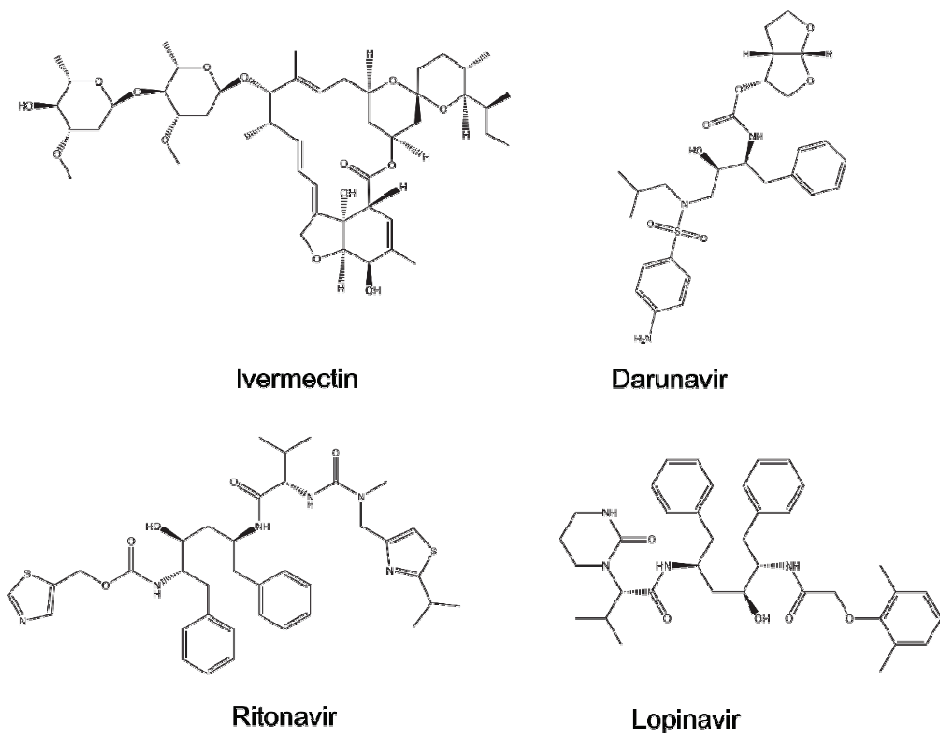


Fig. 1. Chemical structures of tested commercial compounds.

The following chemicals were used during this study: 2-propanol (J.T. Baker, Deventer, Netherlands) HPLC grade; deionized water (TKA water purification system, Niederalbert, Germany); potassium dihydrogen phosphate (Merck); disodium hydrogen phosphate (Merck).

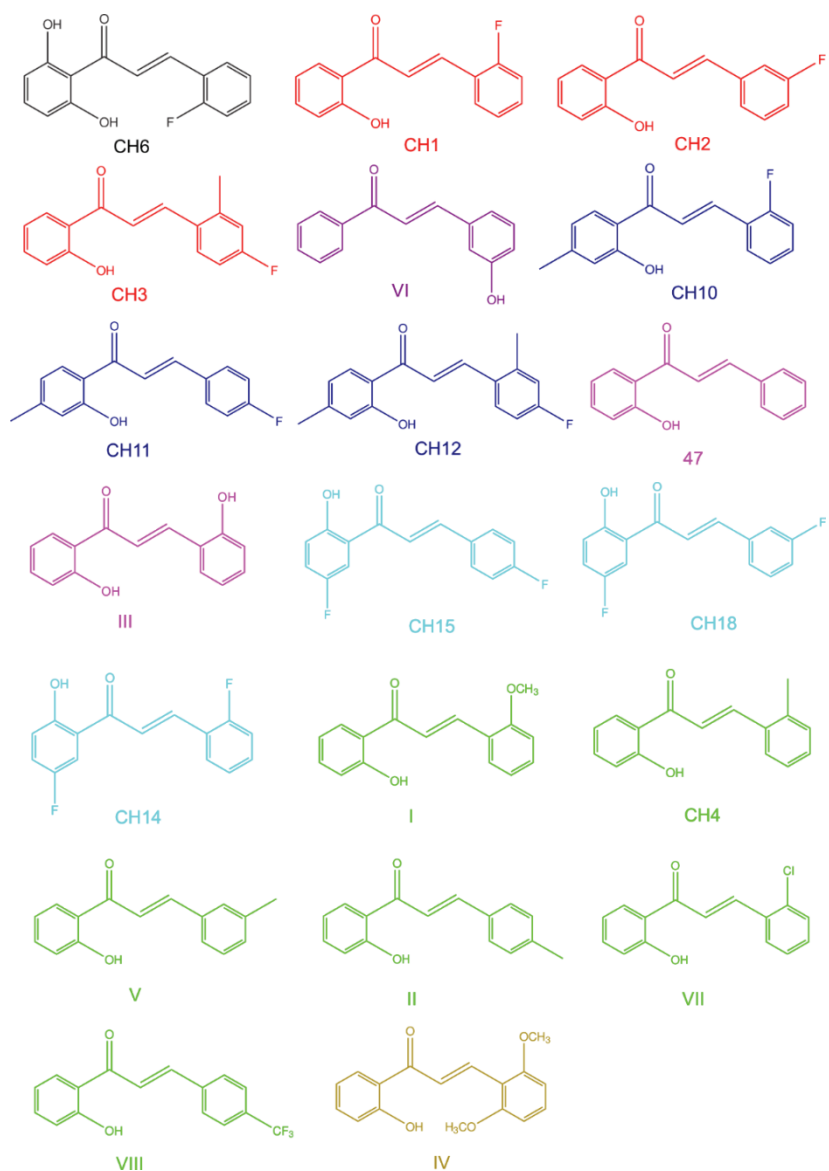


Fig. 2. Chemical structures of tested chalcones. Different colors of the compounds represent different structural groups.

#### *Chromatographic conditions*

HPLC analysis was performed on Agilent Technologies 1200 HPLC chromatograph (Santa Clara, CA, USA) at 25 °C. The retention behaviour of selected compounds was examined on CHIRALPAK®HSA column 150 mm×4 mm I.D. packed with HSA chemically bound to silica particles size of 5 µm (Daicel corporation, Illkirch-Graffenstaden, France). The mobile phase consisted of 80 vol. % phosphate buffer (pH 7.0; 0.01 M) and 20 vol. % isopropyl

alcohol. The flow rate was 0.5 mL min<sup>-1</sup>. UV detection was performed at 254 nm. Standard solutions of the investigated compounds were prepared in methanol at a concentration of 1 mg mL<sup>-1</sup> and then diluted with the mobile phase to the final concentration of 0.1 mg mL<sup>-1</sup>. The retention characteristics of the selected chalcones are defined based on the value of the logarithm of the retention factor ( $\log k$ ),  $\log k = \log ((t_r - t_0)/t_0)$ , where  $t_0$  is the dead time of the column and  $t_r$  is retention time.

The HPLC conditions were selected with the aim of achieving satisfactory retention characteristics of all tested compounds which show a strong interaction with HSA column. At low proportions of modifiers in the mobile phase ( $\phi < 20\%$ ), the elution of all tested compounds was not achieved. The analysis is qualitative with the aim of indirect evaluation of the interaction of the tested compounds with HSA through the obtained retention time ( $t_r$ ) values. Through the QSRR modelling approach, the impact of differences in the structural characteristics of the tested compounds on their HSA interaction was also evaluated. Each compound was analysed individually to clearly define its  $t_r$  value. Due to the individual qualitative interpretation of the HSA-interaction for each compound, the simultaneous chromatographic analysis of all 24 compounds was not performed. Common chromatographic conditions were defined, in order to use QSRR analysis to select the common physicochemical properties of compounds that affect their chromatographic behaviour, as well as to determine a reliable correlation with *in silico* binding to HSA. The defined conditions could be applied for the further analysis of newly synthesized chalcones and related compounds.

#### *Calculation of molecular descriptors*

Using the Marvin Sketch 6.1.0, (Chem Axon) the dominant molecular and tautomeric forms of the investigated compounds were selected at pH 7.00.<sup>9</sup> The tested molecular forms were brought to the minimum energy state by the optimization process using the semi empirical PM3 and HartreeFock/3-21G methods, in the Gaussian 09 (ChemBio3D Ultra 13.0).<sup>10,11</sup>

For all tested compounds, the molecular descriptors were calculated using the ADMET Predictor 9.5 (Simulation Plus Inc., 2019) and the SWISS ADME database.<sup>12,13</sup> Descriptors with the greatest influence on the dependent variable ( $\log k$ ) were used in Support Vector Machine (SVM)-QSRR modelling performed in the Statistica (StatSoft Inc., version 13.6, 2019).<sup>14</sup> In SVM-QSRR modelling,  $\log k$  was used as a dependent variable, while the extracted descriptors were used as independent variables.

QSRR analysis included 21 compounds. Due to strong interaction with the stationary phase, compounds VII, VIII and CH6 (Fig. 2) were not included in the QSRR modelling ( $\log k > 1.80$ ). The final training set for QSRR modelling included 16 compounds (47, CH10, CH12, CH14, CH18, CH2, CH3, CH4, darunavir, I, III, IV, ivermectin, ritonavir, V and VI), while the test set contained 5 most important representative compounds (CH1, CH11, CH15, II and lopinavir).

#### *Model validation*

The quality of the obtained models was assessed by calculating internal validation parameters (correlation coefficient ( $r$ ), root mean square error of estimation ( $RMSEE$ ), squared regression coefficient of cross-validation ( $Q^2_{LOO}$ )) and external validation parameters ( $r^2(\text{pred})$ , root mean square error of prediction ( $RMSEP$ )). QSRR models with  $Q^2_{LOO}$  and  $r^2(\text{pred}) \geq 0.5$  are considered to have good predictive ability. Additionally,  $r^2$  metrics ( $r^2_m$ ,  $r'^2_m$ ,  $\bar{r}^2_m$ , and  $\Delta r^2_m$ ) evaluation was applied. This metric is an additional external validation parameter, calculated based on the correlations between the observed and predicted values with

( $r^2$ ) and without ( $r^2_0$ ) intercept for the least squares regression lines, as shown in the following equation (1):

$$r^2_m = r^2 \left( 1 - \sqrt{r^2 - r^2_0} \right) \quad (1)$$

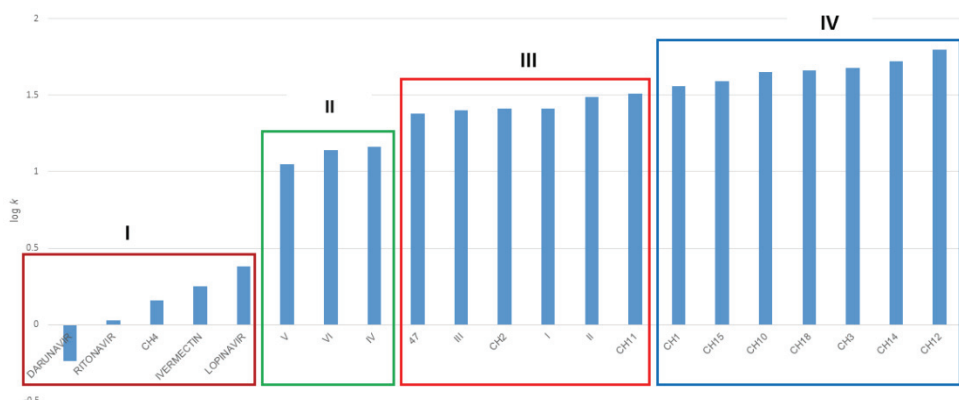
The metric  $r^2_m$  does not consider the differences between individual responses and the training set mean and thus avoids overestimation of the quality of prediction due to a wide response range ( $Y$ -range). For a good predictive QSRR model,  $\bar{r}_m^2$ ,  $r^2_m$  and  $r^2_m \geq 0.50$ , while  $\Delta r^2_m \leq 0.20$ .<sup>15-17</sup>

## RESULTS AND DISCUSSION

The degree of binding of the investigated compounds (chalcones and related compounds) to HSA was evaluated based on their retention behaviour on the stationary phase modified with HSA. The calculated logarithmic values of retention factors ( $\log k$ ) were used to indirectly evaluate and compare the drug-HAS interaction.

### *Classification of interaction of investigated compounds with HSA*

The results of the retention behaviour of the tested compounds are shown graphically in Fig. 3.



( $\log k(\text{lopinavir}) > \log k(\text{ivermectin}) > \log k(\text{ritonavir}) > \log k(\text{darunavir})$ ) is in agreement with the experimentally available data on their total binding to plasma proteins.<sup>18–20</sup>

Based on the obtained values of the retention factors, it is observed that there is a difference in the interaction of the examined compounds with HSA depending on the structural characteristics, *i.e.*, types of substituents in rings A and B. Halogenated derivatives show the strongest HSA-interaction, phenolic and methoxy derivatives show a weaker interaction, while methylated derivatives show the weakest interaction with HSA. From a chemical point of view, this would mean that compounds containing groups with electronegative atoms (fluorine, chlorine, oxygen) show better interaction compared to compounds containing alkyl groups.

The way in which the different type of substituent affects the retention behaviour can be seen on the example of compounds that are *ortho* substituted in ring B (Fig. 4, marked in blue), *e.g.*,  $\log k(\text{CH}_4, \text{methyl substituted}) < \log k(\text{III}, \text{hydroxyl (phenolic group) substituted}) < \log k(\text{I}, \text{methoxy substituted}) < \log k(\text{CH}_1, \text{fluoro substituted}) < \log k(\text{VII}, \text{chloro substituted})$  (Fig. 5a).

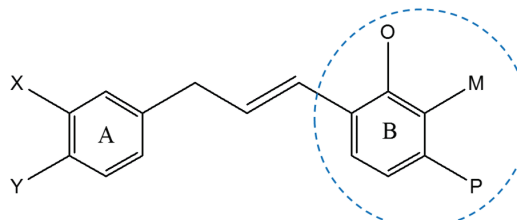


Fig. 4. Basic chemical structure of newly synthesized chalcones.

A similar sequence is also observed with *meta* and *para* structurally related derivatives:

- $\log k(\text{V}, \text{methyl substituted}) < \log k(\text{VI}, \text{substituted with a phenolic group}) < \log k(\text{CH}_2, \text{fluoro substituted})$ ;
- $\log k(\text{II}, \text{methyl substituted}) < \log k(\text{VIII}, \text{trifluoromethyl substituted})$ .

Differences in retention behaviour can also be observed in positional isomers, which indicates the importance of geometry and steric effects of molecules during interaction with HSA (Fig. 5b):

– in the case of isomers that have a methyl substituent in ring B, the order is *ortho* < *meta* < *para*, *e.g.*,  $\log k(\text{CH}_4) < \log k(\text{V}) < \log k(\text{II})$  (Fig. 5b-1);

– in the case of isomers that have a fluoro substituent in ring B, the order is *para* < *meta* < *ortho*, *e.g.*,  $\log k(\text{CH}_15) < \log k(\text{CH}_18) < \log k(\text{CH}_14)$  (Fig. 5b-2).

Compounds CH1 and CH2 differ from each other in the position of the fluoro group in ring B. By introducing an additional methyl group into ring B, (compound CH3), the interaction with HSA increases, so that  $\log k(\text{CH}_2, \text{meta}-$

-fluoro) < log  $k$ (CH1, *ortho*-fluoro) < log  $k$ (CH3, *para*-fluoro, *ortho*-methyl) (Fig. 6a).

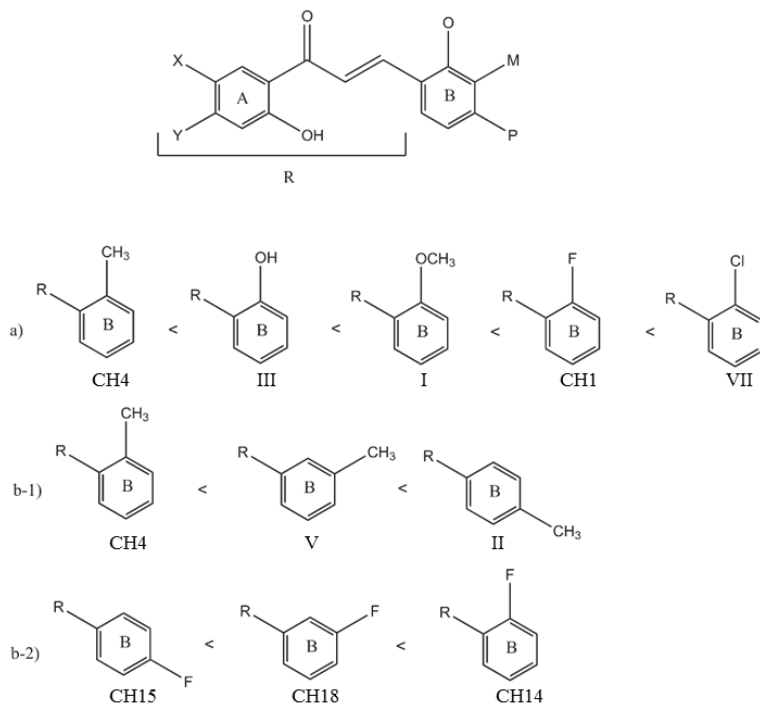


Fig. 5. Comparative presentation of compounds with the influence of: a) different substituent on retention behavior and b) different position of the same substituent (b-1 methylated derivatives, b-2 fluorinated derivatives).

For all investigated compounds from the chalcone group, it was shown that the introduction of an additional X/Y substituent in ring A leads to an increase in the interaction with HSA:

- log  $k$ (CH3) < log  $k$ (CH12, methyl substituent in position Y);
- log  $k$ (CH2) < log  $k$ (CH18, fluorine atom in position X);
- log  $k$ (CH11, methyl substituent in position Y) < log  $k$ (CH15, fluorine atom in position X);
- log  $k$ (CH1) < log  $k$ (CH10, methyl substituent in position Y) < log  $k$ (CH14, fluorine atom in position X) (Fig. 6b).

There is a satisfactory correlation between the obtained log  $k$  values and the *in silico* (ADMET Predictor 9.5 programme (Simulation Plus Inc, 2019)) estimated binding to total plasma proteins ( $r = 0.86$ ).

For darunavir and ritonavir, the chromatographically estimated interaction with HSA showed a deviation from their *in silico* estimated binding to total

plasma proteins including alpha-1-acid glycoprotein (AGP). It was found that the HIV protease inhibitors such as darunavir and ritonavir bind primarily to AGP.<sup>21</sup>

The obtained *in silico* estimated binding to total plasma proteins (through the percent of the unbound fraction to human plasma protein – %(hum\_fup)) is available from corresponding author upon request.

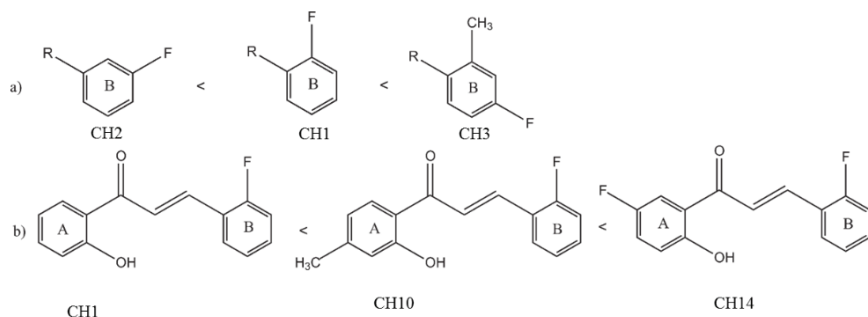


Fig. 6. Comparative presentation of compounds with the influence of an additional substituent on retention behaviour.

#### *Physicochemical characterization of the mechanism of interaction of the examined compounds with HSA*

Using the SVM method, a QSRR model was created that defines the relationship between  $\log k$ , as the dependent variable and the molecular properties of the investigated compounds, as independent variables. Based on the correlation with the values of the  $\log k$  parameter, the molecular features with the greatest influence on the HSA-interaction were selected and then used in SVM modelling (Fig. 7).

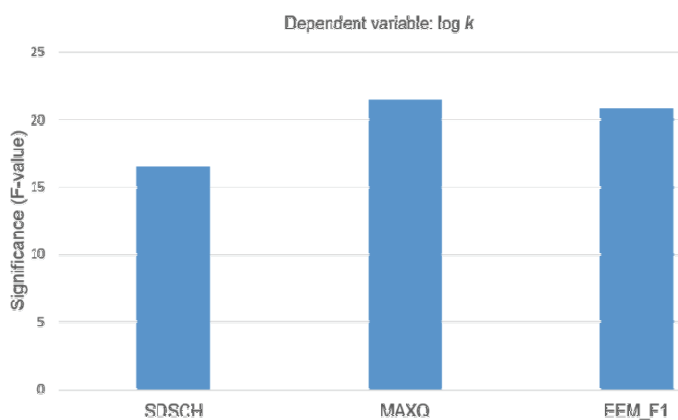


Fig. 7. Selected descriptors in relation to the significance of the influence on the  $\log k$  value.

The most important statistical characteristics of the obtained SVM-QSRR model are shown in Table I, where  $r(\text{train})$  is the correlation coefficient for training set and  $rr^2_m$  is reverse  $r^2_m$ .

TABLE I. The most important statistical characteristics of the obtained SVM-QSRR model

Model	Parameter	Descriptors	$r(\text{train})$	$Q^2_{\text{LOO}}$	$\text{RMSEE}$
SVM (sigmoid function)	$\log k$	SDSCH, MAXQ, EEM_F1	0.76	0.99	0.25
$r^2(\text{pred})$	$\text{RMSEP}$	$r^2_m$	$r^2_m$	$\bar{r}^2_m$	$(rr^2_m - \bar{r}^2_m)/2$
0.95	0.12	0.82	0.77	0.80	0.04

Based on the parameters of internal ( $r = 0.76$ ,  $Q^2_{\text{LOO}} = 0.99$ ,  $\text{RMSEE} = 0.25$ ) and external validation ( $r^2(\text{pred}) = 0.95$ ,  $\text{RMSEP} = 0.12$ ), as well as  $r^2$  metrics parameters ( $r^2_m = 0.82$ ,  $r^2_m = 0.77$ ,  $\bar{r}^2_m = 0.80$  and  $\Delta r^2_m = ((rr^2_m - \bar{r}^2_m)/2) = 0.04$ ), it can be observed that the obtained SVM-QSRR model has satisfactory predictive properties.

Structural characteristics (SDSCH) and electronic properties (maximum partial atomic charge (MAXQ) and electron density in the frontier orbital (EEM\_F1)) have the greatest influence on the interaction of the tested compounds with HSA.

The descriptor SDSCH defines the total number of CH groups that are connected by double or single bonds in the molecule. As the increase in CH groups correlates with the increase in lipophilicity of the investigated compounds based on the obtained results, it can be concluded that the increase in lipophilicity leads to longer retention (interaction) with HSA. Accordingly, for example:

- for the compound CH12 (which contains an additional methyl group in the A ring) in relation to the compound CH3,  $\log k(\text{CH3}) < \log k(\text{CH12})$ ;

- for the compound CH10 (which has an additional methyl group in the A ring) in relation to the compound CH1,  $\log k(\text{CH1}) < \log k(\text{CH10})$ .

Also, the interaction of the examined compounds with HSA depends on MAXQ and EEM\_F1. Compounds with a larger number of electronegative groups showed a greater affinity for HSA, which can be explained by a greater influence of electrostatic interactions or the formation of hydrogen bonds. Accordingly, for example:

- in the A ring, compound CH18 has an additional fluorine atom compared to the compound CH2, which is why  $\log k(\text{CH2}) < \log k(\text{CH18})$ ;

- compound CH14 has an additional fluorine atom in the A ring compared to the compound CH1, which is why  $\log k(\text{CH1}) < \log k(\text{CH14})$ .

#### CONCLUSION

The defined chromatographic conditions can be successfully applied to the investigation of the interaction of chalcone-like compounds and HSA. The formed SVM-QSRR model can be reliably applied for the prediction of retention behaviour of newly synthesized chalcone derivatives on the HSA-stationary

phase. Electrostatic interactions (MAXQ, EEM\_F1) and structural characteristics (SDSCH) showed the greatest influence on the interaction of the investigated compounds with HSA. Increasing lipophilicity and introducing electronegative substituents into the structure of the tested compounds strengthens their interaction with HSA.

#### ИЗВОД

#### ПРИМЕНА ТЕЧНЕ ХРОМАТОГРАФИЈЕ У ДЕФИНИСАЊУ ИНТЕРАКЦИЈА НОВОСИНТЕТИСАНИХ ХАЛКОНА И СРОДНИХ СУПСТАНЦИ СА ХУМАНИМ СЕРУМСКИМ АЛБУМИНИМА

НЕМАЊА ТУРКОВИЋ<sup>1,2</sup>, НАСТАСИЈА АНЂЕЛКОВИЋ<sup>3</sup>, ДАРИЈА ОБРАДОВИЋ<sup>4</sup>, ЗОРИЦА ВУЛИЋ<sup>3</sup>  
и БРАНКА ИВКОВИЋ<sup>3</sup>

<sup>1</sup>Институција за љекове и медицинска средства (ЦИИМЕД), Булевар Ивана Црнојевића 64а, Подгорица,  
Црна Гора, <sup>2</sup>Универзитет Црне Горе, Медицински факултет, Крушевац бб, Подгорица, Црна Гора,  
<sup>3</sup>Фармацеутски факултет, Кафедра за фармацеутску хемију, Универзитет у Београду, Војводе  
Шупље 450, Београд и <sup>4</sup>Иновациони центар, Институција за физику у Београду, Претревица 118,  
11080 Земун, Београд

Дефинисање интеракције новосинтетисаних једињења са протеинима плазме је важан корак у процесу развоја лекова. Хроматографске технике се могу успешно користити у предикцији биофармацеутских и фармакокинетичких особина новосинтетисаних једињења. Циљ овог рада је испитивање и издвајање најзначајнијих молекулских особина које утичу на интеракцију 24 новосинтетисаних халкона и њима сродних једињења са хуманим серумским албумином (HSA). Рetenционо понашање одабраних једињења је испитано на CHIRALPAK®HSA колони. Као мобилна фаза коришћена је смеша фосфатног пулфера (рН 7,0) и изопропанола (запр. однос 80:20). У формирању QSRR модела коришћена је метода вектора подршке. На основу добијених вредности рetenционих параметара уочено је да халогеновани деривати показују најјачу, а метиловани деривати халкона најслабију интеракцију са HSA. Доводећи у корелацију рetenцију и физичко-хемијска својства испитиваних једињења показало се да структурне (SDSCH) и електронске особине (MAXQ,EEM\_F1) група највише утичу на рetenционо понашање и интеракцију испитиваних једињења са HSA. Добијени QSRR модел се може применити у предикцији рetenционих карактеристика нових, структурно-сродних деривата халкона на HSA стационарној фази.

(Примљено 12. децембра 2022, ревидирано 21. јануара, прихваћено 6. јула 2023)

#### REFERENCES

1. H. S. Kim, I. W. Wainer, *J Chromatogr. B* **870** (2008) 22 (<https://doi.org/10.1016/j.jchromb.2008.05.029>)
2. D. S. Hage, S. A. Tweed, *J Chromatogr. B* **699** (1997) 499 ([https://doi.org/10.1016/S0378-4347\(97\)00178-3](https://doi.org/10.1016/S0378-4347(97)00178-3))
3. D. S. Hage, J. Anguizola, O. Barnaby, A. Jackson, M. J. Yoo, E. Papastavros, E. Pfaunmiller, M. Sobansky, Z. Tong, *Curr. Drug Metab.* **12** (2011) 313 (<https://dx.doi.org/10.2174/138920011795202938>)
4. J. Ghuman, P. A. Zunszain, I. Petipas, A. A. Bhattacharya, M. Otagiri, S. Curry, *J. Mol. Biol.* **353** (2005) 38 (<https://doi.org/10.1016/j.jmb.2005.07.075>)

5. B. Ivkovic, *PhD Thesis*, University of Belgrade, Serbia, 2013 (<http://doiserbia.nb.rs/phd/fulltext/BG20130320IVKOVIC.pdf>)
6. Z. Nowakowska, *Eur. J. Med. Chem.* **42** (2007) 125 (<https://doi.org/10.1016/j.ejmech.2006.09.019>)
7. J. V. Basić, B. Ivković, S. Stevanović, A. Lazarević, Z. Vujić, *Hem. Ind.* **70** (2016) 511 ([http://www.ache.org.rs/HI/2016/No5/HEMIND\\_Vol70\\_No5\\_p493-601\\_Sep-Oct\\_2016.pdf](http://www.ache.org.rs/HI/2016/No5/HEMIND_Vol70_No5_p493-601_Sep-Oct_2016.pdf))
8. N. Turkovic, B. Ivkovic, J. Kotur-Stevuljevic, M. Tasic, B. Marković, Z. Vujić, *Curr. Pharm. Des.* **26** (2020) 802 (<https://doi.org/10.2174/1381612826666200203125557>)
9. Chem Axon, *MarvinSketch, Version 6.1.0*, Budapest, Hungary, 2013
10. *Gaussian 09, Revision D.01*, Gaussian, Inc., Wallingford CT, USA, 2009
11. *ChemBio3D Ultra, Version 13.0*, CambridgeSoft Corporation Cambridge, MA, USA, 2013
12. O. Trott, A. J. Olson, *J Comput Chem.* **31** (2010) 455 (<https://doi.org/10.1002/jcc.21334>)
13. *SwissADME*, <http://www.swissadme.ch/index.php> (accessed 15 Dec, 2021)
14. *Statistica data analysis system, Version 13.6*, Tulsa, OK, USA, 2019
15. A. Tropsha, *Mol. Inform.* **29** (2010) 476 (<https://doi.org/10.1002/minf.201000061>)
16. K. Roy, K. Supratik, A. Pravin, *Chemometr. Intell. Lab. Syst.* **145** (2015) 22 (<https://doi.org/10.1016/j.chemolab.2015.04.013>)
17. P. K. Ojha, I. Mitra, R. N. Das, *Chemometr. Intell. Lab. Syst.* **107** (2011) 194 (<https://doi.org/10.1016/j.chemolab.2011.03.011>)
18. *DrugBank Online*, <https://go.drugbank.com/drugs/DB01601> (accessed 17 Feb, 2022)
19. *DrugBank Online*, <https://go.drugbank.com/drugs/DB00503> (accessed 17 Feb, 2022)
20. *DrugBank Online*, <https://go.drugbank.com/drugs/DB01264> (accessed 17 Feb, 2022)
21. D. Maksimovic-Ivanic, P. Fagone, J. McCubrey, K. Bendzen, S. Mijatovic, F. Nicoletti, *Int. J. Cancer.* **140** (2017) 1713 (<https://doi.org/10.1002/ijc.30529>).



## Health risk assessment of toxic elements in sedimentable dust from landfills

UNA MARČETA<sup>1\*</sup>, MILICA VUČINIĆ VASIĆ<sup>2</sup>, JORDANA NINKOV<sup>3#</sup>,  
STRAHINJA ILIĆ<sup>2</sup> and BOGDANA VUJIĆ<sup>1</sup>

<sup>1</sup>University of Novi Sad, Technical Faculty "Mihajlo Pupin", Djure Djakovica bb Street, Zrenjanin 23000, Serbia, <sup>2</sup>University of Novi Sad, Faculty of Technical Sciences, Trg Dositeja Obradovića 6 Street, 21000 Novi Sad, Serbia and <sup>3</sup>Institute of Field and Vegetable Crops, National Institute of the Republic of Serbia, Laboratory for Soil and Agroecology, Maksima Gorkog 30 Street, 21000 Novi Sad, Serbia

(Received 13 April, revised 26 May, accepted 30 June 2023)

**Abstract:** Four monitoring campaigns of sedimentable dust were provided from two large non-sanitary landfills (Zrenjanin and Novi Sad) in Serbia during 2021. Particle size analysis by laser diffraction and inductively coupled plasma-optical emission spectrometry were carried out in order to obtain the particle size distribution (PSD) and the toxic elements (TEs) concentrations. The health risk assessment of the landfill employees was performed according to the United States Environmental Protection Agency methods based on TEs concentrations. The PSD results demonstrated that the majority of sedimentable dust samples mass were not concentrated neither within PM2.5 neither within PM10 fraction. Analysis revealed high concentration of TEs at both landfills: an extremely high concentrations of Cr and Zn in samples from Zrenjanin landfill was detected. Health risk potential of elements was as follows for both landfills: Cr > Co > Pb > Ni > Zn > Cu. According to the results, maximal hazard index for landfill employees in Zrenjanin (0.197) and Novi Sad (0.113) showed that non-cancer risk was very low. For both landfill sites, cancer risk was highest for Cr ( $2.75 \times 10^{-5}$  for Zrenjanin and  $2.02 \times 10^{-7}$  for Novi Sad), though still within the defined threshold for tolerable cancer risk.

**Keywords:** atmospheric deposition; particle size distribution; toxic elements concentrations; hazard index; cancer risk.

### INTRODUCTION

Pollution originating from landfills occupies the attention of the public, scientists, and decision-makers, since it causes environmental degradation.

\* Corresponding author. E-mail: una.tasovac@tfzr.rs

# Serbian Chemical Society member.

<https://doi.org/10.2298/JSC230413032M>

One of the main origins of pollution from landfills is the leachate that can penetrate the soil and water resources.<sup>1</sup> Landfill leachate contains a long list of contaminants: heavy metals, organic compounds, dissolved methane, fatty acids, sulphate, nitrate, phosphates, plastics, calcium, *etc.*<sup>2</sup> The dominant toxic elements (also referred as heavy metals) in leachate are cadmium, chromium, mercury, copper, zinc, lead and arsenic.<sup>3</sup> Likewise, landfills can cause air pollution by emitting different gases, mainly methane and carbon dioxide, that are generated due to a landfill metabolism. Dust is also of great concern when we are speaking about air pollution from landfills. Dust emission from landfills is the result of surface material resuspension related to waste transportation by heavy trucks through the landfill, waste deposition, and cover material handling.<sup>4</sup> Since this dust represents the soil particles from contaminated landfill areas, its composition could be complex, very often containing toxic elements. In addition, commonly, accidentally occurring fires, especially at unsanitary landfills, are sources of other potentially dangerous gases and particles of different sizes. The chemical composition of gases and particles emitted into the air during fires depends on the waste composition.<sup>5</sup>

Although the landfill impact on soil and groundwater has been studied intensively,<sup>6,7</sup> the study of atmospheric pollution from landfills has been less represented due to the complexity of such research. Atmospheric deposition processes from landfills are especially less studied, while publications concerning sedimentable dust in municipal solid waste landfills are very rare.<sup>8</sup> Air contamination by particles, containing toxic elements and emitted from landfills is of great concern with the respect to human health risk assessment since it could be transported to large distances.<sup>9</sup>

The atmospheric fate of particles is influenced by different factors like terrain configuration, meteorological parameters, properties and size of particles, *etc.* Since larger particles ( $>30\text{ }\mu\text{m}$ ) seem to travel shorter distances, it is more likely that they will influence the environment close to the source.<sup>10</sup> Those coarser particles are sedimentable dust that are subject of the process of dry or wet deposition. By deposition from air, particles, and hence all their constituents (organic and organic compounds, toxic elements, *etc.*), enter the aquatic and terrestrial ecosystems, becoming available for living organisms through the food chain.<sup>11</sup>

Hence, humans are influenced by the particles through food, water, skin and respiratory system. The behaviour of particles after entering the human body, as well as the response that it causes, depends on the numerous parameters. In addition to the physiological parameters of the recipient human body (weight, age, *etc.*), the most important are chemical composition, size, and shape of the particles.

In recent studies, the monitoring of particles and its composition analysis provided near the landfills indicate that concentrations of cadmium, chromium, copper, manganese, nickel, and lead exceeded the USEPA standard permissible

limit.<sup>12</sup> Likewise, the analysis of suspended dust from a landfill near Mexico City indicated most abundant elements were silicon and aluminium.<sup>13</sup> In ambient air samples at different distances from the landfill, it was revealed that the highest concentrations of metals (Cd, Cu, Ni, Cr and Zn) were recorded at the sampling sites near the landfills.<sup>14</sup>

A studies on the exposure of landfill employees to dust reveals a higher concentration of arsenite in lung, muscle, and liver, lead in bone and blood and cadmium in kidney and liver.<sup>4,15</sup>

Developing countries, like the Republic of Serbia, face environmental degradation problems because of waste disposal at uncontrolled and non-sanitary landfills without prior selection standard.<sup>16</sup> In Serbia, there are only 12 sanitary landfills and more than 120 non-sanitary landfills. Number of uncontrolled landfills is higher than 3,500. Only 19 % of generated waste is deposited on sanitary landfills. Concerning the location, 40 % of landfills are located near settlements. Also, a huge number of accidentally occurring fires at the unsanitary landfills in Serbia are recorded in past few years, reaching the highest number in 2021.<sup>17</sup>

In this study, four monitoring campaigns of sedimentable dust during the summer period of 2021 at two large landfills in Serbia were provided. The aim of this study was health risk assessment of the employees at the landfills according to quantitative analysis of toxic elements (As, Cd, Co, Cr, Cu, Ni and Pb) and particle size distribution (PSD) for the first time in Serbia.

## EXPERIMENTAL

### *Study area*

Details about the study area are given in Supplementary material to this paper.

### *Sampling and exposure time*

The dust sampling method was performed conforming to recommendations of the Environmental Protection Agency of United States<sup>10</sup> in accordance with the German standard VDI.<sup>18</sup> The Bergerhoff Gauge dust monitoring instrument was used on both locations to measure sedimentable dust. Bergerhoff method is a long-term method, where measurements are usually carried out over a 30-day period. According to the US methods, exposition time should be 30 + 2 days in a minimum of 3 campaigns and at least 2 campaigns should be in the period of May and September.

Sampling was performed during summer and early autumn of 2021, in four campaigns that represent four replicates (following the above-described method that prescribes a minimum of 3 campaigns). The beginning of sample collection was the middle of June, and the end was the middle of October 2021. Each individual campaign had a number of exposed days of 30 or 31. After a sampling period, the collected liquid samples were evaporated, and the solid residue was analysed.

### *Particle size distribution*

Particle size distribution was determined using a Malvern Mastersizer 2000 particle size analyser. Hydro2000 Micro Precision, the dispersion unit for small amounts of a material, was used for measuring. The Malvern Mastersizer 2000 records the light pattern scattered from a

field of particles at different angles. Recorded intensity at a certain angle is the sum of the intensity of light scattered from the surface of particles and the intensity of the secondary scattered light, due to refraction when passing through the particle, which is important for the particles smaller than 50 µm. The device then uses an analytical procedure to determine the particle size distribution that creates the patterns. The composition of the examined samples is inhomogeneous, while the refractive index of dispersed material was impossible to determine precisely, so we used literature data. According to the literature data<sup>19</sup> the real part of the air dust refractive index is in the range 1.48–1.55. We used the value of 1.5. The wavelengths of light used during measurement were 632.8 and 740 nm. Samples were analysed in three replicates. The measurement of the samples was carried out in the dynamic mode. Measurement parameters were: pump speed, 2500 rpm; ultrasonic, off. The results were recorded as the particle volume percentage in 100 discrete size ranges between 0.02 and 200 µm.

#### *Determination of toxic elements concentration in collected samples*

All laboratory analyses were performed at the Laboratory for Soil and Agroecology of the Institute of Field and Vegetable Crops, accredited according to the standard ISO/IEC 17025:2017.<sup>20</sup> The samples were analysed for concentrations of As, Cd, Co, Cr, Cu, Ni, Pb and Zn after microwave digesting the samples in concentrated HNO<sub>3</sub> and H<sub>2</sub>O<sub>2</sub> (0.3 g in 20 ml; 5:1 HNO<sub>3</sub>/H<sub>2</sub>O<sub>2</sub>) by stepwise heating up to 180 °C using a Milestone Vario EL III for 55 min.

The concentration of the elements in prepared samples was determined by ICP-OES (Vista Pro-Axial, Varian) in accordance with the US EPA method 200.7:2001<sup>21</sup> under the following operating conditions: RF power, 1.10 kW; plasma and auxiliary gas flow rate, 15.0 and 1.50 L min<sup>-1</sup>, respectively; nebulizer flow, 1.20 L min<sup>-1</sup>; number of replicates, 3.

Quality assurance and quality control (QA/QC) assessments were conducted using the certified reference materials IRMM ERM-CC141 (Loam soil). The obtained limit of detection (*LOD*) from 0.03 (Cu) to 0.09 (Ni) mg L<sup>-1</sup> and method detection limit (*MDL*) of 1.0 mg kg<sup>-1</sup> for all elements, provided adequate sensitivity for the analysis. In this study, the percentage of recovery, defined as the ratio of measured concentrations and certified values of used reference materials, ranged from 86 to 111 %, which provided adequate analytical accuracy and precision.

#### *Health risk assessment*

Health risk assessment in humans (landfill employees) was determined according to the Exposure Factors Handbook of the Environmental Protection Agency of United States.<sup>22</sup> Firstly, an average daily doses (*ADD* in mg kg<sup>-1</sup> day<sup>-1</sup>) through three dominant exposure pathways, including ingestion (*ADDing*), inhalation (*ADDinh*) and dermal contact (*ADDderm*), were calculated in the following manner:<sup>23</sup>

$$ADDing = \frac{C \times R_{ing} \times CF \times EF \times ED}{BW \times AT} \quad (1)$$

$$ADDinh = \frac{C \times R_{inh} \times EF \times ED}{PEF \times BW \times AT} \quad (2)$$

$$ADDderm = \frac{C \times SA \times CF \times SL \times ABS \times EF \times ED}{BW \times AT} \quad (3)$$

The input parameters for the calculations of employee exposure were: *C* – toxic element concentration (mg kg<sup>-1</sup>), *R<sub>ing</sub>* – ingestion rate (100 mg day<sup>-1</sup>), *R<sub>inh</sub>* – inhalation rate (20 m<sup>3</sup> day<sup>-1</sup>), *EF* – the exposure frequency (74 day year<sup>-1</sup>), *ED* – exposure duration (20 years), *BW* – body weight (70 kg), *AT* – averaging time (365×*ED* days), *CF* – conversion factor (10<sup>-6</sup> kg mg<sup>-1</sup>),

*PEF* – particle emission factor ( $1.32 \times 10^{-9} \text{ m}^3 \text{ kg}^{-1}$ ), *SA* – exposed skin area ( $5000 \text{ cm}^2$ ), *SL* – skin adherence factor ( $1 \text{ mg cm}^{-2} \text{ day}^{-1}$ ), *ABS* – dermal absorption factor (0.001).<sup>24,25</sup>

The non-carcinogenic health risk by toxic elements considered was characterized by the hazard quotient (*HQ*), representing the probability of suffering from an adverse effect. The *HQi* is defined as the ratio of the average daily dose to its reference dose *RfDi* for the same exposure pathway:<sup>23</sup>

$$HQ_i = \frac{ADD_i}{RfDi} \quad (4)$$

*RfDi* values for toxic elements considered are provided by US EPA.<sup>25</sup>

The sum of hazard quotient for ingestion (*HQing*), inhalation (*HQinh*) and dermal exposure (*HQderm*), named hazard index (*HI*):

$$HI = HQ_{\text{ing}} + HQ_{\text{inh}} + HQ_{\text{derm}} \quad (5)$$

has been used to assess the overall potential for noncarcinogenic health effects caused by toxic elements. Hazard index value lower or equal to unity ( $HI \leq 1$ ) implies the absence of health risk. In opposite, hazard index greater than unity ( $HI > 1$ ) indicates a concern for adverse effects.

Cancer risk (*CR*) is assessed by multiplying average daily dose of exposure with cancer slope factors *via* inhalation *SFinh*:

$$CR = ADD \times SFinh \quad (6)$$

Values of *SFinh* are provided by US EPA<sup>25</sup> per individual element. Cancer risk values below  $1 \times 10^{-6}$  present negligible risk, while the ones in the range of  $10^{-6}$ – $10^{-4}$  indicate tolerable cancer risk.<sup>24</sup>

## RESULTS AND DISCUSSION

### Particle size

The particle size distribution (PSD) allowed an estimation of the degree of dispersion of particles over the considered dimensional range. Size distribution of particles differs drastically according to whether it is calculated in terms of particle number, surface area or volume/mass.<sup>26</sup> Fig. 1 represents the average volume-based particle size distribution for samples collected at both landfill sites. Frequency curves are exhibited in Fig. 1. The average particle size distributions were obtained by averaging data for all campaigns at each landfill location. Individual PSD are not presented due to the fact that volume-based PSD for a certain location alters very slightly. The averaged results demonstrate that the particles whose equivalent sphere diameter was between 20 and 30  $\mu\text{m}$  make up the majority of sample mass at both landfill locations. Sample from Zrenjanin (ZR) landfill showed a bimodal distribution with a significant portion of particles larger than 100  $\mu\text{m}$ .

The average percentage of PM2.5 and PM10 fractions, obtained from volume-based particle size distribution cumulative curves are 4.05 and 23.82 for ZR landfill and 4.91 and 27.59 for Novi Sad (NS) landfill, respectively. The obtained results are similar on both landfill locations. It demonstrates that, despite the stochastic emission of particles on investigated landfill sites, the percentage of the mentioned fractions in sedimentable dust is very similar.

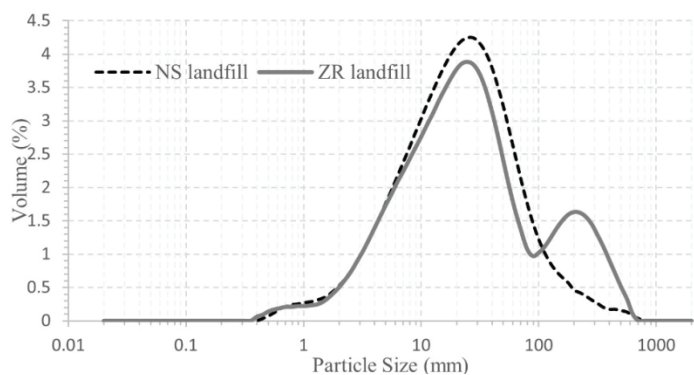


Fig. 1. Average volume-based particle size distribution on landfill sites

Average PM<sub>2.5</sub>/PM<sub>10</sub> ratio in investigated samples was 0.178 and 0.17 for NS and ZR landfill, respectively. That is more than twice lower than found for total suspended particulate matter collected in an industrial and urban areas in Greece, where average PM<sub>2.5</sub>/PM<sub>10</sub> ratio was within range 0.38–0.59.<sup>27</sup> It should be mentioned that sedimentable particles generally contain lower percentage of fine fractions that could penetrate into lungs in comparison with total suspended particles, which can be confirmed by comparing the results of this study with the results related to total suspended particles reported in the literature.<sup>27</sup>

#### Toxic element concentration

In this study, the concentration of As and Cd was not detected in accordance with set method detection limits of 1 mg kg<sup>-1</sup>, therefore, the concentration of these two elements was not processed. Toxic elements concentration (Co, Cr, Cu, Ni, Pb, Zn in mg kg<sup>-1</sup>) in sedimentable dust at two landfills in ZR and NS, and the literature data for landfills and urban areas around the world, were summarized in Table I.

The content of analysed toxic elements varied over a wide range concentration (Table I). Average, maximum and minimum concentrations at both landfills were of the same order of magnitude for the majority of analysed toxic elements. Concentration of Cr and Zn in samples collected at the ZR landfill had the widest range. An inconsistency was established for Cr whose maximum and average concentrations were approximately two orders of magnitude higher at ZR landfill (Table I). Hence, the highest concentrations among all investigated toxic elements were detected for Cr (14910.0 mg kg<sup>-1</sup>) at ZR landfill during the campaign 4. Although Cr occurs in air through soil erosion, most come from anthropogenic sources like various industrial activities and more importantly waste burning.<sup>32</sup> Likewise, high concentration of Zn (1,606.0 mg kg<sup>-1</sup>) was detected during the campaign 1 at the landfill in ZR. This could be explained by the fact that metallic Zn is commonly used for coating of other metals to prevent

corrosion, as well as to make batteries, thus landfills can significantly contribute to its concentration in a particulate matter.<sup>33</sup>

TABLE I. Toxic elements concentration (mg kg<sup>-1</sup>) in atmospheric deposition samples from ZR and NS landfills and literature data

Element Data	Sample						
	Sediment-able dust from ZR landfill	Sediment-able dust from NS landfill	Soil from landfill <sup>28</sup>	Fugitive dust from landfill (PM10) <sup>13</sup>	Urban dust in Novi Sad <sup>29</sup>	Urban dust in Beijing <sup>30</sup>	Road dust <sup>31</sup>
	Co	Aver.	26.8	—	6.01	10.6	
Cr	Max	44.2	73.9	20.41	—	—	
	Min	3.3	1.8	2.08	—	—	
	Aver.	3772.3	60.6	—	70	36.1	86
Cu	Max	14910.0	109.5	108.66	—	—	80.7
	Min	4.1	16.2	13.96	—	—	
	Aver.	50.5	99.3	—	60	50.1	138.4
Ni	Max	90.5	130.7	470.44	—	—	43.9
	Min	22.4	65.4	16.51	—	—	
	Aver.	31.0	10.0	—	30	21	45.2
Pb	Max	77.9	17.7	53.74	—	—	
	Min	5.7	6.0	1.59	—	—	
	Aver.	11.1	15.8	—	50	66.5	167.9
Zn	Max	23.3	22.6	72.76	—	—	66.6
	Min	3.0	9.6	20.97	—	—	
	Aver.	464.2	263.4	—	130	722.7	215
	Max	1606.0	395.8	968.12	—	—	
	Min	54.9	186.1	21.41	—	—	

In comparison to data on toxic elements contamination in the samples from landfill soil published by Thongyuan *et al.*<sup>28</sup> and in fugitive dust from landfill in Mexico City,<sup>13</sup> it was found that average, maximum and minimum concentrations of Co, Cu, Ni, Pb and Zn are of the same order of magnitude. On contrary, average and maximum Cr concentrations at Zrenjanin landfill were two orders of magnitude higher than reported by Vega *et al.*<sup>13</sup> and Thongyuan *et al.*,<sup>28</sup> respectively (Table I).

Additionally, if we compare results from this research to the results obtained from urban dust and soil sampled at the area near studied landfills,<sup>29</sup> toxic elements concentrations in sedimentable dust collected at both landfill sites were significantly higher in general (Table I). This is especially noticeable for Zn and Cr concentrations at samples from ZR landfill sampling site as well as for Cr, Cu and Zn in samples from NS landfill sampling site.

All previously mentioned indicates that the examined landfills significantly contribute to the content of Cr, Zn, Cu and Co in sedimentable dust, though the

same cannot be stated for Pb and Ni. The major sources of Pb in air could be vehicles and different industrial sources.<sup>34</sup> Concentration of lead in urban street areas is generally high and the pollution is still present, even though leaded gasoline has not been used for a long time. This is the reason for the higher concentration of Pb in the street dust than in our samples. Nickel is one of the most common elements on Earth. Its sources in air dust could be local soil,<sup>35</sup> coal and petroleum combustion, as well as electronic waste.<sup>36</sup> Regarding nickel, it is symptomatic that its concentrations in investigated samples were not higher than its average content in the soil of Vojvodina. For this reason, nickel in investigated samples most probably originated from natural sources.

The reason for high concentration of certain elements, especially Cr and Zn, could not be explained with the high confidence, since the samples were collected over the period of one month, thus representing the average monthly concentration. However, it could be based on the fact that sampling campaigns were organized during the summer months when the landfill managing activities could be more intensive and when the landfill fires could occur more frequently because of dry periods with high temperatures. During 2021, when the monitoring campaigns were provided, more than 1715 landfill fires in Serbia were recorded. That is the highest number in the period from 2016–2021.<sup>17</sup> Fires could be one of the main reasons why landfills contributed to the content of Cr, Zn, Cu and Co in our samples.

#### *Health risk assessment*

Health risk assessment of landfill employees was based on TEs concentration obtained by dust analysis. An average daily doses (*ADD* in  $\text{mg kg}^{-1} \text{ day}^{-1}$ ), the non-carcinogenic health risk by toxic elements by the hazard quotient (*HQ*), hazard index (*HI*) and cancer risk (*CR*) were assessed.

According to the results, *ADD* of employees at the landfill in ZR (Table II) was the highest for Cr ( $4.54 \times 10^{-4} \text{ mg kg}^{-1} \text{ day}^{-1}$ ). The lowest total *ADD* was obtained for Pb ( $7.09 \times 10^{-7} \text{ mg kg}^{-1} \text{ day}^{-1}$ ). Most of the toxic elements (Co, Cu and Ni) showed the same magnitude of total maximal exposure amount ( $10^{-6} \text{ mg kg}^{-1} \text{ day}^{-1}$ ) that is an order of magnitude lower than found for Zn ( $10^{-5} \text{ mg kg}^{-1} \text{ day}^{-1}$ ) and two orders of magnitude lower than found for Cr ( $10^{-4} \text{ mg kg}^{-1} \text{ day}^{-1}$ ).

At the landfill in NS (Table III), maximal total daily exposure was the highest for Zn ( $1.21 \times 10^{-5} \text{ mg kg}^{-1} \text{ day}^{-1}$ ) and the lowest for Ni ( $5.38 \times 10^{-7} \text{ mg kg}^{-1} \text{ day}^{-1}$ ). Toxic elements Co, Cr and Cu demonstrated the same magnitude of total maximal exposure amount ( $10^{-6} \text{ mg kg}^{-1} \text{ day}^{-1}$ ) which is still lower in comparison to the magnitude of total exposure amount of Zn ( $10^{-5} \text{ mg kg}^{-1} \text{ day}^{-1}$ ).

Results of the *HQ* values of different exposure pathways and *HI* for both landfills are presented in Tables IV and V.

TABLE II. Average daily doses ( $ADD$  in  $\text{mg kg}^{-1} \text{ day}^{-1}$ ) for employees at ZR landfill

Element	Data	Data type			
		$ADD_{\text{inh}}$	$ADD_{\text{ing}}$	$ADD_{\text{derm}}$	Total exposure
Co	Aver.	$7.59 \times 10^{-10}$	$5.01 \times 10^{-7}$	$2.50 \times 10^{-8}$	$5.27 \times 10^{-7}$
	Max	$1.94 \times 10^{-9}$	$1.28 \times 10^{-6}$	$6.40 \times 10^{-8}$	$1.35 \times 10^{-6}$
	Min	$1.45 \times 10^{-10}$	$9.56 \times 10^{-8}$	$4.78 \times 10^{-9}$	$1.01 \times 10^{-7}$
Cr	Aver.	$1.66 \times 10^{-7}$	$1.09 \times 10^{-4}$	$5.46 \times 10^{-6}$	$1.15 \times 10^{-4}$
	Max	$6.54 \times 10^{-7}$	$4.32 \times 10^{-4}$	$2.16 \times 10^{-5}$	$4.54 \times 10^{-4}$
	Min	$1.80 \times 10^{-10}$	$1.19 \times 10^{-7}$	$5.95 \times 10^{-9}$	$1.25 \times 10^{-7}$
Cu	Aver.	$2.22 \times 10^{-9}$	$1.46 \times 10^{-6}$	$7.32 \times 10^{-8}$	$1.54 \times 10^{-6}$
	Max	$3.97 \times 10^{-9}$	$2.62 \times 10^{-6}$	$1.31 \times 10^{-7}$	$2.76 \times 10^{-6}$
	Min	$9.84 \times 10^{-10}$	$6.49 \times 10^{-7}$	$3.25 \times 10^{-8}$	$6.83 \times 10^{-7}$
Ni	Aver.	$1.36 \times 10^{-9}$	$8.97 \times 10^{-7}$	$4.48 \times 10^{-8}$	$9.43 \times 10^{-7}$
	Max	$3.42 \times 10^{-9}$	$2.26 \times 10^{-6}$	$1.13 \times 10^{-7}$	$2.37 \times 10^{-6}$
	Min	$2.52 \times 10^{-10}$	$1.66 \times 10^{-7}$	$8.31 \times 10^{-9}$	$1.75 \times 10^{-7}$
Pb	Aver.	$4.87 \times 10^{-10}$	$3.21 \times 10^{-7}$	$1.61 \times 10^{-8}$	$3.38 \times 10^{-7}$
	Max	$1.02 \times 10^{-9}$	$6.74 \times 10^{-7}$	$3.37 \times 10^{-8}$	$7.09 \times 10^{-7}$
	Min	$1.32 \times 10^{-10}$	$8.70 \times 10^{-8}$	$4.35 \times 10^{-9}$	$9.15 \times 10^{-8}$
Zn	Aver.	$2.04 \times 10^{-8}$	$1.34 \times 10^{-5}$	$6.72 \times 10^{-7}$	$1.41 \times 10^{-5}$
	Max	$7.05 \times 10^{-8}$	$4.65 \times 10^{-5}$	$2.33 \times 10^{-6}$	$4.89 \times 10^{-5}$
	Min	$2.41 \times 10^{-9}$	$1.59 \times 10^{-6}$	$7.94 \times 10^{-8}$	$1.67 \times 10^{-6}$

TABLE III. Average Daily Doses (ADD in  $\text{mg kg}^{-1} \text{ day}^{-1}$ ) for employees at NS landfill

Element	Data	Data type			
		$ADD_{\text{inh}}$	$ADD_{\text{ing}}$	$ADD_{\text{derm}}$	Total exposure
Co	Aver.	$1.18 \times 10^{-9}$	$7.77 \times 10^{-7}$	$3.89 \times 10^{-8}$	$8.17 \times 10^{-7}$
	Max	$3.24 \times 10^{-9}$	$2.14 \times 10^{-6}$	$1.07 \times 10^{-7}$	$2.25 \times 10^{-6}$
	Min	$8.11 \times 10^{-11}$	$5.35 \times 10^{-8}$	$2.67 \times 10^{-9}$	$5.63 \times 10^{-8}$
Cr	Aver.	$2.66 \times 10^{-9}$	$1.75 \times 10^{-6}$	$8.77 \times 10^{-8}$	$1.85 \times 10^{-6}$
	Max	$4.81 \times 10^{-9}$	$3.17 \times 10^{-6}$	$1.59 \times 10^{-7}$	$3.33 \times 10^{-6}$
	Min	$7.10 \times 10^{-10}$	$4.69 \times 10^{-7}$	$2.34 \times 10^{-8}$	$4.93 \times 10^{-7}$
Cu	Aver.	$4.36 \times 10^{-9}$	$2.88 \times 10^{-6}$	$1.44 \times 10^{-7}$	$3.03 \times 10^{-6}$
	Max	$5.74 \times 10^{-9}$	$3.79 \times 10^{-6}$	$1.89 \times 10^{-7}$	$3.98 \times 10^{-6}$
	Min	$2.87 \times 10^{-9}$	$1.90 \times 10^{-6}$	$9.48 \times 10^{-8}$	$1.99 \times 10^{-6}$
Ni	Aver.	$4.37 \times 10^{-10}$	$2.88 \times 10^{-7}$	$1.44 \times 10^{-8}$	$3.03 \times 10^{-7}$
	Max	$7.76 \times 10^{-10}$	$5.12 \times 10^{-7}$	$2.56 \times 10^{-8}$	$5.38 \times 10^{-7}$
	Min	$2.64 \times 10^{-10}$	$1.74 \times 10^{-7}$	$8.72 \times 10^{-9}$	$1.83 \times 10^{-7}$
Pb	Aver.	$6.93 \times 10^{-10}$	$4.57 \times 10^{-7}$	$2.29 \times 10^{-8}$	$4.81 \times 10^{-7}$
	Max	$9.92 \times 10^{-10}$	$6.55 \times 10^{-7}$	$3.27 \times 10^{-8}$	$6.88 \times 10^{-7}$
	Min	$4.23 \times 10^{-10}$	$2.79 \times 10^{-7}$	$1.40 \times 10^{-8}$	$2.94 \times 10^{-7}$
Zn	Aver.	$1.16 \times 10^{-8}$	$7.63 \times 10^{-6}$	$3.81 \times 10^{-7}$	$8.02 \times 10^{-6}$
	Max	$1.74 \times 10^{-8}$	$1.15 \times 10^{-5}$	$5.73 \times 10^{-7}$	$1.21 \times 10^{-5}$
	Min	$8.17 \times 10^{-9}$	$5.39 \times 10^{-6}$	$2.69 \times 10^{-7}$	$5.67 \times 10^{-6}$

According to the results, total (maximal)  $HI$  for landfill employees in ZR (0.197) and NS(0.113) demonstrated low non-cancer risk. Also, it could be noted that ingestion is the most possible pathway. Hence, in comparison to other path-

ways of exposure, ingestion exposure index for employees at NSlandfill has more than 98 % share.

TABLE IV. Hazard quotients ( $HQ$ ) and hazard indexes ( $HI$ ) for ZR landfill

Element	Data	Data type		
		$HQ_{inh}$	$HQ_{ing}$	$HQ_{derm}$
Co	Aver.	$1.33 \times 10^{-4}$	$2.50 \times 10^{-5}$	$1.57 \times 10^{-6}$
	Max	$3.40 \times 10^{-4}$	$6.40 \times 10^{-5}$	$4.00 \times 10^{-6}$
	Min	$2.54 \times 10^{-5}$	$4.78 \times 10^{-6}$	$2.99 \times 10^{-7}$
Cr	Aver.	$5.79 \times 10^{-3}$	$2.19 \times 10^{-2}$	$2.19 \times 10^{-2}$
	Max	$2.29 \times 10^{-2}$	$8.64 \times 10^{-2}$	$8.64 \times 10^{-2}$
	Min	$6.30 \times 10^{-6}$	$2.38 \times 10^{-5}$	$2.38 \times 10^{-5}$
Cu	Aver.	$5.28 \times 10^{-8}$	$3.96 \times 10^{-5}$	$3.85 \times 10^{-5}$
	Max	$9.46 \times 10^{-8}$	$7.08 \times 10^{-5}$	$6.90 \times 10^{-5}$
	Min	$2.34 \times 10^{-8}$	$1.75 \times 10^{-5}$	$1.71 \times 10^{-5}$
Ni	Aver.	$5.23 \times 10^{-8}$	$4.48 \times 10^{-5}$	$4.48 \times 10^{-5}$
	Max	$1.32 \times 10^{-7}$	$1.13 \times 10^{-4}$	$1.13 \times 10^{-4}$
	Min	$9.69 \times 10^{-9}$	$8.31 \times 10^{-6}$	$8.31 \times 10^{-6}$
Pb	Aver.	$1.38 \times 10^{-7}$	$9.18 \times 10^{-5}$	$3.09 \times 10^{-5}$
	Max	$2.90 \times 10^{-7}$	$1.93 \times 10^{-4}$	$6.48 \times 10^{-5}$
	Min	$3.74 \times 10^{-8}$	$2.49 \times 10^{-5}$	$8.36 \times 10^{-6}$
Zn	Aver.	$6.79 \times 10^{-8}$	$4.48 \times 10^{-5}$	$1.12 \times 10^{-5}$
	Max	$2.35 \times 10^{-7}$	$1.55 \times 10^{-4}$	$3.88 \times 10^{-5}$
	Min	$8.02 \times 10^{-9}$	$5.30 \times 10^{-6}$	$1.32 \times 10^{-6}$
Total	Aver.	$5.92 \times 10^{-3}$	$2.21 \times 10^{-2}$	$2.20 \times 10^{-2}$
	Max	$2.32 \times 10^{-2}$	$8.70 \times 10^{-2}$	$8.67 \times 10^{-2}$
	Min	$3.17 \times 10^{-5}$	$8.46 \times 10^{-5}$	$5.92 \times 10^{-5}$

Health risk potential of elements for ZR and NSis as follows: Cr > Co > Pb > Ni > Zn > Cu.

Results for cancer risk for Co, Cr and Ni are presented in Table VI. Results revealed that the highest cancer risk were calculated at the ZR landfill. At this site, the highest  $CR$  was calculated for Cr ( $2.75 \times 10^{-5}$ ). At the landfill of NS, the highest  $CR$  was calculated also for Cr ( $2.02 \times 10^{-7}$ ). However, calculated  $CR$  for selected toxic elements were in the range of defined threshold of  $10^{-6}$ – $10^{-4}$  that indicates tolerable cancer risk. In the present study, the health risk assessment was completed concerning toxic elements concentration within sedimentable dust at landfills. However, it is known that toxic elements are preferentially bound to fine dust particle size fractions<sup>37</sup> while sedimentable dust consists of bigger particles that tend to sediment by gravity in general. This was also indicative when our results were compared with total suspended particulate matter collected in an industrial and urban areas;<sup>27</sup> average PM2.5/PM10 ratio at landfills was significantly lower indicating lower PM2.5 and higher PM10 content within

investigated samples. Therefore, concerning total suspended particulate matter, health risk would probably be higher than reported here.

TABLE V. Hazard quotients (*HQ*) and hazard indexes (*HI*) for NS landfill

Element	Data	Data type		
		<i>HQ</i> inh	<i>HQ</i> ing	<i>HQ</i> derm
Co	Aver.	$2.06 \times 10^{-4}$	$3.89 \times 10^{-5}$	$2.43 \times 10^{-6}$
	Max	$5.68 \times 10^{-4}$	$1.07 \times 10^{-4}$	$6.69 \times 10^{-6}$
	Min	$1.42 \times 10^{-5}$	$2.67 \times 10^{-6}$	$1.67 \times 10^{-7}$
Cr	Aver.	$9.30 \times 10^{-5}$	$6.14 \times 10^{-2}$	$3.51 \times 10^{-4}$
	Max	$1.68 \times 10^{-4}$	$1.11 \times 10^{-1}$	$6.34 \times 10^{-4}$
	Min	$2.48 \times 10^{-5}$	$1.64 \times 10^{-2}$	$9.38 \times 10^{-5}$
Cu	Aver.	$1.04 \times 10^{-7}$	$7.78 \times 10^{-5}$	$7.57 \times 10^{-5}$
	Max	$1.37 \times 10^{-7}$	$1.02 \times 10^{-4}$	$9.96 \times 10^{-5}$
	Min	$6.84 \times 10^{-8}$	$5.12 \times 10^{-5}$	$4.99 \times 10^{-5}$
Ni	Aver.	$1.68 \times 10^{-8}$	$1.44 \times 10^{-5}$	$1.44 \times 10^{-5}$
	Max	$2.98 \times 10^{-8}$	$2.56 \times 10^{-5}$	$2.56 \times 10^{-5}$
	Min	$1.02 \times 10^{-8}$	$8.72 \times 10^{-6}$	$8.72 \times 10^{-6}$
Pb	Aver.	$1.97 \times 10^{-7}$	$1.31 \times 10^{-4}$	$4.40 \times 10^{-5}$
	Max	$2.82 \times 10^{-7}$	$1.87 \times 10^{-4}$	$6.29 \times 10^{-5}$
	Min	$1.20 \times 10^{-7}$	$7.98 \times 10^{-5}$	$2.68 \times 10^{-5}$
Zn	Aver.	$3.85 \times 10^{-8}$	$2.54 \times 10^{-5}$	$6.36 \times 10^{-6}$
	Max	$5.79 \times 10^{-8}$	$3.82 \times 10^{-5}$	$9.55 \times 10^{-6}$
	Min	$2.72 \times 10^{-8}$	$1.80 \times 10^{-5}$	$4.49 \times 10^{-6}$
Total	Aver.	$3.00 \times 10^{-4}$	$6.16 \times 10^{-2}$	$4.94 \times 10^{-4}$
	Max	$7.36 \times 10^{-4}$	$1.11 \times 10^{-1}$	$8.39 \times 10^{-4}$
	Min	$3.93 \times 10^{-5}$	$1.66 \times 10^{-2}$	$1.84 \times 10^{-4}$

TABLE VI. Cancer risk for Co, Cr and Ni for ZR and NS landfills

Metal	ZR landfill	NS landfill
Co	$1.90 \times 10^{-8}$	$3.18 \times 10^{-8}$
Cr	$2.75 \times 10^{-5}$	$2.02 \times 10^{-7}$
Ni	$2.87 \times 10^{-9}$	$6.52 \times 10^{-10}$

#### CONCLUSION

In this research, a sedimentable dust samples were collected at two large landfills in Serbia during the 4 summer monitoring campaigns, in order to analyse particle size distribution and toxic elements content (As, Cd, Co, Cr, Cu, Ni, Pb, Zn), as well to assess health risk for landfill employees. Since the concentration of As and Cd were not detected in accordance with the set method, the detection limits for these two elements were not taken in consideration.

The results of particle size distribution analysis demonstrate that the particles whose equivalent sphere diameter was between 20–30  $\mu\text{m}$  make up the majority of sample mass at both landfill locations, though the sample from Zrenjanin landfill showed a bimodal distribution with a significant portion of particles larger

than 100 µm. Average PM2.5/PM10 ratio in investigated samples was 0.178 and 0.17 for Novi Sad and Zrenjanin landfills, respectively.

Analysis revealed high concentration of toxic elements in samples at both landfills. Additionally, an extremely high concentration of Cr and Zn in samples from the landfill in Zrenjanin was detected. The high concentration of certain elements (Cr, Zn Cu and Co) was attributed to the frequently occurring landfill fires.

Concerning health risk assessment, we have found that *HI* were in order of magnitude E-01 that indicates that there is low non-cancer risk for the employees at both landfill sites. In general, the highest *CR* was calculated for the employees at Zrenjanin landfill. For both landfill sites, *CR* is highest for Cr, but still within the defined threshold for tolerable cancer risk. If the risk evaluation for total suspended particles is conducted, we assume that the health risk would probably be higher than reported here due to the fact that total suspended particles, in comparison with sedimentable particles, generally contain higher percentage of fine fraction that could penetrate to lungs and that is generally enriched with toxic elements.

Since the study proved the influence of landfill to enrichment dust by toxic elements, especially Cr and Zn, future research is necessary in order to measure toxic elements concentrations in sedimentable, PM2.5, PM10 and total suspended dust during organized campaigns at city landfills.

#### SUPPLEMENTARY MATERIAL

Additional data and information are available electronically at the pages of journal website: <https://www.shd-pub.org.rs/index.php/JSCS/article/view/12335>, or from the corresponding author on request.

*Acknowledgement.* This research (paper) has been supported by the Ministry of Science, Technological Development and Innovation through project No. 451-03-47/2023-01/200156 “Innovative scientific and artistic research from the FTS (activity) domain”.

ИЗВОД

#### ПРОЦЕНА ЗДРАВСТВЕНОГ РИЗИКА ОД ТОКСИЧНИХ ЕЛЕМЕНТА У ТАЛОЖНОЈ ПРАШИНИ СА ДЕПОНИЈА

УНА МАРЧЕТА<sup>1</sup>, МИЛИЦА ВУЧИНИЋ ВАСИЋ<sup>2</sup>, ЈОРДАНА НИНКОВ<sup>3</sup>, СТРАХИЊА ИЛИЋ<sup>2</sup> И БОГДАНА ВУЛИЋ<sup>1</sup>

<sup>1</sup>Универзитет у Новом Саду, Технички факултет „Михајло Пупин“, Бурсе Ђаковића бб, 23000 Зрењанин, <sup>2</sup>Универзитет у Новом Саду, Факултет техничких наука, Трг Доситеја Обрадовића б, 21000 Нови Сад и <sup>3</sup>Институт за прашарство и повртарство, Национални институт Републике Србије, Лабораторија за земљиште и ароекологију, Максима Горког 30, 21000 Нови Сад

На две велике несанитарне депоније у Србији (Зрењанин и Нови Сад) спроведене су четири кампање мониторинга таложне прашине. Анализа расподеле величине честица урађена је ласерском дифракцијом, док је концентрација токсичних елемената (ТЕ) одређена помоћу оптичке емисионе спектрометрије са индуктивно спрегнутом плазмом. Процена ризика по здравље запослених на депонијама спроведена је на основу концентрација ТЕ према методама Агенције за заштиту животне средине Сједињених Америчких Држава. Резултати расподеле величине честица су показали да највећи део

узорака таложне прашине не припада ни PM<sub>2,5</sub> ни PM<sub>10</sub> фракцији. Анализа је показала високу концентрацију ТЕ на обе депоније: установљена је изузетно висока концентрација Cr и Zn у узорцима са Зрењанинске депоније. Потенцијал анализираних токсичних елемената у погледу ризика по здравље за обе депоније је следећи: Cr > Co > Pb > Ni > Zn > Cu. Према резултатима, укупни (максимални) индекс опасности за запослене на депонијама у Зрењанину (0,197) и Новом Саду (0,113) показао је да је ризик од канцера веома низак. За обе депоније, ризик од канцера је био највећи за Cr ( $2,75 \times 10^{-5}$  за Зрењанин и  $2,02 \times 10^{-7}$  за Нови Сад), чија је вредност такође у оквиру дефинисаног прага толеранције за ризик од канцера.

(Примљено 14. априла, ревидирано 26. маја, прихваћено 30. јуна 2023)

#### REFERENCES

1. M. El-Fadel, A. Findikakis, J. Leckie, *Environ. Manage.* **50** (1997) 1 (<https://doi.org/10.1006/jema.1995.0131>)
2. M. Pazoki, M. A. Abdoli, A. Karbassi, N. Mehrdadi, K. Yaghmaeian, *J. Environ. Health Sci. Eng.* **12** (2014) 12 (<https://doi.org/10.1186/2052-336x-12-12>)
3. Z. Chu, X. Fan, W. Wang, W.C. Huang, *Waste Manage.* **84** (2019) 119 (<https://doi.org/10.1016/j.wasman.2018.11.031>)
4. E. Chalvatzaki, V. Aleksandropoulou, M.A. Lazaridis, *Water Air Soil Pollut.* **225** (2013) 1782 (<https://doi.org/10.1007/s11270-013-1782-z>)
5. *Integrated Science Assessment (ISA) for Particulate Matter*, Environmental Protection Agency, United States, 2019, <https://cfpub.epa.gov/ncea/isa/recordisplay.cfm?deid=347534> (accessed 15 July 2022)
6. N. R. Ekeré, M. C. Ugbor, J. N. Ihedioha, N. N. Ukwueze, H. O. Abugu, *J. Environ. Health Sci. Eng.* **18** (2020) 711 (<https://doi.org/10.1007/s40201-020-00497-6>)
7. M. Dubovina, N. Grba, D. Krčmar, J. Agbaba, S. Rončević, Đ. Kerkez, B. Dalmacija, *J. Serb. Chem. Soc.* **87** (2022) 133 (<https://doi.org/10.2298/JSC210830102D>)
8. E. Chalvatzaki, T. Glytsos, M. Lazaridis, *Int. J. Environ. Health Res.* **25** (2015) 551 (<https://doi.org/10.1080/09603123.2014.989491>)
9. B. Vujić, N. Stanisljević, P. Popescu, N. Tosić, U. Marčeta, M. Pardanjac, V. Pode, *Stud. Univ. Babes-Bolyai Chem.* **65** (2020) 305 (<https://doi.org/10.24193/subbchem.2020.1.24>)
10. Campbell, R., Donlon, B., Webster, P., Lynott, D., Carty, G., *Landfill Manuals: Landfill Monitoring*, 2<sup>nd</sup> ed., Office of Environmental Enforcement, Environmental Protection Agency Ireland, 2003, <https://www.epa.ie/publications/compliance-enforcement/waste/EPA-Landfill-Monitoring.pdf> (accessed 26 February 2022)
11. I. Oruc, B. Oktay Akkoyunlu, I. Edogan *J. Serb. Chem. Soc.* **87** (2022) 953 (<https://doi.org/10.2298/JSC211203025O>)
12. D. Espylin, S. N. Ismail, S. M. Praveena, Z. Hashim, E. Z. Abidin, *Malays. J. Med. Health Sci.* **14** (2018) 2 ([http://www.medic.upm.edu.my/upload/dokumen/2018080308584301\\_MJMHS\\_Aug\\_2018.pdf](http://www.medic.upm.edu.my/upload/dokumen/2018080308584301_MJMHS_Aug_2018.pdf))
13. E. Vega, V. Mugica, E. Reyes, G. Sanchez, J.C. Chow, J.G. Watson, *Atmos. Environ.* **35** (2001) 4033 ([https://doi.org/10.1016/S1352-2310\(01\)00164-9](https://doi.org/10.1016/S1352-2310(01)00164-9))
14. M. Rashad, E. Shalaby, *Am.-Euras. J. Agric. Environ. Sci.* **2** (2007) 204 ([http://www.idosi.org/aejaes/jaes2\(3\)/JAES%202\(3\).pdf](http://www.idosi.org/aejaes/jaes2(3)/JAES%202(3).pdf))
15. M. R. Ray, S. Roychoudhury, G. Mukherjee, S. Roy, T. Lahiri, *Int. J. Hyg. Environ. Health* **208** (2005) 255 (<https://doi.org/10.1016/j.ijheh.2005.02.001>)

16. D. Ubavin, B. Agarski, N. Maodus, N. Stanisavljevic, I. Budak, *Integr. Environ. Assess. Manage.* **14** (2018) 105 (<https://doi.org/10.1002/ieam.1967>)
17. *Official document on number of landfill faires, No 65/22*, Republic of Serbia, Ministry of internal affaires, Belgrade, Serbia, 2022
18. *VDI 2119: Measurement of Dustfall, Determination of Dustfall using Bergerhoff Instrument (Standard Method)*, German Engineering Institute, 1972
19. C. Di Biagio, P. Formenti, Y. Balkanski, L. Caponi, M. Cazaunau, E. Pangui, E. Journet, S. Nowak, S. Caquineau, M.O. Andreea, K. Kandler, T. Saeed, S. Piketh, D. Seibert, E. Williams, J.F. Doussin, *Atmos. Chem. Phys.* **17** (2017) 1091 (<https://doi.org/10.5194/acp-17-1901-2017>)
20. *ISO/IEC 17025: General Requirements for the Competence of Testing and Calibration Laboratories*, International Organization for Standardization, 2017
21. *EPA-821-R01-010, Method 200.7: Trace Elements in Water, Solids, and Biosolids by Inductively Coupled Plasma-atomic Emission Spectrometry*, Environmental Protection Agency, United States, 2001
22. *Exposure Factors Handbook: 2011 Edition*, National Center for Environmental Assessment, Environmental Protection Agency, United States, 2011 (<https://cfpub.epa.gov/ncea/risk/recordisplay.cfm?deid=236252>) (accessed 22 July 2022)
23. *Risk assessment guidance for superfund, Human health evaluation manual (Part A)*, Environmental Protection Agency, United States, Office of Emergency and Remedial Response, 1989, [https://www.epa.gov/sites/default/files/2015-09/documents/rags\\_a.pdf](https://www.epa.gov/sites/default/files/2015-09/documents/rags_a.pdf) (accessed 22 July 2022)
24. E. Durmusoglu, T. Fatih, K. Aykan, *J. Hazard Mater.* **176** (2010) 870 (<https://doi.org/10.1016/j.jhazmat.2009.11.117>)
25. *Supplemental Guidance for Developing Soil Screening Levels for Superfund Sites OSWER9355.4-24*, Environmental Protection Agency, United States, Office of Solid Waste and Emergency Response, Washington, DC, 2001
26. M. Vučinić Vasić, A. Mihailović, U. Kozmidis-Luburić, T. Nemes, J. Ninkov, T. Zeremski-Škorić, B. Antić, *Chemosphere* **86** (2012) 585 (<https://doi.org/10.1016/j.chemosphere.2011.10.023>)
27. M. Ochsenkühn-Petropoulou, T. Lyberopoulou, R. Argyropoulou, F. Tsopelas, K.M. Ochsenkühn, *Fresenius Environ. Bull.* **18** (2009) 2210 ([https://www.researchgate.net/publication/230720567\\_Chemical\\_and\\_structural\\_characterization\\_of\\_airborne\\_particulate\\_matter\\_in\\_an\\_industrial\\_and\\_an\\_Urban\\_area\\_in\\_Greece](https://www.researchgate.net/publication/230720567_Chemical_and_structural_characterization_of_airborne_particulate_matter_in_an_industrial_and_an_Urban_area_in_Greece))
28. S. Thongyuan, T. Khantamoon, P. Aendo, A. Binot, P. Tulayakul, *Hum. Ecol. Risk Assess.* **27** (2020) 876 (<https://doi.org/10.1080/10807039.2020.1786666>)
29. B. Škrbić, J. Živančev, I. Antić, M. Buljović, *Environ. Sci. Pollut. Res.* **28** (2021) 16065 (<https://doi.org/10.1007/s11356-020-11794-w>)
30. D. Wan, C. Zhan, G. Yang, X. Liu, J. Yang, *Int. J. Environ. Res. Public Health* **13** (2016) 491 (<https://doi.org/10.3390/ijerph13050491>)
31. F. Li, J. Zhang, J. Huang, D. Huang, J. Yang, Y. Song, G. Zeng, *Environ. Sci. Pollut. Res.* **23** (2016) 13100 (<https://doi.org/10.1007/s11356-016-6458-y>)
32. E. S. Galvão, R. de Cassia Feroni, M. T. D'Azeredo Orlando, *Chemosphere* **269** (2021) 128746 (<https://doi.org/10.1016/j.chemosphere.2020.128746>)
33. A. Eslami, M. H. Saghi, B. Akbari-Adergani, S. Sadeghi, M. Ghaderpoori, M. Rabbani, A. Alinejad, *J. Environ. Health Sci. Eng.* **19** (2021) 133 (<https://doi.org/10.1007/s40201-020-00587-5>)

34. A. Mihailović, Lj. Budinski-Petković, S. Popov, J. Ninkov, J. Vasin, N. Ralević, M. Vučinić Vasić, *J. Geochem. Explor.* **150** (2015) 104  
(<https://doi.org/10.1016/j.gexplo.2014.12.017>)
35. H. A. Al-Swadi, A. R. A. Usman, A. S. Al-Farraj, M. I. Al-Wabel, M. Ahmad, A. Al-Faraj, *Sci. Rep.* **12** (2022) 8972 (<https://doi.org/10.1038/s41598-022-12345-8>)
36. Z. Liu, J. Zhou, J. Zhang, Y. Mao, X. Huang, G. Qian, *J. Clean. Prod.* **244** (2020) 118597  
(<https://doi.org/10.1016/j.jclepro.2019.118597>)
37. J.A. Acosta, A. Faz, K. Kalbitz, B. Jansen, S. Martínez-Martínez, *J. Environ. Monit.* **13** (2011) 3087 (<https://doi.org/10.1039/C1EM10364D>).



SUPPLEMENTARY MATERIAL TO  
**Health risk assessment of toxic elements in sedimentable dust  
from landfills**

UNA MARČETA<sup>1\*</sup>, MILICA VUČINIĆ VASIĆ<sup>2</sup>, JORDANA NINKOV<sup>3</sup>,  
STRAHINJA ILIĆ<sup>2</sup> and BOGDANA VUJIĆ<sup>1</sup>

<sup>1</sup>*University of Novi Sad, Technical Faculty "Mihajlo Pupin", Djure Djakovica bb Street,  
Zrenjanin 23000, Serbia*, <sup>2</sup>*University of Novi Sad, Faculty of Technical Sciences, Trg Dositeja  
Obradovića 6 Street, 21000 Novi Sad, Serbia* and <sup>3</sup>*Institute of Field and Vegetable Crops,  
National Institute of the Republic of Serbia, Laboratory for Soil and Agroecology, Maksima  
Gorkog 30 Street, 21000 Novi Sad, Serbia*

J. Serb. Chem. Soc. 88 (7–8) (2023) 777–791

STUDY AREA

The landfill in Zrenjanin city is situated south-west of the city, on the 5 km distance from the city centre and 1.7 km from the nearest houses (Fig. S-1). The landfill contains ca. 268,400 m<sup>3</sup> mostly of communal waste, waste from construction sites and non-hazardous medical waste.<sup>1</sup> The landfill covers an area of 67,100 m<sup>2</sup>. The average waste height at landfill is 4 m and the modelled annual weight of the waste disposed is 42,116 tons per year.<sup>2</sup>

The landfill In Novi Sad is situated south-west of the city, on the 6 km distance from the city centre and 700 m from the nearest houses (Fig. S-1). Waste separation plant is located nearby the landfill. The landfill site covers an area of 560,000 m<sup>3</sup>, where the landfill itself covers 22,000 m<sup>3</sup>. The height of the landfill varies in the range of 2.5 m to 14 m. The landfill contains ca. 2,000,000 m<sup>3</sup> of the waste. The average quantity of the waste disposed is 629.7 tons per day.<sup>3</sup>

\*Corresponding author. E-mail: una.tasovac@tfzr.rs



Fig. S-1. Layout of the cities of Zrenjanin and Novi Sad (Serbia) and external appearance of the landfills.

#### REFERENCES

1. *Regional Plan for Waste Management in City of Zrenjanin and municipalities Sečanj, Titel i Kovačica*, University of Novi Sad, Faculty of Technical Sciences, Novi Sad, Serbia, 2011,  
[http://www.sepa.gov.rs/download/UpravOtpad/RPUO\\_ZrenjaninSecanjTitelKovacica.pdf](http://www.sepa.gov.rs/download/UpravOtpad/RPUO_ZrenjaninSecanjTitelKovacica.pdf) (accessed 25 December 2021)
2. G. Vujić, Project of recultivation and closing of landfill in Zrenjanin, University of Novi Sad, Faculty of Technical Sciences, Novi Sad, Serbia, 2009
3. Regional waste management plan for city of Novi Sad and municipalities of Bačka Palanka, Bački Petrovac, Beočin, Žabalj, Srbobran, Temerin i Vrbas, University of Novi Sad, Faculty of Technical Sciences, Novi Sad, Serbia, 2012,  
<https://skupstina.novisad.rs/wp-content/uploads/2016/12/SI-26-2.pdf> (accessed 25 December 2021).





## Analysis of the initial education of chemistry teachers and their attitudes towards teaching in the Republic of Serbia

SAŠA A. HORVAT\*#, VERA I. POPOVIĆ, DUŠICA D. RODIĆ#  
and TAMARA N. RONČEVIĆ#

Faculty of Sciences, University of Novi Sad, Trg Dositeja Obradovića 3,  
21000 Novi Sad, Serbia

(Received 22 August, revised 2 October 2022, accepted 10 July 2023)

*Abstract:* This research was aimed to analyse the current state in primary and secondary schools in the Republic of Serbia, regarding chemistry teachers' initial education and self-perceived competencies. As an instrument, a questionnaire of 20 questions was used, which was prepared in the form of a Google questionnaire. The questions were divided into five groups to examine data on the structure of chemistry teachers (gender, age, place and school where they teach), the level of education obtained and the method of acquisition and acquired competencies, and finally the personal opinion of chemistry teachers about the teaching profession, advantages, disadvantages and possible recommendations to his/her students in terms of choosing this profession as a possible career. The questionnaire was sent to 1537 schools and 497 chemistry teachers took part in the questionnaire. The results showed that chemistry teachers are predominantly women, mostly aged 36–55, full-time employed and with an average working experience of over 11 years. Most teachers have appropriate education and acquired competencies. They cite working with children as the biggest advantage of the teaching profession while as the biggest disadvantage, they report a constant increase in the amount of administration from year to year.

*Keywords:* chemistry education; teachers' attitudes; teachers' competencies, teachers' opinions.

### INTRODUCTION

In modern society, the education of young people is experiencing constant changes and improvements in various fields. Teaching relies on professional and personal skills and competencies of teacher and it includes a continuous process of professional development.<sup>1</sup> A teacher is required to constantly learn, develop

\* Corresponding author. E-mail: sasa.horvat@dh.uns.ac.rs

# Serbian Chemical Society member.

<https://doi.org/10.2298/JSC220822039H>

and follow modern innovations and acquire new knowledge and skills. His/her specialization will last throughout their working life. Therefore, modern society needs to successfully support students – future teachers in the learning process to be successful in adequately responding to new requirements and accepting new quality standards. Professional development helps, not only the novice teachers but also those more experienced, to learn new strategic endeavours, which improve the success of students in the process of education and the work of teachers in professional engagement.<sup>2,3</sup>

Chemistry teachers' competences should be obtained through initial teacher education at chemistry education faculties and through continuing professional development. Competencies are a complex combination of knowledge, skills and value judgements needed to perform activities in the classroom.<sup>4,5</sup> They include cognitive and practical skills as well as abilities, experiences, strategies and habits, but also emotions, motivation, *etc.*<sup>3</sup> Due to the complexity of the teaching process, in addition to the knowledge of the scientific content of the subject itself, the teacher is required to have developed a Pedagogical Content Knowledge (PCK) skills.<sup>6</sup> The key role of teachers is the development of educational systems and implementation that contributes in terms of the necessary knowledge, better social skills and greater academic success.<sup>2,7</sup> As education and other spheres of society are subjected to constant change, it is expected of teachers to encourage learning, take care of their personal professional development and to be part of an organization that develops and learns.<sup>2</sup> In addition to possessing specific basic skills acquired at the faculty, more flexible, generic and transferable competencies are needed that will make the teacher complete for active and successful work. This implies acquiring knowledge from the educational subjects Pedagogy, Psychology, Methods of teaching and School practice, so-called PPM block in Serbia. The legal regulations currently in effect require practising teachers to have earned 36 ECTS credits based on subjects belonging to chemistry education with intention to the increase to 60 ECTS.<sup>8</sup> The issue of professional development of teachers in recent years inevitably includes providing quality education that would match the new needs of individuals and society. The assurance of quality and success in competitive working conditions is a professionalism based on competencies. Therefore, the constant professional and personal development of the individual is of great importance.<sup>3</sup>

In addition to external factors (school equipment, regulations governing education, *etc.*)<sup>9</sup>, internal psychological characteristics have a great influence on how successful the teachers will be in performing their professional activities. Society have to be aware that being a teacher is not only teaching, but also being a role-model to the students because a teacher's human qualities are also important.<sup>10</sup> The most of the chemistry teachers from Slovenia and Finland believe that personal characteristics, interest in chemistry, students' development and enjoyment

of teaching and communicating are the most important attributes of good chemistry teachers.<sup>11</sup> The personal characteristics of teachers are reliable indicators of the success of educational activities. Their work, commitment and behaviour should be an example not only to students but also to the entire society.<sup>3,12,13</sup> A successful teacher is a leader of the teaching process, coordinator and mentor, equal associate, and a person who has high organizational skills and who knows different techniques for establishing contacts and interactions with students, colleagues and parents.<sup>3,14</sup>

The teacher must see himself/herself as a professional guide for young people through the process of upbringing and education to knowledge that is usable in real life.<sup>7</sup> Therefore, the two most important roles of teachers are upbringing and educational role. The teachers are expected to be good managers, to possess the skills to teach, adjust to curricula and student changes and cooperate with their colleagues, or simply to carry out different roles in different contexts.<sup>15–17</sup>

The teacher should not pay direct attention only to the teaching content, but also to the development of students as autonomous individuals. An important aspect of the upbringing role is the moral education of students.<sup>18–20</sup> The teacher, as the main leader of the educational process, is obliged to discover and recognize the needs of students for learning and to help them fulfil those needs through their activities. He/she needs to know students' personalities and to direct their learning toward their capabilities. He/she must be aware of the volume and depth of teaching content and correct them as needed.<sup>14,21</sup>

A teacher must have a clear strategy for leading the class based on respect for students and achieving defined learning goals to be a successful professional.<sup>22</sup> The extent to which he/she will be successful in fulfilling his tasks certainly depends on his/her personality, readiness to perform various roles and desire for continuous professional development.<sup>23</sup> The main goal of professional development is for the teacher to improve himself/herself, develop knowledge, skills and abilities, and improve personal characteristics, as well as his/her work in the classroom, which contributes to more complete preparation of students for life and work.<sup>24</sup>

#### EXPERIMENTAL

The aim of this research was to find out what initial education chemistry teachers from Serbia possess and what do they think about the quality of their education and teaching as a profession in general and what measures could be taken to improve the current education system.

For this research, the following tasks have been set:

- to determine the state of the personnel structure of chemistry teachers in schools on the territory of the Republic of Serbia,
- to determine how the subjected teachers acquired their competencies and collect their opinions on PPM subjects and

– to analyse their teachers' attitudes about the advantages and disadvantages of the teaching profession, as well as the reasons why they would or would not recommend their students to study to become chemistry teachers.

#### *The instrument*

The instrument used in this research was a questionnaire that referred to the personal, educational and professional characteristics of chemistry teachers, emphasizing their initial education, the way of acquired competencies and their opinions about working in a school, attitudes about the quality of initial education, their problems in teaching, as well as the attitude about the chosen profession and whether they would recommend it to their students. The research was conducted in the form of a Google questionnaire and was completely anonymous, and the results were used only for scientific purposes. The questionnaire contained 20 questions. The questions were grouped into several sections represented in Table I. The types of questions were single-answer questions, multiple-choice questions and one open-ended question.

TABLE I. Description of sections of a questionnaire according to number and type of questions

Section	Question numbers	Type of questions
General data on respondents	1–2	Single-answer
Employment	3–7	Multiple-choice (Q4) and single-answer
Initial education of chemistry teachers	8–10	Single-answer
Competencies	11–13	Dingle-answer
Chemistry teachers' personal opinions on their professional vocation	14–20	Multiple-choice, single-answer (Q14,19) and open-ended (Q20)

In multiple-choice questions candidates could mark up to three answers. The questionnaire was created by experts whose scientific field is the methodology of teaching chemistry. The team consisted of three assistant professors and one high-school chemistry professor. Choices to single-answer and multiple-choice questions are proposed in a panel discussion. Some answers proposed for choices in some questions (e.g., 16 and 17) came from personal experience and seminars for the development of chemistry teachers created by the authors of this paper. Seminar participants drew attention to the problems they faced in their everyday life in the classroom. Teachers' responses were statistically processed.

#### *The sample*

The research was conducted among chemistry teachers who work in primary and secondary schools in the territory of the Republic of Serbia. Schools from the territory of Kosovo and Metohija were not included in the survey. The questionnaire was sent to the e-mail addresses of the principals of 1078 primary and 459 secondary schools throughout Serbia, who were asked to forward the Google form link to their chemistry teachers. Since there is no reliable data about the number of chemistry teachers in Serbia, the statistical data were calculated based on the number of schools.<sup>8</sup> 497 chemistry teachers took part in the research. They were not asked for any personal information, such as e-mail address or name and surname. The research was conducted during the school year 2020/2021. The total number of schools where the questionnaire was sent and the number of teachers who take part in the survey are shown in Table II.

TABLE II. Total number of schools and number of teachers who participated in the research

Region	Number of schools			Number of respondents
	Elementary schools	High schools	In total	
Vojvodina	344	122	466	227
Belgrade	192	86	278	66
South Serbia	542	251	793	204
In total	1078	459	1537	497

According to the regulations on the appropriate type of teacher education in primary and secondary schools in Republic of Serbia, the educational level of the teachers and the type of school are presented in Table III. Since a part of the teachers work in more than one school, as the primary place of work was taken the workplace with a higher percentage of classes. The table shows that most teachers have the right level of education. As for PPM competences, we see that most of them were acquired at undergraduate studies, but this will certainly be discussed in more detail in the Results and Discussion section.

TABLE III. Educationa level and PPM competencies of teachers according type of school

Education level	Type of schools		
	Elementary	Vocational	Gymnasium
Higher school	16	0	0
Bachelor	176	37	33
Master	121	58	33
Specialisation, Magister, PhD	15	6	2
PPM competencies			
Subjects at Bachelor studies	165	35	25
Subjects at Master studies	32	18	13
Subjects at Integrated studies	13	2	1
Passing the license exam	80	35	22
Further education	24	9	6
No acquired	14	2	1

## RESULTS AND DISCUSSION

The results obtained in the survey are presented in the form of a “pie” or “bar” charts.

### *General data on respondents*

This section contained two questions. The first question was about the respondent age. The respondents’ answers are shown in Fig. 1 as follows: the number of chemistry teachers in the Republic of Serbia is very similar between 46 and 55 years old and 36–45 years old, while the smallest number of teachers belongs to the group over 55. The smallest fractions of the teacher population are those who are either at the end of their working career or at the very beginning, while the majority are teachers with some experience.

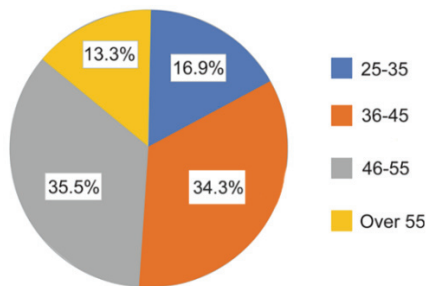


Fig. 1. Chemistry teachers age.

The second question was about the gender of chemistry teachers, and it has been noticed that female teachers are dominantly represented in this profession. Namely, out of 497 respondents, 87.9 % were female teachers. Previous study had shown that gender has no influence on teachers attitudes towards chemistry teaching.<sup>25</sup>

#### *Employment*

This section contained five questions. When asked about the place of work, the respondents had the opportunity to choose a city, a village or both. The results show that the majority of teachers work in the city (59.2 %). The least of them work in rural schools (16.3 %), while about a quarter of respondent teachers work in both urban and rural areas to fulfil the working norm (24.5 %).

The fourth question was a multiple-choice question and it was formulated to ask chemistry teachers about the level of the school they work in. Out of a total of 497 respondents, as many as 71.23 % of them stated that they work in primary schools (Fig. 2). This result could be expected given that the largest number of schools are primary schools, and the greatest demand is for teachers in schools of this type. It was noticed that more than 120 teachers, out of 497, work in several schools to gain their working norm which is 20 classes per week.

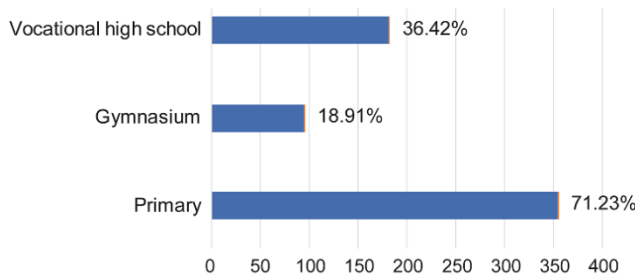


Fig. 2. Representation of chemistry teachers according to the type of school in which they teach.

Regarding the employment status in terms of duration, the respondents had the opportunity to state whether they were admitted to the position of chemistry

teacher in a particular school with a permanent or fixed-term contract. The results showed that 75.5 % of them were hired on a permanent contract.

According to the Rule on the 40-hours working week of teachers and professional associates in high school, the weekly norm of regular classes in high school and vocational and technical schools for chemistry teachers is 20 classes (one class is 45 min). According to the results, the majority of surveyed chemistry teachers work full-time (73.5 %) while only 4.2 % of chemistry teachers work over time. What is concerning is that 22.3 % of teachers do not have full-time or 20 classes per week. The reason for that could be the status of chemistry in the education system because, in The Republic of Serbia, chemistry as a subject is introduced in 7<sup>th</sup> grade with only two classes per week.

Almost half of the chemistry teachers belong to the group of experienced teachers with more than 10 years of working experience, while the most experienced teachers with over 20 years of working experience represent 27.2 % of the total number of respondents. There are a small number of chemistry teachers who have not yet completed one year of work in the educational profession who are most likely young graduate students (Fig. 3). These results are quite similar to Tomašević and Trivić research.<sup>8</sup>

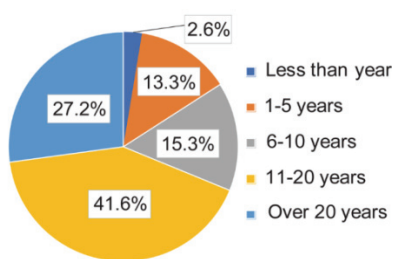


Fig. 3. Representation of chemistry teachers according to their work experience in the field of education.

#### *Initial education of chemistry teachers*

The eighth and the following two questions referred to the initial education of chemistry teachers in Serbia. The answer about academic degree of chemistry teachers is presented in Fig. 4.

From the point of view of the educational system, it is commendable that all surveyed teachers have a certain degree, considering that no respondent has declared himself as an undergraduate. Higher school do not exist now in Serbia. They existed before 2005, followed high school and took 6 semesters to their completion. It is the position 5 of European Qualification Framework. The specialist academic studies grant at least 60 ECTS credits after their completion. Before specialist academic studies student must have completed master academic studies. Graphic representation about the educational level of chemistry teachers in certain types of schools is presented in Fig. 5.

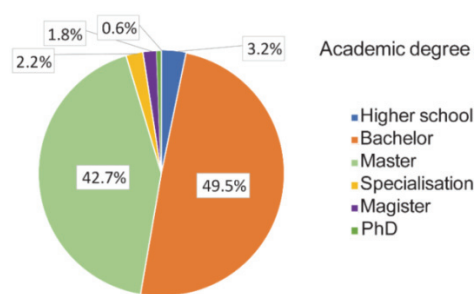


Fig. 4. Representation of chemistry teachers according to their academic degree.

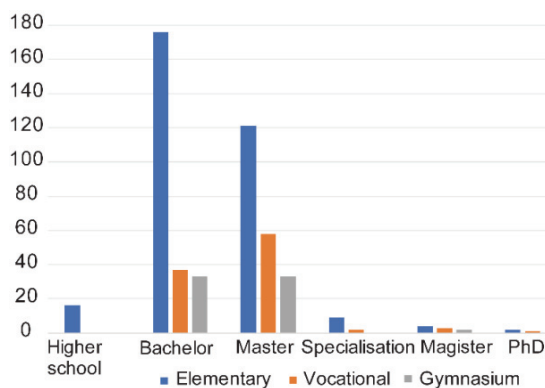


Fig. 5. Representation of chemistry teachers in certain schools according to their level of education.

Since a part of the teachers work in more than one school, as the primary place of work was taken the workplace with a higher percentage of classes. This shows that there is a competent teaching staff at educational positions.

The largest number of chemistry teachers in Serbia graduated from the Faculty of Sciences which has a well-organized program for the education of future chemistry teachers in several university centres. There are 66.8 % of them. Some chemistry teachers graduated at the Faculty of Chemistry which make 20.7 % of respondents, then at the Faculty of Physical Chemistry and the Faculty of Technology or Technology and Metallurgy with 3.6 % of teachers each. The remaining 5.3 % of respondents graduated from undergraduate studies at other faculties. These chemistry teachers completed their studies at the Faculty of Philosophy, or Faculty of Pedagogy or High Pedagogy School (level 5 of European Qualification Framework). They might be the older chemistry teachers who had been studying chemistry when chemistry was subject at these faculties.

When it comes to the Master's degree, the largest number of respondents said they did not have it, as many as 40.4 %. Of those who continued their studies after completing their Bachelor's studies, most of them stated that they had obtained a Master's degree at the Faculty of Sciences, 39.8 %. Three times less

number received their Master's degree at the Faculty of Chemistry, more precisely 13.5 %, and the remaining 6.3 % completed Master's studies at other faculties (Faculty of Physical Chemistry, Faculty of Technology or Faculty of Technology and Metallurgy, *etc.*).

#### *Competences of chemistry teachers*

According to the Law's regulations on a PPM program for work in the teaching of the Republic of Serbia, in addition to the teaching area of the subject, teachers should acquire a certain number of ECTS in subjects related to pedagogy, psychology, subject teaching methods and school practice. The chemistry teachers were asked the next question for three subjects: how they acquired the competencies of chemistry teachers for learning and teaching (subjects: Pedagogy, Teaching Methods, School Practice).

Regarding competencies for learning and teaching chemistry, the largest number of chemistry teachers answered that they acquired competencies through subjects within their initial studies (Fig. 6).

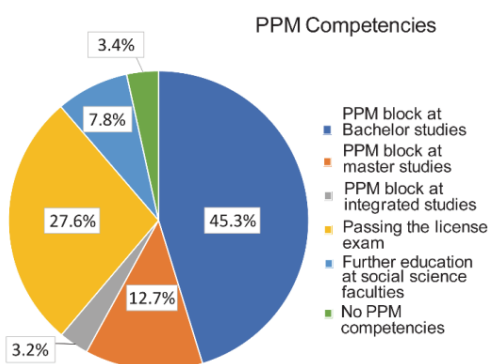


Fig. 6. Representation of chemistry teachers according to obtained competencies.

It is a matter of concern that teachers believe that they acquired competencies by passing the licence exam and through additional education at the Faculty of Philosophy, Faculty of Pedagogy, Faculty of Teaching or Singidunum Faculty. Namely, the chemistry teaching methods and school practice in chemistry can only be obtained at the chemistry education faculties as only these faculties have employees who are engaged in chemical education and who within their education completed courses in all areas of chemistry as well as the pedagogical and the psychological courses. Teacher with no competencies are probably teachers with less than a year of working experience who have not completed their study program in teaching.

It is reassuring to know that the vast majority of respondents believe that PPM block subjects are necessary for a chemistry teacher (93.4 %). Only a small percentage of teachers (6.6 %) believe that this is not the case. As already men-

tioned in the paper, the subjects of this type are certainly needed by future teachers, because thanks to them they acquire all the necessary knowledge and skills to perform the tasks that require critical responsibility to help their students in their development and encourage self-development.

In the process of education reform, the Law on the Basics of the Education System as a novelty introduced the work permit known as license exam, as a condition for the work of teachers in schools. The licence exam checks the trainee's ability to independently perform the work of a teacher after completing the induction program (the duration of the program is one year in a school where the teacher works). The exam is taken in another institution, in front of a committee formed by the Ministry of Education. A candidate with a written preparation of a lesson or activity, or a written essay, approaches the exam. Carrying out the appropriate form of educational work takes one school hour (45 min). The oral part of the exam lasts up to 90 min and consists of the candidate's conversation with the committee about the class held, or the presentation of the activity; solving the specific pedagogical situation and knowing the regulations in the field of education. Success in the exam is evaluated with: "passed" or "failed". Most chemistry teachers who participated in the research have passed the licence exam (80.3 %) while 12.9 % of teachers have completed the internship program and are waiting for an invitation to the exam. At the time of the research, 6.8 % of them were in the process of doing an internship.

#### *Chemistry teachers' personal opinions on their professional vocation*

The last 7 questions were about personal opinions of chemistry teachers about their profession, satisfaction with their job, the advantages and disadvantages of a teacher's job and would they advise their students to study chemistry education.

The 14<sup>th</sup> question was about the possible opportunity to change the job of a teacher. Of the total number of surveyed teachers, 44.7 % enjoy working with children. Teachers' job satisfaction has been recognized as very important.<sup>1</sup> On the other hand, 20.1 % of respondents did not find themselves in the role of teachers and if they could, they would change their profession. 35.2 % of them said that they might apply for another job. Teachers who want to change their profession have work experience between 11 and 20 years and bachelor and master completed studies. This is graphically illustrated in Fig. 7. Similar findings are presented in research conducted in the Southeast part of the USA where 58.7 % wanted to leave teaching after 10 years in the profession.<sup>26</sup>

Those respondents who answered the previous question that they would like to change their profession, were requested to write where they would like to work instead of school. 184 chemistry teachers said that they love the educational profession and would not change their teaching job. However, the largest number of

respondents would still change their job at school for a job in the laboratory, which is 45.88 %. In new research it has found that only a quarter of teachers believe that teacher profession is valued in modern society.<sup>27</sup> The distribution of answers to question 15 is shown in Fig. 8.

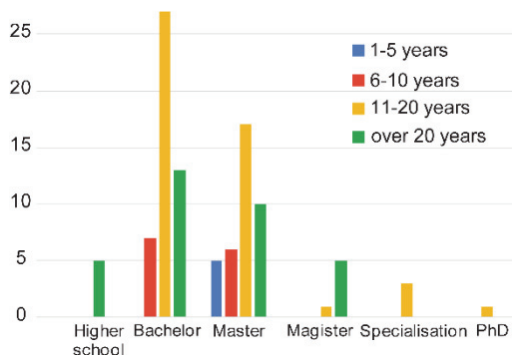


Fig. 7. The level of education and years of working experience of chemistry teachers who want to change teacher job.

*If you were to change the job of a chemistry teacher, which job would suit you?*

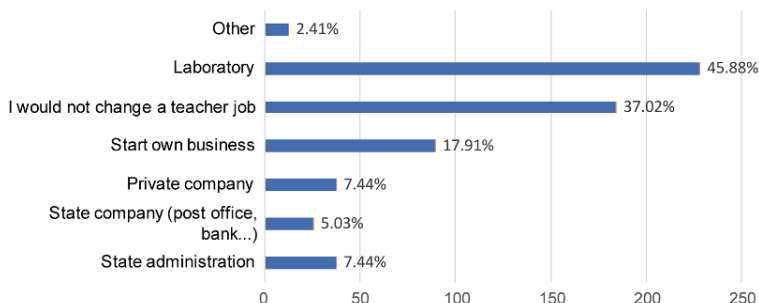


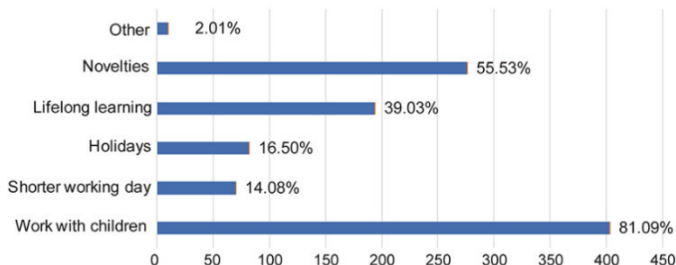
Fig. 8. Representation of chemistry teachers according to a personal opinion about alternative work.

The next two questions were multiple-choice questions about the advantages and disadvantages of the chemistry teacher profession. Answers to questions 16 and 17 are represented in Fig. 9.

The biggest advantages of working in a school, according to the results of the research, are working with children, novelties – the fact that no day is the same as another, and lifelong learning. Bivona claims that teachers need to deal with many challenges during their worktime and that daily routine is not a routine at all.<sup>28</sup> Chemistry teachers stated that they are most concerned about the amount of administration in the teaching profession, which is an integral part of the job. Teachers often feel overloaded with other requirements placed upon them in addition to the teaching they have every day.<sup>29</sup> Teachers spend a greater number of working hours in administrative tasks than in the preparation of teaching

classes, according to a previous survey in the Republic of Serbia.<sup>30</sup> Working with children and novelties as an advantage of chemistry teacher job dominate among teachers aged 36–55 years and with work experience of 10–20 years. On the other hand, teachers cited the lack of laboratory equipment as a big disadvantage of this profession. Chemistry is an experimental science, this is not just a problem for teachers and schools, but the entire educational system of the state. 300 chemistry teachers indicated a low salary as the biggest problem of the teaching profession, while 269 of between them, a small fund of chemistry classes as a disadvantage of this profession. Teachers often fulfil their norm by working in several schools, which requires a high organization of time and schedule of classes by schools. An interesting fact is that a smaller number of teachers stated the need for continuous improvement as a disadvantage. It is commendable that teachers do not see this as a problem but as a need to raise educational activity to the highest possible level. The desire for continuous professional development has been confirmed in previous research in some countries.<sup>31</sup>

*In your opinion, what are the advantages of the chemistry teacher job?*



*In your opinion, what are the disadvantages of the chemistry teacher job?*

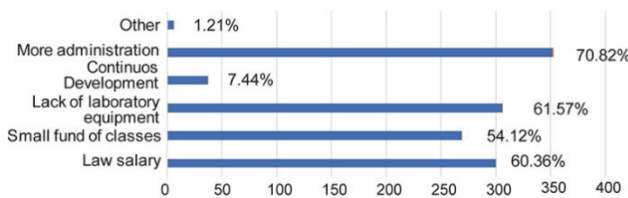


Fig. 9. Representation of chemistry teachers according to personal opinion on the advantages and disadvantages of the teaching profession of chemistry teacher.

As for the shortcomings, the problem with a small salary and a small fund of classes is seen by the same group of teachers. It is interesting that a small salary is not a problem for those under the age of 35. As for the lack of equipment of the laboratory, this is mostly indicated by colleagues with experience over 10

years of and 45–55 years of age. The problem of increasing administration is indicated by all colleagues over 10 years of service and 36–55 years of age.

Question 18 was asked to find out would chemistry teachers work as mentors to students who study chemistry education programs. It was also a multiple-choice question. The majority of respondents answered “Yes, because it is important to share experiences with future chemistry teachers”, which is in the interest of the education system and collegiality among teachers. Some teachers saw this as an opportunity for extra money, more precisely, 30.78 % of the respondents. The smallest number would answer negatively to this question (7.44 % of them). Answers to question 18 are represented in Fig. 10. Mentoring is an effective method in the development of pre-service teachers’ PCK.<sup>32</sup>

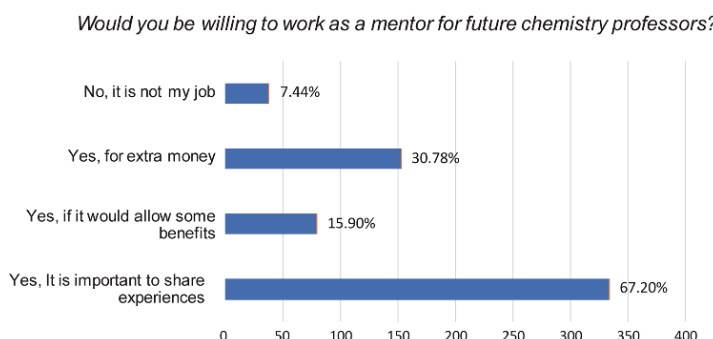


Fig. 10. Representation of chemistry teachers who want to work as a mentor to students.

Questions 19 and 20 asked chemistry teachers about their personal opinions on the recommendation of the teaching profession to students. The first question was about chemistry teachers’ recommendations about teachers’ profession to their students, and the next one was to write a reason for their answer. Distribution of answers is shown in Table IV.

TABLE IV. Distribution of answers on question 19: “Would you recommend your students to be chemistry teachers?”

Yes	No	Maybe
34.5 %	24.3%	41.2 %

The results of this study are in line with the results obtained in a study in Australia where almost 35.4 % of respondents would recommend teaching as a career.<sup>33</sup> The reasons for such answers were explained in question 20. Those teachers who answered “yes” to the previous question to recommend the job of a chemistry teacher, cited the following: “Working with children is beautiful, creative and dynamic”; “chemistry is an important science that gives us constant acquisition of new information”; “chemistry allows us to observe the world with

different view and understand the processes that take place around us every day”; “teachers job provides the opportunity to participate in other people’s progress and development as a person, as well as the opportunity to transfer knowledge and skills to younger generations”. In other words, teachers who would recommend chemistry teachers’ jobs to students are in love with chemistry as a science and their profession as chemistry teachers. A group of teachers who stated that they would not recommend their students to work at school explained the answer through the following statements: “Students do not want to study natural sciences, and generally there is no one who could recommend a job as a chemistry teacher”; “there is more and more administration, the work does not end with the bell, but continues at home”; “for the number of tasks required by this job the salary is very small”; “the profession is not valued enough in society”; “the faculty needed for this job is difficult and the job is difficult to obtain”; “a small norm of chemistry classes concerning other subjects that are studied four or five times a week and disparagement not only by students but also their parents”; “lack of laboratory equipment, no room for improvement regardless of the length of service”. The answers that the respondents wrote as a reason why they would not recommend teaching profession to their students is in a line with a general opinion about the shortcomings of this profession, regardless of all the advantages of this job. The reasons are also in line with previous research.<sup>33</sup> The third group consists of those teachers who cannot say with certainty whether they would recommend the job of chemistry teacher to their students. They explained their answer in the following ways: “I would recommend this job only if the position of educators changes in society, if conditions improve in all schools, if they provide a sufficient norm of classes, otherwise the job is unprofitable”; “Only if they are ready to work with children, I would recommend the job of a teacher, but some other subject because chemistry is a very complex science”. This group of respondents includes those teachers who love their job and the science they do, but would only recommend the job of a chemistry teacher if most of the shortcomings are eliminated.

#### CONCLUSION AND IMPLICATIONS

The conducted research was aimed at the analysis of the initial education of chemistry teachers and their attitudes towards the teaching profession in the territory of the Republic of Serbia. However, the key findings of this study can be summarized in next points. The number of female chemistry teachers were higher than male teachers. Mid-career teachers are the most respondents and they work in primary school. Three-quarters of respondents are indefinite-term employed and the same number are provided with a full-time job. In the part where the data on employment were examined, the result was obtained that in Serbian schools, those teachers who have at least 10 years of working experience in the field of

education are mostly employed. According to the questionnaire results, the chemistry teachers in Serbia have competence in the necessary qualifications in terms of academic, social, and personality traits. The largest number of chemistry teachers obtained their Bachelor's degrees at the Faculty of Sciences and most of the teachers have passed the professional exam.

In the fifth and last part, the personal opinion of the teacher on the teaching vocation was analysed. The results of the survey led to the following finding: most of the surveyed teachers love their job and would not change it for someone else, while the minor group of teachers said that they would change their job if they had the opportunity, giving the work in laboratories as an example of what they would rather do. Teacher competencies are the key to the practical application of a safe and efficient teaching process. Students' positive attitudes towards chemistry and their motivation to learn and provide appropriate feedback to learning activities significantly depend on how teachers have influenced them.<sup>34</sup> Therefore, it is necessary to deal as much as possible on the issue of initial education of future teachers and the implementation of activities for their personal and professional development.

Perceptions of the status of the teaching profession have changed, and accordingly, the former importance of the teaching profession has disappeared.<sup>35</sup> Some chemistry teachers have specified that factors such as enjoy teaching, love of children, being a teacher is a dream job, and the fact that teachers' working conditions are more comfortable than many other professions are effective in the choice of teaching. The biggest disadvantage of this job are the growing demands of the administration, which takes up too much free time, low salaries, poor position of teachers in society and a small number of classes. When asked if they would work as mentors to students who come to practice at the school where they work, most teachers said that they would be very happy to do so, because in that way they pass on their own experience to younger colleagues.

Despite all the shortcomings of the teaching profession, teachers are a pillar of education and progress in a country. For that reason, joint efforts are urgently needed to develop teachers' competencies and obtain resources and practical equipment to create a scientifically literate society in Serbia.

*Acknowledgement.* The authors acknowledge the financial support of the Ministry of Education, Science and Technological Development of the Republic of Serbia (Grant No. 451-03-9/2021-14/200125).

## И З В О Д

АНАЛИЗА ИНИЦИЈАЛНОГ ОБРАЗОВАЊА НАСТАВНИКА ХЕМИЈЕ И ЊИХОВИХ  
СТАВОВА ПРЕМА НАСТАВНИЧКОМ ПОЗИВУ У РЕПУБЛИЦИ СРБИЈИ

САША А. ХОРВАТ, ВЕРА И. ПОПОВИЋ, ДУШИЦА Д. РОДИЋ И ТАМАРА Н. РОНЧЕВИЋ

*Природно-математички факултет, Универзитет у Новом Саду, Три Доситеја Обрадовића 3, 21000  
Нови Сад*

Ово истраживање је рађено с циљем да се сагледа тренутно стање по питању наставника хемије који раде у основним и средњим школама на територији Републике Србије. Као инструмент је коришћен упитник са 20 питања, урађен у форми Google упитника. Питања су подељена у пет група с циљем да се испитају подаци о структури наставника хемије (пол, старосна доб, место и школа у којој раде), стеченом степену образовања и начину стицања, стеченим компетенцијама и њиховом мишљењу о наставничком позиву, предностима, манама и препорукама младима за избор наставничког позива. На упитник је одговорило 497 наставника. Према добијеним резултатима међу наставницима хемије доминирају особе женског пола, претежно старости 36–55 година, запослене на неодређено радно време и с просечним радним стажом преко 11 година. Већина наставника има одговарајуће образовање и стечене компетенције. Као највеће предности наводе рад са децом, а сматрају да је највећи недостатак професије, због којег не би препоручили својим ученицима да се образују за наставнички позив, све више администрације.

(Примљено 22. августа, ревидирано 2. октобра 2022, прихваћено 10. јула 2023)

## REFERENCES

1. B. Cristina-Corina, A. Valerica, *Procedia Soc. Behav. Sci.* **51** (2012) 167 (<https://doi.org/10.1016/j.sbspro.2012.08.139>)
2. D. Popović in *Montenegro in XXI Century — In The Era Of Competitiveness: Education*, P. Vukotić, S. Milić, Ž. Jaćimović, V. Kaščelan, Z. Bogićević, D. Radonjić, R. Šendelj, D. Popović, T., Novović, Z. Minić, K. Popović, V.A., Lubarda, M. Popović, B. Šišević, Z. Kotri, Eds., Crnogorska akademija nauka i umjetnosti, Podgorica, Montenegro, **73**, 2010, 239 (in Serbian) (<https://canupub.me/bli3>)
3. M. Danilović, in *Proceedings of 6<sup>th</sup> International Symposium Technology, Informatics and Education for Learning and Knowledge Society*, 2011, Čačak, Serbia, *Tehnologija, informatika i obrazovanje*, TIO 6, Tehnički fakultet, Čačak, 2011, 371.12 (in Serbian)
4. R. Deakin Crick, in *Getting involved: Global citizenship development and sources of moral values*, F. Oser, W. Veugelers, Eds., Sense Publishers, Rotterdam, 2008, p. 31
5. B. Tomašević, D. Trivić, *J. Serb. Chem. Soc.* **80** (2015) 435 (<https://doi.org/10.2298/JSC141002121T>)
6. L. S. Shulman, *Educ. Researcher* **15** (1986) 4 (<https://doi.org/10.2307/1175860>)
7. K. Lasić, *Putokazi*, **1**(2019), 157 (in Serbian) (<https://putokazi.eu/web/aktualni-broj/>)
8. B. Tomašević, D. Trivić, *Chem. Educ. Res. Pract.* **15** (2014) 239 (<https://doi.org/10.1039/C3RP00116D>)
9. R.R. Edmonds, *Search for effective schools: The identification and analysis of city schools that are instructionally effective for poor children (final report)*, Detroit, MI, 1977 (<https://eric.ed.gov/?id=ED142610>)
10. N. Oruç, *Int. J. Humanit. Soc. Sci.* **1** (2011) 83 ([http://www.ijhssnet.com/journals/Vol.\\_1\\_No.\\_4;\\_April\\_2011/11.pdf](http://www.ijhssnet.com/journals/Vol._1_No._4;_April_2011/11.pdf))

11. V. Ferk Savec, B. Urankar, M. Aksela, I. Devetak, *J. Serb. Chem. Soc.* **82** (2017) 1193 (<https://doi.org/10.2298/JSC161221083S>)
12. K. Lasić, *Putokazi* **3** (2015) 101 (in Serbian) (<https://putokazi.eu/wp-content/uploads/2015/03/KL.pdf>)
13. G. Handley, *Personality, learning and teaching*, Routledge & K. Paul, London, 1973
14. H. Požar, *Sinteze – časopis za pedagoške nauke, književnost i kulturu* **5** (2016) 23 (<https://doi.org/10.5937/sinteze0-11315>) (in Serbian)
15. G. Đigić, *PhD Thesis*, Faculty of Philosophy, Niš, <https://nardus.mpn.gov.rs/handle/123456789/4000> (accessed 28.11.2021) (in Serbian)
16. L. W. Anderson, D.R. Krathwohl, *A taxonomy for learning, teaching, and assessing: A revision of Bloom's taxonomy of educational objectives*, Longman, New York, 2001 (<https://www.uky.edu/~rsand1/china2018/texts/Anderson-Krathwohl - A taxonomy for learning teaching and assessing.pdf>)
17. K. Funda Nayir, S. Cinkir, *Anthropologist* **20** (2015) 1 (<https://doi.org/10.1080/09720073.2015.11891718>)
18. S. Stojiljković, *Zbornik Instituta za pedagoška istraživanja* **33** (2001) 190 (in Serbian) (<https://www.ipisr.org.rs/images/arhiva-zbornika/Zbornik-33.pdf>)
19. S. Stojiljković, Z. Dosković, *Zbornik Instituta za pedagoška istraživanja* **22** (1990) 63 (in Serbian) (<https://www.ipisr.org.rs/images/arhiva-zbornika/Zbornik-22.pdf>)
20. S. Stojiljković, Z. Dosković, *Godišnjak za psihologiju* **4** (2006) 237 (in Serbian)
21. D. Ješić, *Časopis za društvene i prirodne nauke* **1** (2010) 195 (in Serbian) (<https://www.psихологијанис.rs/arhiva-godisnjak/godisnjak-2005-2006/Godisnjak-Vol-4-No-4-5-%282005-2006%29-237-251.pdf>)
22. V. Simeunović, P. Spasojević, *Savremene didaktičke teme: nacrt za savremenu didaktičku koncepciju i strategiju nastavnog rada u osnovnoj školi*, Pedagoški fakultet, Bijeljina, 2005 (in Serbian)
23. S. Stojiljkovic, *Psihološke karakteristike nastavnika*, Filozofski fakultet, Niš, 2012, (in Serbian)
24. E. M. Uslu, T. Özgün, *Research on Education and Psychology* **6** (2022) 68 (<https://doi.org/10.54535/rep.1134110>)
25. S. W. Wachanga, M. Ngary, D. R. Muchiri, *ZJER* **15** (2003) (<https://opendocs.ids.ac.uk/opendocs/handle/20.500.12413/5376>)
26. B. Scafidi, *An analysis of the retention rates of Georgia public school teachers. The Governor's Office of Student Achievement* (accessed 30.11.2022 from [www.gosa.georgia.gov](http://www.gosa.georgia.gov))
27. OECD, *TALIS 2018 Results (Volume II) Teachers and School Leaders as Valued Professionals* (accessed 02.12.2022 from [https://www.oecd-ilibrary.org/education/annex-bmain-breakdown-variables\\_d1ba43b3-en](https://www.oecd-ilibrary.org/education/annex-bmain-breakdown-variables_d1ba43b3-en))
28. K. Bivona, *Teacher moral: The impact of teaching experience, workplace conditions, and workload*, 2002 (accessed 02.12.2022 from <http://eric.ed.gov/?id=ED467760>)
29. S. Black, *Am. Sch. Board J.* **190** (2003) 36 (<https://eric.ed.gov/?id=EJ674597>)
30. B. Tomašević, D. Trivić, *Pedagogija* **4**(2014) 605 (in Serbian)
31. D. Sikošek, B. Čagran, *J. Elementary Educ.* **9** (2016) 75 (in Slovenian) (<https://journals.um.si/index.php/education/article/view/351>)
32. D. Can-Kucuk, S. Gencer, H. Akkus, *Chem. Educ. Res. Pract.* **123** (2022) 599 (<https://doi.org/10.1039/d2rp00033d>)

33. F. Longmuir, B. Gallo Cordoba, M. Phillips, K.A. Allen, M. Moharami, *Australian Teachers' Perceptions of their Work in 2022*, Monash University, 2022 (<https://doi.org/10.26180/21212891>)
34. J. Copriady, *Med. J. Soc. Sci.* **5** (2014) 312 (<https://dx.doi.org/10.5901/mjss.2014.v5n8p312>)
35. L. Hargreaves, M. Cunningham, A. Hansen, D. McIntyre, C. Oliver, T. Pell, *The status of teachers and the teaching profession in England: Views from inside and outside the profession*, The Chancellor, Masters and Scholars of the University of Cambridge, Cambridge, 2007.